Ignition and combustion of future oxygenated fuels in compression-ignition engines

Elina Koivisto

University College London

Submitted in partial fulfilment of the requirements for the degree of Doctor of Philosophy at University College London

October 2015

I, Elina Koivisto, confirm that the work presented in this thesis is my own. Where information has been derived from other sources, I confirm that this has been indicated in the thesis.

Elina Koivisto

18th October 2015

Abstract

Biodiesel and ethanol-diesel blends are currently commercially available but further engine research is required so as to develop new, more efficient and environmentally friendly, alternative fuels for diesel engines. Although natural sources of feedstock can provide a wide range of potential fuel molecules, their combustion characteristics are generally not yet well understood. This PhD project contributes to the development of alternative fuels by systematically investigating in a single cylinder direct injection diesel engine the fundamental effects of chemical and physical fuel properties on combustion characteristics, exhaust gas formation and engine thermal efficiency of over 70 potential alternative fuel molecules. These molecules included oxygen-bearing ones, alkylbenzenes and diesel refinery streams. Chemical kinetic studies available in literature were applied to explain the differences in ignition delays of different molecules. The results showed that oxygenated fuels have longer ignition delays, higher levels of NO_x and lower particulate emissions compared to hydrocarbon fuels. It was concluded that the shorter ignition delays of biodiesel, compared to fossil diesel fuel, which have been reported by several previous studies, are caused by the longer carbon chain of the biofuel molecules despite the oxygenated fuel structure, as well as by the lower content of aromatic and cyclic compounds. Additionally, it was observed that although adding oxygen into the fuel molecular structure lowers the overall particulate emissions, it increases the number of small particulates. Furthermore, it was found, based on experimental engine tests and a zero dimensional thermodynamic simulation, that development of alternative fuels could provide more opportunities for reducing pollutant exhaust gas emissions than improving efficiency, because molecular fuel structure does not appear to have a substantial effect on engine thermal efficiency. The results of this work can be used in the selection and development of new alternative fuels, with environmentally friendly combustion characteristics and improved thermal efficiency.

Acknowledgements

First and foremost, I would like to express my sincere gratitude to my supervisor Professor Nicos Ladommatos for his guidance and knowledge, as well as motivation and patience as my PhD supervisor. Additionally, I wish to thank Dr Ramanarayanan Balachandran for his support as my second PhD supervisor.

I am also grateful to Dr Martin Gold for acting as my supervisor at British Petroleum and Dr John Rogerson and Dr Philip Sorin for their assistance in interpreting the experimental results.

I wish to express my sincere thanks to the employees of the workshop at UCL's Department of Mechanical Engineering, especially to Richard, Barry and Phil for their help with the experimental setup.

Special thanks for the excellent company, countless lunches and support to Aaron, Babtiste, Mart, Midhat, Taaha, Anne, Aadil, and Paul.

And, as always, I wish to thank my parents and my sisters for their unconditional love and support. Kiitos kullat pienet suppilovahverot!

Contents

List of figures

List of tables

Nomenclature

A	area
BTE	brake thermal efficiency
CI	compression ignition
CN	cetane number
CAD	crank angle degrees
CO	carbon monoxides
CO_2	carbon dioxide
DAQ	data acquisition
DEE	diethyl ether
ddHRR	second derivative of heat release rate
dHRR	first derivative of heat release rate
DME	dimethyl ether
DPF	diesel particulate filter
d	droplet diameter
EOC	end of combustion
ETBE	ethyl tertiary butyl ether
FAME	fatty acid methyl esters
γ	ratio of the specific heat
GC-MS	gas chromatography–mass spectrometry
H	enthalpy
HO_2•	hydroperoxyl radical
H_2O	water
H_2O_2	hydrogen peroxide
HRR	heat release rate
IFFMS	instantaneous fuel flow measurement system

IMEP	indicated mean effective pressure
ITE	indicated thermal efficiency
k	vaporization rate constant
l	distance
m	mass
MTBE	methyl tertiary butyl ether
η	efficiency
n	amount of substance
N_2	nitrogen
NO	nitrogen oxide
NO_x	nitrogen oxides
NO_2	nitrogen dioxide
OH•	hydroxyl radical
O_2	oxygen
p	pressure
PAH	polycyclic aromatic compounds
pHRR	peak value of the heat release rate
PID	proportional integral derivative
PM	particulate matter
Q_{ch}	gross heat release rate
Q_{HV}	heating value of the fuel
Q_{ht}	heat transfer to the cylinder walls
Q_n	net heat release rate
r	radius
ρ	density

R	ideal gas constant
RCM	rapid compression machine
RME	rapeseed methyl ester
$RO_2\bullet$	alkyl peroxy radical
SCR	selective catalytic reduction
SMD	sauter mean diameter
SME	soybean methyl ester
SOC	start of combustion
SOI	start of injection
T	temperature
θ	crank angle degrees
t	time
TDC	top dead centre
UHC	unburned hydrocarbons
ULDCFS	ultra-low volume fuel system
V	volume
W_C	power output per engine cycle
W_i	indicated work output per cycle

Chapter 1

Introduction

1.1 Motivation

Fossil diesel fuel has been used to power passenger vehicles since the compression ignition (CI) engine was invented by Rudolph Diesel in 1892. Besides fossil diesel fuel, vegetable oils have been used as alternative fuels in CI engines since Rudolph Diesel first tested peanut oil in an engine. In 1970s, research into vegetable oils as potential fuels was increased once it was discovered that the viscosity of vegetable oils can be reduced by the chemical process of transesterification, which breaks the oil structure down making it better suitable for CI engines [1]. Currently there is a growing interest in alternative transportation fuels, which could replace fossil diesel fuel, because of (1) diminishing reserves of petroleum, (2) increasing demand for transportation, (3) concerns about the security of energy supply in several countries, and (4) the need for more environmentally friendly fuels due to both global warming and growing concern about the effect of exhaust gas emissions on human health.

In order to allow a faster transition from fossil to alternative fuels, alternative fuels should be compatible with the existing diesel engines at least in the short to medium term. The development of alternative fuels provides opportunities for the development of sustainable fuel molecules with more efficient and clean combustion than fossil diesel fuels. The natural feedstock for alternative fuels provides a wide variety of molecules for a range of production processes. Therefore, the focus of global fuel research is increasingly on the types of molecules which could provide the desirable performance in compression ignition engines, and which could be produced from sustainable resources. Oxygenated molecules are particularly promising ones due to their lower overall carbon emissions and potential to increase the security of energy supply. However, as was suggested by Fiorese et al. [2], although the technical difficulties of several production routes are likely to be overcome by 2030, the production of alternative fuels may not become cost effective compared to fossil fuels by then unless new policies are introduced encouraging production and adoption of alternative fuels.

The motivation of this dissertation was the need to obtain better understanding of compression ignition combustion with potential alternative fuels, which could be developed from environmentally friendly sources and combusted with low exhaust gas emissions and with high engine thermal efficiency. Therefore, if molecular structure could be identified, which met these requirements, then fuel developers could be guided in their selection and development of future environmentally friendly and efficient alternative fuels. Fuel molecular structure is of high importance when considering the development of new, alternative fuels, because it governs the physical and chemical properties of the fuel, which in turn determine the chemical kinetics of ignition and the physical aspects of the combustion processes. Several studies have investigated the effect of fuel properties on ignition, combustion, and exhaust gas emissions. However, the wide range of apparatus and engines used, and differences in experimental conditions, make comparison between the results of these studies difficult. Additionally, previous research has mainly focused on first generation biofuels, such as methyl esters, alcohols and ethers with little research being conducted on other potential fuel molecules, such as ketones [3]. This dissertation presents a systematic study of a wide variety of potential alternative fuel molecules, which includes non-oxygen bearing as well as oxygenated molecules, such as alcohols, esters and ketones. Particular efforts were made to determine the effects of a range of sub molecular, structural features on engine combustion, pollutant emissions and thermal efficiency.

1.2 Aims and objectives

The aim of this dissertation was to systematically investigate the effect of chemical and physical fuel properties of several potential alternative fuels on combustion characteristics, exhaust gas emissions and engine thermal efficiency of a diesel engine. To this end, a literature review and several experimental studies were conducted. The main objectives of this PhD project can be listed as follows:

1. To investigate the compression ignition and exhaust gas emissions of several potential alternative oxygenated fuel molecules in order to gain an extensive database of the effects of fuel molecular structure on diesel engine

combustion. The alternative oxygenated fuel molecules included alcohols, carbonyl compounds and ethers.

2. To investigate the engine thermal efficiency of these oxygenated fuel molecules and to identify the key factors which may determine the engine thermal efficiency of a CI engine.
3. To apply the knowledge gained from the two studies above to explain the combustion characteristics, exhaust gas emissions and engine thermal efficiency of several lignocellulosic compounds proposed as potential alternative fuels. The lignocellulosic compounds included valeric esters, levulinates and ketones.
4. To investigate the compression ignition and exhaust gas emissions of alkylbenzenes, because the relatively high content of cyclic compounds in fossil diesel fuel is one of the most significant structural differences between the fossil diesel fuel and the aliphatic alternative fuel molecules.
5. To investigate the compression ignition and exhaust gas emissions of five refinery streams which are used for blending fossil diesel fuel and compare the results for these streams with results for alternative oxygenated fuels, namely rapeseed methyl esters and soybean methyl esters.

1.3 Structure of the thesis

This thesis consists of a literature review, description of the experimental setup and the result analysis methods, followed by several chapters of results of experimental combustion studies, ending with a chapter on conclusions with recommendations for future work.

The literature review of this dissertation describes briefly the composition of fossil diesel fuel and several potential alternative fuel molecules, followed by the current knowledge of the effect of chemical and physical fuel properties on chemical kinetics of combustion, physical combustion processes, diesel engine thermal efficiency and exhaust gas emissions. The key findings of the literature review are concluded at the end of the literature review chapter. After the literature review, the experimental systems and analytical methods utilized in the experimental studies are described. In the six chapters following this, the results of each of the main six experimental studies

conducted as part of this PhD project are presented and discussed. Lastly, the main conclusions drawn in this PhD project are summarized and further work is suggested.

1.4 Publications

The following publications were produced as part of this PhD study:

1. Koivisto E, Ladommatos N, Gold M. Systematic study of the effect of the hydroxyl functional group in alcohol molecules on compression ignition and exhaust gas emissions. Fuel 2015;153;650–63.
2. Koivisto E, Ladommatos N, Gold M. The influence of various oxygenated functional groups in carbonyl and ether compounds on compression ignition and exhaust gas emissions. Fuel 2015;159;697-711.
3. Koivisto E, Ladommatos N, Gold M. Compression Ignition and Exhaust Gas Emissions of Fuel Molecules Which Can Be Produced from Lignocellulosic Biomass: Levulinates, Valeric Esters, and Ketones. Energy Fuels 2015; 29; 5875-5884.
4. Koivisto E, Ladommatos N, Gold M. Compression ignition and pollutant emissions of large alkylbenzenes. Fuel 2016; 172; 200-208.
5. Koivisto E, Ladommatos N, Gold M. The Effect of physical and chemical properties of fuel molecules on the engine efficiency of a compression ignition engine (Under review. Fuel 06/02/2016)

Chapter 2

Literature Review

2.1 Introduction

This literature review first describes the molecular structures of several potential alternative fuels compatible with compression ignition engine. The literature review then moves on to discuss the effect of fuel molecular structure on chemical kinetics of combustion, the physical processes of combustion, thermal engine efficiency, and the formation of exhaust gas emissions. Previous, publically available studies conducted with the alternative fuels are reviewed during the discussions when available.

2.2 Composition of fossil diesel fuel and several alternative fuels

The chemical composition of a fuel governs its physical and chemical properties, which in turn affect the engine performance and exhaust gas emissions. Therefore, it is important to consider the structure of the fuel molecules available from natural renewable resources when developing alternative fuels. This section describes, first, the general composition of fossil diesel fuel, so as to allow comparison between it and the alternative fuel molecules. This is followed by brief descriptions of the properties of potential alternative fuels molecules, which included biodiesel (esters), alcohols, ethers and ketones. Additionally, the production routes of these alternative fuel molecules were considered briefly.

2.2.1 Fossil diesel fuel

Fossil diesel fuel is a fractional distillate of crude oil and a complex mixture of several hundred chemical compounds. A typical diesel fuel contains approximately 66% paraffins and cycloparaffins ranging from C_{12} to C_{22}, 30% aromatics and 4%

olefins. The exact composition of fossil diesel fuel is usually determined by the composition of the crude oil and the refining methods [4,5].

Fossil diesel fuel is distilled from crude oil in order to achieve a cetane number (CN) suitable for compression ignition engines. A typical CN of diesel fuels is about 49 and the boiling point range is approximately 450-630K. As a comparison, hexane (C6) CN has been measured by ASTM method D6890 to be 53 and CN of 105 has been suggested for heptadecane (C17) [6]. Other diesel fuel properties that affect engine operation are viscosity and cold flow properties: high viscosity diesel fuel may require heated fuel lines; the high molecular mass components of diesel fuel can precipitate at low temperatures and form a waxy deposit, which may plug fuel filters. Several different diesel fuel additives can be used to improve the CN, viscosity and cold flow properties of diesel fuel [7].

It should also be noted that, besides crude oil refining, hydrocarbon fuels can be produced through bioprocessing from renewable sources. However, hydrocarbons are not currently produced through bioprocessing because crude oil refining is the most economical way to produce diesel fuels. Hence the production of hydrocarbons though a bioprocess, such as metabolic engineering, has mainly been used as validation for a concept to produce alternative fuels, rather than for the commercial mass production of hydrocarbons [8–10].

2.2.2 Esters as biodiesel

Biodiesel is a commercially available first generation biofuel composed of fatty acid methyl esters (FAME), which has many similar properties compared to fossil diesel fuel and can therefore be used in diesel engines as pure biodiesel (B100) or as diesel blends. Huber et al. estimated that 80% of biofuels produced in 2006 were biodiesels [11]. The main difference between fossil diesel fuel and biodiesel is the higher oxygen content of biodiesel, which reduces the fuel energy density. However, because of the higher density of biodiesel the volumetric energy content of biodiesel is only 5-6% lower than that of fossil diesel fuel. Biodiesel in general has higher viscosity, higher surface tension and poorer cold flow properties compared to diesel fuels [12,13]. Knothe [14] suggests a CN of 57 for a general commercial biodiesel

and Yean et al. [15] a boiling point of 622-632K. For comparison, a CN of 34.2 has been measured for methyl heptanone with ASTM method D6890 [6].

Biodiesel is produced from vegetable oils and animal fats: potential vegetable oils include corn, cotton, soybean, camelina, sunflower, canola, rapeseed, Jatropha, coconut, palm oil and algae. Pure vegetable oils and animal fats are difficult to combust in a diesel engine due to the large molecule size of their main compounds, the triglycerides [16]. Therefore, the triglycerides are reacted with alcohol, typically methanol or ethanol, in the presence of a catalyst (e.g. sodium or potassium hydroxide), to form FAME and glycerol, as shown in Figure 1. Biodiesel consists of a mixture of FAME molecules, which combust in diesel engines due to their long carbon chains. [12] Higher alcohols, such as ethanol, isopropanol and butanol can also be used in the transesterification process to produce biodiesel with longer carbon chains. However, methanol is the most common alcohol used in transesterification process due to its lower price compared to the larger alcohols. Summaries of the most common biodiesel production methods currently available can be found in the review articles by Abbaszaadeh et al. [17], Borugadda and Goud [18], Aransiola et al. [19], Adewale et al. [20], Bharathiraja et al. [21] and Daud et al. [22].

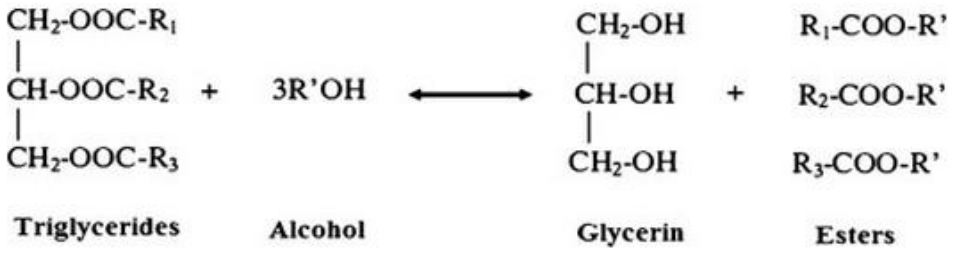

Figure 1. Production of biodiesel from triglycerides through transesterification [17].

Biodiesel composition is defined mainly by the type of triglycerides in the feedstock. Vegetable oils in general have more unsaturated triglycerides compared to animal fats. The most common fatty acids in biodiesel have carbon chain lengths from 12 to 22, which is similar to the carbon chain length of the diesel fuel molecules. The dominant fatty acids of biodiesel are palmitic acid (16:0), stearic acid (18:0), oleic

acid (18:1), linoleic acid (18:2) and linoleic acid (18:3), where the first number in brackets denotes the length of the carbon chain and the second the number of double bonds in the molecule [12,23]. As an example of the differences between feedstock, coconut oil contains more of the light fatty acids than the other vegetable oils and camelina oil is mainly composed of linolenic acid (18:3) with smaller amounts of heavier fatty acids [12]. Comprehensive reviews of the composition and properties of biodiesel can be found in the review articles by Hoekman et al. [12], Silitonga et al. [24], Kumar et al. [25], Ashraful et al. [23], Atabani et al. [16] and Takase et al. [26].

2.2.3 Alcohols

First generation ethanol-diesel blends are currently commercially available for CI engines and the production of second generation alcohols, both ethanol and heavier alcohols, is under development. Compared to fossil diesel fuel, alcohols have significantly lower heating values and lower vapour pressure due to their oxygen content. Additionally, the polarity of alcohol molecules makes them more soluble to water than hydrocarbons. However, alcohols have good ignition properties and are therefore attractive alternative fuel molecules [27]. For example, CN of 29.5 has been measured for heptanol with ASTM method D613. Higher alcohols have generally higher CN compared to shorter alcohols, making longer chain alcohols (> C5) more attractive biofuels than shorter chain alcohols (< C5) [6].

First generation ethanol is mainly produced from microbial fermentation of sugar cane and corn starch. The promising second generation bio-alcohol fuel production methods use lignocellulosic biomass as feedstock and the third generation bio-ethanol production, which is at an early development stage, uses algal biomass [27,28]. The main production technologies of bioethanol were described e.g. in review articles of Vohra et al. [29] and Baeyens et al. [28] and the production methods of bioethanol from lignocellulosic biomass were recently reviewed by Mood et al. [30] and Kang et al. [31]. Alcohols with longer carbon chains than that as ethanol can in general be produced with the same production methods as ethanol, but the low production yields prevent the utilization of long chain alcohols on commercial scale [32]. For example, in acetone-butanol-ethanol fermentation, the

ethanol yield is 10-30 times higher than the butanol yield [33]. As further examples of n-butanol production methods Morone and Pandey [34] described the production of n-butanol from lignocellulose and Jin et al. [33] from microorganisms through fermentation.

Besides the aforementioned production methods, alcohols can also be produced through metabolic engineering. The yields are rather low, making production of ethanol unattractive, but the production of alcohols with long carbon chains through metabolic engineering has become increasingly a research focus. Several strains can be used, out of which Escherichia coli is commonly considered a good potential strain for production of biofuel molecules on industrial scale. However, further development is required before the production methods can be applied on industrial scale [35–37]. Different possible production methods of isopropanol and butanol through metabolic engineering have been reviewed by Singh et al. [38]. Additionally, both Cann and Liao [32] and Zhang et al. [39] discussed the production of pentanol isomers from microorganisms, and Youngquist et al. [40] demonstrated a metabolic pathway to produce 1-dodecanol and 1-tetradecanol.

2.2.4 Ethers

Ethers have been suggested as diesel additives because of their high cetane numbers and low emission combustion. For example a CN of 140 has been suggested for diethyl ether, compared to the 49 CN of diesel fuels. However, ethers do in general have lower heating values and higher vapour pressure, compared to fossil diesel fuel, due to their oxygenated structure [41]. Currently, when considering ethers, only dimethyl ether (DME) is commercially used as a diesel additive due to its relatively easy production process and high availability. However, several studies are researching the production routes of second generation ethers from lignocellulosic biomass.

DME has similar physical properties to liquefied petroleum gas, CN about 55, and is considered as a good ignition improver in diesel engines [41,42]. Commercially, DME is produced from natural gas and through gasification of coal, but several studies have also focused on the direct conversion of syngas to DME using a bi-

functional catalyst [43]. The production methods of DME were discussed further in a review article by Azizi et al. [43]. Although the combustion behaviour of DME is desirable, the physical properties of DME, which is gas at ambient temperature, require modifications in the traditional diesel fuel injection systems [44]. Because of these requirement liquid diethyl ether (DEE) has recently been proposed as diesel additive. DEE can be produced from ethanol through a dehydration process, has a CN above 125, broad flammability limits and high miscibility with hydrocarbons despite its high oxygen content [45]. Additionally, longer chain ethers with higher CN, such as dibutyl ether, can also be produced through dehydration process from the corresponding alcohol [46]. Besides straight chain ethers, branched ethers such as ethyl tertiary butyl ether (ETBE) have also been suggested as alternative fuels. ETBE can be synthetized from bioethanol and isobutene. It has a low boiling point and good solubility in hydrocarbons [47]. Furthermore, ETBE and methyl tertiary butyl ether (MTBE) have been suggested as possible additives to improve diesel and ethanol miscibility [48].

2.2.5 Ketones

Methyl ketones have been suggested as potential diesel additives because of their suitable cetane numbers [49]. For example, a CN of 30 has been measured with ASTM method D6890 for 2-heptanone [6]. The research in production of methyl ketones as biofuels has been relatively scarce, due the relatively low yields of the suggested production methods, but is continuously increasing. Production of methyl ketones via several biological pathways, such as aerobic alkane/alkene degradation and fatty acid oxidation, has been suggested [50]. Methyl ketones can be produced for example via direct conversion of lignocellulosic biomass by endophytic fungi [51] or from E.coli through metabolic engineering [49]. It should also be noted that isopropyl ketone has been studied as a potential biofuel [52].

2.3 Effect of fuel molecular structure on chemical kinetics of combustion

When the fuel-air mixture in a diesel engine combustion chamber is homogeneous the rate of combustion is mainly controlled by the chemical kinetics of combustion. The chemical kinetics of combustion is specific to the molecular structure of the fuel: atoms and chemical bonds within the fuel molecules, as well as bonds between the fuel molecules, determine the reaction routes available for the fuel to combust. Combustion kinetics is temperature dependent and thus an artificial division is usually made between low (600-800 K), intermediate (800-1000 K) and high temperature (1000-3000 K) kinetics [53]. In this section, the general combustion reaction mechanism is presented first, followed by a slightly more detailed description of the low and intermediate temperature kinetics and a brief description of the high temperature kinetics. Lastly, the H_2O_2 mechanism is briefly described due to its significant effect on ignition. Because of the extreme complexity and quantity of the suggested kinetic mechanisms available, only the generally accepted key mechanisms are presented in this section. The main focus is on the kinetics of aliphatic hydrocarbons because they form the desirable main component of fossil diesel fuel. However, in order to provide a comprehensive overview on the effect of fuel molecular structure on chemical kinetics, the kinetics of alternative fuel molecules are also described, when available in the literature.

2.3.1 General combustion kinetics

The general stoichiometric complete combustion reaction between hydrocarbons (C_aH_b) and air (oxygen O_2 and nitrogen N_2) produces carbon dioxide (CO_2), water (H_2O) and nitrogen as follows [1]:

$$C_aH_b + \left(a + \frac{b}{4}\right)(O_2 + 3.773N_2) = aCO_2 + \frac{b}{2}H_2O + 3.773\left(a + \frac{b}{4}\right)N_2 \quad \text{(R 1)}$$

The general combustion reaction (R 1) cannot occur directly because it would require simultaneous breaking and formation of several fuel molecule bonds. Combustion in general occurs through a radical chain reaction mechanism, also known as the Semenov mechanism, which includes four main reaction types: initiation, propagation, branching and termination. An example of the radical chain mechanism is presented in Figure 2 for alkanes with less than five carbon atoms. Alkanes with more than five carbon atoms also combust through the main steps presented in Figure 2, but intermediate steps have to be added. For example, several thousand elementary reactions occur during the auto ignition of diesel fuel [1]. It should be noted, that because the chain reaction mechanism will start at different times in different regions of the combustion chamber during real diesel engine combustion, all of the chain reaction mechanisms occur practically at the same time and the species from reaction routes of different molecules may interact.

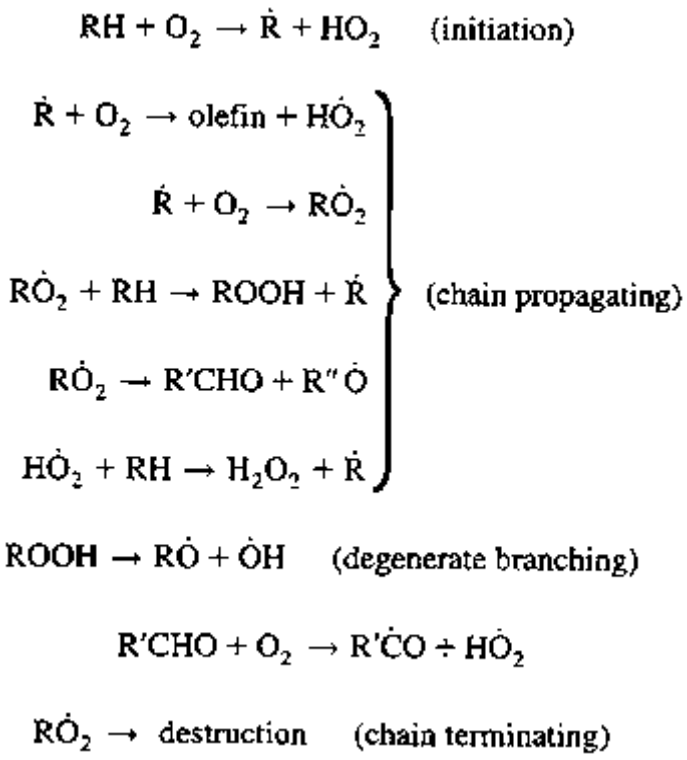

Figure 2. Example of the radical chain mechanism of alkanes with less than five carbon atoms [54].

The radical chain mechanism, an example of which is shown in Figure 2, starts when energy input into the compressed air-fuel mixture from the engine compression process reaches the minimum activation energies of the endothermic initiation reactions between fuel molecules and either molecular oxygen or radical species. Activation energy is defined as the minimum energy that must be introduced to a chemical system in order for a chemical reaction to occur [1]. Fuel radicals formed in the initiation reactions react further in exothermic propagation and branching reactions. In propagation reactions one radical is formed for each one consumed, whereas in branching reactions two radicals are formed for each one consumed, thus increasing the amount of radicals exponentially. Besides the propagation and branching reactions, the fuel radicals may also undergo a chain terminating reaction route. The radical chain mechanism ends in the termination reactions, in which no further radicals are formed. The most common chain carriers of the radical chain mechanism are radical species O•, H•, OH•, CH_3•, and HO_2• [55]. Combustion reactions tend to have low selectivity, which allows several different chain carrier

radicals to react via the same reaction, thus increasing the complexity of combustion kinetics [56].

Auto-ignition occurs once the initially slow, low and intermediate temperature reactions generate a large enough radical pool to sustain and accelerate fuel oxidation. Hence, ignition is determined by the competition between the heat generation from both the compression and the exothermic reactions, and heat loss by convection, radiation and the endothermic reactions within the combustion chamber [1,7]. Combustion can be enhanced by adding more radicals, for example by ignition improving additives or though laser ignition, and ceased by removing radicals: for example halogens are used in some fire extinguishers [56].

Several authors, e.g. Westbrook [57], have stated that ignition delay is mainly controlled by the low temperature kinetics. High temperature kinetics, on the other hand, affect greatly both combustion phasing and combustion duration. Under the high temperature regime, after ignition, chain propagation and chain branching reactions become dominant [55]. Combustion starts to slow down when the chain termination reactions have consumed most of the radicals available: temperature in the combustion chamber starts to decrease due to the lack of exothermic reactions, and in many cases also due to the increasing volume during the engine expansion stroke. Terminating reactions are generally not temperature sensitive, and can thus be effective also in relatively low-temperature zones. Combustion ends when either all of the fuel molecules have been consumed or not enough energy is available to enable further combustion reactions [58].

2.3.2 Low and intermediate temperature kinetics

The low and intermediate temperature region (600-1000 K) generally includes ignition and start of combustion before the temperature in the combustion chamber rises above 1000K due to both the compression stroke and the exothermic reactions [53,59]. The general radical chain mechanism of hydrocarbons starts with the initiation reaction (R 2), where the fuel molecule (RH) is attacked by a radical (X•) which removes a hydrogen atom from the fuel molecule creating an alkyl radical (R•). When considering the radical species, hydroxyl radical (OH•) is the main

attacking radical in H-abstraction (R 2) at temperatures below 700 K, because it can form water with the abstracted hydrogen radical in a highly exothermic reaction. It should be noted, that the hydroxyl radical is less selective of the H atom position in H-abstraction, compared to the other radical species. At higher temperatures the hydroperoxyl radical (HO_2•) plays a significant role [53,58,60]. Further reactions of the hydrogen radical formed in H-abstraction have a significant effect on the duration of low temperature combustion: hydrogen radicals may take part in the hydrogen peroxide (H_2O_2) mechanism, which is described briefly in subsection 2.2.4, and lead to the main branching reaction at temperatures 800-1200K producing hydroxyl radicals. In general, easier H-abstraction enhances the ignition quality of a fuel molecule [61].

$$RH + \mathrm{X}\bullet \rightarrow R\bullet + \mathrm{XH} \qquad \text{(R 2)}$$

The rate and location of H-abstraction (R 2) depends significantly on the fuel molecular structure: H-abstraction will occur from the weakest C-H bond of the fuel molecule. In the case of an alkane, the weakest C-H bond is on a tertiary carbon atom (numbered 3 in alkane in Figure 3), the second weakest on a secondary carbon atom (2 in alkane in Figure 3), and the strongest C-H bonds are on a primary carbon atom (1 in alkane in Figure 3) [58]. These differences in the C-H bond strengths were explained by e.g. Kemnitz et al. [62] by the differences in the stability of the resulting fuel radical: branching stabilizes the resulting hydrocarbon radical by allowing greater electron delocalization over the higher number of neighbouring carbon atoms. When considering the carbon chain length of an alkane, it can be concluded that longer carbon chains result in faster ignition because of the higher relative number of secondary carbon atoms in the molecule. There is a diminishing effect on ignition delay of increasing carbon chain length when the carbon chain length becomes large due to the smaller relative changes in the ratio between secondary and primary hydrogen atoms [63]. In the case of alkane branching, the H-abstraction from tertiary carbons atoms is easier than form the corresponding secondary carbon atoms of the straight chain alkanes. However, branching also increases the amount of primary carbon atoms with more difficult H-abstraction compared to the secondary carbons.

This was suggested to contribute to the increase in ignition delays with increased level of branching, which has been observed by several studies, e.g. by Liu et al [64] and Ji et al. [63].

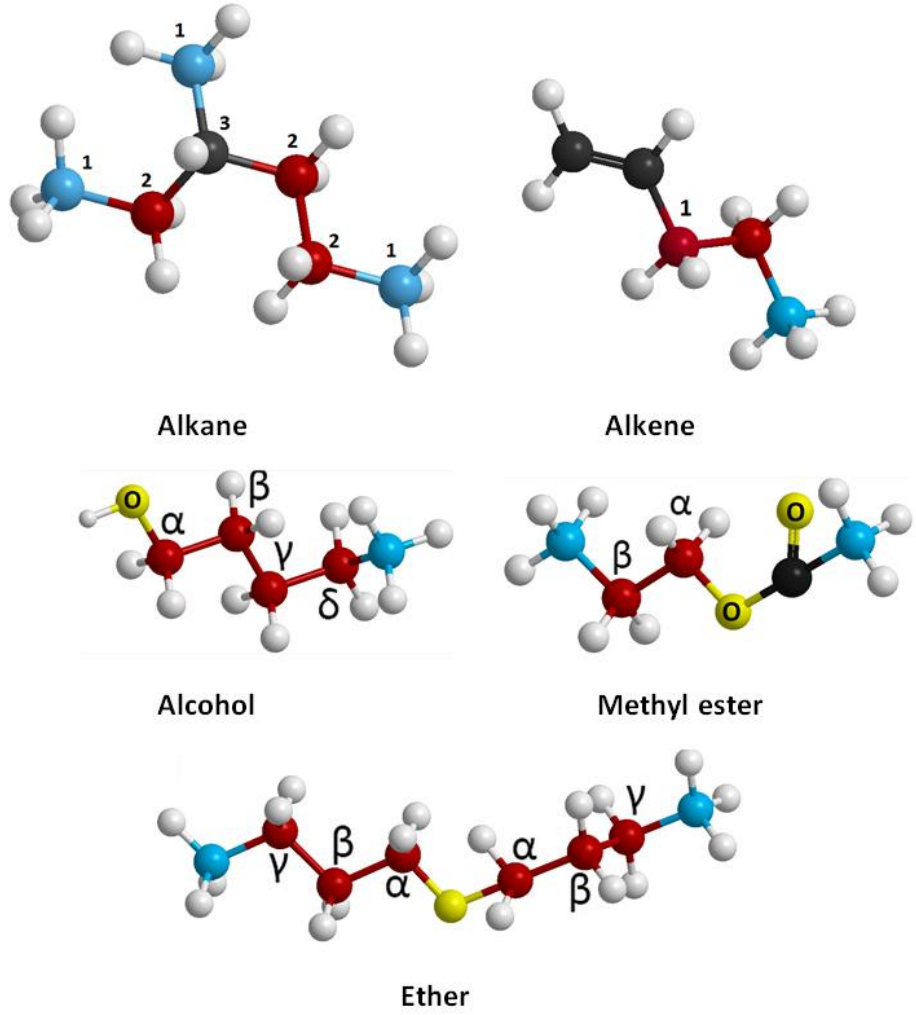

Figure 3. Molecular structures of an alkane, an alkene, an alcohol, a methyl ester and an ether.

The C-H bond strength is affected by the type of bonds between the carbon atoms and is also affected by what other type of atoms (e.g. oxygen atom) are bonded to the carbon atom. Several studies have investigated the effect of unsaturation level on H-abstraction, because both fossil diesel fuel and biodiesel contain molecules with double bonds: e.g. Westbrook et al. [65] has modelled the combustion of biodiesels

and Sun and Law [66] the combustion of butene isomers and Mehl et al. [67] the combustion of n-hexene isomers. They showed that double bonds between carbon atoms make the C-H bonds on the double bonded carbon atoms stronger and C-H bonds on the allylic carbon atoms (1 in alkene in Figure 3) weaker than those on the single bonded carbon atoms. The easy H-abstraction from allylic sites was explained by the resonantly stabilized structure of the resulting allylic radicals. It should be noted, that besides H-abstraction from the double bonded carbon atoms, radical additions of mainly hydroxyl and hydroperoxy radicals to the double bond can also occur, as was shown in a rapid compression machine (RCM) by Minetti et al. [68] and jet-stirred reactor experiments by Battin-Leclerc et al. [69]. However, according to the flow reactor experiments of Prabhu et al. [70] and Mehl et al. [67], hydrogen abstraction is expected to dominate for long chain alkenes.

When considering H-abstraction from oxygenated alternative fuels, several studies have shown that an oxygen atom in the fuel molecular structure affects the bond strengths of the C-H bonds close to it. This has been attributed to the higher electronegativity of the oxygen atom compared to that of carbon and hydrogen atoms. In the case of alcohols, the shock tube and RCM experiments of Heufer et al. [71], shock tube measurements of Black et al. [72], RCM experiments of Weber et al. [73] and several experiments of Sarathy et al. [74] showed that H-abstraction from higher alcohols was easiest from the alpha carbon (alcohol in Figure 3), followed by H-abstractions from gamma, beta, delta etc. carbons and the most difficult from the hydroxyl group. According to Heufer et al.[71], the changes in C-H bond strengths caused by the hydroxyl group in an alcohol are in general significant enough to cause H-abstraction from alpha position of an alcohol to be faster than from the secondary carbon atom of an alkane, H-abstraction from the beta and gamma carbon atoms of an alcohol to be more difficult and slower than from the primary carbon atom of an alkane and H-abstraction from delta position to be of similar difficulty to that for a primary carbon atom of an alkane. Hence, the overall H-abstraction is more difficult from alcohols compared to alkanes.

In the case of carbonyl compounds, the theoretical and kinetic study of Wang et al. [75], a modelling study of Lin et al. [76] and the theoretical study of Osmont et al. [77] concluded that the electronegativity of the carbonyl group weakens the C-H bonds on the alpha carbon (methyl ester in Figure 3), making H-abstraction from this

site faster than the abstraction from corresponding secondary carbon atoms of an alkane. However, the carbonyl group strengthens the C-H bonds on the beta carbon atom (methyl ester in Figure 3), compared to the secondary carbon atom of an alkane. It was suggested that, as was the case with alcohols, the overall H-abstraction from carbonyl compounds is more difficult than from the corresponding alkanes.

Unlike alcohols and carbonyl compounds, ethers have an oxygen atom bonded between two carbon atoms of the carbon chain. The laminar flow reactor study Cai et al. [78], shock wave experiments of Guan et al. [79], and theoretical calculations of both Ogura et al. [80] and Rashidi et al. [81] have shown that the ether linkage makes the H-abstraction from the two alpha carbon atoms easier than H-abstraction from a secondary carbon atom of an alkane (ether in Figure 3). Additionally, the ether linkage makes H-abstraction from the two gamma carbon atoms easier than from the two beta carbon atoms (ether in Figure 3). It was suggested, that the overall H-abstraction is easier from ethers, compared to the corresponding alkanes, unlike from any other oxygenated alternative fuel molecules considered here. Interestingly, Cai et al. [78] concluded, based on experiments with DME and butanol, that alcohols have longer ignition delays than ethers.

The fuel radical remaining after H-abstraction(R 2) generally react with molecular oxygen through either reaction (R 3) or reaction (R 4). The transition between low and intermediate temperature combustion is defined to large extent based on the competition between these two propagating reactions. [58] Reaction (R 3) is favoured at temperatures below 850K according to Faravelli et al.[53] and below 650K according to Griffiths and Barnard [61], whereas at higher temperatures reaction (R 4) becomes more significant. The hydroperoxyl radical formed in (R 4) reacts further in the H_2O_2 mechanism described in subsection 2.2.3, but at low temperatures the activation energy for this reaction is not reached.

$$R\bullet + O_2 \rightarrow RO_2\bullet \quad \text{(R 3)}$$

$$R\bullet + O_2 \rightarrow alkene + HO_2\bullet \quad \text{(R 4)}$$

When considering alkenes, Mehl et al. [67] observed that allylic radicals, which were the preferred product of H-abstraction form alkenes, cannot bond with molecular oxygen to undergo isomerization. Instead, the alkyl peroxy radicals with oxygen in the allylic site decomposes easily back to the reactants. The difficulty of molecular oxygen to bond with an allylic radical is caused by the loss of resonance stability. This reduces the low temperature reactivity of alkenes significantly compared to the corresponding alkanes. In the case of alcohols, oxidation, after H-abstraction has occurred, from the alpha carbon atom does not lead into alcohol radical formation. Instead, oxidation of a primary alcohol via reaction (R 3) has been shown to lead to formation of an aldehyde and a hydroperoxy radical, and oxidation of a secondary alcohol to formation of a ketone and a hydroperoxy radical [58,71].

The alkyl peroxy radical ($RO_2\bullet$) formed in (R 3) undergoes branching through endothermic isomerization reaction (R 5), which leads to multiple branching reactions. Due to the relatively fast formation of the alkyl peroxy radical in reaction (R 3), the isomerization reaction (R 5) typically controls the overall chain branching sequence and hence has a significant effect on the formation rate of the radical pool: greater ability of a fuel molecule to undergo isomerization results in faster formation of radicals and earlier ignition. Isomerization occurs through a transition state ring formation, where rings of five and six carbon atoms are favoured due to their low ring strain energies. Therefore fuel molecules with more than five or six carbon atoms as a straight carbon chain have a better ability to form transition rings, compared to molecules with shorter carbon chains, and therefore have a significantly faster isomerization [58,61]. The greater ability of fuel molecules with long carbon chains to undergo isomerization has also been suggested to cause the greater tendency for these molecules to knock [58].

$$RO_2\bullet \rightarrow QOOH\bullet \qquad \text{(R 5)}$$

According to Mehl et al. [67], alkenes generally have rigid transition state caused by the double bonds, which further increases the ignition delay of alkenes compared to the corresponding alkanes. This reduces the CN of alkenes further, compared to

alkanes, and leads to the longer ignition delays of alkenes in CI engines, as was observed by Puhan et al. [82], Lapuerta et al. [83] and Benjumea [84]. Furthermore, Battin-Leclerc et al. [69] and shock tube experiments of Wang et al. [85] have shown that moving the double bond towards the centre of the molecule decreases the ability of a methyl ester to isomerize further.

In the case of alcohols, Heufer et al. [71] and Sarathy et al. [74] have suggested that alcohols may undergo isomerization in the cases where H-abstraction has not occurred from the alpha carbon atom. In the case of H-abstraction from the alpha carbon atom, the oxidation of an alcohol in reaction (R 3) does not lead to formation of a stable peroxy radical and the main branching reactions of alcohols at low temperatures are H-abstractions. This increases the ignition delay of alcohols compared to that of the corresponding alkanes. Only a few CI engine studies have been conducted on alcohols with longer chains than ethanol. However, butanol [86,87] and pentanol [88,89] addition to diesel has been shown to increase the ignition delay.

When considering carbonyl compounds, the carbonyl group in esters has been suggested by several studies to impose extra strain on the transition rings and thus lower the reaction rate of isomerisation and increase the ignition delay of carbonyl compounds compared to alkanes: this is evidenced by modelling studies of Da Silva et al [90], Lin et al. [76] and Osmont et al. [52], review article of Tran et al. [91] and an engine study with gas chromatography–mass spectrometry (GC-MS) conducted by Zhang et al. [92]. The only engine studies available regarding carbonyl compounds have investigated the combustion of esters. Several studies (e.g. vegetable oil biodiesel studies of Buyukkaya [93], Sahoo et al. [94] and Özener et al. [95], fish oil biodiesel study of Sakthivel [96], animal fat biodiesel study of Awas et al. [97]) have observed biodiesel to have a shorter ignition delay compared to diesel fuel in a CI engine. The shorter ignition delay of biodiesel compared to diesel fuel has been attributed to a chemical breakdown of the biodiesel FAMEs during injection, in which low-molecular weight gases combusting early would be formed. This shorter ignition delay of biodiesel compared to diesel fuel is contradictory with the ignition hindering effects of both the ester group and the higher level of unsaturation described in this subsection, if diesel is considered to consist mainly of aliphatic alkanes. Hence it is suggested that the long carbon chains of biodiesel

FAMEs is the reason for their faster ignition compared to the diesel fuel, because although the carbon chain lengths of diesel fuel molecules are similar to those of biodiesel molecules, diesel fuel contains higher proportions of cyclic structures and aromatics, which have ignition hindering qualities.

On the contrary to carbonyl compounds, Cai et al. [78], Ogura et al. [80] and Guan et al. [79] state that isomerization of ethers can occur in the same way as isomerization of alkanes, because hydrogen may undergo migration across the central oxygen atom of an ether group. Additionally, the peroxide decomposition of ethers has in general a lower energy barrier for ethers during isomerization, compared to alkanes. The ability of ethers to isomerize, together with faster H-abstraction compared to alkanes, is assumed to result in the faster ignition of ethers. Several experimental studies have shown that DME addition to diesels fuel reduces CI engine ignition delay, as summarized in a review article of Park and Lee [98]. Imtenan et al. [99]. Sivalakshmi and Balusamy [100] concluded that adding DEE to biodiesel reduces the ignition delay. Similar observation was made in the case of diesel fuel blends by Paul et al. [101] and in the case of a biodiesel-diesel mixture by Qi et al. [102]. However, studies of longer chain ethers are scarce. However, when considering the branched ethers, Kajitani et al. [103] concluded that adding MTBE to diesel increases the ignition delay and de Menezes et al. [48] has shown that ETBE addition to diesel reduces the cetane number in engine tests.

2.3.3 High temperature kinetics

Chemical kinetics of combustion at high temperatures of 1000-3000K is complicated due to the instability of fuel radicals under such conditions and the large variety of different intermediate species resulting from thermal decomposition. Thermal decomposition of the fuel molecule, presented in reaction (R 6), starts to compete with initiation reactions of the low temperature combustion when the combustion chamber temperature reaches 850K and becomes the dominating initiation reaction at temperatures above 850K. In alkane decomposition a C-C bond (bond energy 348 kJ/mol) is broken because of its lower average bond energy compared to that of a C-H bond (bond energy 413 kJ/mol). Nonetheless, initiation reactions where C-H bonds are broken may also occur for alkanes at high temperatures. Additionally, the

initiation reaction shown in Figure 2, a reaction between the fuel molecule and molecular oxygen, forms a small fraction of the radicals at high temperatures [58,59].

$$R \rightarrow R' + R'' \qquad \text{(R 6)}$$

The thermal decomposition of an alkene is initially faster than that of a corresponding alkane due to the cleavage of the allylic C-C bond: cleavage of the allylic C-C bond is energetically favoured to that of the corresponding C-C bond of an alkane because of the formation of resonantly stabilized radicals [61,67,104]. Thermal decomposition of an alcohol, on the other hand, can occur through either the removal of a hydroxyl group (C-O bond bond energy 358 kJ/mol) or breakage of a C-C bond (C-C bond energy 348 kJ/mol) of the alkyl chain. [58] Glassman and Yetter [58] and Kuo [105] state that in the initiation reaction of methanol combustion the hydroxyl group is displaced, but as the chain length of an alcohol increases the initial thermal decomposition of the C-C bonds becomes more prevalent. Heufer et al.[71] and Black et al. [72] showed that compared to alkanes hydroxyl group weakens the C-C bonds between the alpha and beta carbons, and therefore this is the first C-C bond to be broken during thermal decomposition of an alcohol. In the case of carbonyl compounds, Osmont et al. [77] and Ali and Violi [106] concluded, based on theoretical calculations of ester combustion, that the C-C bond between alpha and beta carbon atoms of the long carbon chain of methyl esters was the first to be broken in thermal decomposition of the molecule. When considering ethers, Guan et al. [79] observed that during thermal decomposition of an ether the first C-C bond to break is the alpha and beta carbon atoms, followed by the bond between beta and gamma carbon atoms, and lastly breaks the bond between gamma and delta carbon atoms.

Alkyl radicals ($R\bullet$) formed in the high temperature radical attack (R 2), decay further into alkenes and smaller species, such as aldehydes and ketones, according to the reaction (R 7). Reaction (R 7) follows the β-scission rule, which states that the bond to be broken is one position away from the radical site. According to Glassman and Yetter [58], it can be concluded that all aliphatic fuel molecules oxidize primarily to ethylene or propene. These small alkenes react further through the reaction sequence of methane and ethane combustion, eventually producing carbon monoxide, part of which is oxidized further to CO_2 as part of complete combustion.

$$R \bullet\rightarrow\ alkene + R' \qquad \text{(R 7)}$$

2.3.4 H2O2 mechanism

When discussing chemical kinetics of combustion, it is important to include the hydrogen peroxide (H_2O_2) mechanism, because it defines the ignition timing to large extent. At low temperatures and high pressures the reaction between hydrogen radicals and molecular oxygen generally leads towards formation hydroperoxyl radicals, as shown in reaction (R 8). When the in-cylinder temperature increases, this reaction will increasingly start to produce oxygen and hydroxyl radicals in reaction (R 9) and at temperatures of about 1000K this reaction route becomes dominant. At temperatures 800-1200 K, hydroperoxyl radicals react with each other in reaction (R 10) to form molecular oxygen and a hydrogen peroxide. The hydrogen peroxide then decomposes through reaction (R 11) into two hydroxyl radicals [53,58,107]. The hydroxyl radicals produced are the most reactive radicals at temperatures below 700K and therefore the decomposition reaction of hydrogen peroxide is the main branching reaction at temperatures 800-1200 K: reaction (R 11) generally enhances the radical build up to such a degree that ignition occurs at about 900-1100K. Therefore, ignition timing can be roughly determined by the decrease of hydrogen peroxide concentration in the reaction mixture [53,107].

$$\mathrm{H} \bullet + \mathrm{O_2} \rightarrow \mathrm{HO_2} \bullet + M \qquad \text{(R 8)}$$

$$\mathrm{H} \bullet + \mathrm{O_2} + \mathrm{M} \rightarrow \mathrm{O} \bullet + \mathrm{OH} \bullet \qquad \text{(R 9)}$$

$$\mathrm{HO_2} \bullet + \mathrm{HO_2} \bullet \rightarrow \mathrm{H_2O_2} + O_2 \qquad \text{(R 10)}$$

$$\mathrm{H_2O_2} + M \rightarrow OH \bullet + OH \bullet + M \qquad \text{(R 11)}$$

$$H \bullet + O_2 \rightarrow O \bullet + OH \bullet \qquad \text{(R 12)}$$

The concentration of fuel molecules available in the reaction mixture affects the rate of the H_2O_2-mechanism, and thus the ignition timing and the overall rate of combustion. At low temperatures, fuel addition (i.e. increase in fuel concentration) increases the overall rate of combustion reactions: at low temperatures reaction (R 8) is dominant over reaction (R 9) and a fuel molecule may react with the hydroperoxy

radical produced in reaction (R 8), producing hydrogen peroxide, which results in chain branching reactions through (R 11). At high temperatures, however, fuel molecules compete with the reaction (R 9) for the hydrogen radicals and because the rate of several reactions between fuel molecules and hydrogen radicals is faster than that of the reaction (R 9) an increase in fuel concentration can reduce the rate of combustion [58,59].

It should be noted, that because of the high significance of the H_2O_2-mechanism on ignition, ignition delay can be shortened by adding a peroxide-based additive to the reaction mixture, as was shown by Nandi et al. [108]. Furthermore, hydrogen and/or oxygen addition at high temperatures can enhance the formation of radicals and thus decrease the ignition delay and accelerate the overall rate of combustion. This was supported by the results of Mardani and Tabejamaat [109] and Wang et al. [110], who observed that hydrogen addition to a jet-in-hot-co-flow burner to resulted in both increased flow temperature and increased flame entrainment, which increased the chemical reaction rate. Furthermore, Christodoulou and Megaritis [111], Bose and Maji [112] and Antunes et al. [113] have observed an increase in break thermal efficiency of a CI engine with hydrogen addition.

2.4 Effect of physical fuel properties on diesel engine combustion

In the previous section, the rate of combustion of a homogenous fuel-air mixture was stated to be determined by the chemical kinetics of combustion. However, when homogenous charge combustion is not applied, the fuel-air mixture is rarely homogenous during combustion in a diesel engine. Under non-homogenous air-fuel conditions the rate of combustion is controlled by both the chemical kinetics of combustion and the rate of fuel-air mixing, because the rate of fuel-air mixing determines the availability of oxygen for the combustion reactions. The mixing rate of fuel and air is, in turn, mainly controlled by the physical fuel properties through the four main physical stages of the combustion process: atomization, spray formation, spray vaporization, and vapour-air mixing. The rate of these four stages affect the resulting local air-fuel concentration within the combustion chamber and

therefore the combustion rate, local temperature and the local formation of pollutant species. The following section will review the effect of physical fuel properties on each of the above four main physical stages of the combustion process. The three main fuel physical properties of fuel discussed in this section are density, viscosity and surface tension. Examples of experimental studies conducted on the physical combustion processes of alternative fuels are mentioned, where available.

2.4.1 Atomization

Liquid fuels are atomized prior to combustion in order to enhance the fuel-air mixing by increasing the total fuel surface area, and thereby its vaporisation rate. During injection, the liquid fuel passes through an injector nozzle which atomizes the fuel by converting the bulk of liquid into smaller droplets that from a spray within the combustion chamber. The effectiveness of atomization depends mainly on the injector nozzle geometry and the injection velocity. Higher injection velocity enhances atomization by dispersing the fuel into finer droplets with smaller Sauter mean diameter (SMD). The air density in the combustion chamber also affects the fuel jet disintegration process, with higher air density resulting in smaller SMD of the fuel droplets [114].

When considering the effects of physical fuel properties on atomization, fuel atomization can be seen as the breakup of the fuel jet, due to the turbulent conditions within the combustion chamber, against the stabilizing influences of fuel surface tension and fuel viscosity: increasing fuel surface tension leads to poorer atomization by opposing the droplet formation from the liquid jet; and increasing fuel viscosity leads to poorer atomization by decreasing fuel velocity for a given injection pressure, as well as by supressing the instabilities required for the fuel jet to break up and disperse [7]. Additionally, increasing fuel viscosity affects the dynamic operation of an injector by making the needle lift slower. Therefore high injection pressures are required for fuels with high viscosity in order to keep the injected amount of fuel constant over a given injection period [13]. An increase fuel density also leads to a decrease in fuel velocity, and hence to poorer atomization. When short injection durations and low injection pressures are applied the effect on atomization of fuel viscosity is greater than the effect of fuel density, whereas with longer injection

durations and higher injection pressures the effect of fuel density becomes more significant [115]. For example, Dernotte et al. [116] observed that with injection pressures of 550 bar or higher, fuel density remained the only fuel property driving the injection mass flow rate.

In the case of alternative fuels, several studies [117–125] have shown that biodiesels have poorer atomization compared to diesel fuels due to the higher surface tension, viscosity and density of biodiesels. For example, Galle et al. [126] concluded, based on optical CI engine studies, that rapeseed oil, palm oil and animal fat had poorer atomization compared to rapeseed methyl ester, which in turn had slightly poorer atomization compared to fossil diesel fuel. On the other hand, Ejim et al. [13] observed in injector experiments that B100 biodiesels of palm oil, soybean oil, cotton seed, peanut and canola had similar SMD compared to that of fossil diesel fuel: B100 coconut biodiesel had a slightly lower SMD compared to diesel fuel and B100 rapeseed biodiesel slightly higher. Ejim et al. [13] concluded that the higher viscosity of biodiesel compared to fossil diesel fuel contributed to about 90% change in SMD, whereas the higher density of biodiesel caused only about 2% change. When considering alcohols, Park et al. [127] concluded based on both injector and CI engine tests, that bio-ethanol has smaller SMD compared to diesel fuel due to the lower kinematic viscosity and lower surface tension of ethanol. Additionally, Park et al. [128] observed in an earlier injection study that 20% ethanol addition to biodiesel decreased SMD due to the lower viscosity of ethanol compared to that of biodiesel. In the case of ethers, Suh et al.[129] observed in diesel engine experiments that DME atomized better (smaller SMD) compared to diesel fuel because of the lower viscosity, surface tension and density of DME. Additionally, Kim et al. [130] observed in injector experiments that SMD of isobutene was decreased with DME addition. Similarly, Guan et al. [131] showed in a constant volume chamber, that blending di-n-butyl ether into biodiesel decreased the SMD and attributed this decrease to the lower values of both viscosity and surface tension of the ether.

2.4.2 Spray formation

Besides atomization, the process of forming a spray also distributes fuel through the combustion chamber for efficient utilization of the trapped air. The main

characteristics of the cone shaped spray produced by the spray holes of a diesel injector are spray cone angle and spray tip penetration, as shown in Figure 4. Wide spray cone angle and long spray tip penetration are desirable because they lead to larger spray volumes, more efficient air entrainment into the fuel spray, enhanced fuel air mixing and, thereby, lower local equivalence ratio. Larger spray volumes are also associated with enhanced atomization of the spray: SMD becomes smaller with both axial and radial distance from the injector nozzle due to enhanced vaporization and secondary droplet break up caused by aerodynamic interaction between the fast moving droplet and surrounding high density air [132]. Although a larger spray angle and larger spray penetration are both desirable, in practise they have an inverse relationship. Additionally, it has been observed that spray tip over-penetration may lower the air-fuel mixing rate due to impingement of the liquid fuel on cool combustion chamber surfaces [1].

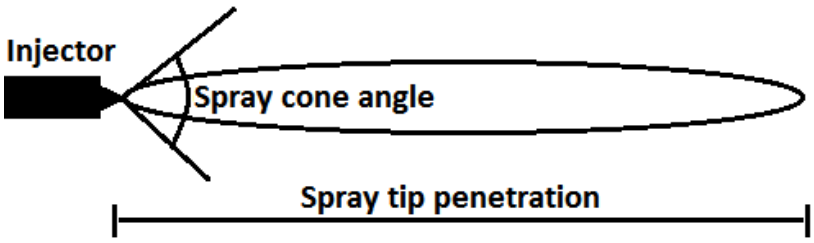

Figure 4. Spray characteristics: spray cone angle and spray penetration

Higher injection pressure results in longer spay trip penetration, as well as improved dispersion and smaller SMD. However, too high injection pressures may cause the spray to become too finely atomized and thus to have insufficient momentum to penetrate far from the injector nozzle. Increasing the in-cylinder air density is likely to shorten the spray tip penetration further, but it also widens the spray cone angle. [114] When considering the physical fuel properties, a combination of high fuel density, high fuel viscosity and high fuel surface tension tends to result in large droplets with high momentum, which leads to longer the spray tip penetration and narrower spray cone angle, resulting in a smaller spray volume and thus decreasing the mixing rate of air and fuel. The consequence of this is higher fuel local

concentration and poorer combustion efficiency, with greater amount of some pollutants generated (e.g. soot and unburned hydrocarbons) [1,114].

Studies investigating the spray characteristics of alternative fuels have mainly focused on biodiesel sprays. No [121] concluded in a review article that, compared to fossil diesel fuels, both neat vegetable oils and biodiesels have smaller spray cone angles and the longer spray tip penetration due to their higher viscosity, surface tension and density. Smaller spray cone angle and longer spray tip penetration in general result in smaller spray area and smaller spray volume for biodiesels compared to diesel fuels [133]. The smaller spray volume of biodiesels compared to diesel fuels has been observed for example by Lahane and Subramaniana [122] for karanja methyl ester; by Mohan et al. [123] for biodiesel derived from waste cooking oil; by Gao et al. [119] for jatropha, palm oil and used fried oil; and by Balaji et al. [120] for methyl oleate, methyl stearate and methyl linoleate. It should also be noted that due to the long spray tip penetration of methyl esters, Mancaruso et al. [134] observed flame impingement with B100 rapeseed methyl esters and B100 soy methyl esters in an optical CI engine. In the case of alcohols, Park et al. [127] showed that bioethanol maintained similar spray penetration length as diesel fuel but had a wider spray cone angle, and thus larger spray volume, due to the smaller SMD of ethanol. When considering ethers, Suh et al.[129] and Wu et al. [135] showed DME to have shorter spray tip penetration and wider spray cone angle than fossil diesel fuel at high temperatures due to the better atomization of DME. Kim et al. [130] observed that DME had wider spray cone angle and similar spray tip penetration compared to DME-isobutene blends. Compared to biodiesel, however, DME has been shown by Bang and Lee [136] to have a smaller spray cone angle together with shorter spray tip penetration. Lastly, Guan et al. [131] observed that blending di-n-butyl ether into biodiesel decreased the spray tip penetration and increased both the spray cone angle and the spray area due to decreased fuel droplet size.

2.4.3 Spray vaporization

During and after spray penetration, the in-cylinder conditions cause fuel spray to vaporize, allowing the fuel vapour to mix with air. Therefore, faster vaporization rate in general leads to faster mixing rate of fuel and air and hence to shorter ignition

delay times. In a diesel engine, combustion occurs both in a locally near-homogenous air-fuel vapour mixture and around individual droplets. Spray vaporization behaviour is often considered to be taking place mostly around individual droplets and is therefore taken as the sum of the vaporization behaviour of individual droplets. After a droplet has formed through atomization, heat transfer causes the droplet first to undergo liquid expansion and then to heat up to its local equilibrium temperature, i.e. saturation temperature corresponding to the in-cylinder pressure. The heating phase accounts for approximately 90% of the droplet lifetime. Once the droplet liquid saturation temperature is reached, all further heat transferred to the droplet goes towards the vaporization enthalpy of the liquid fuel [137]. The fuel vapour, leaving the droplet at the liquid fuel saturation temperature, reaches the cylinder gaseous ambient temperature relatively quickly. Many investigations have observed that the droplet surface area, represented by the droplet diameter squared, decreases linearly with time according to d^2-law during the entire droplet evaporation process. The d^2-law is presented in equation

(E 1), where d is droplet diameter at time t, d_o is the original droplet diameter and k is a vaporization rate constant [138]. The d^2-law, also called Quasi-Steady Model, is a theorethical model developed based on the pioneering experimental works of Godsave [139] and Spalding [140] in 1950s and is still currently applied to model droplet evaporation, as was shown by Law [138] in 1980s and more recently e.g. by Hsia et al. [141] and Sagna and Almeida [137], although the model relies on several simplifying assumptions.

$$d^2 = d_o^2 - kt \qquad \text{(E 1)}$$

Modelling results, e.g. by Sazhin et al. [142], suggest that high fuel surface tension slows the rate of spray vaporization by hindering the evaporation from the droplet surface, especially at its initial heating stage. However, as Faeth [143] states in his review article in the 1970s , it is generally accepted that this effect of surface tension is not significant in diesel engine combustion conditions. The main factors affecting the rate of spray vaporization are droplet size, vapour thermal conductivity, liquid droplet heat capacity, droplet enthalpy of vaporization, droplet boiling point at in-

cylinder conditions, in-cylinder temperature, in-cylinder pressure and the fuel vapour concentration in the air surrounding the droplet. Decreasing droplet size by enhancing atomization leads to faster overall spray vaporization, because smaller droplet volumes reach the saturation temperature faster than larger droplets and increasing the number of droplets increases the vaporization surface area [144]. High thermal diffusivity from the air to the droplet, and hence high vapour thermal conductivity, low liquid droplet heat capacity, low droplet enthalpy of vaporization and low droplet boiling point, all intensify the droplet heating and the spray vaporization [1,145]. Lower in-cylinder pressures and higher in-cylinder temperatures lead to faster spray vaporization: higher in-cylinder temperatures increase the temperature gradient inside a droplet, which leads to a substantial increase of the droplet surface temperature and thus decrease in droplet surface tension, resulting in a faster break-up of droplets and hence in faster spray vaporization [105,144]. When considering the fuel vapour concentration in the air surrounding the droplet, low fuel vapour concentration causes a large concentration gradient between the droplet surface and its surroundings, which enhances the spray vaporization [146]. For a given droplet, this concentration depends on the initial droplet spacing, which is mainly affected by the overall spray geometry and vapour-air mixing efficiency: larger overall spray area and efficient vapour-air mixing enhance the rate of spray vaporization. It should be noted, that the effect of the droplet spacing on spray vaporization is more significant when droplets are closer to each other, due to inter-droplet interactions [147,148].

When considering alternative fuels, biodiesels generally vaporizes slower than diesel fuels due to poorer atomization and smaller spray volumes of biodiesels, as was concluded e.g. in a review article by Xue [149]. Additionally, e.g. Daho et al. [150] observed that domestic fuel oil vaporizes faster than pure vegetable oils of cotton seed, jatropha and rapeseed under the temperature range of 578K – 917K. In addition to the experimental work, several mathematical models have been developed to predict the biodiesel fuel droplet heating and evaporation, e.g. by Qubeissi et al. [151] and by Sazhin et al. [152]. Birouk and Toth [153] concluded based on experiments in a pressure vessel that soybean biodiesel droplets follow the d^2 law in **a** turbulent environment. In the case of alcohols, Park et al. [127] observed that ethanol droplets evaporated faster than diesel fuel droplets due to the better atomization and larger

spray volume of ethanol and the lower boiling point of ethanol. When considering ethers, Suh et al.[129] observed that DME evaporates more rapidly than diesel fuel because of both the smaller SMD and the lower boiling point of DME, despite its shorter spray tip penetartion. Park et al. [154] explined the fast evaporation of DME by the flash boiling effect.

2.4.4 Vapour-air mixing

Once the fuel has vaporized, the fuel vapour mixes with air in an engine combustion chamber through turbulent mixing and molecular diffusion. Efficient mixing increases the rate of combustion by allowing maximum air utilization for combustion reactions, as was recently shown in CI engine experiments of Han et al. [155]. Additionally, mixing enhances the rate of combustion further by supplying the droplet with heat energy from the surrounding gases for vaporization**,** by removing the already vaporized fuel from the droplet surface to allow further vaporization, and by transporting rapidly the products of combustion away from the droplet [61]. When fuel is available in the form of a non-premixed spray, at high temperatures, the rate of chemical combustion reactions is faster than the rate of fuel-air mixing and therefore mixing is considered as the rate controlling step of the overall combustion process, as was stated in a combustion review article by Gao and Chow [156] and in a modelling study of Arregle et al. [157].

Turbulent entrainment, also called turbulent convection, is caused by the turbulent conditions of CI combustion and aided by the piston movement, the bulk air flow and the turbulence in the air flow. Turbulent entrainment is generally much more rapid and relevant to the overall rate of combustion than molecular diffusion [105]. Therefore, the rate of mixing is determined by the bulk air flow rate and the level of turbulence, as well as by the quality of atomization, spray volume and the rate of fuel vaporization. Hence, some alternative fuels result in poorer mixing compared to diesel fuel, as was for example observed in the case of RME biodiesel by Yamane et al. [158]. It should be noted, that the influence of turbulence on vapour-air mixing decreases with decreasing droplet diameter, as shown by droplet vaporization experiments of Gökalp et al. [159]. Additionally, Birouk and Fabbro [160] showed experimentally that turbulence increases droplet vaporization more effectively under

elevated ambient pressures and higher turbulence intensities. However, the effect of turbulence on mixing in the presence of evaporating droplets is not yet fully understood. Status on the research on droplet evaporation in turbulent flows in 2006 was presented in a review article by Birouk and Gökalp [161].

Molecular diffusion is the thermal motion of molecules from higher concentration to lower concentration, which causes gradual mixing of fuel and air. The rate of vapour transport by molecular diffusion is mainly determined by the in-cylinder temperature and the size and spacing of fuel molecules. Higher in-cylinder temperatures and smaller fuel molecules with smaller spacing enhance the rate of molecular diffusion. [162,163] Molecular diffusion is usually too slow to have a substantial influence the bulk air/vapour mixing, but it is important locally. According to a modelling study of Kemenov and Pope [164], the degree of molecular diffusion is comparable or exceeds the significance of turbulent entrainment in the case of a spray. However, the relative importance of turbulence grows when moving downstream of the fuel nozzle, along the spray core, or away from the spray centre line, as well as with increasing in-cylinder temperature. This modelling result was supported by the numerical study of Mardani et al. [165], which demonstrated that molecular diffusion has a higher influence on the combustion in the region near the nozzle than turbulent entrainment. Additionally, Kelly-Zion et al. [166] observed from evaporation experiments that molecular diffusion contributes to the vapour transport even for conditions where a strong turbulent convective flow is apparent. They explained this by hypothesizing a diffusive sub-layer where diffusion is dominant over turbulent convection. Molecular diffusion modelling in the complex environment of diesel engine combustion is still a major challenge, with several different diffusion rate coefficients being proposed to describe different situations [162,167].

2.5 Engine thermal efficiency

Engine thermal efficiency is dependent on the combustion phasing relative to the position of the piston and the profile of the heat release rate. The heat release rate profile of an engine is dependent on the engine design, engine operating conditions, and fuel properties. In theory, high thermal efficiency would be achieved with an Otto-like engine cycle, where all of the injected fuel would combust very rapidly in

the premixed combustion phase at the top dead centre (TDC). This is not, however, possible in practical applications due to significant time required for the physical and chemical processes associated with diesel combustion. A typical CI engine heat release rate diagram is presented in Figure 5. In order to develop alternative fuels with high engine thermal efficiency, it is important to understand the factors affecting engine thermal efficiency. In this section, the engine thermal efficiency is first defined, followed by a brief review of the effect of fuel properties on engine thermal efficiency. Lastly, the engine efficiency of alternative fuels is discussed.

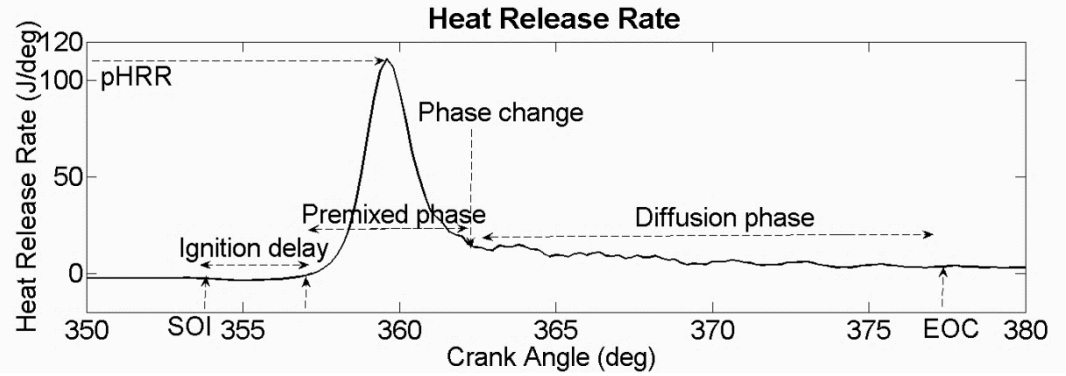

Figure 5. Typical CI engine heat release rate diagram (where SOI indicates start of combustion, EOC end of combustion and pHRR peak heat release rate)

2.5.1 Definition of engine thermal efficiency

Engine thermal efficiency is a dimensionless performance measure defined as the ratio between the work output of an engine and the chemical energy supplied to the engine from the fuel. There are two often quoted versions of thermal engine efficiency: indicated thermal efficiency (ITE) and brake thermal efficiency (BTE). ITE defines the power output of an engine as the gas work done on the pistons, whereas BTE considers the power output of an engine to be the power developed at the engine output shaft and absorbed by a brake dynamometer. ITE is higher than BTE and the difference between the two is accounted for by friction losses between surfaces with reaction movement (piston, bearings) and (if included) auxiliary driven subsystems such as fuel and water pumps [1] .

ITE is calculated as a ratio of the power output of an engine (W_C) to the chemical energy supplied in the fuel during one engine cycle, as shown in equation

(E 2). In the equation

(E 2) η_F is the ITE, W_C is power output per engine cycle, m_F is mass of fuel injected per engine cycle and Q_{HV} is the heating value of the fuel. The power output can be either the indicated power, corresponding to the indicated thermal efficiency, or the break power output corresponding to the break thermal efficiency. In this thesis the power output is from here onwards considered as indicated power and engine efficiency as indicated engine efficiency [1].

$$\eta_F = \frac{W_C}{m_F Q_{HV}} \quad \text{(E 2)}$$

The characteristics of the heat release rate profile, an example of which was shown in Figure 5, affecting engine efficiency are the amount of energy released at TDC and the overall combustion duration. If most of the fuel energy is released close to TDC, for example through near-premixed combustion, then the exposed combustion chamber surface, from which energy can be lost to the walls, is minimized; on the other hand, the combustion temperature is higher which tends to encourage a greater rate of energy transfer to the exposed surfaces of the combustion chamber. Therefore, in terms of energy loss through heat transfer, there is no great advantage if most of the fuel energy is released close to TDC. In terms of conversion energy released into work, if most of the fuel energy is released close to TDC, the pressure will be higher, as the cylinder volume would be small; however, the higher pressure cannot be utilized effectively until some expansion has taken place, and therefore the turning momentum generated by the gas force on the piston would be small. Consider now the case when energy is released slowly during the expansion stoke, for example by means of mostly diffusion controlled combustion. The energy loss to the combustion surface through heat transfer can be expected to be greater due to the lower cylinder gas temperature (lowered by the increasing cylinder gas volume). The lower expected gas pressure will act over a greater movement length, enabling the lower pressure to develop a significant turning moment. However, the later energy release can also

result in greater energy loss, reject from the energy cylinder when the engine exhaust gas valves open [1,168]. Experimental efficiency optimization in internal combustion engines often demonstrates that a significant amount of premixed combustion early during the combustion stroke results in the highest indicated thermal efficiency. It is therefore useful to consider how different fuels can contribute towards a heat release rate profile in which a substantial amount of energy is released rapidly during the early premixed stage of combustion.

2.5.2 Effect of fuel molecular structure on engine thermal efficiency

Fuel molecular structure affects engine thermal efficiency through the shape of the heat release rate. When considering the amount of energy released at TDC, the most relevant properties of the heat release rate are the ignition delay and the overall combustion duration. Ignition delay plays a significant role in controlling the proportion of the rapid premixed fuel combustion and it also has an effect on the combustion timing relative to piston motion: the premixed phase increases with longer ignition delays due to the higher quantity of fuel mass injected prior to ignition and the greater amount of time available for fuel vaporization and fuel-air mixing. Larger premixed phases, and hence longer ignition delays, tend to result in more of the fuel burning rapidly. The degree to which chemical and physical fuel properties affect, separately, the ignition delay is not as yet well understood, especially with alternative fuels. Nevertheless, several studies [1,7,105,162,169,170] have suggested that ignition delay is mainly controlled by the chemical kinetics of combustion, while the physical processes of combustion are of secondary importance in determining the ignition delay. The effect of fuel molecular structure on the chemical kinetics of combustion was discussed above in the section 2.2, where several alternative fuel molecules were suggested to have longer ignition delays, compared to the corresponding alkanes.

The overall combustion duration includes both the premixed phase and the diffusion phase (also called the mixing-controlled phase). In general, longer overall combustion duration leads to a smaller portion of the fuel to be burned rapidly over a short period of time, and therefore reduces the engine thermal efficiency. After the premixed air-fuel fraction has been consumed rapidly, the radical chain reactions are

relatively fast due to the high pressure and high temperature reached during the premixed combustion phase. Therefore, once premixed combustion has been completed, during the diffusion controlled combustion, the chemical reaction rates are usually considered to be faster than the physical processes that form the ignitable fuel-air mixture by turbulent convection and molecular diffusion in the rich combustion zone. [105] Several studies, such as a spray study by Sornek et al. [171], a modelling study by Allegré et al.[157] and a review article on combustion modelling by Gao and Chow [156], have concluded that the mixing rate of air and fuel is the rate controlling step of the duration of diffusion controlled combustion phase. The effect of molecular structure on the air-fuel mixing was described above in section 2.3, where alternative fuels such as biodiesel were described to have slower mixing rates compared to fossil diesel fuel.

It should be noted that the combustion conditions affect the physical fuel properties and that hence the changes in the heat release rate profile have to all be considered together. For example, although a short overall combustion duration is desirable to reach high engine efficiency, an overall rise in the combustion duration may in practice be inevitable, for example with an increase in engine load (increase in indicated mean effective pressure (IMEP)), although an increase in IMEP results in a reduction in ITE [1,172,173]. This was observed e.g. in an experimental study by Kasiraman et al. [173], who reported an increase in the BTE with increasing combustion duration for both fossil diesel fuel and cashew nut shell oil.

When considering the effects of fuel molecular structure on engine efficiency, it should also be noted that the heat released from a given amount of fuel depends on the heating value of the fuel. Heating value (Q_{HV}) is a fuel specific quantity, which denotes the magnitude of the heat of a combustion reaction at a standard temperature and at either constant pressure or at constant volume for a complete combustion of a unit mass of fuel [1]. Higher heating values are desirable, because they facilitate higher peak heat release rates during combustion and thus enhance engine thermal efficiency. Heating value of a fuel depends on the fuel molecular structure: it has been shown by several modelling studies [174–177] that a higher number of carbon atoms in fuel increases the heating value while, in general, a higher number of oxygen molecules in fuel decreases it. For example, Sadrameli et al. [178] observed in bomb calorimeter studies a positive linear correlation between the heating value and the

molecular weight of fatty acids. Additionally, Tompkins et al. observed that B100 palm oil biodiesel and fossil diesel fuel had similar combustion durations under low load conditions, whereas under high load conditions biodiesel had shorter combustion duration. They suggested that the lower ratio of specific heats in the case of biodiesel, compared to fossil diesel fuel, counteracts the benefit of shorter combustion when considering ITE. It is interesting to note in passing that heating value correlates with some of the physical properties of fuel, for example the heating value has a negative correlation with fuel density and a strong positive correlation with fuel viscosity [178–180].

2.5.3 Engine efficiency of several alternative fuels

Most biofuels have lower heating values than fossil fuels (due to their higher oxygen content), which prolongs the overall combustion duration and tends to reduce the ITE. The degree to which the oxygen content of fuel affects ITE is not yet fully understood due to the complex nature of engine combustion. For example, Nabi [181] concluded, based on a theoretical investigation of several different kinds of biofuels, that the ITE remained almost unchanged with oxygen content below 30 wt-%, despite the changes in heating value. Above 30 wt-% of oxygen content the ITE of biofuels was observed to decrease slightly with increasing oxygen content.

When considering biodiesels, Arab et al. [182] and Ashraful et al. [23] concluded in their review articles that adding low percentage of biodiesel into fossil diesel fuel can reduce the fuel consumption and result in higher brake power due to more complete combustion. The percentage at which a biodiesel/diesel blend reaches the maximum engine efficiency depends on the engine and the operating conditions. For example, CI engine experiments of Labeckas and Slavinskas [183] showed an upper limit in the biodiesel/diesel blend ratio of 10 wt-% of RME/diesel, after which ITE starts to decline rapidly. This corresponds to about 1.45 wt-% of oxygen in the fuel. The decline in ITE above this level of oxygen content was attributed partly to the poorer volatility of RME compared to fossil diesel fuel. Agarwal et al. [184] stated that the highest ITE for blends of diesel fuel and linseed oil methyl ester in a CI engine was achieved with 20 wt-% of linseed methyl ester, which improved the ITE by 2.5 percentage points compared to diesel fuel. The initial increase in ITE with linseed oil

methyl ester addition was partly attributed to improved self-lubricity of the fuel, which e.g. reduced the fuel pump power required. Vallinayagam [185] reported a BTE increase of 10 and 5 percentage points when comparing B100 pine oil to fossil diesel fuel under both low and high load conditions in a diesel engine, respectively, and attributed these increases in engine efficiency to better atomization with pine oil. Agrawal et al. [125] observed that addition of Karanja biodiesel up to 10 v-% to diesel increased BTE of a single cylinder research engine. Chauhan et al. [186] reported a reduction in BTE of a CI engine with addition of 5-100% jatropha oil, with 5% jatropha oil addition having the highest efficiency compared to the other blends. Can [187] concluded that 5% and 10% additions of waste cooking oil to diesel reduced the BTE up to 2.8% in a diesel engine. Sakthivel et al. [96] reported that BTE decreased with adding fish oil biodiesel to diesel in 20-100% blends and explained this decrease in BTE by the decreasing ignition delays of the fuel blends with increasing proportion of fish oil.

In the case of alcohols, a few studies have observed an increase in ITE with alcohol addition to diesel fuel despite the lower heating values of alcohols compared to diesel fuel. Balamurugan et al. [188] showed 1.6%, 7.6%, 9.0% and 10.5% increase in BTE for the addition of 4% n-propanol, 8% n-propanol, 4% n-butanol and 8% n-butanol in fossil diesel fuel, respectively, with butanol having a more significant effect on the BTE. The higher BTEs of the alcohol-diesel blends, compared to diesel fuel BTE, were attributed to larger premixed phases caused by better spray characteristics and longer ignition delays of alcohol-diesel blends. Zhang et al. [189] observed a slight, under 1%, increase in ITE with 20 v-% and 40 v-% butanol addition to diesel in a diesel engine with EGR. Sahin et al. [190] showed that 2 v-% butanol addition to diesel fuel increased the engine efficiency level of a turbocharged diesel engine by 2.16, 2.12 and 2.36% for selected loads at 2000, 3000 and 4000 rpms, respectively, whereas 4 v-% butanol addition had no significant effect on the efficiency compared to the 2 v-% addition, and 6 v-% addition tended to decrease the engine efficiency slightly. Zheng et al. [191] observed that adding 20 or 40 v-% isobutanol, sec-butanol, n-butanol or tert-butanol to diesel fuel increased the thermal efficiency of a diesel engine in a certain EGR region. Karabektas and Hosoz [192] reported that 5% and 10% addition of isobutanol into diesel fuel slightly increased the BTE of a single cylinder CI engine, and attributed this to the decrease in cetane number. With 15%

and 20% addition of isobutanol they observed a noticeable decrease in BTE, which they attributed to decrease in break power and increase in fuel consumption ratio. Campos-Fernández et al. [193] observed in diesel engine experiments that adding 10-30 v-% of either 1-butanol or 1-pentanol to diesel fuel lead to slightly higher BTE compared to diesel fuel due to greater premixed phases and more complete combustion of the alcohol-diesel mixtures, despite the lower heating values of the alcohols. Wang et al. [194] observed in a CI engine, that pentanol combustion achieved higher ITE by approximately 1.3 percentage points compared to diesel fuel with pilot injection. They attributed the higher ITE of pentanol to leaned combustion atmosphere, combustion closer to TDC and lower heat losses due to lower in-cylinder peak temperature. However, Wei et al. [88] observed no change in BTE of a diesel engine when up to 30 v-% of pentanol was added to diesel.

When considering the engine efficiency of ethers, Rakopoulos et al. [45] observed that adding up to 25 v-% diethyl ether in fossil diesel fuel did not change the BTE. They explained this by suggesting that the decrease in the calorific value of fuel by diethyl ether addition was simply offset by the increase in brake specific fuel consumption. Kannan and Marappan [195] reported that adding 20% of DEE into either biodiesel or cotton seed oil increased the engine efficiency by about 1.2 percentage points due to decrease in viscosity and the consequent improvement in atomization. Paul et al. [101] reported that 5 v-% addition of DEE to diesel fuel increased the thermal engine efficiency slightly and 10 v-% addition decreased it slightly.

It should be noted that only few studies have compared the engine thermal efficiency of different alternative fuels. Recently, Rakopoulos et al. [196] observed in a diesel engine study that pure cotton seed oil, cottonseed biodiesel (B10,B20 and B50), ethanol-diesel blends of 5, 10 and 15 v-%, as well as both butanol and diethyl ether blends with diesel of 8,16 and 24 v-%, all had little higher BTE, compared to diesel fuel, excluding the diethyl ether blends which did not change the BTE. They attributed the slightly higher BTE of these alternative fuels to the larger premixed combustion phases of the alternative fuels. Interestingly, their results showed the alternative fuels to be in the following order according to decreasing BTE: ethanol-diesel blends; butanol-diesel and biodiesel-diesel blends; cotton seed oil: diethyl ether blends with diesel. Additionally, Imtenan et al. [99] have observed in a multiple

cylinder diesel engine, that B20 jatropha biodiesel had higher BTE compared to diesel fuel by 2.74%. Also, replacing 5% and 10% of jatropha in the B20 biodiesel with n-butanol decreased the ITE about 3.9% and 7%, respectively, and replacing the corresponding amounts with diethyl ether instead of n-butanol resulted in slight further reduction in ITE.

2.6 Exhaust gas emissions

Besides engine thermal efficiency, the level of pollutant exhaust gas emission is one of the most important measures of diesel engine performance. The aim of an optimal combustion process is high ITE and low levels of exhaust emissions. Compression ignition engines have generally about 98% fuel combustion efficiency, and therefore only about 2% of fuel converts into exhaust gas emissions. However, the growing demand for better protection of the environment has made emission control increasingly important and resulted in continuously, albeit slowly, tightening regulations of the diesel engine exhaust gas emissions. Difficulties are caused in reducing pollutant emissions, especially with nitrogen oxides (NO_x), because they tend to have a negative correlation with ITE. This is because both ITE and NO_x increase with higher combustion temperatures [197]. Therefore, understanding the correlations between exhaust gas emission levels and engine thermal efficiency is highly relevant when developing new alternative fuels. In this section the typical levels of the main pollutant exhaust emissions, namely NO_x, carbon monoxide (CO), unburned hydrocarbons (UHC) and particulate matter (PM), are stated and compared to the current exhaust gas emission limits for diesel engine passenger vehicles in the EU Euro 6 standard (Regulation (EC) No 715/2007 [198]). Additionally, the formation mechanisms of these emissions are presented and the correlations between the emission levels and the engine thermal efficiency are described briefly. It should be noted, that the pollutant formation mechanisms are of great complexity in non-premixed systems, such as compression ignition engines, because emissions in such systems depend on the specific details of the system and local equivalence ratio. Furthermore, the most common exhaust gas treatment systems of diesel engines are briefly described at the end of this section.

2.6.1 Nitrogen oxides

Nitrogen oxides are one of the principal toxic pollutants emitted from combustion processes in the exhaust gas of a diesel engine. NO_x level in diesel engine exhaust gas is typically around 100-2000 ppm [1], corresponding to around 125-250 mg/l. The Euro 6 limit for NO_x emissions is 80 mg/km [198]. NO_x is mostly present in the exhaust gas as nitrogen oxide (NO) with 10 to 30% of NO_x being nitrogen dioxide (NO_2) and smaller amounts of other compounds [199]. NO_x can react with ammonia, moisture and other compounds to form small particles that can aggravate existing heart diseases and penetrate into lungs causing respiratory diseases, such as bronchitis [200].

The formation mechanisms of NO_x have been widely researched for decades. The three main routes proposed for NO_x formation are the prompt NO (Fennimore) route, the thermal (Zeldovich) NO route and the oxidation of fuel bound nitrogen. The case of fuel-bound nitrogen is not considered relevant for this PhD. The dominating NO_x formation route is determined by the reaction conditions in the combustion chamber. At lower pressures and lower temperatures under about 1800-2000 K, the prompt NO (Fennimore) route dominates the rate of NO formation. In hydrocarbon flames NO is mainly formed through rapid reactions of fuel radicals with molecular nitrogen producing amines and hydrocyanic acid, which reacts to form NO. Hence, the prompt NO route is highly significant for hydrocarbon fuels especially under fuel-rich conditions. The main kinetically controlling factors of the prompt NO route are the fuel radical concentration, the rate of reactions between fuel radicals and molecular nitrogen, and the mixing of fuel radicals and nitrogen. At high pressures and high temperatures above about 1800-2000 K, fuels with no nitrogen in their molecular structure form NO_x mainly through the thermal (Zeldovich) NO route, which is the dominant NO_x formation route in the combustion processes. The thermal NO route proceeds through the reactions (R 13), (R 14) and (R 15). Due to the high activation energy of the rate controlling reaction (R 13), the rate of NO_x formation through the thermal NO mechanism depends mainly on the peak temperature achieved during combustion: higher peak temperatures and longer residence time of combustion products at high temperatures result in higher NO levels in the exhaust gas. This peak temperature during combustion is affected, for example, by the equivalence ratio, fuel composition, amount of diluents present, and the initial temperature of the fuel-

air mixture. Therefore, NO is typically formed via the thermal NO route at the flame front and in the post-flame gases. Additionally, due to the temperature dependency of NO formation, EGR can be used to reduce the rate of NO formation [58,105].

$$N_2 + O \bullet \rightarrow NO + N \quad \text{(R 13)}$$

$$N + O_2 \rightarrow NO + O \bullet \quad \text{(R 14)}$$

$$N + OH \bullet \rightarrow NO + H \bullet \quad \text{(R 15)}$$

After the peak combustion temperature has been reached, the in-cylinder temperature decreases due to the expansion stroke and mixing of combustion gases and relatively cooler air within the combustion chamber. This decrease in temperature causes the NO equilibrium concentration initially to readjusts to lower levels. However, with further temperature decrease into the expansion stroke, the NO_x kinetics slow down and eventually freeze partly half way through the expansion stroke. NO_x concentration generally increases with higher peak combustion temperatures and higher premixed-burning fractions, as has been shown by several experimental studies [1]. Higher peak temperature and higher premixed fraction also tend to increase the ITE, and hence there is typically a trade-off between ITE and NO_x levels [1,201].

Alternative fuels generally produce higher levels of NO_x compared to fossil diesel fuel, as was stated in a review article by Westbrook [202]. It has been well established in several experimental studies that biodiesel combustion produces higher levels of NO_x compared to diesel fuel combustion. Based on the review articles of Bann-Weis [203], Hoekman et al. [204] and Palash et al. [205], the higher NO_x emissions of biodiesels, compared to diesel fuel, are mainly caused by the following factors: poorer fuel-air mixing because of higher viscosity, higher density and higher surface tension; higher CN and faster combustion, generally due to longer carbon chain length; less radiated heat loss by particulates; lower fuel vapour heat capacity; higher adiabatic flame temperature mainly due to higher level of unsaturation; and higher heat release rate during the premixed combustion phase due to higher oxygen content. However, slower fuel vaporization due to lower liquid thermal conductivity may

reduce the peak combustion temperature of biodiesels compared to diesel fuels. Therefore, it should be noted, that although most of the experimental studies have observed an increase in NO_x emissions for biodiesels, compared to diesel fuel, some studies have reported no changes or a slight reduction, as was discussed in the review articles of Lapuerta et al. [206] and Palash et al. [205]. For example, Serrano et al. [207] observed a slight increase of about 2% in the NO_x emissions of a EURO 5 passenger vehicle using New European Driving Cycle with 7% addition of soybean/palm to fossil diesel fuel, but a slight reduction of about 9% with 20 v-% addition. Labeckas et al. [183] observed in a CI engine study that NO_x emissions continued to increase with increasing amount of oxygen in fuel, despite the deterioration of combustion efficiency for RME/diesel blends with RME content higher than 10 v-% (1.45 v-% oxygen). They surmised that the effect of extra oxygen available from the fuel for the combustion reactions in the fuel rich zones might have a more significant effect in NO_x formation than the flame temperature. Additionally, Peirce et al. [208] concluded based on CI engine tests that under 40 Nm load RME generated about 100 ppm less and under 80 Nm load only slightly more NOx emissions than fossil diesel fuel for start of combustion timings between 20 CAD before TDC and 6 CAD after TDC.

In the case of alcohols, Giakoumis et al. [209] reported in a review article that the trend of ethanol and butanol percentages in diesel fuel on NO_x emissions is not clear and seems to depend on the specific alcohol percentage: the NO_x emissions are increased by the higher oxygen content and the lower CN of alcohols, compared to fossil diesel fuel, but decreased by the higher heat of vaporization and lower C:H ratio of alcohols. Several diesel engine studies have observed that addition of C2, C3 and C4 alcohols to diesel fuel reduces the NO_x emissions compared to diesel fuel. For example, Labeckas et al. [210] observed that adding 5, 10 or 15 v-% ethanol to diesel fuel resulted in a decrease in NO_x emissions, of about 15% in the case of B15, with equivalence ratios 3.0 and 1.5, although a slight increase in NO_x emissions was observed with high equivalence ratio of 5.5; Guariero et al. [211] concluded that 6 v-% ethanol addition to a B5 soybean biodiesel reduced NO_x emissions slightly compared to the B5 biodiesel due to both the higher latent heat of vaporization and the lower CN of ethanol compared to the biodiesel; Balamurugan and Nalini [188] observed that 4 or 8 v-% addition of propanol, as well as 4 or 8 v-% addition of

butanol to diesel fuel, decreased NOx emissions by 6.1%, 19.7%, 11.9% and 14.3%, respectively; Ylimaz et al. [86] reported a slight reduction in NO_x emissions, with 5, 10 or 20 v-% addition of butanol to biodiesel due to decreased exhaust gas temperatures; Merola et al. [87] observed in a turbocharged diesel engine, that 20 v-% butanol in diesel fuel resulted in formation of less NO_x by about 7%, compared to diesel fuel, due to the longer ignition delay and enhanced fuel volatility of fuel; Karabektas and Hosoz [192] reported a decrease of about 11%, 8%, 16% and 20% in NO_x emissions with 5, 10, 15 and 20 v-% isobutanol addition to diesel fuel, respectively, at engine speed 1800 rpm; Rakopulos et al. [212] concluded that adding 8, 16 or 24 v-% butanol to diesel fuel reduced the NO_x emissions by about 2, 3 and 3.5% with 2.75 bar IMEP. However, some diesel engine studies have reported an increase in the NO_x emissions with butanol addition. For example, Chen et al. [213] concluded based on results from a turbocharged diesel engine, that under low load conditions NO_x emissions decreased slightly with increasing addition of butanol to diesel fuel (30, 40 and 50 v-%), whereas at high loads NO_x emissions increased with increasing addition of butanol, for example by 13.4% and 15.8% for B40 butanol with 2000rpm and 4000rpm, respectively; Sahin and Aksu [190] reported that 2 v-% addition of butanol to diesel decreased the NOx emissions 1.47%, 2.74% and 5.03% at 2000, 3000 and 4000 rpms, respectively but both 4 and 6 v-% additions increased NO_x emissions; Zhu et al. [214] observed that with 15% exhaust gas recirculation 20 and 40 v-% butanol addition to diesel slightly increased the NO_x emissions by about 7% and 5%, respectively; Chen et al. [215] reported an increase in NO_x emissions with 40 v-% butanol addition to diesel fuel in a heavy duty diesel engine, and attributed this increase to a wider high-temperature combustion region.

When considering ethers, Arcoumanis et al. [41] and Thomas et al. [216] concluded in their review articles, that DME produces significantly lower levels of NO_x emissions, compared to diesel fuel, due to the shorter ignition delay, smaller injection rate, smaller premixed phase and higher local equivalence ratio of DME. For example Rakopoulos et al. [45] reported a reduction in NO_x emission, compared to fossil diesel fuel, by about 4%, 8% and 20% from a diesel engine with 8, 16 and 24 v-%, respectively, addition of DEE to diesel fuel at 5.37 bad BMEP. Additionally, Cinar et al. [217] observed that increasing the ratio of DEE in the premixed combustion in a HCC engine from 0 to 40 v-% decreased the NO_x emissions by up to 19.4%.

Interestingly, Paul et al. [101] observed a slight increase in the NO_x emissions of a diesel engine when adding 5 or 10 v-% of DEE to fossil diesel fuel at low loads, but a slight decrease in NO_x under higher loads above 1.8 kW. However, some studies have observed higher NO_x emissions for DME compared to diesel fuel, as was discussed in the review article of Park and Lee [98].

2.6.2 Carbon monoxide

The Euro 6 limit for CO emissions is 500 mg/km [198]. CO emissions can result in harmful health effects, such as reduced oxygen conveyed to heart, by reducing the oxygen delivery to main organs of the body [200]. Formation of CO depends mainly on the fuel-air equivalence ratio: under fuel rich conditions there is not enough oxygen in the combustion chamber to convert all CO, formed as an intermediate species of hydrocarbon combustion, into CO_2. Thus CO concentration in the exhaust gas increases with increasing equivalence ratio. Exhaust CO is generated throughout the combustion process, but most of the CO is formed when the engine is cold started or during acceleration under high load, due to a temporarily change in equivalence ratio, lack of air, and transient incomplete combustion. However, diesel engines operate under globally lean conditions and therefore CO emissions of diesel engines are generally low enough to be a lesser challenge than NO_x and particulate emissions [1,199].

It should be noted, nonetheless, that both Sharma et al. [218] and Shahir et al. [201] concluded in review articles that biodiesels generally reduce the CO emissions by about 27%, compared to fossil diesel fuel, due to their higher oxygen content and lower C:H ratio. They also reported that engine load and engine speed have a substantial influence over CO emissions, which makes the comparison between engine studies difficult. When considering alcohols, both an increase and a decrease in UHC have been reported with the addition of C3, C4 and C5 alcohols in diesel fuel. However, most of the diesel engine studies have observed an increase in CO emissions with alcohol addition to diesel fuel. For example, Labeckas et al. [210] observed an increase in CO emissions with 5, 10 and 15 v-% ethanol addition, nearly 85.6% higher CO emissions being observed for the E15 fuel at equivalence ration of 5.5 and 2200 rpm speed; Ylimaz et al. [86] reported an increase of 0.03% to 0.05%

with 5, 10 and 20 v-% butanol addition to biodiesel at 46% load; Zhu et al. [214] observed an increase in CO emissions with 20 and 40 v-% butanol addition; Chen et al. [215] reported a 58% increase in CO emissions with 40 v-% butanol addition to fossil diesel fuel. However, a decrease of about 7% to 20.5% in CO emissions of a diesel engine was reported by e.g. Karabektas and Hosoz [192] with 5, 10, 15 and 20 v-% isobutanol addition to diesel fuel at engine speeds above 2000 rpm. With the same addition levels at engine speeds between 1200 and 2000 rmp Karabektas and Hosoz [192] reported an increase of about 0 to 3.5% in CO emissions. Rakopulos et al. [212] observed a decrease of 0 to 7% in CO emissions with 8, 16 and 24 v-% butanol addition. Interestingly, Chen et al. [213] concluded, based on results from a turbocharged diesel engine, that under low load conditions CO emissions increased by about 4% to 35% with increasing addition of butanol to diesel fuel (30, 40 and 50 v-%), whereas under high load conditions CO emissions decreased by about 2.5% to 25% with increasing addition of butanol. Additionally, Balamurugan and Nalini [188] observed that 4 and 8 v-% addition of propanol, as well as 4 and 8 v-% addition of butanol to diesel fuel, reduced the CO emissions of a diesel engine under 60% load ranges by about 0.03 to 0.05 %-units, but increased the CO emissions by 0.02 to 0.06 %-units at higher loads. In the case of ethers, Arcoumanis et al. [41] and Park and Lee [98] concluded in their review articles, that experimental studies show both higher and lower levels of CO in DME combustion compared to diesel fuel. An increase in CO compared to diesel fuel was attributed to the longer injection duration, spray impingement and faster evaporation of DME. On the other hand, DME can reduce the CO emissions, compared to fossil diesel fuel, due to more efficient fuel-air mixing, lower C:H ratio and high oxygen content of DME compared to fossil diesel fuel. Raopoulos et al. [45] reported a reduction in CO emission of a diesel engine of 11% to 72% with 8, 16 and 24 v-% addition of DEE to diesel fuel at 5.37 BMEP.

2.6.3 Unburned hydrocarbons

Unburned hydrocarbons are formed due to incomplete combustion of hydrocarbon fuel. The levels of UHC in the exhaust gas of a diesel engine are typically in the range of 1000-6000 ppm, which is roughly the equivalent of 125-750 mg/kg [1]. The

combined Euro 6 limit for hydrocarbon and NO_x emissions is 170 mg/km [198]. The formation of UHC depends mainly on the fuel-air equivalence ratio: under fuel rich conditions less of the fuel injected into the combustion chamber combusts completely. Therefore, increasing the equivalence ratio generally results in higher levels of UHC. Additionally, fuel composition affects the magnitude and composition of UHC significantly. Compounds with poorer combustion characteristics, such as aromatics compared to alkanes, result in higher levels of UHC. Other factors enhancing the formation of UHC include incomplete mixing of air and fuel, flame quenching caused either by a layer of unreacted air/fuel mixture on the combustion chamber wall or by exhaust residuals, fuel mixture in crevice volumes out-going late in the exhaust stroke and not burning, leaks past the exhaust valve, valve overlap, fuel vaporization after injection out of the injector nozzle holes and sac, deposits on combustion chamber walls and oil on combustion chamber walls and over dilution of fuel vapour, below its flammability limits, sometimes due to long ignition delay. These factors lead to formation of UHC during the compression and expansion stokes and release of UHC late in the expansion stroke with insufficiently high temperature and time available for complete oxidation. It should be noted, that ITE increases with more complete combustion and therefore ITE in general has a negative correlation with the level of UCH in the exhaust gas [1,199].

Alternative fuels, when compared to diesel fuel, tend to decrease UCH emissions. Sharma et al. [218] and Shahir et al. [201] concluded in review articles that biodiesels generally tend produce less UHC compared to diesel fuel, although few contradictory engine study results are available. Additionally, they reported that the effect of engine load on UHC emissions is not yet fully understood. According to Giakoumis et al. [209], the effect of alcohols on UHC emissions is not yet clear: alcohols can reduce the amount of UHC, compared to diesel fuel, by reducing the number of fuel-rich local regions due to their oxygenated molecular structure, but the formation of UHC is enhanced by the higher heat of vaporization and poorer spray characteristics of alcohols. However, several diesel engine studies have also reported an increase in UHC emissions with alcohol addiction. An increase in UHC emissions of about 1% to 42% with 4 and 8 v-% addition of both propanol and butanol to diesel fuel has been reported e.g. by Balamurugan and Nalini [188]. Additionally, Guariero et al. [211] reported an increase of about 38% with 6 v-% ethanol addition to a B5 soybean

biodiesel, compared to the B5 biodiesel, due to both the higher latent heat of vaporization and the low CN of ethanol. For example, Ylimaz et al. [86] reported an increase of 400% to 600% with 5, 10 and 20 v-% addition of butanol at 46% load; Rakopulos et al. [212] observed a rise of around 4% to 15% with 8, 16 and 24 v-% addition of butanol; Zhu et al. [214] reported that compared to 20 v-% butanol addition to diesel fuel 40 v-% addition doubled the UHC emissions when 15% of the exhaust gas was recirculated; Karabektas and Hosoz [192] reported a rise of 7% to 56% with 5, 10, 15 and 20 v-% isobutanol; and Chen et al. [213] concluded based on results from turbocharged diesel engine, that 20% addition of butanol to diesel fuel decreased the UHC emissions slightly, 30% addition caused no significant changes and 40% addition increased the UHC emissions slightly. Interestingly, Labeckas et al. [210] observed that addition of 5, 10 and 15 v-% ethanol to diesel fuel increased the UHC emissions, in the case of E15 by 33.6%, 27.9% and 25.5% at equivalence ratio 5.5 for speeds 1400, 1800 and 2200, respectively. In the case of ethers, Arcoumanis et al. [41] and Park and Lee [98] concluded in their review articles, that DME tends to have lower UHC emission, compared to diesel fuel, due to the shorter ignition delay and efficient fuel-air mixing of DME. Paul et al. [101] observed the UHC emissions of a diesel engine to decrease by about 0 to 80% with addition of 5 and 10 v-% of DEE to diesel fuel. However, Raopoulos et al. [45] reported an increase of about 6% to 24% in UHC emission of a diesel engine with 8, 16 and 24 v-% addition of DEE to diesel fuel at 5.37 BMEP.

2.6.4 Particulate matter

Diesel engine particulate emissions consists mainly of solid carbonaceous material, called soot, generated during combustion, on to which some organic compounds become adsorbed. Although most of the PM comes from the fuel (0.2-0.5% of the fuel becomes soot), up to 25% of PM is formed from the lubricating oil [199]. For light-duty diesel vehicles the PM emission rates are typically 200-600 mg/km [1]. The Euro 6 limit for particulate emissions is 5 mg/km [198]. Particulate emissions can cause several health problems, including irregular heartbeat, aggravated asthma, decreased lung function, increased repertory systems, cancer, and even premature death in people with heart or lung disease [200].

Particulates are formed in diesel engines at temperatures about 1000-2800K at pressures 50-100 atm. First, the soot precursors condense from the gas phase and form the first very small (diameter below 2 nm) observable soot particles. These precursors include typically unsaturated compounds, especially acetylene, and polycyclic aromatic hydrocarbons (PAH). At temperatures below 1700K only aromatics and highly unsaturated species form soot, whereas in diffusion flames at temperatures above 1800K all hydrocarbon fuels can lead to soot formation [1]. The soot formation propensity of hydrocarbons can be presented in a descending order as follows: aromatics > alkynes > alkenes > alkanes [58]. After the particulates are generated, they grow through surface growth, coagulation and aggregation, as shown for soot formation in Figure 6. Surface growth contributes to the initial particulate growth: hydrocarbon intermediates from the gas phase are deposited on the surface of the particulate nuclei in agglomerating collisions. At the early stages of the particle growth, two particulates may collide and coagulate into a single spheroid. Once surface growth ceases, the coalescence of particulates continues to form chain like structures in aggregation. Eventually large clusters of solid carbon spherules with diameters from 10 nm to 80 nm are formed. In diesel engines, the particulate concentration is highest in the fuel-rich fuel spray core. Efficient atomization and mixing reduce the soot levels by increasing air concentration in the fuel rich spray core, which enhances the oxidation of both soot precursors and the soot particles that have already formed. Therefore higher soot levels indicate lower ITE. The highest particulate concentration occurs when the engine is under full load and the overall engine equivalence ration is high, even approaching the stoichiometric value [1,219].

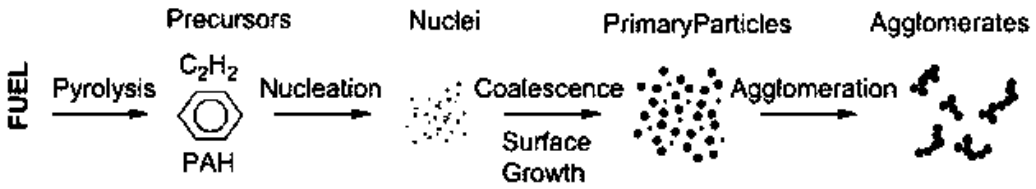

Figure 6. Schematic diagram of soot and particulate formation [219]

Alternative fuels, such as alcohols, ethers and esters, generally produce lower levels of PM mass emissions compared to diesel fuel, as was stated in a review article by Westbrook [202]. Diesel fuel tends to produce higher PM levels, compared to alternative fuels, because of its higher content of aromatics and sulphur compounds, which can act as soot precursors. Additionally, the oxygen in the molecular structure of alternative fuels can reduce the locally fuel-rich regions and thus reduce PM formation compared to diesel fuel. Several articles, e.g. the review articles of Sharma et al. [218], Bergthorson and Thomson [220] and Shahir et al. [201], have reported that biodiesels produce less PM emissions compared to diesel fuel.

In the case of alcohols, Giakoumis et al. [209] concluded in their review article that blending alcohols to diesel fuel tends to reduce the PM emissions due to the better volatility of alcohols compared to diesel fuel. Reduction in PM emissions of a diesel engine with alcohol addition to diesel fuel has been reported by e.g. Merola et al. [87], who observed a reduction of about 20 % in smoke with 20 v-% butanol addition in a turbocharged diesel engine with start of combustion occurring either 3 CAD before TDC of 5 CAD after TDC. Balamurugan and Nalini [188] reported an increase of 10% to 15% in smoke density with 4 and 8 v-% addition of either propanol or butanol under both medium and high load ranges. Interestingly, Guariero et al. [211] observed that 6 v-% ethanol addition to a B5 soybean biodiesel resulted in an increase in the number of particulates from $9.6*10^6$ to $1.1*10^7$ particulates in cm^3 due to a shift from larger particulates to smaller, lighter particulates. Furthermore, Zhang and Balasubramanian [221] reported that both 15 and 20 v-% butanol blended to diesel fuel reduced the total mass and number of particulates in diesel engine exhaust gas, but increased the number of particulates with diameter less than 15 nm. Additionally, they observed an increase in PAH emissions with butanol addition to diesel fuel.

When considering ethers, the review articles of both Arcoumanis et al. [41], Park and Lee [98] and Thomas et al. [216] concluded that DME produces significantly lower levels of PM, compared to diesel fuel, due to the high oxygen content. For example, Yoon et al. [222] reported that DME produced low PM emissions compared to fossil diesel fuel at advanced injection timing. Raopoulos et al. [45] reported a reduction in smoke opacity of a diesel engine of about 14% to 29% with 8, 16 and 24 v-% addition of DEE to the diesel fuel. Paul et al. [101] observed the particulate emissions of a diesel engine to decrease by about 2% to 90% with addition of 5 and 10 v-% of DEE

to diesel, the decrease being more significant at higher loads. Cinar et al. [217] observed with DEE that increasing the ratio of premixed combustion in a HCC engine from 0 to 40 v-% decreased the soot emissions up to 19.4%. They attributed the reduction in soot to the reduced number of fuel rich regions in the combustion chamber, the oxygen in the DEE and the lower C:H ratio of DEE compared to diesel fuel.

2.6.5 Exhaust gas treatment of a diesel engine

When comparing the typical exhaust gas pollutant levels formed in diesel engines to the Euro 6 limits, it can be concluded that the typical exhaust gas levels can be higher than the Euro limits. The level of exhaust gas pollutant emissions of diesel engines can be affected by the engine design and the engine operating conditions. However, even with the engine technologies available today, the level of some diesel exhaust pollutants, such as particulates and NO_x, still do not meet the legislation limits. Therefore, in practise, further reductions in exhaust gas emissions through exhaust gas after treatment are required [1].

Gas phase emissions of CO and THC are in diesel engines typically removed by oxidizing them in either thermal or catalytic converters [1]. Thermal converters are high-temperature chambers that promote further oxidation reactions in the exhaust gas flow once the flow has exited the combustion chamber. Catalytic converters are, however, more efficient and compact than thermal converters, and therefore catalytic converters are commonly used in CI engines. In the catalytic converters the exhaust gas is directed, after exiting the combustion chamber, to flow through an oxidizing catalyst bed in a metal casing. The most common catalysts are mixtures of palladium and platinum, which can remove 98-99% of CO and above 95% of gaseous UHC from the exhaust gas. It should be noted that the effectiveness of catalysts deteriorates with time due to both catalyst poisoning and sintering of the catalyst. Furthermore, the operational high temperature limit of these oxidizing catalysts is around 523 K, and they are therefore ineffective during high load or cold start engine conditions [1,199].

NO_x emissions are typically reduced in dried exhaust gas either by selective catalytic reduction (SCR) and a NO_x trap or by NO_x adsorber. SCR is generally used for reducing NO_x emissions in diesel engines instead of NO_x adsorbers, which contain precious metals. SCR reduces NO_x to diatomic nitrogen, water and small amounts of carbon dioxide through an active reductant on a catalyst surface. The reductant is usually automotive grade urea [1,223].

For the solid particulates a diesel particulate filter (DPF) can be used to physically trap the particulates. The main problems with DPF usage are the accumulation of particulate mass within the trap and the following increase in the exhaust manifold back pressure which reduces engine ITE. The trapped particulates can be burned away from the filter by either using an oxidative catalyst in the trap or with an external heat source. Generally 60-90% of the PM in the engine exhaust can be removed by using such traps [1,199].

2.7 Conclusions of the literature review

The literature review above presented the molecular structure of several alternative compression ignition fuels and then discussed the effects of the fuel molecular structure on combustion kinetics, physical processes of combustion, engine thermal efficiency and the formation of exhaust gas emissions. The alternative fuels considered were biodiesel, alcohols, ethers and ketones. It can be concluded, that currently the most common biofuels are biodiesels and ethanol/diesel blends, although the research focus is increasingly on the longer alcohols due to their high CN, on ethers due to their high CN and low exhaust gas emissions, as well as on ketones due to their suitable CN and improving production technologies.

When considering the effect of fuel molecular structure on compression ignition combustion, several studies suggest that the ignition delay is mainly controlled by the chemical kinetics of combustion and the combustion after ignition by the physical properties of the fuel. The two main reaction mechanisms affecting the ignition delay have been shown to be hydrogen abstraction from the fuel molecule and isomerization of the fuel peroxy radicals. Faster reaction rates of these two mechanisms are associated with increased rate of radical production and hence the

formation of a radical pool large enough to initiate and sustain ignition. H-abstraction and isomerization have both been shown to be hindered by the increasing degree of both unsaturation and branching. In the case of alternative fuels, studies have shown that H-abstraction and isomerization are more difficult for alcohols than for the corresponding alkanes due to the high electronegativity of the oxygen in the hydroxyl group of the alcohols. Additionally, it is suggested here that, based on results available in literature, a carbonyl group similarly results in harder H-abstraction and isomerization compared to a corresponding alkane. Furthermore, studies have shown H-abstraction to be easier from ethers compared to alkanes, and that the ether group does not hinder isomerization. The main four physical combustion phenomena considered were atomization, spray formation, spray vaporization and vapour-air mixing. It has been established that, in general, lower viscosity, lower density, lower boiling point and lower surface tension decrease the overall duration of overall combustion, because they result in better atomization, larger spray area, faster spray vaporization and higher vapour-air mixing rate. Several studies have shown that compared to fossil diesel fuel, biodiesels tend to result in poorer atomization, smaller spray area and slower evaporation; short chain alcohols have better atomization and faster evaporation; and ethers have been observed to have improved atomization, slightly increase the spray area and lead to faster evaporation. However, no studies on ketone combustion or systematic comparisons between the combustion rates of the alternative fuel molecules were available in the literature.

Engine thermal efficiency was concluded to be determined by both the timing and the rate of heat release rate. Both engine operating conditions, such as engine speed, fuel injection rate and air flow rate, as well as fuel molecular structure were shown to affect the engine thermal efficiency. Fuel molecular structure was concluded to affect engine thermal efficiency through the shape of the heat release rate profile of combustion. Therefore the duration of ignition delay, the size of premixed combustion phase, the overall combustion duration and the heating value of fuel can have a significant effect on engine thermal efficiency. It can be concluded that, based on the literature, most biofuels have lower engine efficiency than fossil diesel fuel due to the oxygenated structure of biofuels. However, low percentages of biodiesel in fossil diesel fuel have also been reported to increase the engine efficiency due to more complete combustion. In the case of alcohols, several studies have observed an

increase in engine efficiency with alcohol addition to fossil diesel fuel. Interestingly, both decrease and increase in engine efficiency has been reported for ethers. It should be noted, that studies comparing the engine efficiency of alternative fuels were scarce and no studies investigating the engine efficiency of ketones were available.

The main diesel engine exhaust gas emissions considered in the literature review were NO_x, CO, UHC and PM. It can be concluded that NO_x emissions and PM emissions are the most critical pollutant emissions, compared to CO and UHC, considering the relatively high amount formed during fossil diesel fuel combustion and the severity of the effects on human health of these emissions. The formation of NO_x emissions was shown to be highly temperature dependent. Several studies have shown that this temperature dependency results in higher NO_x levels of alternative fuels, compared to fossil diesel fuel, mainly due to the poorer fuel-air mixing, higher in-cylinder temperatures, higher adiabatic flame temperatures and higher oxygen content of alternative fuels. However, the effect of biodiesel and alcohol addition to fossil diesel fuel on NO_x formation is not yet fully understood. In the case of ethers, several studies have reported a decrease in NO_x emissions with ether addition to fossil diesel fuel. In contrast to NO_x emissions, alternative fuels in general produce less PM, compared to fossil diesel fuel, due to the lower content of aromatic and cyclic compounds and the higher oxygen content: studies have shown that blending biodiesel, alcohol or ether to fossil diesel fuel reduces PM emissions. However, it should be noted that the smaller particulate can penetrate deeper into the human lungs than the larger particulates, and may thus be more dangerous to human health.

It can be seen, from the conclusions above, that understanding the effect of fuel molecular structure on combustion characteristics is important in order to identify alternative fuel molecules with high engine thermal efficiency and low exhaust gas emissions. However, systematic experimental studies comparing the combustion characteristics, exhaust gas emissions, and engine thermal efficiency of several alternative fuels are scarce. Therefore, the experimental studies of this PhD project aimed to aid in the selection of raw materials and production processes of alternative fuels by assessing the compression ignition and the exhaust gas emissions of several potential fuel molecules.

Chapter 3

Experimental and analytical methods

3.1 Introduction

The present chapter describes the experimental systems used in the fuel combustion experiments. Additionally, the instrumentation and software used to measure and record the experimental data are described. Furthermore, the last subsection presents the main analytical methods used in the results analysis.

3.2 Diesel research engine

The diesel research engine was a custom built, naturally aspirated 4-stroke direct injection single cylinder, compression ignition engine. The cylinder head, piston with omega-shaped bowl, piston liner and connecting rod were from a 2.0 litre, 4 cylinder turbocharged automotive diesel engine (Ford Duratorq CD132 130PS). These were mounted on a Ricardo Hydra single cylinder research engine crank case. The engine was motored by a David McClure direct-current motor dynamometer, which was controlled by a Cussons test-bed console and driven by a thyristor power unit. Exhaust gas was lead to the laboratory extraction system through a silencer. The engine specifications are presented in Table 1. The engine was already operational at the beginning of this PhD project, and a more detailed description of the engine setup can be found in the thesis of Schönborn [224]. However, the engine was overhauled by the author at the beginning of this PhD project due to a substantial drop in the in-cylinder gas pressure when comparing the current values to historic values. The compression ratio of 18.2:1 presented in Table 1 is the value measured after this overhaul.

Table 1. Engine specifications

Engine head model	Ford Duratorq
Crank case model	Ricardo Hydra
Number of cylinders	1
Number of valves	4
Cylinder bore (mm)	86
Crankshaft stroke (mm)	86
Swept volume (cc)	499.56
Compression ratio	18.2 : 1
Maximum cylinder pressure (MPa)	15
Piston bowl design	ω – bowl
Minimum engine running speed (rpm)	755±5
Maximum engine speed (rpm)	5500 ± 50
Injector type	6-hole (DELPHI DF 1.3)
Injector control	1µs steps (EMTRONIX EC-GEN 500)
High pressure fuel system	160 MPa common rail (BOCH CRS2)

3.3 Fuel injection system

The experimental setup allowed supplying fuel to the fuel injector through two different routes: (a) directly via a common rail from a header tank or (b) from an ultra-low volume fuel system (ULVFS). The experimental setup with both the header tank and the ULVFS is presented in Figure 8. The engine experiments for this PhD project were conducted using the ULVFS. Direct injection with the common rail was used in the commissioning tests and also to check the injector operation at the beginning of each test day.

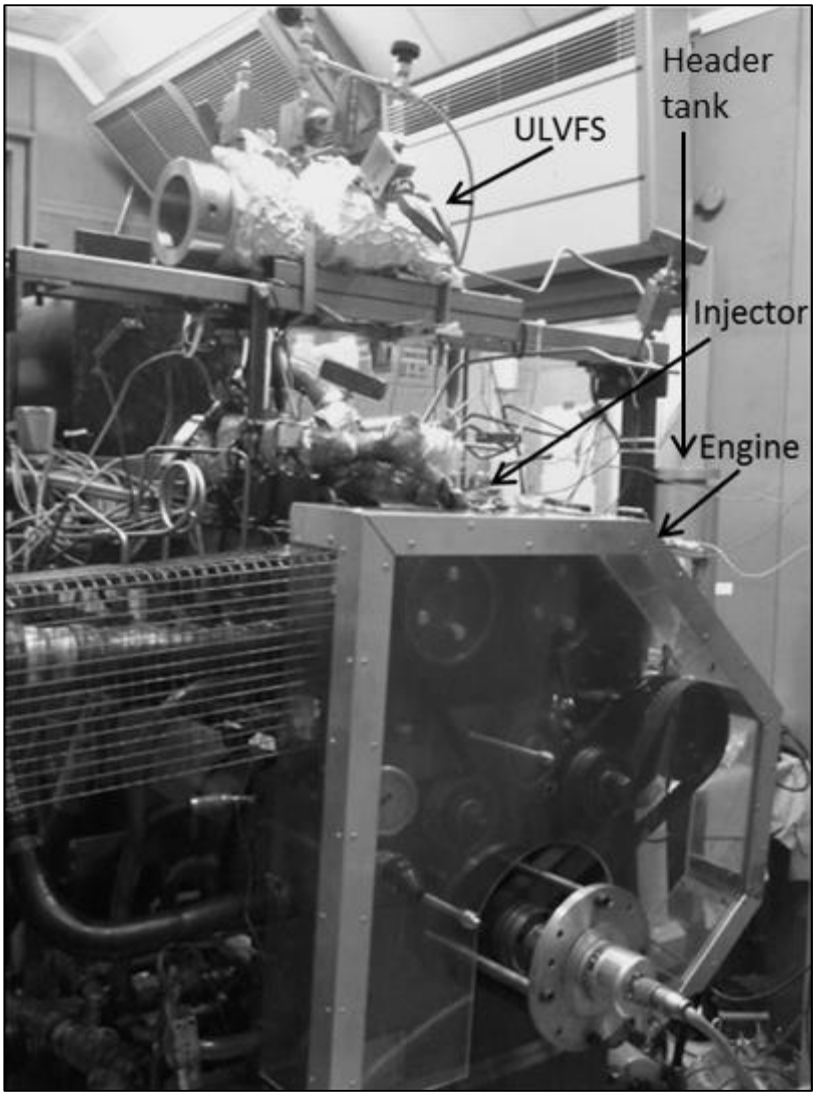

Figure 7. Header tank and the ultra-low volume fuel system (with left end-cap removed).

When injecting via the common rail from a header tank, fuel was led from the header tank to a crank-shaft driven fuel pump (BOSCH CP3), which pumped the fuel through the common rail to the injector. The injection pressure in the common rail was maintained by a PID feedback control loop, which used the signal from the common rail pressure sensor plus a solenoid pressure control valve (BOSCH CRS2). This solenoid valve, controlled by an EmTroniX system, relieved pressure from the common rail by bleeding controlled amounts of the fuel back to the low pressure fuel pump inlet, thus maintaining constant pressure in the common rail at the set value.

The ULVFS allowed testing with small fuel samples of 120-180 ml. This small fuel sample quantities were a significant advantage because many of the fuel samples were costly to purchase even in small quantities. The schematic diagram of the ULVFS is presented in Figure 8: diesel flow from the common rail was utilized in the right hand side of the ULVFS to push the two pistons leftwards, which in turn pressurized the fuel sample on the left hand side of the pistons and supplied this sample fuel to the injector at the same injection pressure as that in the engine common rail. The original design of this ULVFS can be found in the thesis of Schönborn [224] and later modifications in the thesis of Hellier [225].

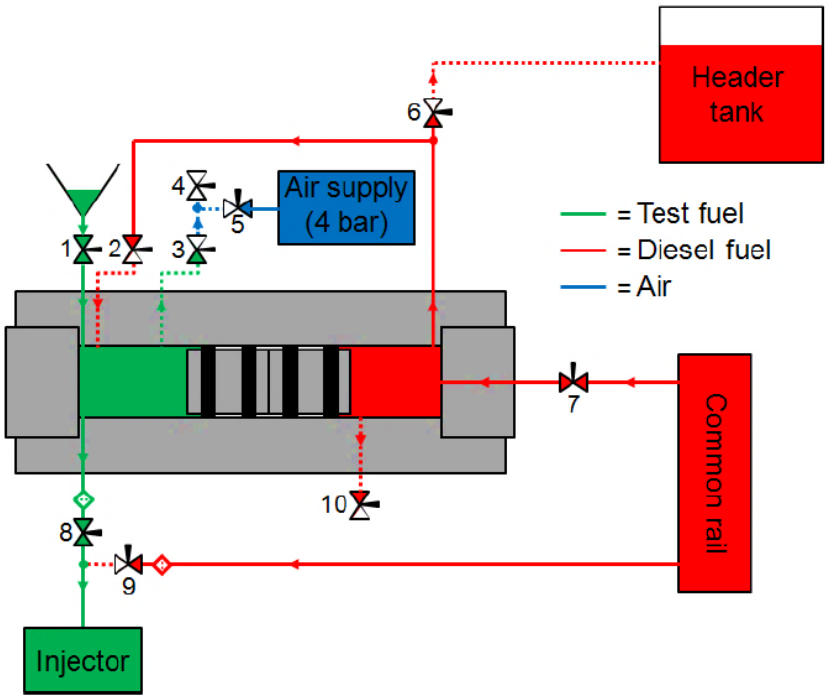

Figure 8. Ultra-low volume fuel system [225]

3.4 Injection fuel flow measurement

In order to allow calculations of engine thermal efficiency and the magnitude of the premixed combustion phase, the amount of fuel injected into the engine combustion chamber at any given time had to be known. However, measuring the amount of fuel injected at any given time was not possible with the existing experimental setup at the beginning of this PhD project. Therefore, an injection fuel flow measurement

system was developed by the author. This consisted of an instantaneous fuel flow measurement system (IFFMS), which measured the fuel flow from the ULVFS to the fuel injector, and this was combined with an additional system which measured the injector spill flow. In this section a general description of the injection fuel flow measurement system is presented first, followed by more detailed descriptions of the IFFMS and the injector spill flow measurement system.

3.4.1 Injection fuel flow measurement system

A schematic drawing of the injection fuel flow measurement system is shown in Figure 9. Together, the instantaneous fuel flow measurement from the IFFMS ($V_{from\ ULVFS}$) and the injector spill flow measurement (m_{spill}) allowed the calculation of injection fuel flow rate ($m_{injected}$) according to the equation (E 3) below. It should be noted that the density of the sample fuel (ρ_{sample}) was determined with a Gay-Lussac bottle (Cole-Parmer WZ-34580-42) at the temperature of the ULVFS prevailing during the experiment.

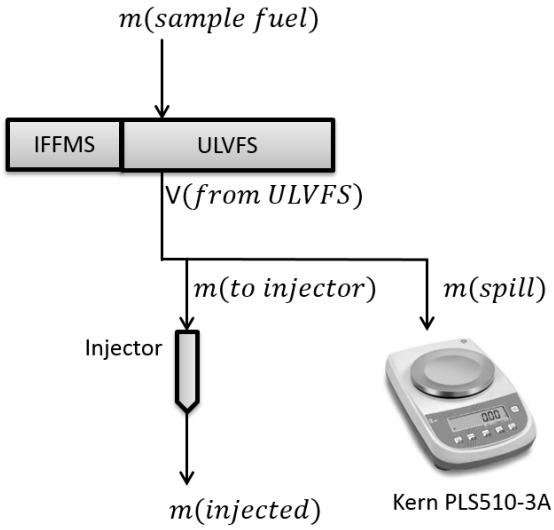

Figure 9. Schematic drawing of the injection fuel flow measurement system.

$$m_{injected} = m_{to\ injector} - m_{spill} = V_{from\ ULVFS} * \rho_{sample} - m_{spill} \quad \text{(E 3)}$$

3.4.2 Instantaneous fuel flow measurement

A mechanical IFFMS was developed to measure the fuel flow from the ULVFS to the injector, because no flow measurement equipment was available at the start of this PhD which would allow fuel flow measurement in-line with the ULVFS. The experimental setup with the IFFMS attached to the ULVFS, positioned above the research engine, is shown in Figure 10.

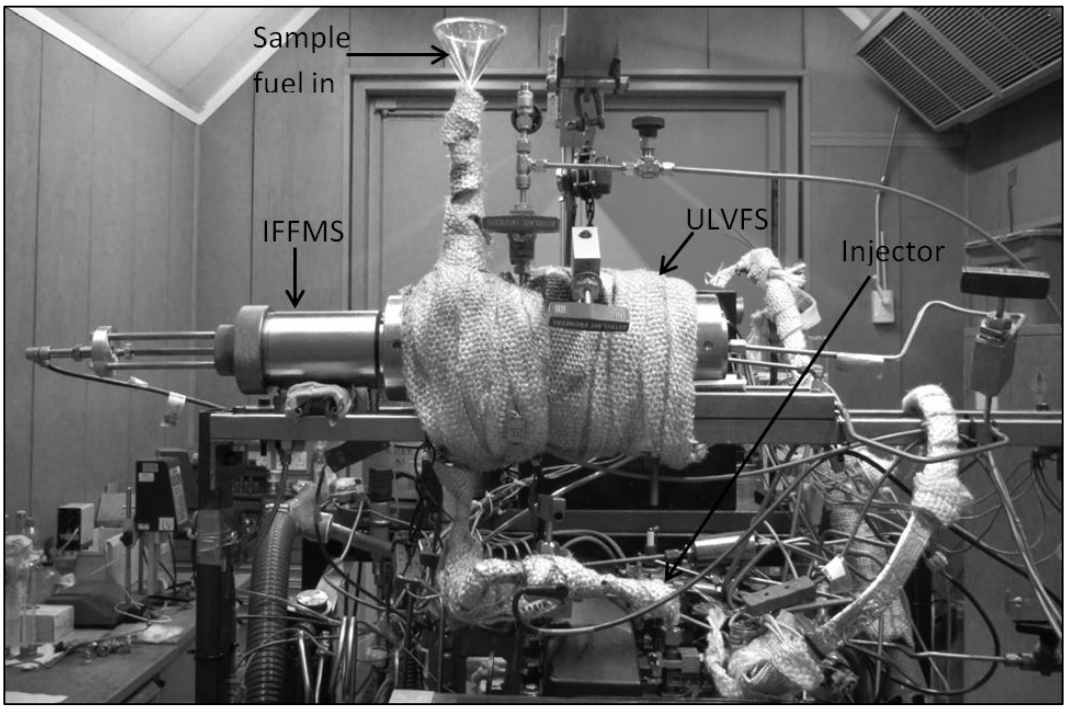

Figure 10. Experimental setup with IFFMS and ULVFS.

When designing the IFFMS it was decided that this new piece of equipment would be integrated to the existing ULVFS, because it would have been impossible to find a system measuring fuel flow from the ULVFS at injection pressures up to 1300 bar. Inside the ULVFS the two pistons push the fuel sample to pressurize it and to supply the fuel sample to the injector (Figure 8). Therefore, the IFFMS was designed to measure the movement of these pistons. In order to develop a durable fuel flow measurement system for the various tested fuels, it was decided to use a stainless

steel rod which would be in contact with the ULVFS pistons, instead of measuring the movement of the ULVFS pistons with a sensor which would have had to be in contact with the fuel sample. Such sensor would have had to be able to withstand 1300 bar pressure and contact with corrosive fuels, and was not obtainable. The rod used in the IFFMS, in contact with the ULVFS pistons, is shown in Figure 11 (see Figure 12 for cross sectional diagram of the system). Viton O-rings were used to seal the fuel sample in the ULVFS and the movement of the rod was measured with a proximity sensor. Several proximity sensors with different functioning principles were evaluated before an ultrasonic proximity sensor (UB120-12GM-U-V1), shown in Figure 11, was selected based on its sensing range and accuracy.

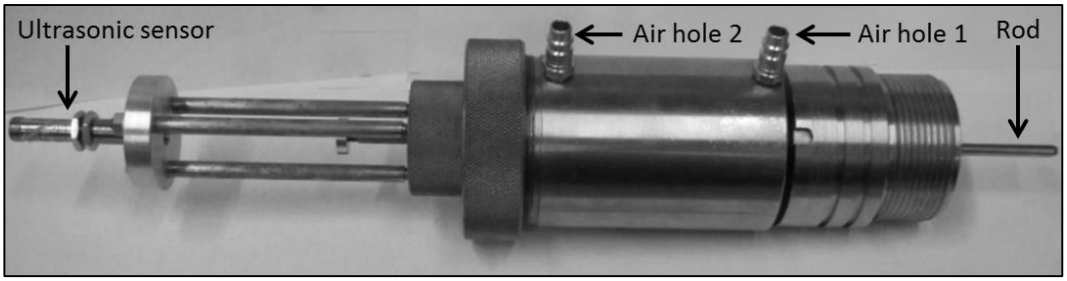

Figure 11. Instantaneous fuel flow measurement system (IFFMS).

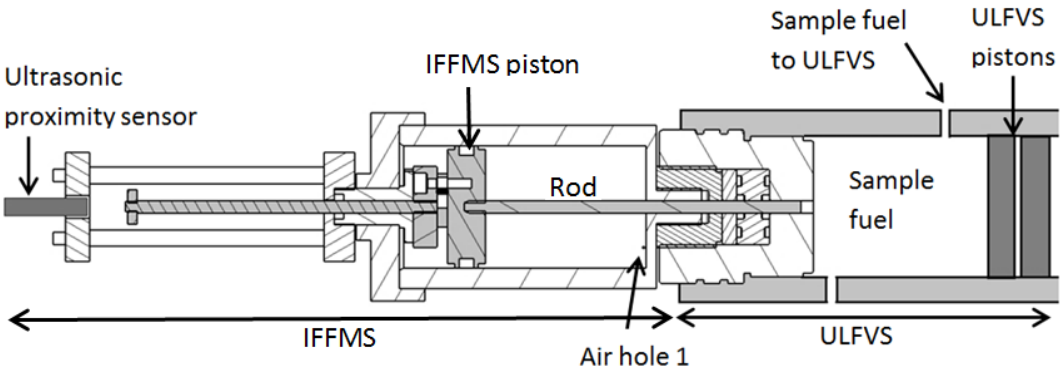

Figure 12. IFFM at the beginning of an experiment

Measures were needed to prevent the rod of the IFFMS from being pushed (extruded) out from the ULVFS by the very high fuel pressure in the ULVFS acting on the end

of the rod. Thought was given to embedding the rod in the outer sample fuel piston of the ULVFS, but this option was not followed because it would have interfered with the dismantling of the ULVFS after each experiment to clean it. Therefore, a compressed air system was developed to create backpressure for the rod so as to offset the force on the rod generated by the high pressure in the ULVFS: the end of the rod, which extended outside the ULVFS, was embedded into a new piston (labelled IFFMS piston in Figure 12), which moved inside the IFFMS cylinder, so as to allow pressurizing the other side of the IFFMS piston with air in order to create a back-pressure for the fuel pressure in the ULVFS. Air holes, shown in Figure 11, were used to move the IFFMS piston with pressurized air.

Both the piston diameter and the rod diameter were designed in order to require only low compressed air pressure to act as back-pressure on the rod. Buckling stress calculations were performed so as to determine the minimum rod diameter required. The thickness of the IFFMS cylinder walls were determined through Hoop stress calculations based on the air pressure required to counter-act the force on the rod from the maximum fuel sample injection pressure. Viton O-rings, selected according to ISO 3601-2, were applied to seal the rod on both ends of the IFFMS cylinder.

Besides finding the most suitable proximity sensor for the IFFMS, the main challenge faced in designing of the IFFMS was sealing the right hand side end of the moving rod system where the rod entered the ULVFS and was exposed to the high fuel sample pressure. Due to the high fuel pressures in the ULVFS (450–1300 bar), the O-rings on the rod tended to fail as the O-ring surface was scraped by the rod surface. Additionally, the stepwise movement of the ULVFS piston, which was shown in the thesis by Hellier [225], exacerbated the scraping of the O-rings on the rod. This resulted into sealing failures during early experiments, causing the fuel to leak from the ULVFS into the IFFM**S** and this prevented accurate calculation of the fuel flow from the ULVFS to the injector. The three main reasons for these sealing failures were: the original small rod diameter, the rod surface finish, and insufficiently tight rod-hole tolerance. The small rod diameter limited the cross section of the O-rings available: both 4mm and 6mm rods were tried before the 6mm rod was selected. Stainless steel rods were originally used but they scraped the O-ring surface even when surface polished. Hence a surface- hardened high-carbon steel rod, which was surface-ground, was eventually used. When considering the rod-hole tolerances a

sliding fit H7/g6 was specified, but the manufacturing to such tight tolerance proved difficult. Nevertheless, these improvements solved the leak problem from the high pressure fuel sample past the rod.

The operation of the IFFM**S** during an engine experiments can be described in three stages: beginning, pressurization and experiment. At the beginning of each experiment the IFFM**S** was screwed into the left end of the ULVFS to double up as a cap, after which the sample fuel was fed to the ULVFS. The pistons of ULVFS were on the right-most position to allow the sample fuel to be fed to the left side of the ULVFS cylinder (Figure 12). At this stage, the piston system in the IFFM**S** was on the left-most position having been pushed there either by a previous test or by applying 1.2 bar absolute pressurized air through the air hole 1 (Figure 12). Once the sample fuel was fed to the ULVFS, this sample fuel in the left hand side of the ULFVS pistons was pressurized up to the injection pressure by feeding diesel under the common rail pressure to the right hand side of the ULFVS pistons. The common rail pressure caused the ULVFS pistons to move to the left until the sample fuel was under the injection pressure. After pressurization, the piston system of the IFFM**S** was pushed to its right-most position, where the rod was in contact with the pistons in the ULVFS, as shown in Figure 13. This was done by applying pressurized air through the air hole 2 (Figure 13). The pressurized air connection to air hole 2 was left connected for the duration of the experiment and the air pressure was increased to 1 bar higher than the injection pressure divided by hundred, so as to act as the back-pressure: a systematic study of the back-pressure was conducted and it was concluded that IFFM**S** back-pressure of 1 bar higher than the injection pressure divided by 100 was sufficient to prevent the sample fuel pressure from moving the IFFM**S** rod.

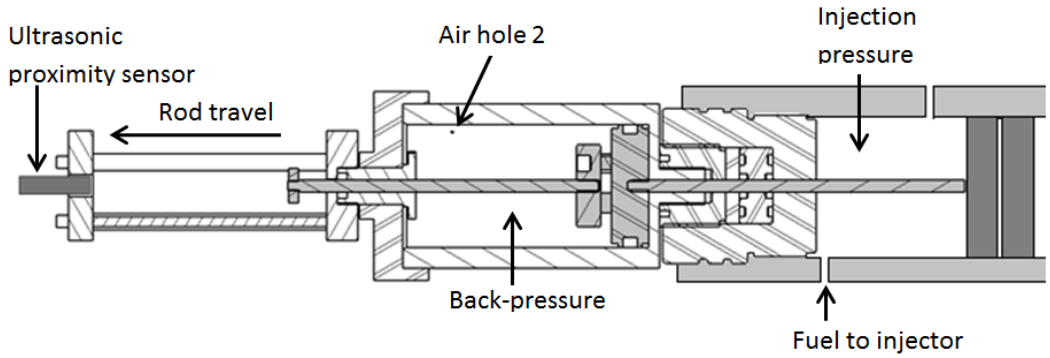

Figure 13. IFFM at the end of an experiment.

During the experiment, the IFFM**S** rod was pushed gradually to the left by the ULVFS pistons, which fed the sample fuel to the injector. The ultrasonic proximity sensor (Figure 13) recorded this movement of a target at the end of the rod (and hence the movement of the rod – see Figure 11 and Figure 12) and sent an analogue output to the low speed DAQ NI card. Based on this signal, the LabVIEW interface calculated the rod travel. In turn, the rod travel measurement allowed the calculation of the sample fuel volume flow ($V_{from\ ULVFS}$ in equation (E 3)) to the injector, based on the known cross sectional area of the ULVFS cylinder and the position of the rod, measured with the ultrasonic proximity sensor. At the end of each fuel sample experiment, the IFFM**S** was screwed out of the ULVFS to allow dismantling and cleaning of the ULVFS.

3.4.3 Injector spill flow measurement

Before deciding to use a mass balance to measure the injector fuel spill flow, several commercial positive displacement fuel flow meters were considered for the measurement of the injector spill flow. However, due to the very small spill flow from the injector (maximum flow about 0.06g/s) and the wide range of fuels tested, very few suitable fuel flow meters were available and these were discarded as either expensive or unreliable options. One such fuel flow meter, a positive displacement meter (Max machinery 213-310), was initially used to measure the injector spill flow, but the required accuracy was not reached despite much effort to do so.

Table 2 2 shows that good repeatability of the fuel flow could not be obtained with this positive displacement meter, and that this meter had an unacceptably large test-to-test standard deviation.

Table 2. Standard deviations of injector spill flow measurements mode with a positive displacement flow meter (five repeat tests were conducted under each test conditions).

Test conditions	Mass based (pulses/g)		Volume based (pulses/cc)	
	Average	Standard deviation	Average	Standard deviation
Initial	22.1	1.41	18.4	3.5
Shorter outlet fuel tube	25.2	1.48	19.5	3.4
Shorter inlet fuel tube	14.9	1.27	11.7	0.9

After the positive displacement meter was discarded as an option, a mass balance (Kern PLS510-3A) continuously monitored with a RS232 interface card was tried and selected to be the instrument that was subsequently used for injector spill flow measurement, due to the good repeatability shown in Table 3 (see Figure 9). The injector spill mass flow value was recorded continuously via the low speed DAQ NI card to the LabVIEW interface and logged against time together with the output from the ultrasonic proximity sensor of IFFMS.

Table 3. Standard deviations of mass balance tests (results of five tests with duration of one minute were conducted during each test series).

Test series number	Average mass (g)	Standard deviation
1	7.59	0.0476
2	7.58	0.0809
3	7.58	1.33E-08

3.4.4 Experimental error of the injection fuel flow measurement

Engine indicated thermal efficiency was calculated as the ratio of the indicated work over one engine cycle to the chemical energy supplied in the fuel during one engine cycle, as shown in section 2.5.1. The measurements of the injection fuel flow measurement system were used as m_F, the mass of fuel injected per engine cycle, and W_C, the power output per engine cycle, was considered as the indicated work output per cycle (W_i) and was calculated as shown in section 2.7.6. The experimental error caused by the measurement of injection fuel flow to the calculation of the engine thermal efficiency was evaluated according to the equation (E 4). In equation (E 4) η_F is the engine thermal efficiency, $V_{from\ Fuel\ System}$ the volume of sample fed to the injector measured by the instantaneous fuel flow measurement system, ρ_{sample} is the sample density measured with a Gay-Lussac bottle, m_{spill} is the mass of spill measured by the mass balance and the carat over $\eta_F$indicates the estimated value of the η_F.

$$\Delta\widehat{\eta_F} = \sqrt{\{[\widehat{\eta_F}(\Delta V_{from\ ULFVS})]^2 + [\widehat{\eta_F}(\Delta\rho_{sample})]^2 + [\widehat{\eta_F}(\Delta m_{spill})]^2\}} \qquad \text{(E 4)}$$

Table 4 presents the experimental errors caused by the three measurements allowing the calculation of injection fuel flow (ultrasonic sensor measurement of the fuel flow from the ULFVS to the injector, density measurement and injector spill flow mass balance measurement) and the total experimental error. The total estimated experimental error in engine thermal efficiency values was estimated as 0.62%, which was concluded to be acceptable. Additionally, it was concluded that the experimental error could not be improved, due to the small quantities of both the fuel supply to the injector and the injector spill.

Table 4. Experimental error in the calculation of engine thermal efficiency.

Instrument	Average value of the measurement	Standard deviation of the measurement	± Total experimental error in engine thermal efficiency (%) caused by the standard deviations of the measurement
Ultrasonic sensor (cm)	na	0.0197	-0.329
Density measurement (g/ml)	6.42	0.0061	-0.524
Mass balance (g)	7.58	0.0737	0.052
Total error (%)	38.09	na	0.62

The actual repeatability of the engine thermal efficiency measurement was also measured experimentally by accumulating the results of 26 repeat reference diesel fuel tests conducted on 13 different days (two measurements each day at start and at end of working day). Table 5 shows that the standard deviation of the measured engine thermal efficiency was 0.47 percentage points. This standard deviation is only 1.2% of the average engine thermal efficiency value of 38.09% and therefore the engine thermal efficiency calculation was judged to be acceptable, as it was concluded that it would be difficult to improve further the experimental repeatability of the efficiency measurement.

Table 5. Repeatability of the engine thermal efficiency

Fuel sample	Injection pressure (bar)	Number of repeat data points	Average efficiency (%)	Standard deviation (percentage points)
Reference diesel	600	26	38.09	0.47

3.5 Instrumentation

Several measurement instruments were utilized to allow monitoring and controlling of the engine operating conditions. The in-cylinder gas pressure was measured by a piezoelectric high-pressure transducer (Kistler 6056AU38) located in a glow plug adapter and connected to a charge amplifier (Kistler 5011). The injection fuel pressure was measured in the high-pressure fuel pipe between the ULVFS and the fuel injector with a thin-film piezoresistive pressure transducer (Gems 3100R2200S2TE000RS). The air intake manifold pressure was measured after an intake air filter with a piezoresistive pressure transducer (Druck PTX 7517-3257), which was also used to peg the in-cylinder pressure measurements at the intake stroke before TDC. The air flow into the intake manifold was monitored upstream of the inlet manifold pressure transducer, by means of the atmospheric air supplied to the engine passing through a positive displacement air flow meter (Romet G40), followed by a plenum damping chamber which had a capacity of approximately 60 litres (approximately 120 times engine displacement). Additionally, the experimental setup included an option to heat the intake air with an inline air heater (Secomak 571) controlled by a proportional integral derivative (PID) controller (CAL 9900). Several heating elements controlled by PID controllers were also installed on both the fuel pipework to the fuel injector and the ULVFS, in order to allow heating the fuel sample before it reached the injector. K-type thermocouples were used to measure the temperature of the heating elements where they contacted the ULVFS external wall surfaces, and to also measure the fuel temperature before injection into the combustion chamber.

The exhaust gas pressure was measured with a piezoresistive pressure transducer (Druck PTX-7517- 3257). The exhaust gas sampling points for the gas analysers were 180 mm downstream from the exhaust port. The gas sample was led via heated lines maintained at 353K to two gas analysers: Horiba MEXA 9100HEGR and Cambustion DMS500. The Horiba system was used to measure the concentrations of CO_2, CO, O_2, UHC and NO_x in the exhaust gas. These concentrations were measured by several methods: CO_2 and CO with a non-dispersive infrared absorption analyser (Horiba AIA-120), O_2 with a magneto-pneumatic cell (Horiba FMA-125), THC with a flame ionisation detector (Horiba FIA OV-04 and Horiba FMA-125) and NOx with

a chemiluminescence analyser (Horiba CLA-150). [226] The particle size distribution and mass and number concentration in the exhaust gas were measured by a differential mobility spectrometer DMS500, which analysed particles in the size range of 5 nm to 1000 nm [227].

Additionally, the composition of several refinery fuel stream samples, used for some of the tests, were analysed by the author with a gas chromatograph-mass spectrometer (Agilent Technologies 5977A Series GC/MSD System).

3.6 Software

A PC user interface NI LabVIEW 2011 was used to record and display the measured experiment data. The temperature and pressure data recordings were carried out via two multifunction data acquisition (DAQ) systems. One of the DAQs was a high speed card (NI PCI-6251) with sampling rate of 1.25MS/s (where S denotes the number of samples) using a single analogue to digital converter and a multiplexer. This card received analogue signals from the pressure transducers of in-cylinder pressure, air inlet manifold, exhaust pipe and fuel line, as well as the engine speed signal from the Cussons test-bed console. These signal values were analysed and logged against the crank angle degrees (CAD) at 0.2CAD intervals (PCI-6251 card was actually triggered by the shaft encoder TDC signal and clocked by the encoder 0.2 CAD pulses. The other DAQ card was a slow speed one (NI PCI-6224) with sampling speed of 250KS/s, and also had a single analogue to digital converter and a multiplexer. This card recorded 10 times per second the values of the signals from nine temperature thermocouples, the ultrasonic sensor of the IFFMS, the air flow measurement and the pressure transducer of the ULVFS fuel sample side. The measurement values were displayed on the LabVIEW screen interface against time with the exception of the air flow measurement, which was used to calculate the mass flow rate of air. Additionally, the Horiba exhaust gas measurements were read via a General Purpose Interface Bus output from the Horiba control unit to a LabVIEW interface and recorded by manually adding a file number stamp, which corresponded to the pressure and temperature record files. DMS500 signals were recorded with Cambustion DMS User Interface software (versions 4.07 and 4.11). The data logged with LabVIEW and the Cambustion DMS User Interface was analysed

mathematically after each experiment using both MathWorks Matlab and Microsoft Excel to calculate the heat release rate, ignition delay, in-cylinder temperature, adiabatic flame temperature and indicated mean effective pressure as described in section 3.7, as well as to calculate engine thermal efficiency according to equation (E2) described in section 2.5.1..

3.7 Analytical methods

3.7.1 Heat release rate

The net heat release rate, denoting the rate at which work was done on the piston plus the rate of sensible internal energy change of the cylinder contents, was calculated according to the first law of thermodynamics, the law of conservation of energy. The net heat release rate (Q_n) was considered as the difference between the chemical energy released to the engine cylinder contents by combustion (Q_{ch}) and the heat transfer (energy dissipation) from the engine cylinder contents (Q_{ht}), as shown in equation (E5). The in-cylinder contents were assumed to be at uniform pressure and temperature and were modelled as an ideal gas. These assumptions allowed the net heat release rate to be calculated as a function of the in-cylinder pressure (p), engine cylinder volume (V) and crank angle (θ), according to the equation (E5). Time was defined in equation (E5) as crank angle degrees (θ) of the engine cycle (from 0 to 720 CAD) and engine cylinder volume (V) at any given crank angle was calculated according to the equation (E6). Values of the ratio of the specific heat (γ) suggested by Heywood [1] were applied: 1.35 during the compression stroke and 1.28 during the expansion stroke. In the equation (E6) V_{clear} is the clearance volume, A_{bore} is the surface area of the bore, l_{conrod} is the length of the connecting rod, r_{crank} is the radius of the crank shaft rotation and the distance between the crank axis and the piston crank pin axis ($l_{ca,ppa}$) was calculate according to equation (E7) [1].

$$\frac{dQ_n}{d\theta} = \frac{dQ_{ch}}{d\theta} + \frac{dQ_{ht}}{d\theta} = \frac{1}{1-\gamma} p \frac{dV}{d\theta} + \frac{1-\gamma}{1} V \frac{dp}{d\theta} \qquad \text{(E 5)}$$

$$V(\theta) = V_{clear} + [A_{bore}(l_{conrod} + r_{crank} - l_{ca,ppa})] \quad \text{(E 6)}$$

$$l_{ca,ppa} = \text{acos}(\theta) + \sqrt{{l_{con\,rod}}^2 - {r_{crank}}^2 \sin^2(\theta)} \quad \text{(E 7)}$$

3.7.2 Ignition delay

Ignition delay was defined as the time interval, in CAD, between the start of injection (SOI) and the start of combustion (SOC). SOI was considered to occur when the injector actuating signal was sent via EmTroniX to the injector. The heat transfer from the cylinder gases (heat dissipation) during the combustion process is a relatively small fraction (about 10-15%) of the released fuel energy and therefore the SOC was defined as the time of the minimum cumulative heat release rate value, as shown in Figure 14. The heat losses become significant after combustion has been completed and the piston travelled down the engine cylinder, causing a reduction in the cumulative heat release rate within the engine cylinder. Hence, the end of combustion (EOC) was considered to be the time of the maximum cumulative heat release rate value (Figure 14).

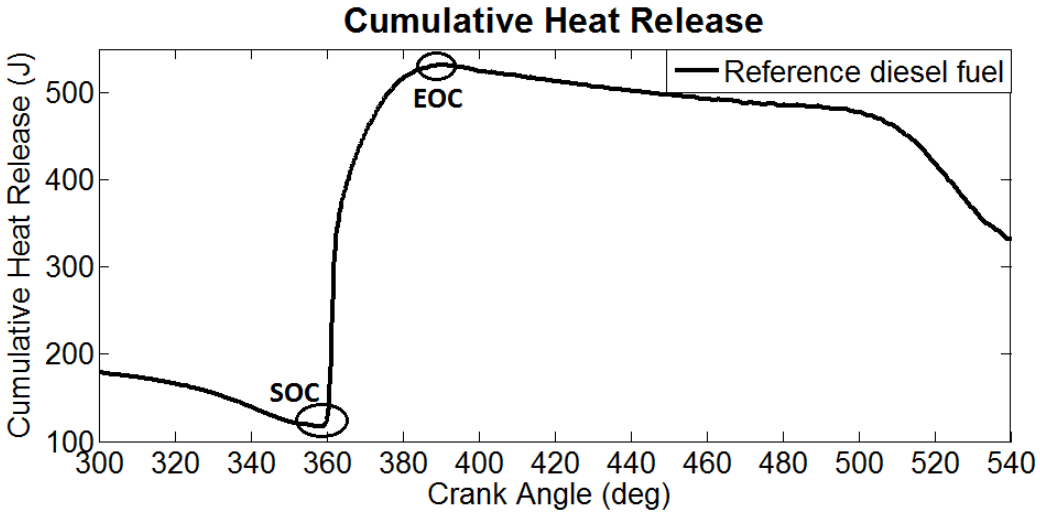

Figure 14. A typical cumulative heat release rate diagram for diesel fuel combustion.

3.7.3 Combustion phasing

The combustion split into the premixing-controlled and the diffusion-controlled combustion phases was carried out by a graphical method based on the HRR curve. Premixed fuel-air burns rapidly at the beginning of combustion, while the diffusion controlled phase that follows occurs over a longer period of time with lower heat release rate. Therefore, the time at which the premixing controlled phase ended was defined as the highest maximum value of the second derivative of HRR (ddHRR), an example of which is shown in Figure 15. The percentage of fuel burned during the premixing controlled phase, usually denoted as the premixed burnt fraction or the premixed phase, was calculated as the ratio of the cumulative HRR that occurred between SOC and the end of the premixed phase to the measured chemical fuel energy injected during the engine cycle.

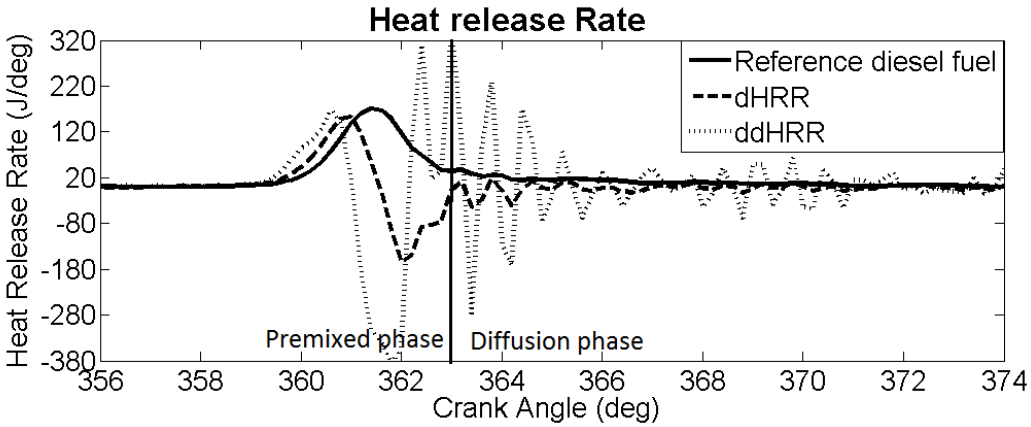

Figure 15. A typical heat release rate diagram with the first (dHRR) and second (ddHRR) derivatives (the vertical line indicates the switch-over point between the combustion phases).

3.7.4 Maximum average in-cylinder temperature

The maximum average in-cylinder temperature, also known as global gas temperature, was calculated from the instantaneous in-cylinder temperature (T_{cyl}), which in turn was calculated for any given time using the ideal gas law as shown in equation (E 8). In the equation (E8) p_{cyl} is the cylinder pressure, V_{cyl} is the cylinder

volume, n_{air} is the amount of air in the combustion chamber and R is the gas constant. Combustion conditions were assumed to be lean and the number of air moles present in the engine cylinder were estimated by the air flow rate measurement (see subsection 3.4). The recorded values of in-cylinder temperature for hundred consecutive engine cycles were averaged for the calculation of the maximum average in-cylinder temperature value.

$$T_{cyl} = \frac{p_{cyl} * V_{cyl}}{n_{air} * R} \quad \text{(E 8)}$$

3.7.5 Adiabatic flame temperature

The adiabatic flame temperature at constant pressure was calculated from the iteration of the equivalence of the absolute enthalpy of the reactants (H_{react}) at the initial in-cylinder temperature (T_i) and that of the products (H_{prod}) at the adiabatic flame temperature (T_{ad}), as shown in equation (E9)

$$H_{react}(T_i, p) = H_{prod}(T_{ad}, p) \quad \text{(E 9)}$$

The iteration was conducted as presented by Turns [162]. The initial temperature was defined as the minimum average in-cylinder temperature during the ignition delay period and the change in the enthalpy during complete combustion was calculated according to the Joback method [228].

3.7.6 Indicated mean effective pressure

IMEP was calculated as the ratio of the indicated work output per engine cycle (W_i) and the swept volume (V_{swept}) according to the equation (E 10) [1]. The indicated work output per cycle (W_i) was calculated as the integral of in-cylinder pressure (p) with respect to the cylinder volume (V), whereas the swept volume (V_{swept}) was

calculated from the area of the engine cylinder bore (A_{bore}) and the piston stroke length ($l_{piston\ stroke}$).

$$IMEP = \frac{W_i}{V_{swept}} = \frac{\int pdV}{A_{bore} * l_{piston\ stroke}} \quad \text{(E 10)}$$

3.8 Repeatability and experimental error

The repeatability of the combustion experiments and the exhaust gas composition analysis were estimated from repeated experiments with the reference diesel fuel. Reference diesel properties are presented in Appendix I. The repeated tests with reference diesel fuel on different days and at the same engine running conditions, allowed evaluation of average values, standard deviation and the standard error of the mean of the exhaust gas emission measurements. A similar approach was used for the valuation of the repeatability of the engine thermal efficiency measurements. These repeatability values are quoted in the various chapters of the thesis, where appropriate. To minimize repeatability errors, each test series was conducted within as short a time period of time as possible. That is, for example, tests of a homologous set of fuels were conducted on consecutive days and in as small a number of days as possible. In the limited number of days, when some data appeared to be outlying on result plots, the tests for an outlying data point were repeated to confirm or otherwise of the outlying point was there due to an experimental malfunction. Only in a very limited number of a handful of cases, an outlying point was found to be due to a malfunction of equipment or an operation error.

3.9 Constant injection timing test conditions

All combustion experiments of this PhD project were conducted with constant injection timing. Initial tests with some of the oxygenated fuel molecules, which were assumed to be difficult to ignite, showed that an injection timing of 7.5 CAD before TDC allowed long enough air-fuel mixing time for these difficult-to-ignite molecules to ignite. Therefore, an injection timing of 7.5 CAD BTDC was used throughout the

combustion tests of this PhD project. During these tests, the injection duration was varied so as to ensure a constant desired IMEP value of 4 bar, and in a small number of cases, a desired value of IMEP greater than 4 bar (i.e. 6 bar).

Chapter 4

Systematic study of the effect of the hydroxyl functional group in alcohol molecules on compression ignition and exhaust gas emissions

4.1 Introduction

The low temperature chemistry (600-1000 K) leading to auto-ignition is well established for hydrocarbons, which is the main component of fossil diesel fuels. However, the low temperature kinetics of alcohols, which are alternative fuel molecules, is less well understood. The differences in ignition delay between hydrocarbons and alcohols are mainly caused by the higher electronegativity of the oxygen atom in the alcohol molecule compared to that of a carbon or hydrogen atom in the corresponding hydrocarbon molecule. This higher electronegativity of the oxygen atom affects the bond strengths of adjacent atoms in the fuel molecule and hence changes the kinetic combustion mechanisms. Additionally, the different molecular structure affects the formation of exhaust gas emissions, partially through a lengthening of the ignition delay. [27] Several authors have investigated experimentally with equipment such as rapid compression machines and jet-stirred reactors the combustion of higher alcohols [71,203,229] and discussed their ignition delay times [72,74,230,231], but a significantly low number of engine studies have been conducted on this subject [86–89,232,233]. Furthermore, the engine studies of higher alcohols have generally investigated the combustion of alcohol-diesel blends, instead of the combustion of higher alcohol molecules.

This chapter discusses the results of a systematic experimental study conducted in a single cylinder compression ignition research engine using several different higher alcohol molecules. Seventeen alcohol molecules, which could potentially be used in compression ignition engines as biofuels, were investigated. These alcohol molecules included primary alcohols with carbon chain length of eight to 16 carbon atoms, alcohols with the hydroxyl functional group in different positions within the molecule, unsaturated alcohols and branched alcohols. Ignition delays observed in the combustion engine experiments are compared with low temperature ignition mechanisms found in published literature. Hydrogen abstraction from the fuel

molecule and the following isomerization, following fuel radical oxidation, have been shown to be the two main initial reactions with significant effect on the duration of ignition delay [53,107]. Therefore, the comparison between ignition delays of different fuel molecules was carried out by discussing the rates of these two reactions. Corresponding alkanes and alkenes were also tested to provide reference data for comparison with the ignition and emissions data of alcohols. The analysis of exhaust gas emission focuses on NOx and PM. The results of this study may be used in the development of future biofuels by identifying alcohol molecular structures with desirable ignition properties and combustion profiles and which could lead to lower pollutant exhaust emissions.

4.2 Experimental methods

4.2.1 Experimental conditions

All the combustion experiments were conducted with a fixed injection timing of 7.5 CAD before TDC, engine speed of 1200 rpm, 600 bar injection pressure, and 4 bar IMEP. Each test day was started and ended with a reference diesel fuel test, so as to detect any day to day drift in the experimental equipment and instrumentation. Additionally, the reference diesel fuel tests were used to generate a historic record of day to day variations in the results obtained with the same fuel and same experimental procedures. When considering the repeatability of emission measurements, the mean value for NO_x was 918ppm, standard deviation of mean 28.6 and standard error of mean 7.2. The corresponding values for PM mass were 0.0552µg/cc, 0.00716 and 0.00179; for the number of particulates 57.6 $*10^6$N/cc, $6.96*10^6$ and $1.74*10^{6.}$

Most of the combustion experiments were conducted with the test fuels maintained at ambient conditions (305 ±3K). For the tests with fuel molecules which had melting points above this temperature, the fuel in the injection system and the supply pipes was heated to 343 ±3K. The test temperature for each fuel experiment can be seen in Appendix II. To determine the effect on combustion and exhaust emissions of heating a fuel from 305K to 343K, three molecules were tested at both temperatures (undecane, 1-decanol and 1-undecanol). The 38K rise in temperature caused only a small decrease in ignition delay (0, 0.23, 0.06 CAD, respectively). By comparison,

the day-to-day standard deviation of ignition delay with reference diesel fuel was found to be 0.1 CAD. Therefore, the changes in ignition delay caused by varying the fuel temperature by 38K were deemed to be of low significance. Nevertheless, differences in fuel temperatures are noted in the results section for information, where applicable.

4.2.2 Fuel molecules investigated

Seventeen alcohols and nine hydrocarbons of various chain lengths from C8 to C16 were studied experimentally. The molecular structures of these fuel molecules are shown in Table 6 and the physical properties of the fuel molecules investigated are listed in Appendix II [234–238].

The purpose of the experiments was to investigate the effects of the following molecular structural features on combustion and exhaust emissions:

a) Adding a hydroxyl group to an alkane
b) Position of a hydroxyl group within the fuel molecule
c) Degree of unsaturation in alcohol molecule
d) Degree of branching in alcohol molecule

Table 6. Molecular structure of the fuel molecules.

Fuel molecule	Molecular structure
Alkanes	
Octane	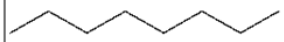
Nonane	
Decane	
Undecane	
Dodecane	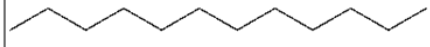
Tetradecane	
Hexadecane	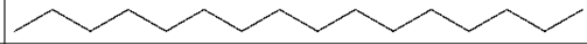
Alkenes	
1-Octene	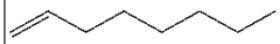
1-Decene	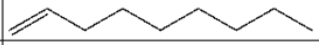
Alcohols	
1-Octanol	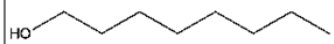
2-Octanol	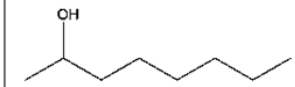
3-Octanol	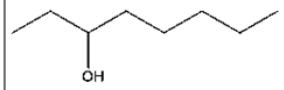
1-Octen-3-ol	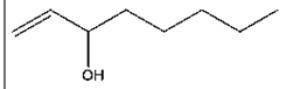
1-Nonanol	
2-Nonanol	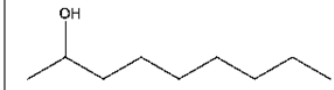
5-Nonanol	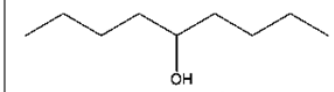
1-Decanol	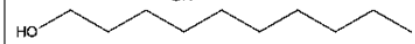
1-Decen-3-ol	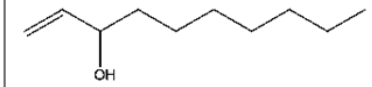
1-Undecanol	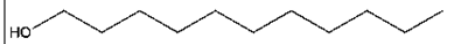
2-Undecanol	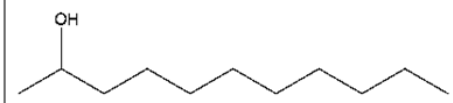
10-Undecen-1-ol	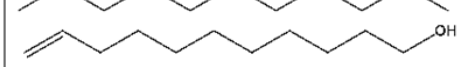
3,7-Dimethyl-1-octanol	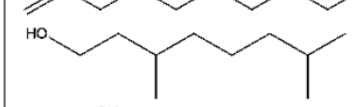
3,7-Dimethyl-3-octanol	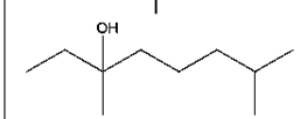
1-Dodecanol	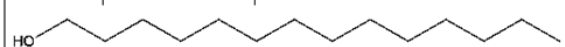
1-Tetradecanol	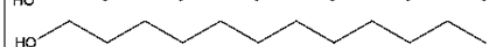
1-Hexadecanol	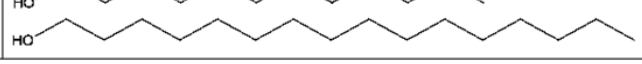

4.3 Results and discussion

4.3.1 Effect of the carbon chain length

Figure 16a shows the ignition delay for primary and secondary alcohols and for comparison the delays for alkanes and the reference diesel fuel. The figure shows that ignition delay became lower with increasing carbon chain length for both the hydrocarbons and the alcohols. It is suggested that this increase in ignition delay occurs due to the changes in the rate of hydrogen abstraction and the ability of the fuel molecule to isomerize.

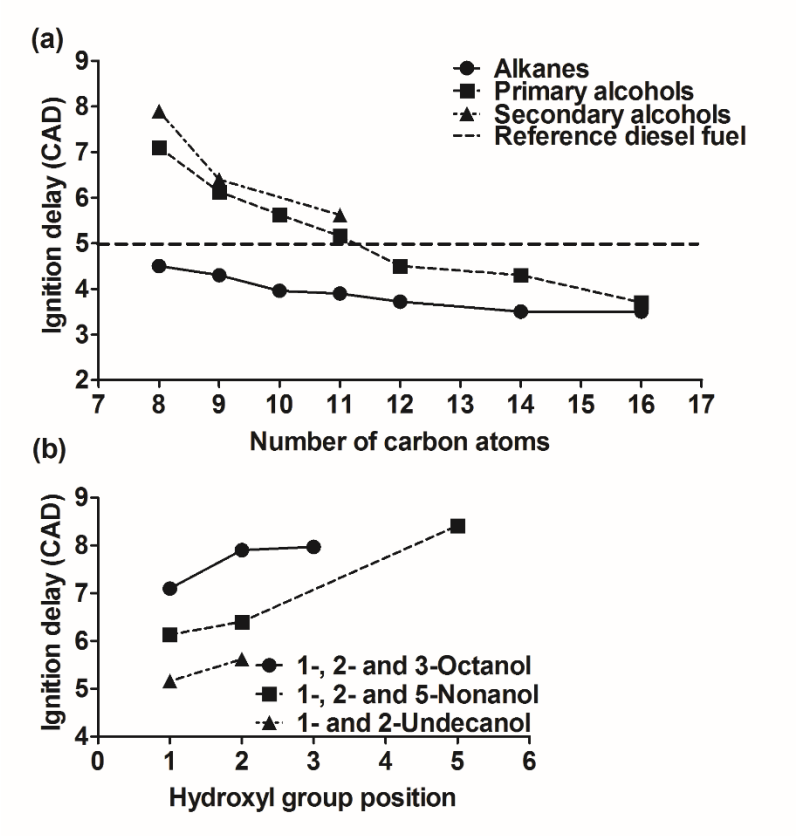

Figure 16. (a) Ignition delays for straight chain saturated molecules (secondary alcohols have the hydroxyl group bonded to the second carbon atom of the carbon chain); (b) Effect on ignition delay of moving the hydroxyl group along the carbon chain of a molecule.

According to Westbrook [107] compression ignition in engines in the temperature range of 850K to 1200K occurs principally through the H_2O_2-mechanism This mechanism involves the production of two hydroxyl radicals (OH) for each hydrogen radical consumed, and it therefore leads to a rapid increase in the radical pool. The availability of hydrogen radicals, through abstraction from the fuel molecule, is therefore of key importance to the H_2O_2-mechanism. In general, hydrogen abstraction from hydrocarbon chain occurs, firstly, from the weakest C-H bonds. In the case of alkanes H-abstraction is easiest from the tertiary carbon atoms, followed by the secondary and the primary carbon atoms [53].One could, therefore, expect that as the chain length increases and, consequently, the number of secondary carbon atoms increases, the ease of H-abstraction from the longer chain molecule would generally increase. It is suggested that this is reflected in the progressive shortening of ignition delay with longer chain molecules shown in Figure 16a.

The fuel radical that remains after H-abstraction is oxidized and then undergoes isomerization, leading to branching reactions which enhance radical pool formation further. Isomerization occurs through transition rings, with six-membered transition rings being a preferred state [53,107]. As the fuel molecule chain length increases, the propensity of the molecule to form six-membered transition rings and to isomerize increases. It is therefore suggested that this improved propensity to isomerize results in further shortening of the ignition delay for longer molecules, seen in Figure 16a.

4.3.2 Effect of the hydroxyl group

Primary alcohols (R-CH_2-OH) are observed from Figure 16a to have higher ignition delays than corresponding alkanes with the same number of carbon atoms. One way to explain the greater resistance of primary alcohols to ignition, compared to that of the corresponding alkane, is to consider a primary alcohol as an alkane with the primary hydrogen atom substituted by a hydroxyl group. This is illustrated for octane and 1-octanol in Figure 17. As it will become apparent from the following discussion, the introduction of the hydroxyl group at the end of the molecule has significant

knock-on effects on the adjacent carbon-carbon (C-C) and carbon-hydrogen (C-H) bonds, weakening some of them and strengthening some others.

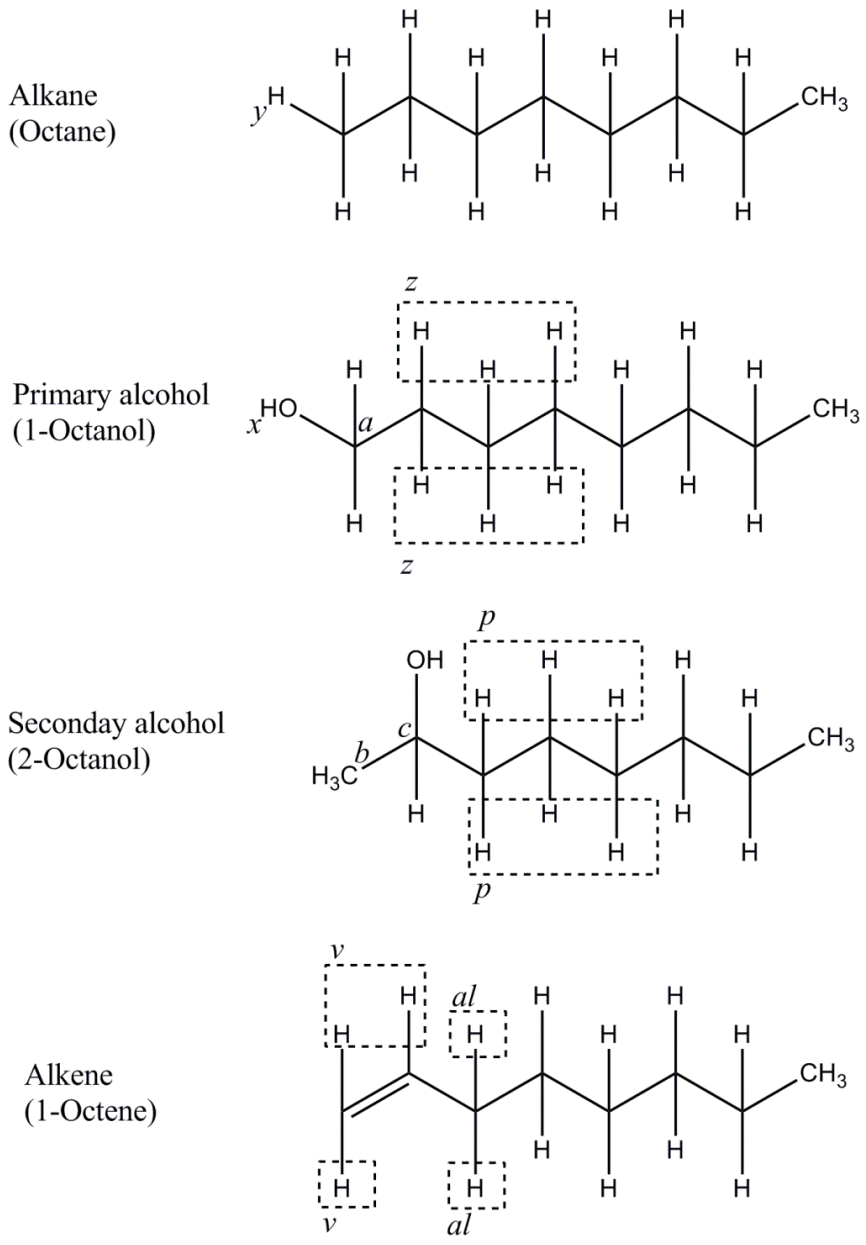

Figure 17. Molecular structures of an alkane, an alcohol and an alkene molecule, with C8 molecules used as the example.

Consider, first, the bonding strength between the oxygen and hydrogen atoms of the hydroxyl group. Referring to Figure 17, the hydrogen atom of the hydroxyl group

(labelled x in 1-octanol) is more difficult to abstract than the corresponding hydrogen atom in the alkane molecule (labelled y in octane) due to the higher electronegativity of an oxygen atom compared to that of a carbon atom. As a result, the hydrogen radical pool associated with compression-ignition of the alcohol becomes somewhat smaller than that of the corresponding alkane, and the compression-ignition delay can be expected to increase somewhat [27]. Next, consider the carbon chain and the abstraction of the six hydrogen atoms labelled z in 1-octanol (Figure 17). The presence of the OH group (rather that the corresponding y H-atom in Octane - Figure 17), makes the abstraction of these six hydrogen atoms more difficult than the abstraction of the corresponding hydrogen atoms in the alkane molecule; this resistance to hydrogen abstraction is related to the progressive weakening of the C-C bonds of the 3 carbon atoms adjacent to the carbon onto which the electronegative OH group is bonded. As a result, one would expect the ignition delay to, again, increase somewhat. Lastly, the introduction of the OH group has one converse effect in lowering the compression-ignition delay, by weakening the two H-C bonds of the primary carbon atom (labelled a in 1-octanol - Figure 17). The weakening of these two H-C bonds has been suggested to occur because the electrons of these two carbon atoms are closer to the hydroxyl group thus decreasing the degree to which they participate in forming the two H-C bonds. The changes in H-C bond strengths described above were demonstrated by Heufer et al. [71] using shock tube and RCM experiments conducted with n-pentanol and n-hexanol. Additionally, this order of the H-C bond strengths was supported by the experimental study of 1-hexanol combustion in an opposed-flow diffusion flame conducted by Yeung and Thomson [239].

As mentioned previously, the ease or difficulty of hydrogen abstraction controls the magnitude of the hydrogen radical pool and, thereby, affects the period of the compression-ignition delay. There is also another way in which the presence of the hydroxyl group affects ignition delay. That is the ability of a fuel radical to initiate the further branching reactions through isomerization. It has been demonstrated [240,241] that the reaction between an α-hydroxyalkyl radical (R·-CHOH) (formed through hydrogen abstraction from alpha carbon atom) with oxygen may produce an aldehyde (R-CHO) and an HO_2 radical. Hence, the oxidation of an α-hydroxyalkyl radical appears to lead mainly to chain propagation reactions, instead of chain

branching reactions through isomerization, as is the case with alkanes. This suppresses the low temperature reactivity of primary alcohols and lengthens their ignition delay further, in comparison to alkanes.

4.3.3 Position of the hydroxyl group

Figure 16a shows that the secondary alcohols (R- CHOH-CH3) have slightly longer ignition delays than the primary alcohols. It should be noted that these secondary alcohols have the hydroxyl group bonded to the second carbon atom of the carbon chain. The longer delays of secondary alcohols are believed to be partly due to the substitution of a secondary hydrogen atom by the hydroxyl group. This is illustrated in Figure 17 for 1-octanol and 2-octanol. Based on the results of Heufer et al. [71] and Yeung and Thomson [239], the hydroxyl group can be expected to: weaken the C-H bond for the alpha carbon atom (labelled c in 2-octanol – Figure 17); strengthen the C-H bonds for the adjacent primary carbon atoms (labelled b in 2-octanol –Figure 17); and strengthen the C-H bond for the three neighbouring secondary carbon atoms, making their hydrogen atoms more difficult to abstract (labelled p in 2-octanol – Figure 17). Therefore, taken together, the effect of the OH group is to make the overall H-abstraction from secondary alcohols more difficult than from primary alcohols and reduces the rate of radical pool formation. As a result of the smaller pool of hydrogen radicals available for further reactions the duration of ignition delay for secondary alcohols is longer in comparison to that for primary alcohols.

Next, consider the ability of a secondary alcohol radical, which is formed in the H-abstraction, to initiate further branching reactions through isomerization. According to Sarathy et al. [240], oxidation of a secondary alcohol radical after H abstraction from the alpha carbon atom usually produces a methyl ketone and an HO_2 radical. This leads to lower reactivity of the secondary alcohols compared to that of alkanes. However, no comprehensive comparison between the duration of further reactions of the methyl ketone and an aldehyde, which is formed during the oxidation of a corresponding primary alcohol radical, was available in the literature. Therefore, it remains unclear whether changes in the ability of a fuel molecule to isomerise contributed to the change in ignition delay observed between secondary and primary alcohols in Figure 16a.

The effect of moving a hydroxyl group further along the carbon chain of alcohols beyond the first and second carbon atoms of the chain was investigated with molecules of three different chain lengths. Figure 16b shows the effect of moving a hydroxyl group along the carbon chain of an octanol from the first carbon atom in the chain to the second and then to the third carbon atom. Similarly, a hydroxyl group was moved from the first carbon of a nonanol to the second and to the fifth carbon; and, in the case of Undecane, from the first carbon to the second carbon. It was observed that moving the hydroxyl group towards the centre of the carbon chain increased the ignition delay, as can be seen from Figure 16b. It is suggested that this greater resistance to ignition is due to reduced length of the un-substituted carbon chains on either side of the hydroxyl group. These shorter carbon chains have a higher number of secondary carbons that are affected by the hydroxyl group, which will result in slower overall H-abstraction and thus in longer ignition delay. Additionally, the ability of a fuel molecule to form six-membered transition rings and go through isomerization reactions, decreases with the reducing length of the un-substituted carbon chains.

4.3.4 Degree of unsaturation

To assess the effect on ignition delay of unsaturation in an alcohol both saturated and unsaturated C8, C10 and C11 alcohols were tested. For comparison, two alkenes, namely 1-octene and 1-decene were tested and their ignition delays compared to those of the corresponding saturated hydrocarbons, namely octane and decane. The alkenes were observed from Figure 18a to have longer ignition delays than the alkanes of same carbon chain length. This result is supported by several previous studies, for example those of Vanhove et al.[242] and Mehl et al. [104]. One way to explain the increase in ignition delay caused by the addition of a double bond is to consider the changes in the C-H bond strengths of the neighbouring carbon atoms. This is illustrated in Figure 17 for octane and 1-octene.

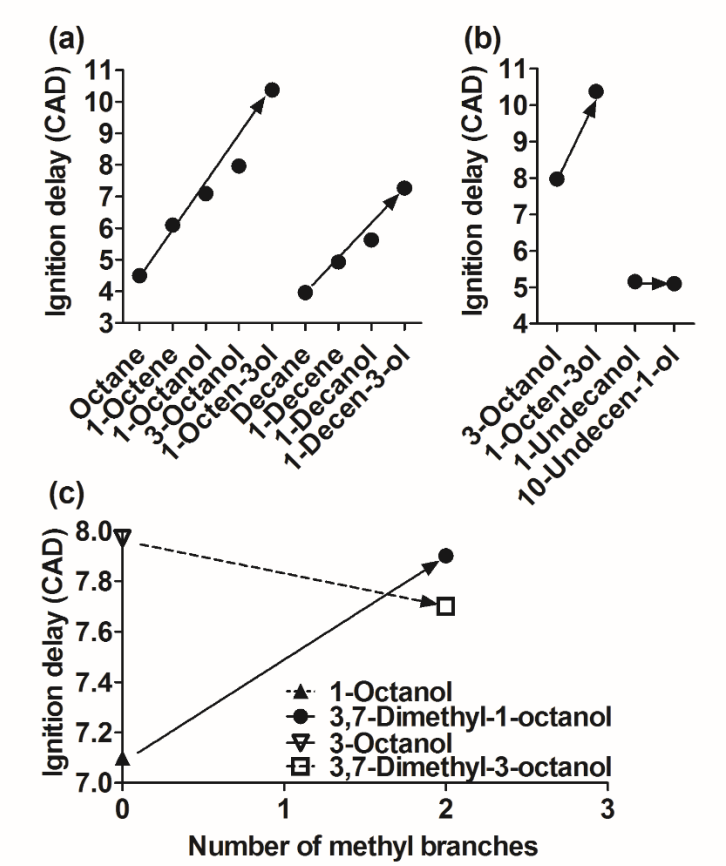

Figure 18. Ignition delays for molecules with different (a, b) degrees of unsaturation (arrows show roughly the direction of adding a double bond to a saturated molecule); (c) levels of branching (arrows show the direction of adding two methyl groups to a molecule with straight carbon chain).

A double bond affects the C-H bond strengths of both the three vinylic (labelled v in 1-octene -Figure 17) and the two allylic carbon atoms (labelled al in 1-octene - Figure 17). The vinylic C-H bonds are stronger than the corresponding C-H bonds of an alkane, which makes the H-abstraction from these sites more difficult and, thereby, increases the ignition delay of alkenes compared to alkanes. In the case of allylic C-H bonds the C-H bonds are weaker than the corresponding C-H bonds of an alkane and hence the H-abstraction is less difficult than from the corresponding carbon atom of an alkane. This makes the allylic C-H bond the favoured site for H-abstraction from alkenes. Superficially this may appear to make compression ignition easier and shorten the ignition delay. However, the chemistry is complicated by the oxidation of hydrocarbon radicals left after the abstraction of the allylic hydrogen atoms. The

oxidation reactions results in intermediate alkyl peroxy radicals with weak C-O_2 bonds. Due to the weak C-O_2 bonds, the alkyl peroxy radicals dissociate easily back to hydrocarbon radicals and molecular oxygen, instead of initiating the isomerization reaction sequence that leads to further branching reactions in the case of alkane radicals. Therefore, the dissociation of the alkyl peroxy radicals decreases the formation rate of the radical pool significantly, during alkene compression-ignition, compared to compression ignition of the corresponding alkane. Hence the relatively easy H-abstraction from an allylic site does not decrease the ignition delay of an alkene compared to an alkane, but rather increases it somewhat. These changes in C-H bond strengths of an alkene have been observed for example through kinetic modelling by Westbrook et al. [65].

The effect of unsaturation in alcohols on ignition delay was investigated though comparison of the following pairs: 3-octanol and 1-octen-3-ol and 1-undecanol and 10-undecen-1-ol, as shown in Figure 18b. Adding one double bond to the alcohol structure increased the ignition delay for the C8 alcohol, as was expected based on the previous comparisons between C8 and C10 hydrocarbons. Figure 18b shows that the increase in the alcohol chain length from C8 to C11 reduces the ignition delay substantially, from about 8 CAD to approximately 5 CAD. Figure 18b also shows that adding a double bond to the undecanol alcohol had no effect on ignition delay. It is therefore possible that the longer chain length of the C11 alcohol compared to that for the C8 alcohol eliminates any additional impact that the addition of a double bond might have on ignition delay.

The effect of potential interaction between the hydroxyl group and a double bond was investigated further by comparing the ignition delays of several C8 and C10 molecules. This was carried out by comparing octane with 1-octene and 1-octanol; and by a similar comparison of the corresponding C10 molecules in Figure 18a. It can be seen from Figure 18a that adding a double bond to the primary carbon atom of octane to form 1-octene increases the ignition delay less than the addition of a hydroxyl group to form 1-octanol. This result is also confirmed in Figure 18a in the case of decane, where the addition of a double bond to the first carbon atom of decane increases the ignition delay less than the addition of a hydroxyl group. Interestingly, adding a hydroxyl group to the first carbon atom of 3-octanol to form a 1-octen-3-ol results in a significantly higher ignition delay than for any of the other molecule

configurations. Similarly high ignition delay is observed for 1-decen-3-ol. Taken together, these results suggest that the two structural features, degree of unsaturation and a hydroxyl group, when combined tend to increase the ignition delay of a fuel molecule very substantially.

4.3.5 Degree of branching

Figure 18c shows that the addition of two methyl branches to 1-octanol to form 3,7-dimethyl-1-octanol increases the ignition delay. This result was expected based on several previous studies regarding alkane branching, such as those of Silke et al. [243] and Ribaucour et al. [244] with RCM. The longer ignition delays of branched molecules can be explained by the stabilizing effect of branching due to greater electron delocalisation, as was shown among others by the calculations of Kemnitz et al.[62]. The greater stability of the fuel molecule results in slower H-abstraction in addition to the smaller number of secondary hydrogen atoms available for abstraction in branched molecule compared to straight chain molecules. Additionally, according to Ribaucour et al [244], branching inhibits isomerization by reducing the number of sites available for transition ring formation. Both of these changes in low temperature combustion kinetics will result in slower formation of a radical pool large enough to sustain ignition and, therefore, increase the ignition delay of branched molecules compared to that of the straight chain molecules with same carbon chain length.

Returning to Figure 18c, the figure does not show the same trend of increased ignition delay when two branches are added to 3-octanol to form 3,7-dimethyl-3-octanol. Instead, Figure 18c shows a decrease in ignition delay which can be explained by a two-stage pattern of ignition of 3,7-dimethyl-3-octanol. Although the first ignition occurred early at 7.70 CAD, the second, main ignition occurred later, resulting in a significant increase in ignition delay to about 13.5 CAD, which falls into line of a trend of branching increasing the ignition delay. The rather long ignition delay of 13.5 CAD, corresponding to the second main ignition, is believed to arise because the hydroxyl group in 3,7-dimethyl-3-octanol is bonded to the same carbon atom as the methyl group. As a result, there is one less secondary hydrogen atom available for H-abstraction compared to 3,7-dimethyl-1-octanol, reducing the hydrogen radical pool and thus delaying the main ignition. Furthermore, a hydroxyl group in the

middle of the carbon chain is likely to hinder the isomerization reactions more than when the hydroxyl group is bonded to the end of the carbon chain. These two effects are expected to have hindered the growth of the radical pool, causing the ignition delay to increase.

4.3.6 Effect of fuel molecular structure on heat release rate

The rate at which energy is released during combustion can have a significant effect on engine performance, affecting such aspects as thermal efficiency and formation of pollutant emissions [1]. The three key parameters of heat release are as follows: the fraction of the total energy released during the premixed combustion phase; the peak value of the heat release rate (pHRR); and the timing of the pHRR. Figure 19 shows the effect of ignition delay on these three parameters for all of the investigated molecules, excluding 3,7-dimethyl-3-octanol and 1-octen-3-ol. These two molecules were excluded due to their unusually long ignition delays and double-ignition.

Figure 19a shows that the ignition delay has a strong positive correlation with the fraction of the fuel burnt in the premixed phase, as one would expect, since longer delays result in a greater amount of premixed fuel-air mixture, which combusts rapidly after ignition. With the experiments conducted with fixed injection timing of 7.5 CAD and ignition delays changing from about 4 to 8 CAD, much of the rapid premixed phase combustion takes place close to TDC, in near constant-volume conditions. It is therefore not surprising that Figure 19b shows that longer ignition delay, and therefore greater amounts of rapidly combusted premixed mixture, resulted in higher peak heat release rates. The moderate slope of this peak HRR curve for ignition delays longer than 7 CAD is probably due to the peak HRR occurring further away from TDC (as shown in Figure 19c), during the expansion stroke and increasing in-cylinder volume.

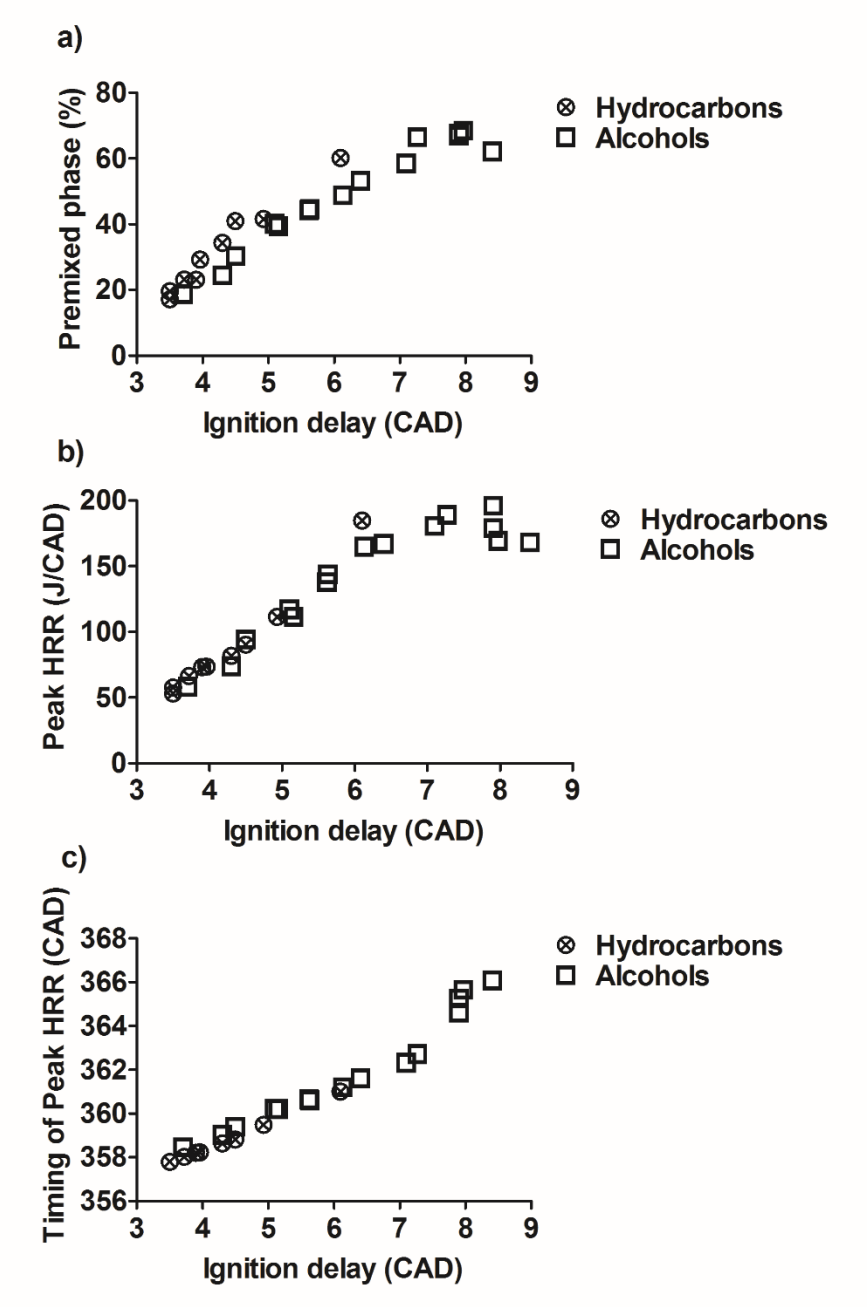

Figure 19. Effect of ignition delay on (a) premixed phase, (b) value of pHRR and (c) timing of pHRR for the tested fuel molecules, excluding 1-octen-3-ol and 3,7-dimethyl-3-octanol.

4.3.7 Effect of fuel molecular structure on nitrogen oxides

NO_x emissions form mainly according to the Zeldovich mechanism, which is exponentially highly dependent on in-cylinder temperature and less so on the availability of oxygen [245]. In general, higher in-cylinder temperatures and higher availability of oxygen increase the formation rate of NO_x emissions. Longer ignition delays are observed from Figure 20a to result in higher average in-cylinder temperatures, for the reasons discussed in the previous section. It is therefore somewhat surprising that the generally positive correlation between the NO_x emissions and the maximum average in-cylinder temperature of Figure 20b shows a significant amount of scatter when all of the investigated molecules are considered together. However, when molecules were split into subgroups based on their molecular structure strong positive correlations were observed for hydrocarbons, primary alcohols and secondary alcohols. When all the data was considered together, considerable scatter was also observed for the correlation between NO_x emissions and ignition delay (Figure 20c), as well as between NO_x emissions and premixed phase (Figure 20d) for all molecules; whereas strong correlations were observed within the subgroups from both of these figures. The strong correlations when subgroups shown in Figure 20a are considered, suggest that the molecular fuel structure has a significant effect on NO_x emissions through other factors than the maximum average in-cylinder temperature and ignition delay. These other factors may include the local air-fuel ratio, which is affected by the fuel physical properties through e.g. the efficiency of fuel-air mixing.

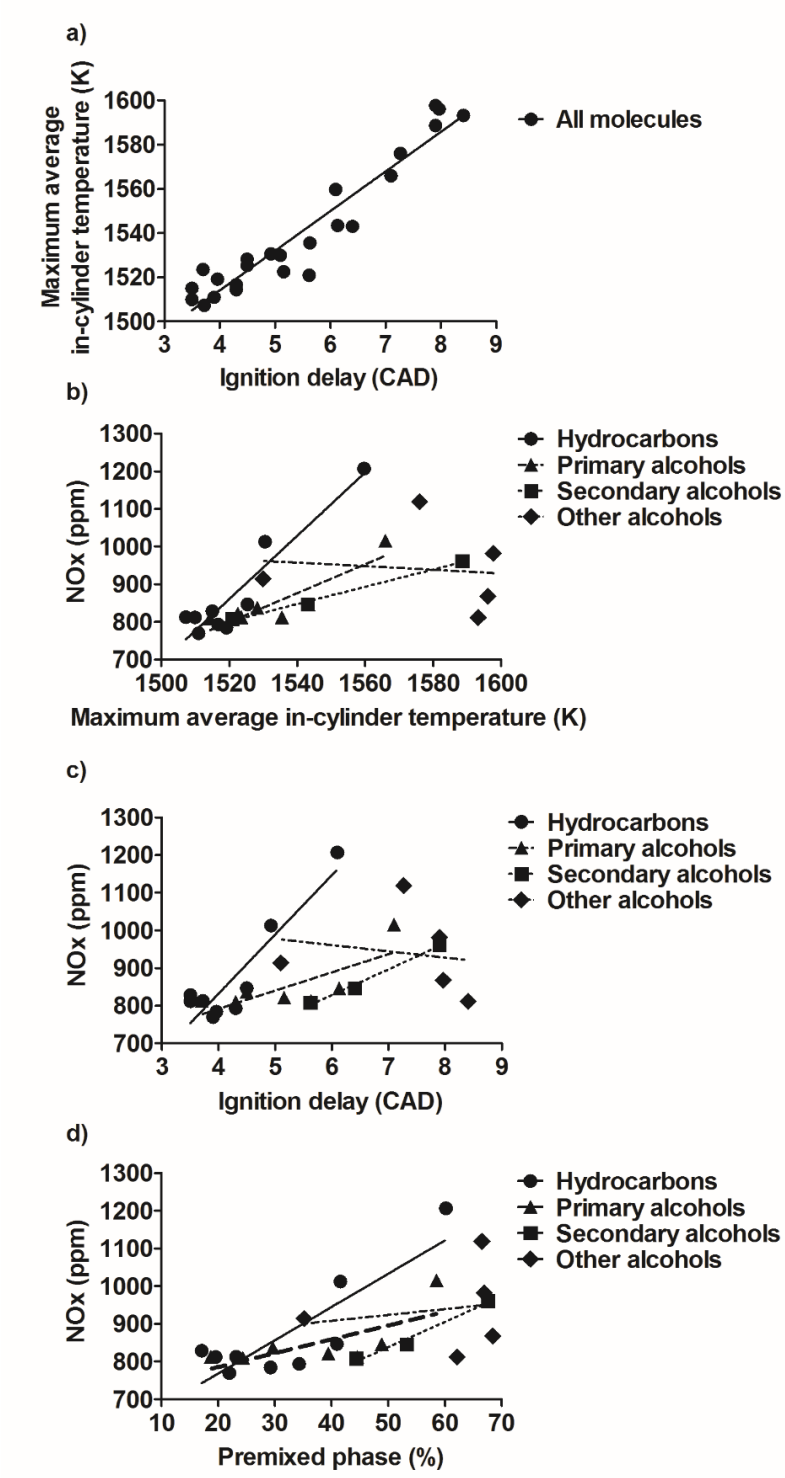

Figure 20. Correlation between (a) maximum average in-cylinder temperature and ignition delay, and (b, c) the effect of both of these, as well as (d) the size of premixed combustion phase, on NO_x emissions (1-octen-3-ol and 3,7-dimethyl-3-octanol excluded).

A similar observation could also be made from Figure 21a, which shows no conclusive correlations between NO_x and adiabatic flame temperatures for the tested molecules. However, if the data point for Octane with an unexpectedly high NO_x value (847 ppm) was excluded from Figure 21a, a weak positive correlation (R-square of 0.24) would be observed for the alkane molecules. A weak positive correlation (R-square of 0.33) was also observed for the tested alcohols (Figure 21a). The adiabatic flame temperatures were calculated for a stoichiometric mixture at constant pressure assuming no dissociation [162].

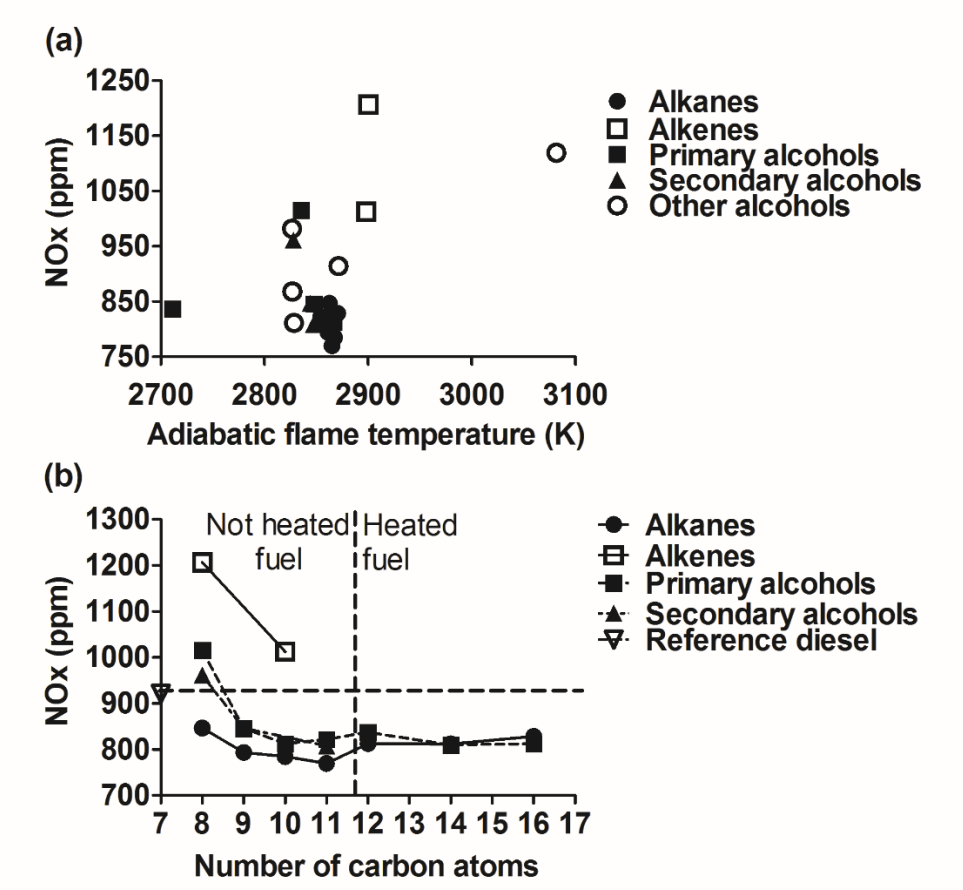

Figure 21. Effect on NO_x emissions of (a) adiabatic flame temperature and (b) the number of carbon atoms in a fuel molecule (excluding 1-octen-3-ol and 3,7-dimethyl-3-octanol).

Following on from the somewhat unexpected weak correlations between NO_x and maximum average in-cylinder temperature and adiabatic flame temperature when all molecules were considered together and the strong correlations within subgroups, further analysis of the data was carried out. Figure 21b shows a tendency for NO_x to decrease with increasing carbon chain length, and thus with decreasing ignition delay, for molecules with chain lengths shorter than 11 carbon atoms. For molecules with 12 or more carbon atoms the NO_x concentration is seen in Figure 21b to stay the same. The combustion experiments for molecules with carbon chain length of more than 12 carbon atoms were conducted under heated conditions in order to ensure that they remained in liquid phase and flowed freely. Therefore, it is possible that any tendency towards lower NO_x due to increasing chain length may have been offset by somewhat increased NO_x due to the increased fuel temperature.

Figure 21b also shows that primary and secondary alcohols had higher NO_x emissions than alkanes. This result is contradictory with several previous studies, which have shown that an increased ethanol or butanol percentage in alcohol-diesel blends resulted in lower in-cylinder temperatures and lower NO_x emissions, ascribed by various investigations to the higher heat of vaporization of alcohols [86,213,246,247]. The higher NO_x emissions of alcohols compared to those of alkanes shown in Figure 21b could perhaps be explained by the higher in-cylinder temperatures of alcohols compared to those for the alkanes having the same carbon chain length. The shorter ignition delays of alkanes compared to those for the alcohols (Figure 16a) resulted in combustion for alkanes starting a few CAD before TDC. In the case if the alcohols, their longer ignition delays resulted in ignition and premixed combustion occurring closer to TDC, causing somewhat higher combustion temperatures. The enhanced supply by the alcohols of oxygen molecules into the combustion zone might have also raised NO_x.

The location of a hydroxyl functional group within an alcohol molecule was observed to affect NO_x exhaust emissions. Figure 22a shows that NO_x emissions were reduced when moving the hydroxyl group along the carbon chain towards the centre of molecule. In the case of undecanol, which had the shortest ignition delay, it is suggested that the slight NO_x reduction was due to the decrease in maximum average in-cylinder temperature (Figure 22b) and possibly lower adiabatic flame temperatures (Figure 22c). In the case of octanol and nonanol there is less clarity as

to the reason why the NO_x decreased when the hydroxyl group was located progressively towards the middle of the molecule (Figure 22a). There is a strong suggestion in Figure 22c that this was due to reduced adiabatic flame temperature. However, the experimental values of maximum average in-cylinder temperature show increasing average temperature (Figure 22b), while NO_x emission was reducing (Figure 22a). A possible but rather tentative explanation for the decrease in NO_x for octanol and nonanol, despite rising average in-cylinder temperature, is the following. Figure 16b shows that for 2- and 3-octanol the ignition delay rose by 1 CAD to 8 CAD after TDC (ATDC) and for 5-nonanol by about 2.5 CAD to 8.5 CAD ATDC. For these molecules, therefore, ignition occurred after TDC, when the in-cylinder air and turbulence levels would have been rising, due to interacting swirl and reverse squish [1], as the piston started to recede away from the cylinder head. It is therefore possible that flame quenching locally due to cooler air entrainment, resulted in NO_x reduction, despite the rising in-cylinder global average in-cylinder temperature.

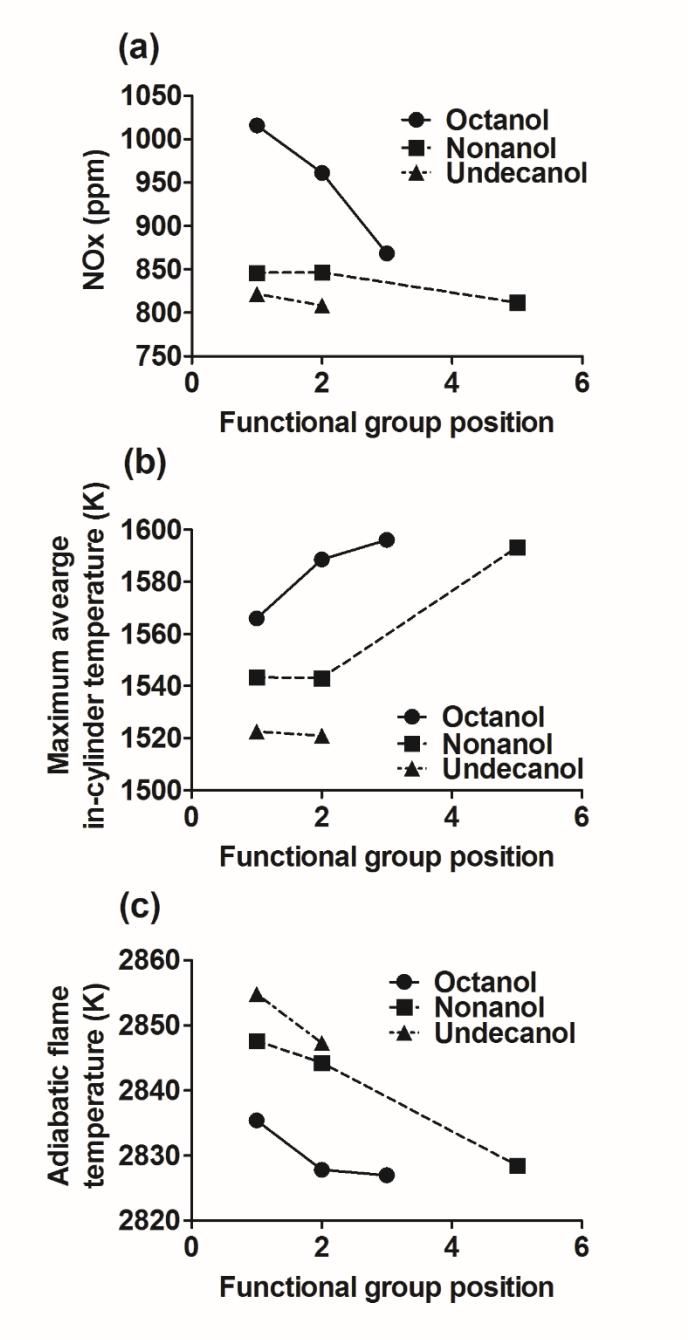

Figure 22. Changes in (a) NO_x emissions, (b) maximum average in-cylinder temperature and (c) adiabatic flame temperature caused by moving a hydroxyl along the carbon chain of a fuel molecule.

Figure 23a shows that higher degree of molecule unsaturation resulted in higher NO_x levels for 10-undecen-1-ol compared to 1-undecanol. This could possibly be explained by the higher values of both adiabatic flame temperature (Figure 23b) and

maximum in-cylinder temperature (Figure 23c) of 10-undecen-1-ol. Considering 1-octen-3-ol, Figure 23a shows that introducing a single double bond to the 3-octanol to form 1-octen-3-ol reduced the NO_x level to almost zero. Figure 23c shows that this reduction in NO_x could perhaps be explained by a very large reduction in the average in-cylinder temperature, from about 1600K to about 1475K. In turn, the large reduction in average temperature was the result of very late main ignition (4 CAD ATDC, as shown in Figure 18b) and slow combustion taking place during the engine expansion stroke.

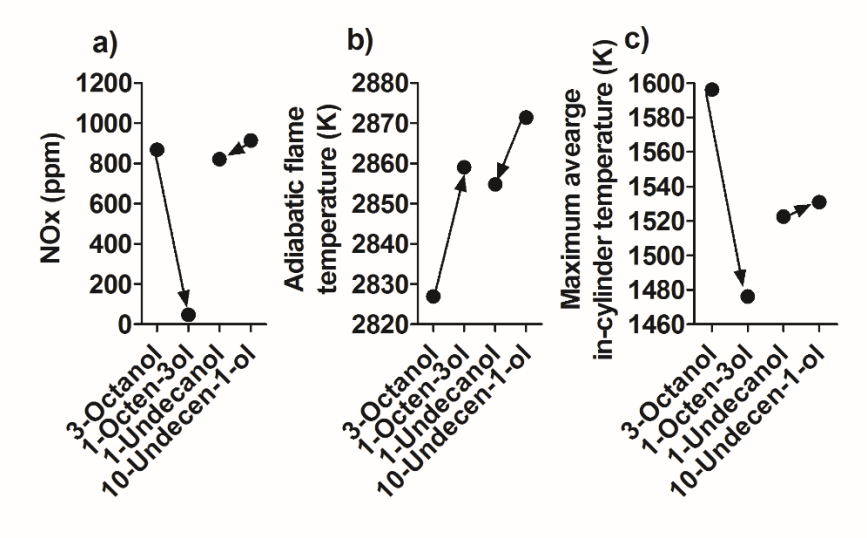

Figure 23. Changes in (a) NOx emissions, (b) maximum average in-cylinder temperature and (c) adiabatic flame temperature caused by increasing the degree of saturation of a fuel molecule.

Figure 24a shows that adding two methyl group branches to 1-octanol to form 3,7-dimethyl-1-octanol slightly decreases the NO_x emissions despite the increase in maximum average in-cylinder temperature (Figure 24b). The increase in maximum average in-cylinder temperature was caused by the longer ignition delay and the larger premixed combustion phase. It is possible, that the decrease in adiabatic flame temperature (Figure 24c) may have had an impact in regarding the NO_x emissions. The significant decrease in NO_x emissions when comparing 3-octanol and 3,7-dimethyl-3-octanol (Figure 24a) is very likely to have been due to the late ignition of

3,7-dimethyl-3-octanol. The late ignition resulted in a low maximum in-cylinder temperature (Figure 24b) which, combined with lower adiabatic flame temperature (Figure 24c), could have caused the reduced NO_x emission.

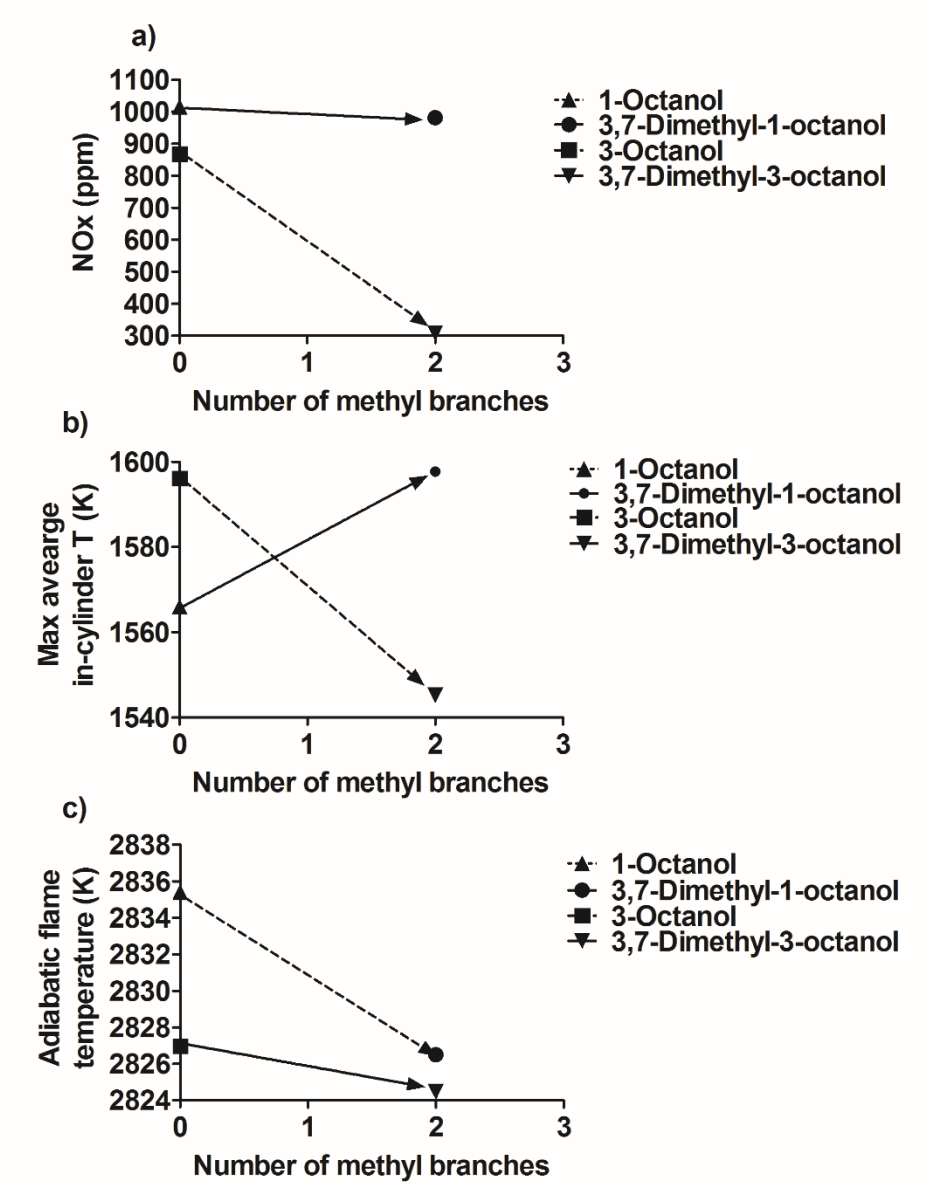

Figure 24. Changes in (a) NO_x emissions, (b) maximum average in-cylinder temperature and (c) adiabatic flame temperature caused by adding two methyl branches to a fuel molecule.

4.3.8 Effect of fuel molecular structure on particulate matter

Particulate matter emissions are formed in locally fuel-rich regions in the combustion chamber and comprise mainly of agglomerated solid carbonaceous material and organic compounds. Larger particulates are formed when small nucleus particles (diameter 0-50 nm) combine together to form accumulation particles (diameter 50-1000 nm), which in turn may form larger agglomerates [248]. Three main factors controlling PM formation are the local fuel/air stoichiometry, percentage of fuel that burns during the premixed combustion phase, and the in-cylinder temperature. All three factors, in turn, are significantly affected by the ignition delay: longer ignition delay allows the formation of a leaner and larger premixed fraction, which leads to a larger fraction of the fuel being burned instantaneously close to TDC, resulting in increased in-cylinder temperature. Higher premixed fraction combusted at high temperature generally leads to formation of fewer and smaller particulates, due to fewer fuel-rich pockets and limited time available for soot formation and growth (Figure 25a). Conversely, smaller premixed phase will increase diffusion burning which is slower, exposes rich mixture regions to high temperature and provides more time for particle agglomeration and growth, leading to smaller number of larger particles. Higher in-cylinder temperature generally leads to formation of fewer particulates due to accelerated oxidation, but can also lead to higher formation rate of particulates in the rich core of the spray (Figure 25b) by speeding up pyrolysis and soot formation reactions in this oxygen-deficient region. Put together, these factors generally appear to lead to smaller and more numerous particles when ignition delay is longer and, hence, the premixed combustion fraction is greater (Figure 25).

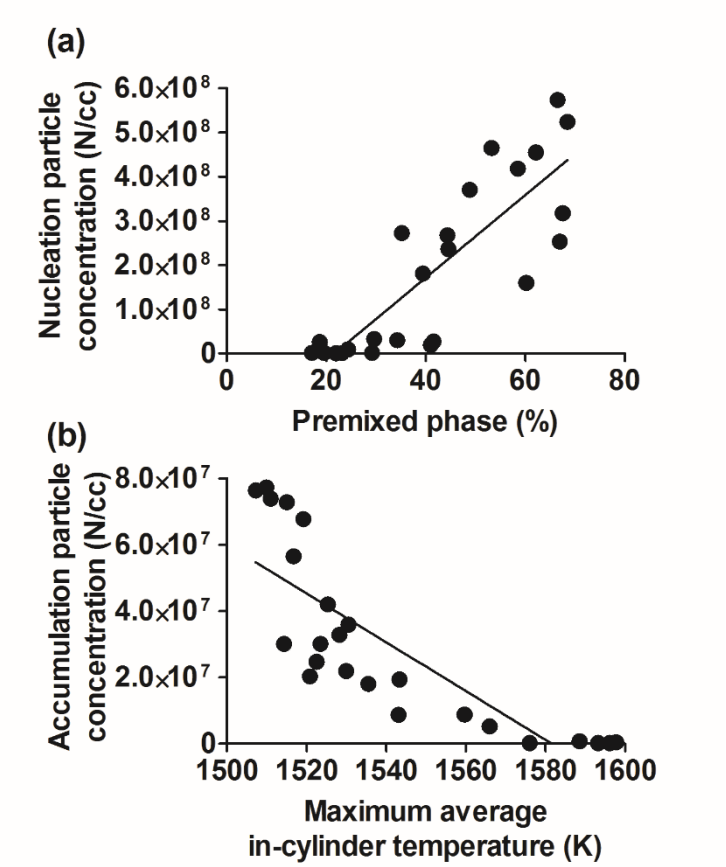

Figure 25. Effect of (a) premixed phase on nucleation particle concentration and (b) the effect of maximum average in-cylinder temperature on accumulation particle concentration for all of the tested fuel molecules (excluding 1-octen-3-ol and 3,7-dimethyl-3-octanol).

In this study, the non-oxygen bearing hydrocarbons (alkanes and alkenes), were observed from Figure 26a to produce a greater mass concentration of particulates than the alcohols. This result was also observed by several other investigations, e.g. Xue et al. [249] and Wei et al. [88], who have reported reduced particulate emissions with alcohol fuels compared to hydrocarbon fuels. However, despite the lower overall mass concentration of particulates, Figure 26b indicates that the alcohols produce, in general, more but smaller particles than the hydrocarbons. Possible reasons for the smaller particulates of alcohols are their longer ignition delays and greater premixed fractions compared to hydrocarbons.

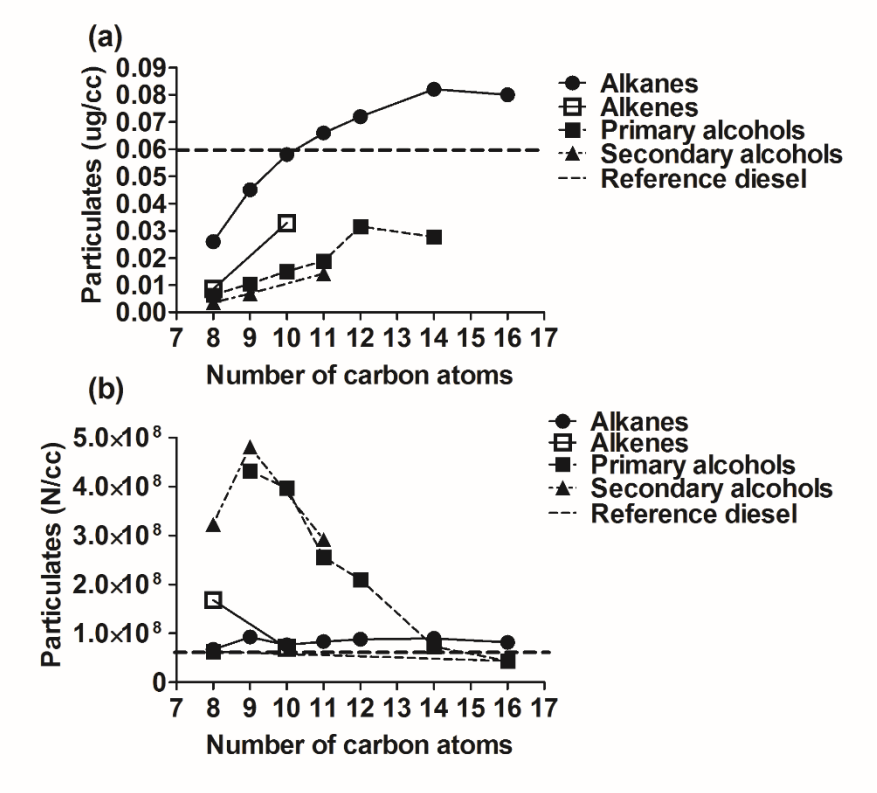

Figure 26. (a) Number and (b) mass of particulates in the 5-1000 nm size range emitted in the engine exhaust as a result of combustion of different oxygenated molecules.

Figure 27a shows that moving a hydroxyl group towards the centre of the molecule resulted in a very strong tendency for the number of nucleation particles to increase. It is possible to ascribe this increase in the number of nucleation particles to the longer ignition delays and to a greater fraction of the fuels burnt in the premixed combustion mode. Figure 27b shows that adding a double bond to the C8 alcohols caused increased mass and number of particulates. In the case of 1-octen-3-ol, two-stage ignition was observed with a small premixed phase and a prolonged diffusion combustion phase, which could have increased both the number and size of the particulates. In the case of 10-undecen-1-ol, no significant change in the mass of particulates was observed although there was a small rise in particulate number density. A possible explanation for the smaller rise in particulate concentration with the C11 alcohols, in comparison with the results for C8 alcohols, would be the significantly longer chain length of the C11 alcohol: due to the longer chain length,

the relative increase in ignition delay with the increasing degree of unsaturation was smaller for the C11 alcohol than for the C8 alcohol. Increased methyl group branching is shown in Figure 27c to have led to lower number concentration of particulates. It is possible that this is due to abnormally late combustion and partial burning taking place at low temperatures. The lower combustion temperature reduced the rate of the time-consuming processes required for soot formation.

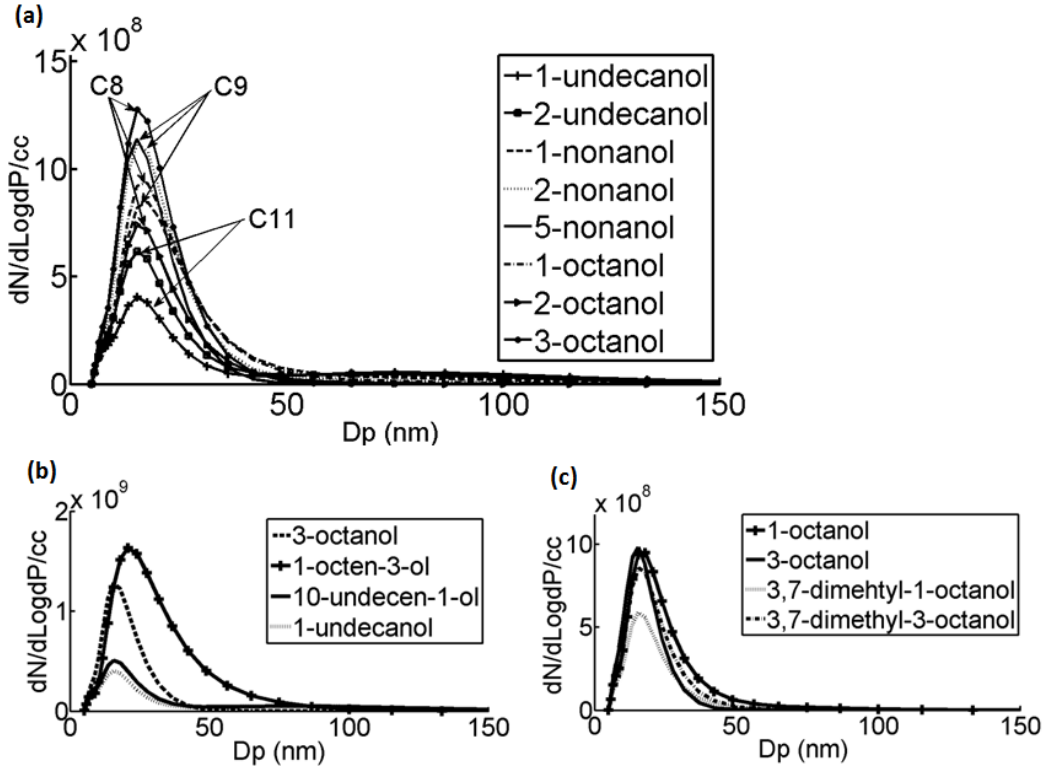

Figure 27. Size distribution of particulates 0-150 nm formed in combustion of (a) molecules with a hydroxyl group in different position, (b) straight chain hydrocarbons and alcohols with different degrees of unsaturation and (c) straight chain and branched C8 alcohols.

4.4 Conclusions

The hydroxyl group in a wide variety of alcohol molecules was observed to have a significant effect on compression ignition delay and exhaust emissions. The key results were as follows:

1. Compared to alkanes, alcohols had longer ignition delays, which lead to larger premixed phases and higher maximum average in-cylinder temperatures. Higher in-cylinder temperatures tended to increase the NO_x emissions; larger premixed phases resulted in lower mass of particulate emissions and higher particle number emissions for alcohols compared to alkanes.
2. Moving a hydroxyl group towards the centre of the alcohol carbon chain resulted in longer ignition delays. NO_x emissions decreased with increasing ignition delay, despite the increasing maximum average in-cylinder temperatures. This reduction in NO_x emissions was suggested to be caused by both the decrease in adiabatic flame temperatures and the later combustion. Although the maximum average in-cylinder temperature increased with increasing ignition delay, the later combustion was assumed to result in a shorter overall time during which the in-cylinder temperature remained high, partly due to the possible flame quenching. The shorter duration of high in-cylinder temperature lead to formation of less NO_x. Longer ignition delays resulted in formation of greater number of small nucleation particulates, as was expected due to the larger premixed phases.
3. Higher degree of unsaturation led to longer ignition delays. NO_x emissions increased due to increases in both the maximum average in-cylinder temperatures and the adiabatic flame temperatures. As expected, the number of small nucleation particulate emissions was observed to increase with increasing ignition delay.
4. Higher degree of branching in alcohols increased the ignition delay. NOx emissions decreased slightly despite the increase in both premixed phase and the maximum average in-cylinder temperature, perhaps partly due to decrease in adiabatic flame temperature. The number of PM particles increased slightly with increasing ignition delay.

It is suggested that the observed increase in ignition delay for alcohols compared to the delay for alkanes was mainly due to the higher electronegativity of the oxygen atom present in alcohols, compared to that of carbon and hydrogen atoms in hydrocarbon molecules. This higher electronegativity of the oxygen atom makes the

overall hydrogen abstraction more difficult and decreases the ability of fuel molecules to initiate further branching reactions through isomerization. The differences in NO_x emissions were suggested to be caused mainly by the changes in the rate of rapid thermal NO_x formation. When considering the PM emissions, the number of particles in the exhaust gas was observed to decrease with increasing magnitude of premixed phase, and the mass of particulates to increase with increasing in-cylinder temperature.

It can be concluded that, both adding a hydroxyl group and moving it along the carbon chain of a hydrocarbon fuel molecule can be used to alter the combustion profile and the exhaust gas emissions of a fuel. It should also be noted that a slight trade-off between the NO_x emissions and PM emissions was observed with the hydroxyl group addition to a hydrocarbon; the NO_x emissions generally increased, whereas the PM emissions decreased.

Chapter 5

The influence of various oxygenated functional groups in carbonyl and ether compounds on compression ignition and exhaust gas emissions

5.1 Introduction

The aim of the study presented in this chapter was to investigate systematically in a single cylinder CI research engine the auto ignition behaviour and emission formation of a wide range of oxygen-bearing fuel molecules, including ketone, carboxylic acid, methyl ester and ether molecules. The chapter makes an assessment of their combustion characteristics of these molecules and exhaust pollutant emissions. The assessment includes the impact of altering the position of the carbonyl group in a molecule and the level of carboxylic acid unsaturation. A comparison is then made of the results from these molecules and those of the several alcohol molecules from the previous chapter. It was suggested in a previous chapter that the two key aspects to understanding how molecular structure affects ignition delay are the relative difficulty of hydrogen abstraction from the fuel molecule and the subsequent ability of the fuel peroxy radical to isomerize through hydrogen transfer [53,107]. Therefore, the assessment of the ignition delays of various molecules reported in this chapter was made in the context of this hypothesis. Taken together, the results reported here provide a broad picture of the combustion and exhaust emissions of almost 50 oxygenated molecules which could potentially be produced from renewable energy sources.

5.2 Experimental methods

5.2.1 Experimental conditions

All combustion experiments were conducted at engine speed of 1200 rpm, 600 bar injection pressure, 4 bar IMEP and a fixed engine injection timing of 7.5 CAD before TDC. Each test day was started and ended with a reference diesel fuel test to detect

any day to day drift or longer term change in the experimental equipment and instrumentation. From this data it was possible to calculate for diesel fuel the long term mean value, standard deviation and the standard error of the mean value for NO_x as follows: 921 ppm, 29.4 ppm and 5.76 ppm, respectively. The corresponding values for the mass of particulates in the exhaust gas were 0.0563 µg/cm^3, 0.00779 µg/cm^{3}and 0.00179 µg/cm^3, respectively, and for the number of particulates 57.1*10^6 units/ cm^3, 8.99*10^6 units/ cm^3 and 1.74*10^6 units/ cm^3 respectively. This data, therefore, provided a measure of the test-to-test repeatability of the emissions over several dozens of tests.

The fuel temperature during most of the combustion experiments was 305 ±3K. For fuel molecules with melting points above this temperature, the fuel was heated to 343 ±3K (Appendix II). To determine the effect of fuel heating on combustion and emissions results, several molecules were tested at both temperatures of 305K and 343K (nonanoic acid, methyl octanoate and methyl nonanoate). The 38K rise in temperature was observed to cause only a small decrease in ignition delay (0.20, 0.28, 0.20 CAD, respectively). These changes in ignition delay were deemed insignificant compared to the shaft encoder resolution of 0.2 CAD, and the 0.1 CAD test-to-test standard deviation of ignition delay with reference diesel fuel. Nonetheless, the fuel test temperatures are mentioned in the results section where applicable.

5.2.2 Fuel molecules investigated

Altogether, 46 oxygen bearing molecules were investigated having eight to 16 carbon atoms each and incorporating the following functional groups; hydroxyl (ROH), carbonyl (RR'CO), carboxyl (RCOOH), ester (RCOOR') and ether (ROR'). Additionally, seven alkanes and two alkenes were tested to provide reference data for comparison with the oxygenated molecules. The molecular structures and physical properties of the alkanes, alkenes and alcohols were presented in the previous chapter and the molecular structure of the ketones, carboxylic acids, esters and ethers are presented in Figure 28. Appendix II lists the physical properties of the ketones, carboxylic acids, esters and ethers [234–238,250].

The aim of the experiments was to investigate the effects on combustion and exhaust emissions of the following molecular features:

a) The type of oxygenated functional group incorporated in a fuel molecule and the functional group position within the molecule; more specifically, the following effects on ignition and emissions were investigated:
    i. Addition of a carbonyl group to the second carbon atom of an alkane carbon chain to form a methyl ketone.
    ii. Moving the carbonyl group along the carbon chain.
    iii. Replacing the first carbon atom of the carbon chain next to the carbonyl group of a ketone with a hydroxyl group to form a carboxylic acid.
    iv. Replacing the hydrogen atom of the hydroxyl group in a carboxylic acid with a methyl group to form a methyl ester.
    v. Introducing an oxygen atom into the alkane carbon chain to form an ether.
    vi. Increasing the number of ether linkages (R-O-R') in a molecule.
b) The degree of unsaturation of various fuel molecules

Fuel molecule	Molecular structure
<u>Ketones</u>	
2-Octanone	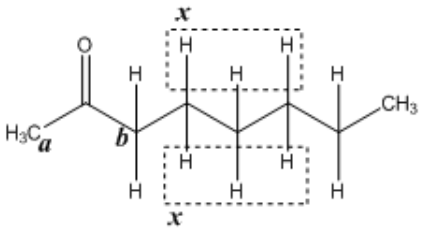
2-Nonanone	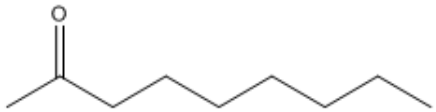
5-Nonanone	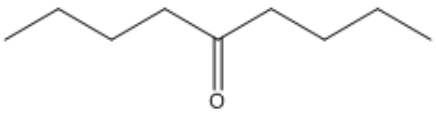
2-Decanone	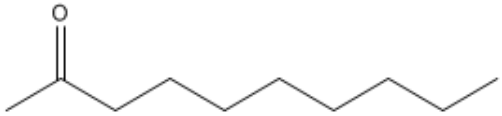
3-Decanone	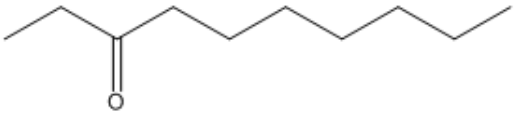
2-Undecanone	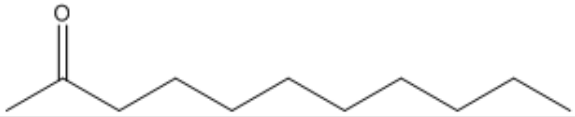
<u>Esters</u>	
Methyl octanoate	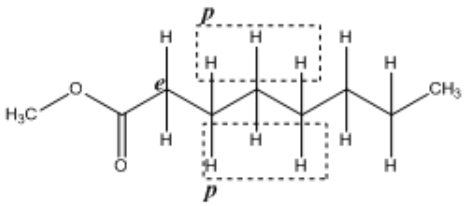
Methyl nonanoate	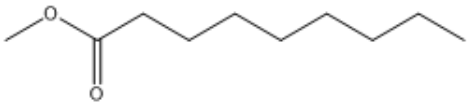
Methyl decanoate	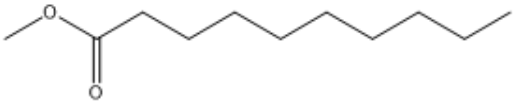
Methyl hexadecanoate	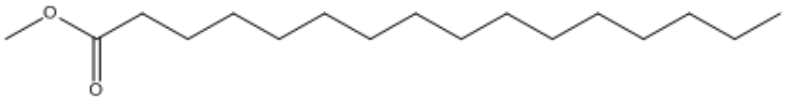

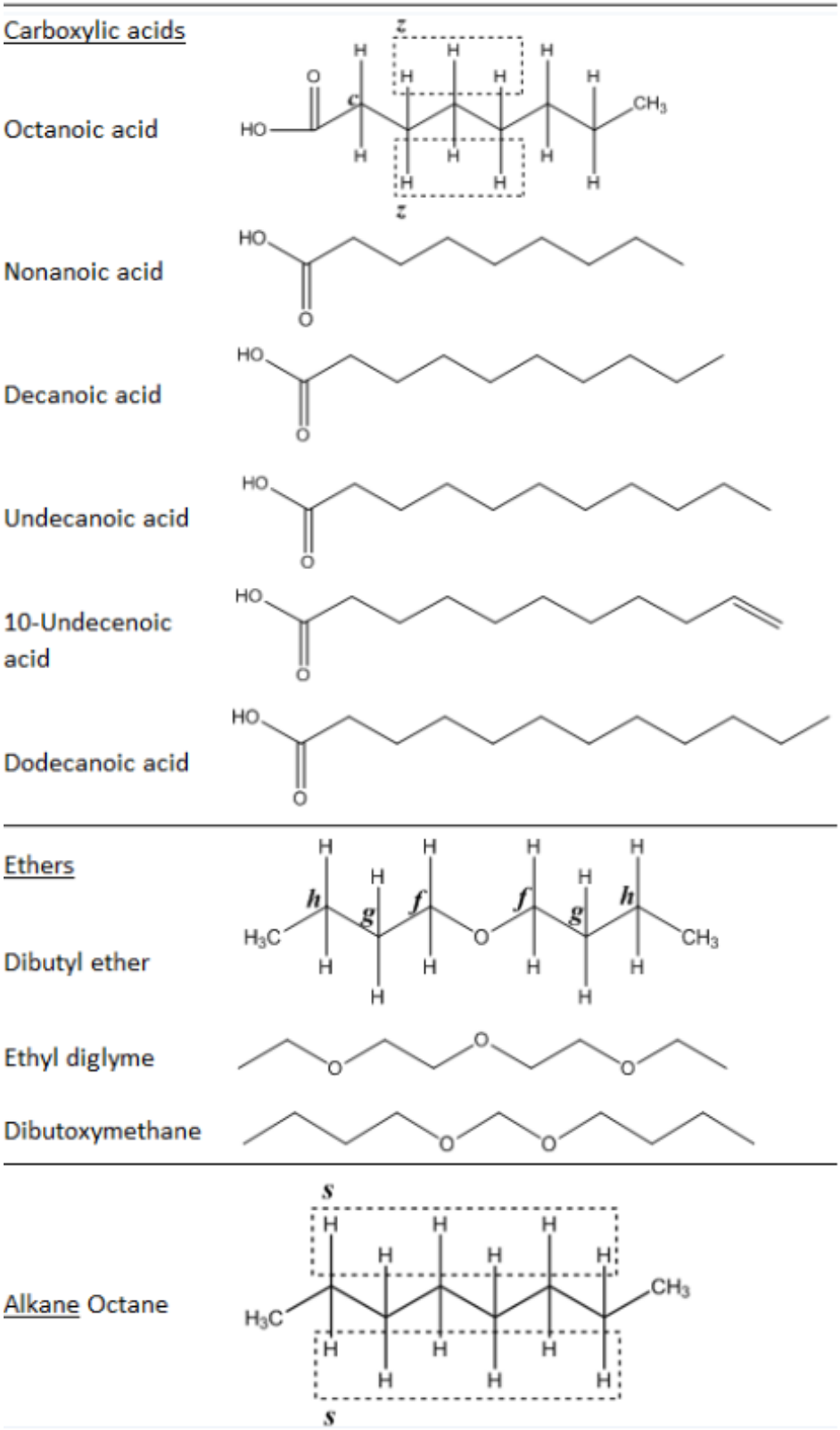

Figure 28. Molecular structures of the tested ketones, carboxylic acids, ethers and esters with an alkane structure provided for comparison.

5.3 Results and discussion

5.3.1 Effect of carbon chain length on ignition delay

Figure 29a shows that ignition delay decreased with increasing carbon chain length for all functional groups. This result is in agreement with both the theoretical discussion of Westbrook et al. [107] and the experimental engine studies of Schönborn et al. [224]. It is suggested that this decrease in ignition delay with increasing carbon chain length is partly due to the increase in the number of secondary C-H bonds and the greater ability of the fuel peroxy radicals to isomerize. The higher number of easily abstracted secondary H atoms results in faster overall H-abstraction and thus in faster radical pool formation, which reduces the ignition delay. Longer carbon chain also allows the fuel peroxy radical to form a larger number of six-membered transition state rings during isomerization, which increases the rate of isomerization and results in faster increase of the radical pool, hence decreasing the ignition delay further. Additionally, it can be seen from Figure 29a that the curves become shallower with increasing carbon chain length. This is likely to be due to diminishing rate of increase in the ratio of secondary to primary hydrogen atoms; and also, due to the smaller relative change in the ability of a fuel peroxy radical to isomerize.

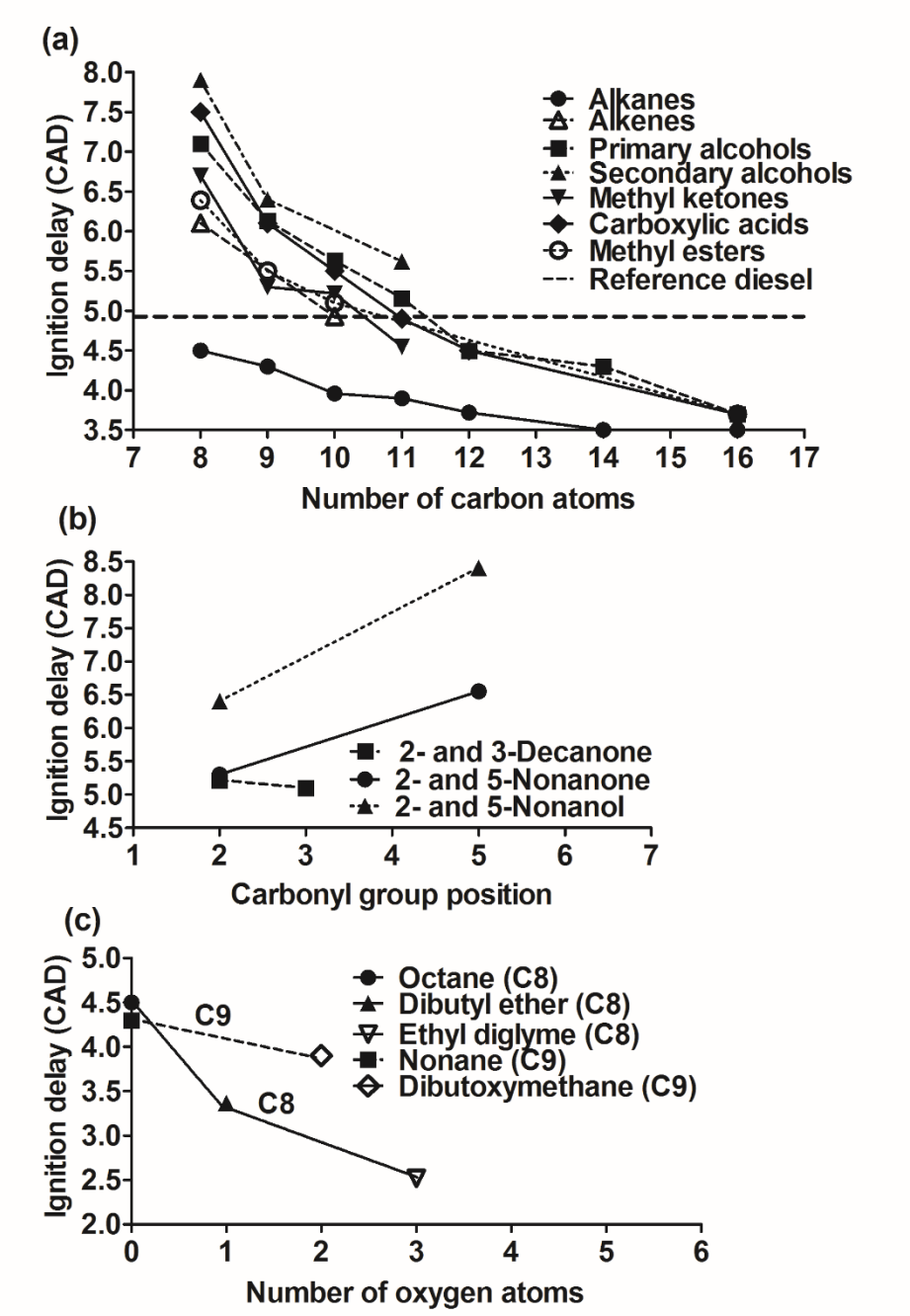

Figure 29. (a) Ignition delays of straight chain saturated molecules (secondary alcohols have the hydroxyl group bonded to the second carbon atom of the carbon chain); (b) Effect on ignition delay of moving a carbonyl group or a hydroxyl group along the carbon chain of a molecule; (c) Effect on ignition delay of adding oxygen into an alkane carbon chain.

5.3.2 Methyl ketones

Methyl ketones are observed from Figure 29a to have higher ignition delays than the corresponding alkanes with the same carbon chain length. One way to explain the longer ignition delays of methyl ketones is to consider the effect of oxygen in the carbonyl group of ketones on H-abstraction. Firstly, compared to a corresponding alkane, the carbonyl group in a methyl ketone reduces by two the number of secondary hydrogen atoms available for H-abstraction. This is illustrated, for example, for octane and 2-octanone in Figure 28. Secondly, several studies [3,251–253] indicate that the higher electronegativity of the oxygen atom compared to that of a hydrogen atom affects the strengths of the nearby C-H bonds in the fuel molecule. As a result, H-abstraction from the neighbouring secondary carbon atom (labelled b in 2-octanone – Figure 28) becomes easier than abstraction of the corresponding secondary hydrogen atom of an alkane (labelled s in alkane – Figure 28). However, abstraction of the six hydrogen atoms (labelled x in 2-octanone - Figure 28) from the three following carbon atoms, as well as abstraction of the three primary hydrogen atoms from the primary carbon atom next to the carbonyl group (item labelled a in 2-octanone – Figure 28) becomes more difficult than abstraction of the corresponding secondary hydrogen atom of an alkane (labelled s in alkane – Figure 28). These changes result in increased difficulty of the overall H-abstraction from methyl ketones compared to alkanes and, therefore, increase the duration of ignition delay.

Besides H-abstraction, the ignition delay of methyl ketones is also likely to be affected by the further reactions of fuel radicals. These fuel radicals react, first, with oxygen into ketonyl peroxy radicals. Hoare and Li [251] and Anderson and Hoare [252] suggested, on the basis of low temperature oxidation experiments, that the ketonyl peroxy radicals undergo mainly propagation reactions, instead of branching reactions, via hydrogen transfer through transition ring formation. Additionally, Allen et al. [52] showed, by means of experiments conducted in a RCM with di-isopropyl ketone, that the carbonyl group hinders the formation of six-membered transition rings, thus making the isomerization of ketonyl peroxy radicals more difficult than that of alkyl peroxy radicals in alkane combustion. Isomerization of the fuel peroxy radicals initiates the low temperature branching reactions, and therefore

the lower ability of ketones to undergo this reaction is assumed to contribute to their higher ignition delays compared to alkanes, as shown in Figure 29a.

The effect of moving a carbonyl group along the carbon chain of ketones was studied for two chain lengths, one with 9 and the other with 10 carbon atoms. Figure 29b shows that moving the carbonyl group from the second carbon atom of nonanone to the fifth carbon atom increased the ignition delay significantly. This change in ignition delay could be partly due to the higher number of secondary C-H bonds affected by the carbonyl group in 5-nonanone compared to the number affected in 2-nonanone. This is expected to result in a slower overall H-abstraction from 5-nonanol compared to 2-nonanone, which in turn leads to slower formation of the radical pool and hence to later ignition. Furthermore, moving the carbonyl group towards the centre of the molecule decreases the lengths of the hydrocarbon chains on either side of the carbon atom of the carbonyl group, and therefore is suggested to decrease the ability of the fuel peroxy radicals to isomerize through transition ring formation. Lower ability of fuel peroxy radicals to isomerize hinders the overall rate of branching reactions and hence increases further the ignition delay of 5-nonanone compared to 2-nonanone. In the case of decanone, Figure 29b shows that moving a carbonyl group from the second carbon atom of a decanone to the third carbon atom results in very little change in ignition delay (below 0.2 CAD). It therefore appears, in the case of a C10 ketone, that the effect of moving a carbonyl group by only one carbon atom towards the centre of a molecule on low temperature ignition chemistry is insignificant.

5.3.3 Carboxylic acids

Carboxylic acids would make poor biofuels due to their ionic (hence corrosive) nature and therefore their combustion in an engine has not been studied extensively [254]. Nevertheless, within the context of this study, they provide useful insights to molecular effect on ignition and emissions. Figure 29a shows that carboxylic acids had higher ignition delays than those of the corresponding alkanes. It is suggested that the longer ignition delays of carboxylic acids, compared to alkanes, is partly due to the changes in C-H bond strengths caused by the two oxygen molecules in the carboxyl group. Having both a hydroxyl group and a carbonyl group bonded to the

same carbon atom as a carboxyl group could be assumed to make H-abstraction from the neighbouring carbon atom (labelled c in octanoic acid - Figure 28) easier than the abstraction of a secondary hydrogen atom of an alkane (labelled s in alkane – Figure 28). However, H-abstraction of the six hydrogen atoms (labelled z in octanoic acid - Figure 28) from the next three carbon atoms of the chain could be assumed to be more difficult than the abstraction of a secondary hydrogen atom of an alkane (labelled s in alkane – Figure 28). Additionally, the carboxylic acids have three fewer primary hydrogen atoms available for H-abstraction than the corresponding alkanes, as is illustrated in Figure 28 for octane and octanoic acid. These changes in the molecular structure tend to increase the difficulty of overall H-abstraction of carboxylic acids, compared to alkanes, and resulted in longer ignition delays.

When considering the further reactions of the fuel radicals formed by H-abstraction of carboxylic acids, the ability of fuel peroxy radicals to isomerize has a significant effect on the rate of radical pool formation. The results of Silva [90] show that the fuel peroxy radicals of a carboxylic acid may undergo isomerization leading to further branching reactions and increasing the radical pool. However, the carboxyl group in the structure of carboxylic acids makes the formation of transition rings during isomerization more difficult compared to alkanes. This lower ability to undergo isomerization decreases the rate of radical formation and further increases the ignition delays of carboxylic acids compared to those of alkanes.

5.3.4 Methyl ester

Figure 29a shows that methyl esters had longer ignition delays than alkanes. The ester group could be considered as being formed by replacing the hydrogen of the hydroxyl group in carboxylic acid with either a methyl group or a longer alkyl chain. This is illustrated for octanoic acid and methyl octanoate in Figure 28. The electronegativity of the carbonyl group weakens the C-H bonds of the neighbouring carbon atom (labelled e in methyl octanoate - Figure 28), making H-abstraction from this site faster than the abstraction of corresponding secondary hydrogen atoms of an alkane (labelled s in alkane – Figure 28). However, the carbonyl group strengthens the C-H bonds of the next three carbon atoms in the carbon chain making H-abstraction of the six hydrogen atoms (labelled p in methyl octanoate - Figure 28)

bonded to these carbon atoms more difficult than abstraction of hydrogen atoms bonded to secondary carbon atoms of an alkane (labelled s in alkane – Figure 28) [75,77]. It is suggested that this strengthening of the C-H bonds hinders the radical pool formation compared to alkanes, leading to the observed higher ignition delays of methyl esters compared to alkanes.

When considering further reactions of methyl esters after H-abstraction, Fisher et al. [255] suggested that the methyl-ester peroxy radical may go through a similar isomerization route to alkane isomerization. This similarity of the reaction routes has been supported by several engine studies, for example in a CFR engine study by Zhang and Boehman [92]. However, the oxygen atoms within esters may impose extra strain to the transition rings and thus lower the reaction rate of isomerisation and increase the ignition delay of esters further compared to alkanes [91,92].

5.3.5 Ethers

Unlike all the other oxygenated molecules of this study, ethers had lower ignition delays than alkanes, as shown in Figure 29c Short chain ethers, such as dimethyl ether (DME) and diethyl ether (DEE), have been shown to be compatible with diesel engines as diesel blends and therefore their combustion mechanism is relatively well researched. Both of these ethers have shorter ignition delays compared to diesel fuel [98,100]. However, only a few combustion mechanism studies have been conducted with longer chain ethers. Based on the results of these studies, the lower ignition delays of ethers shown in Figure 29c compared to alkanes (octane and nonane) can be explained by the effect of the oxygen atom in the ethers on the neighbouring C-H bonds and by the ability of the alkyl peroxy radicals to undergo isomerization.

First consider the changes in the C-H bond strengths. Cai et al. [78] observed for Di-n-butyl ether in a laminar flow reactor that the ether linkage (R-O-R') within the carbon atom chain makes the H-abstraction from the two alpha carbon atoms (labelled f in dibutyl ether – Figure 28) easier than the abstraction of a secondary hydrogen atom of an alkane (labelled s in alkane – Figure 28). Additionally, the oxygen atom in the carbon chain makes H-abstraction from the two gamma carbon atoms (labelled h in dibutyl ether – Figure 28) easier than from the two beta carbon

atoms (labelled g in dibutyl ether – Figure 28). These changes in the C-H bond strengths result in faster H-abstraction from ether, compared to the corresponding alkanes, and lead to faster ignition. The results of Cai et al. have been supported by several studies, such as the shock tube experiments of Guan et al. [79] and theoretical calculations of Ogura et al. [80].

Now consider the ability of an alkyl peroxy radical, which has been formed through oxidation of an ether radical, to isomerize. Cai et al. [78] concluded that isomerization of ethers may occur with hydrogen migration across the central oxygen atom. Furthermore, the energy barrier of the peroxide decomposition to facilitate further chain branching reactions has been shown to be lower for ethers compared to alkanes [78,80]. These two factors were assumed to increase the rate of isomerization, and thus radical pool formation of ether combustion, compared to alkanes leading to shorter ignition delays for ethers.

In order to investigate further the effect of adding oxygen into the carbon chain of an alkane, the ethers and alkanes were grouped based on the number of carbon atoms in their structure; octane was grouped with dibutyl ether and ethyl diglyme, and nonane with dibutoxymethane. It can be seen from Figure 29c that higher number of oxygen linkages in a carbon chain of constant length decreased the ignition delay, as was expected. Additionally, it can be seen that the changes in ignition delay for the longer C9 molecules were slightly smaller than the changes for the shorter C8 molecules, indicating that the effect of ether linkages decreases with increasing carbon to oxygen atom ratio. This result was also supported by the decreasing slopes of the curves in Figure 29a.

5.3.6 Degree of unsaturation

The effect of unsaturation in a carboxylic acid was investigated by comparing undecanoic acid to 10-undecenoic acid (C11). As was expected, unsaturation was observed to increase the ignition delay by 1.8 CAD. Interestingly, in the previous chapter 4 when a double bond was added to the last position of undecanol, no change in ignition delay was observed (Fig. 4b in [256]). This suggests that the hydroxyl group has a more significant effect on ignition delay than the carboxyl group, making

the effect of adding a double bond to an alcohol less significant than adding it to a carboxylic acid. It is suggested that the higher electronegativity of the hydroxyl group, compared to that of the carboxylic acid, may be a contributing factor to the greater insensitivity of the alcohol to unsaturation.

5.3.7 Comparison between the functional groups

Taking an overview of the various functional structures discussed above, it can be seen from Figure 29a and Figure 29c that hydrocarbons had lower ignition delays than the oxygenated molecules, excluding ethers. It should also be noted that the ignition delay of the reference diesel was close to that of alkanes, as was expected, because a substantial portion of petroleum diesel consists of C10 to C22 alkanes. This suggests that the shorter ignition delay of commercial biofuels compared to diesel fuels cannot be caused by the oxygen-bearing functional groups in their molecules, as generally believed. Rather, it is suggested that biofuel molecules, such as esters, have shorter ignition delays because of their longer carbon chains compared to the average alkane chain length in diesel.

A main difference between the oxygenated functional groups tested in this study is the way the oxygen atom is bonded to the carbon chain of the molecule. Based on the results presented in Figure 29a, the functional groups with longer ignition delays, compared to diesel fuel, can be ranked approximately in the order of increasing ignition delay as follows:

1. Methyl ketones and methyl esters (shortest delay)
2. Primary alcohols and carboxylic acids (longer delay)
3. Secondary alcohols (longest delay)

First, consider the functional groups with similar ignition delays. For example, no significant difference was observed between the ignition delays of methyl ketones and methyl esters. This result was unexpected due to the lower electronegativity of methyl esters compared to methyl ketones [257]. Due to the lower electronegativity, the effects of oxygenated functional groups that increase the ignition delay of a fuel molecule were assumed to be less significant, and thus lower ignition delays were expected for methyl esters compared to methyl ketones. The similar ignition delays

of methyl esters and methyl ketones indicate that the ether linkage in an ester group had no significant effect on the ignition delay for C8-C11 molecules. In the case of primary alcohols and carboxylic acids, shorter ignition delays were expected for primary alcohols due to their lower electronegativity compared to carboxylic acids [258]. However, no significant difference was observed between the ignition delays of primary alcohols and carboxylic acid, which suggests that the carbonyl group in a carboxyl group had a less significant effect on ignition delay compared to the hydroxyl group, which is present in both carboxylic acids and primary alcohols.

Comparing now the ignition delays of methyl ketones and methyl esters to the higher ignition delays of primary alcohols and carboxylic acids the following arguments apply. The carbonyl group in methyl ketones and methyl esters, and the hydroxyl group in primary alcohols and carboxylic acids play a major role in the differences in ignition delays. These functional groups affect the bond strengths both within and in between the molecules. When considering bond strengths within the molecules, the lower electronegativity of a carbonyl group compared to a hydroxyl group is expected to make the H-abstraction easier from methyl ketones and methyl esters compared to H-abstraction from primary alcohols and carboxylic acids [259]. It is suggested that this occurs due to higher stability of the fuel radical formed from a molecule with a carbonyl group, compared to a radical from a molecule with a hydroxyl group: the double bonded oxygen of a carbonyl group allows greater electron delocalization after H-abstraction than the single bonded oxygen of a hydroxyl group [260]. When considering intermolecular forces, the dipole moment of a carbonyl group makes the methyl ketones and methyl esters more polar than alkanes, alkenes and ethers, which only have weak Van der Waals intramolecular forces [258]. However, the ability of primary alcohols and carboxylic acids to form hydrogen bonds, due to their hydroxyl group, results in even higher polarity compared to methyl ketones and methyl esters. Higher polarity of molecules increases the strength of the intermolecular forces. As a result, primary alcohols and carboxylic acids are less volatile compared to methyl ketones and methyl esters. The lower volatility of those alcohols and acids results in more time required in the engine for the fuel and air to mix, and hence tends to increase the ignition delay of these compounds.

Secondary alcohols were observed from Fig. 1a to have the longest ignition delays of all tested molecules. Primary alcohols can be seen from Fig. 1a to also have long ignition delays, but somewhat shorter than those for secondary alcohols. The reasons for the longest delay for the secondary alcohols were discussed in more detail in the previous chapter 5; having the hydroxyl group in the second, instead of the first, carbon atom of the carbon chain hinders both the H-abstraction and the isomerization of fuel peroxy radicals and therefore increases the ignition delay significantly.

An interesting comparison can be made between secondary alcohols and methyl ketones, where the second carbon of the carbon chain is bonded to either a carbonyl or a hydroxyl group, respectively. The only difference between the molecules is, therefore, whether the oxygen atom is double bonded to a carbon atom, or it is single bonded to a carbon atom plus a hydrogen atom. It is possible that tertiary hydrogen abstraction from secondary alcohols may lead to formation of methyl ketones and HO_2 radicals, instead of leading to a branching reaction. This would suggest that on at least some occasions, secondary alcohols might have an additional step in the oxidation chain reaction compared to methyl ketones, thus making the ignition delays of secondary alcohols longer than those of methyl ketones, as observed in Fig. 1a.

To investigate the effect of the hydroxyl and carbonyl groups on ignition delay further, the effects of moving these functional groups along the carbon chain were compared. Moving the carbonyl group from the second to the third carbon atom of Decanone caused a very small reduction (0.12 CAD) in the ignition delay (Fig. 1b). On the other hand, Fig. 1b shows that moving the carbonyl and hydroxyl groups from the second carbon atom to the fifth carbon atom of a C9 molecule caused a larger increase in ignition delay for the alcohol (2.0 CAD) than for the ketone (1.3 CAD). Based on these results, one might suggest that the position of a hydroxyl group has a more significant effect on ignition delay than the position of a carbonyl group. One reason for this could be that the higher electronegativity of the hydroxyl group, compared to that of the carbonyl group, has a more significant effect on neighbouring bond strengths.

Figure 29c shows that C8 and C9 ethers had shorter ignition delays than the corresponding C8 and C9 alkanes. It is suggested that the lower ignition delays of ethers were due mainly to greater ease of hydrogen abstraction and greater ability to

undergo isomerization, as was discussed above. In terms of intermolecular forces, ethers are not significantly polar and therefore their intermolecular forces are broadly similar to those of alkanes.

5.3.8 Effect of fuel molecular structure on heat release rate

Several aspects of engine performance are affected significantly by the timing and the rate of heat released from combustion of the fuel during an engine cycle. The rate of heat release in the study reported here was calculated from first law of thermodynamics analysis [1], using the in-cylinder gas pressure in the engine, recorded digitally every 0.2 CAD. Three main parameters are often used to characterise the heat release in a diesel engine, namely the amount of fuel burned during the premixed combustion phase, the value of pHRR, and the timing of pHRR. The premixed phase energy release was calculated as the percentage of the total chemical energy of the fuel injected into the combustion chamber. Figure 30 shows good correlations of these three parameters with ignition delay for the molecules investigated. Three molecules were excluded from Figure 30, namely 3,7-dimethyl-3-octanol, 1-octen-3-ol and diglyme; the former two molecules had unusually long ignition delays and double-ignition, while ethyl diglyme had an unusually short ignition delay and very small premixed phase. Figure 30 highlights the substantial effect that ignition delay has on the rate of heat release in the engine. For example, just 1 CAD increase in the ignition delay added as much as 20 percentage points to the fuel burned in the premixed phase (Figure 30a); increase of 1 CAD in ignition delay also caused a substantial increase in the peak heat release rate (Figure 30b), for example increasing pHRR from 75 to 125 J/CAD when the ignition delay was increased from 4 CAD to 5 CAD. Figure 31a shows a clear correlation between the average in-cylinder temperature and the ignition delay. As ignition delay increases, one can expect a greater amount of the fuel burned rapidly in the premixed phase, around TDC, when the combustion volume is at a minimum (Figure 30c), resulting in higher average in-cylinder temperature.

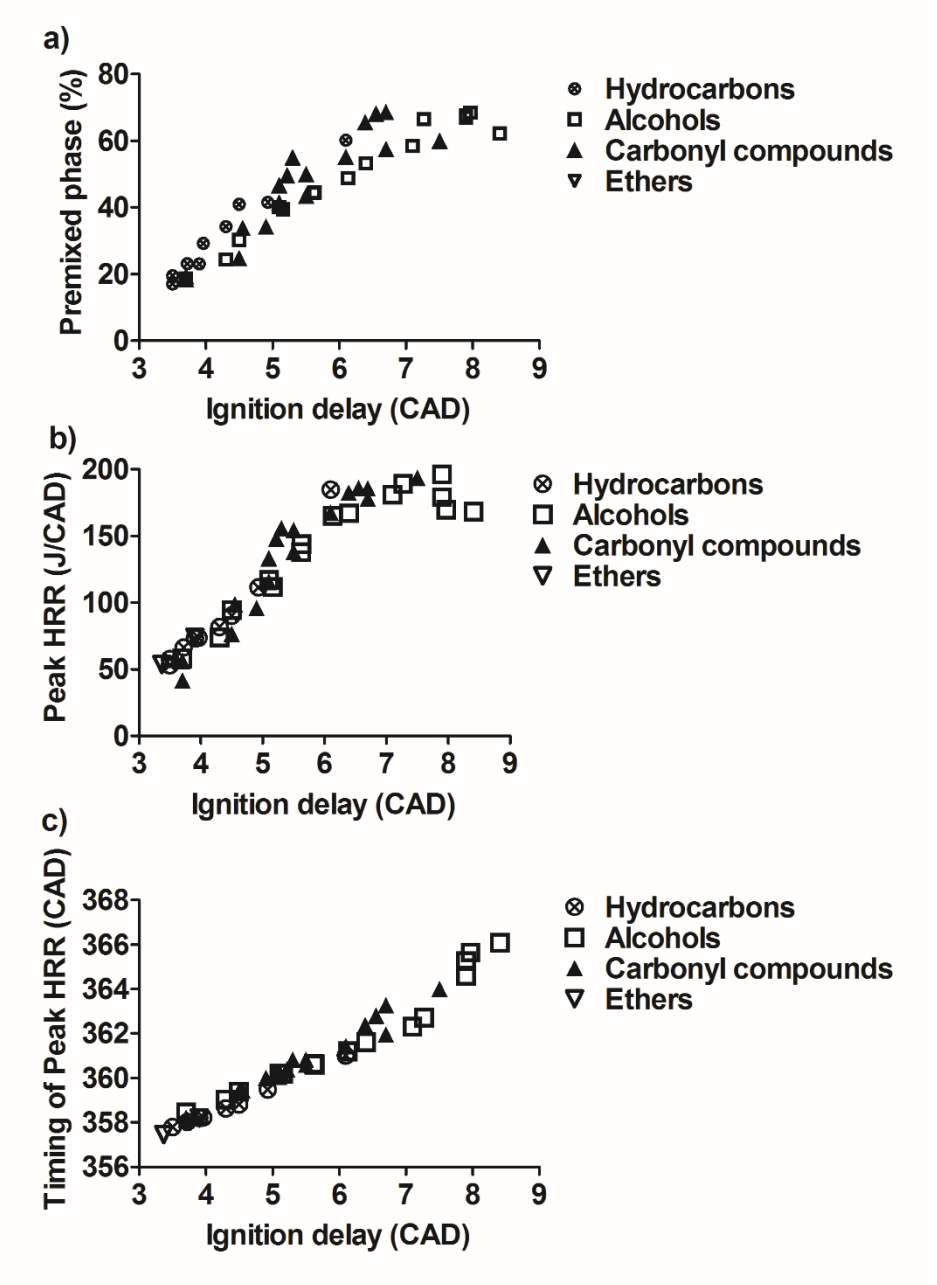

Figure 30. Effect of ignition delay on (a) premixed phase, (b) value of peak heat release rate and (c) timing of peak heat release rate for the tested fuel molecules (excluding 1-octen-3-ol, 3,7-dimethyl-3-octanol and ethyl diglyme).

5.3.9 Effect of fuel molecular structure on nitrogen oxides

In general, NO_x can be formed in diesel engines through a number of routes, including prompt reactions of fuel fragments with atmospheric nitrogen, conversion of fuel bound nitrogen, and, predominantly, a thermal mechanism involving atmospheric nitrogen oxidation. Therefore, NO_x emission generally increase rapidly with both the engine in-cylinder temperature and the fuel adiabatic flame temperature, as well as with the amount of oxygen available in the reaction areas [245]. Figure 31b shows, perhaps surprisingly, a rather poor correlation between the average in-cylinder temperature and NO_x concentration in the engine exhaust. Similarly, Figure 31cshows a rather poor correlation between the ignition delay and NO_x emissions.

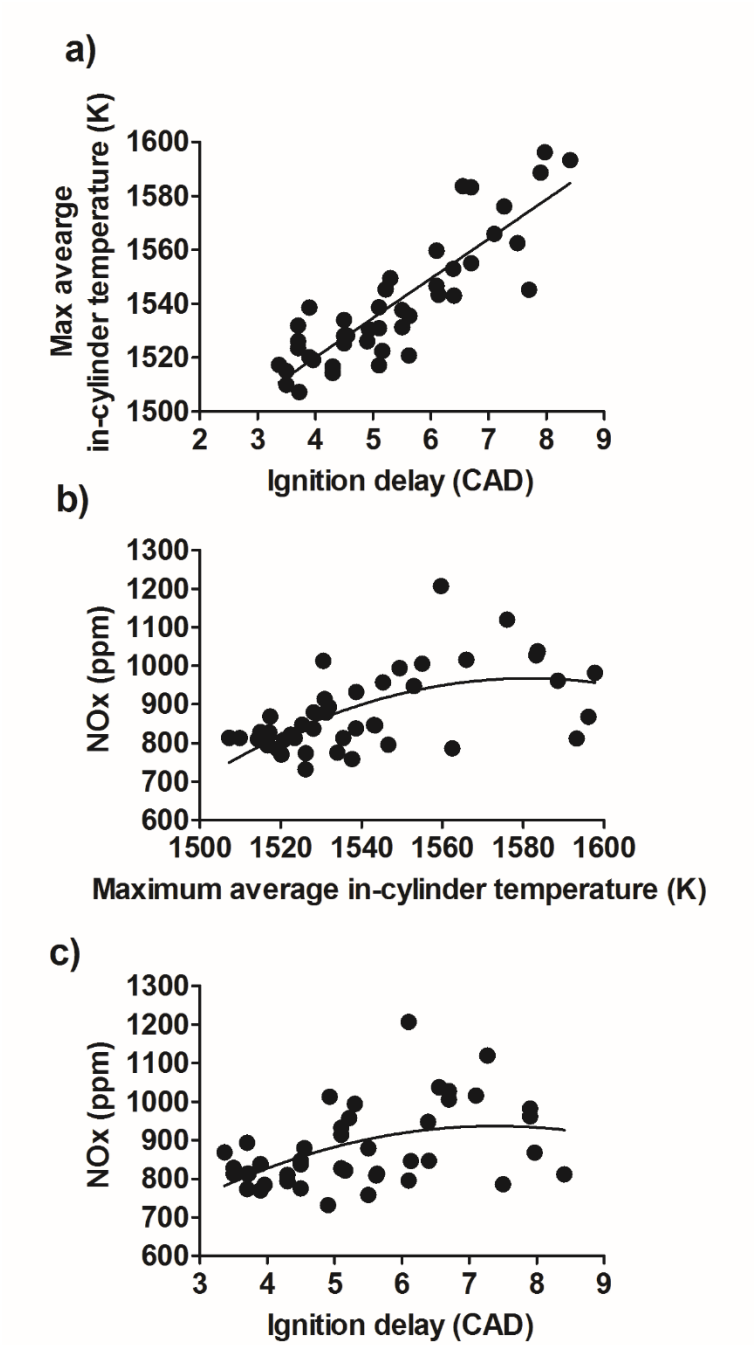

Figure 31. Correlations between (a) maximum average in-cylinder temperature and ignition delay; (b) NO_x emissions and maximum average in-cylinder; (c) NO_x emissions and ignition delay for the tested fuel molecules (excluding 1-octen-3-ol, 3,7-dimethyl-3-octanol and ethyl diglyme).

Further analysis was carried out with the NO_x emission data divided into subgroups based on the structure of the fuel molecules. Figure 32a shows that the NO_x emission decreased with increasing carbon chain length for all subgroups, and it is suggested that this is due to the decreasing ignition delay. In other words, when individual molecules are considered a correlation between NO_x and ignition delay becomes apparent. Similar correlations have been observed for methyl esters in several other studies [204]. It should be noted, that the combustion experiments of molecules with carbon chain longer than 12 carbon atoms were conducted under heated fuel conditions. Therefore, a combination of the fuel higher temperature and diminishing increment in number of carbon atoms may have resulted in NO_x level remaining roughly constant for chains with more than 12 carbon atoms. Figure 32a shows that the oxygenated fuel molecules, excluding carboxylic acids, have higher NO_x emission compared to the alkane fuels. The lower NO_x of alkanes can be explained by their lower in-cylinder temperatures, which are believed to be mainly the result of the shorter ignition delays, compared to those for oxygenated molecules (Figure 29a). This result agreed with several previous studies which have observed that oxygenated biofuels have tend to increase the production of NOx emission [205]. Figure 32a also shows the methyl esters (biodiesel components) to have higher NO_x levels than fossil diesel fuel. Within the oxygenated fuel molecules, shown in Figure 32a, methyl ketones were observed to have the highest NOx emission.

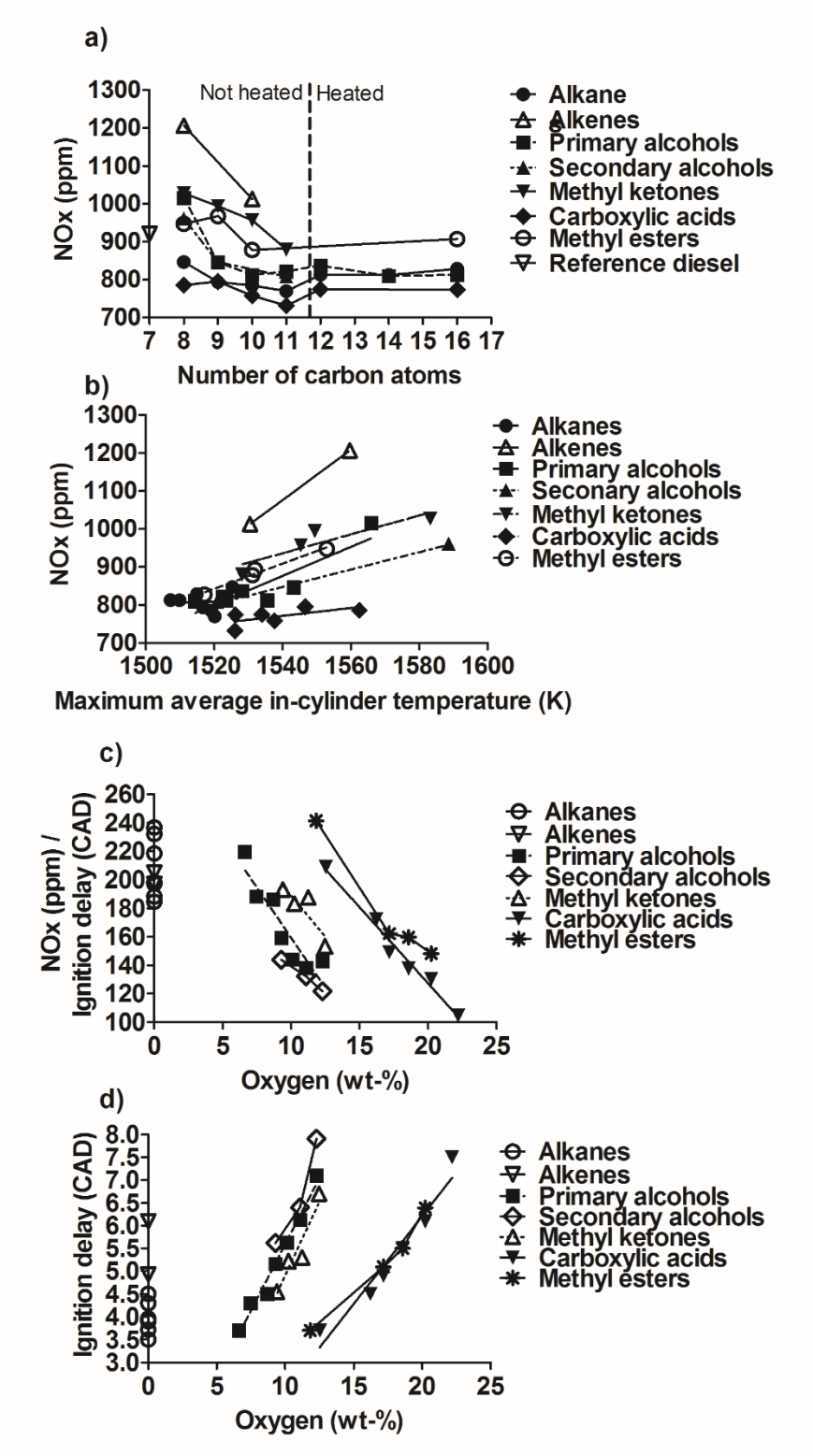

Figure 32. Effect of (a) number of carbon atoms and (b) maximum average in-cylinder temperature on NO_x emissions and effect of oxygen wt-% in the fuel molecule on (a) NO_x emissions normalized with ignition delay and (b) on the ignition delay.

Unlike Figure 31b, where no global correlation was found between NOx and average in-cylinder temperature, Figure 32b shows positive correlations for individual molecule structures. Of the carbonyl and ether compounds shown in Figure 32bthe R square was below 0.8 only for the carboxylic acids correlation (R square is 0.41). In contrast, no significant correlation between the adiabatic flame temperature and NO_x was observed. This absence holds true when NO_x was plotted against the adiabatic flame temperature for all of the molecules combined and for individual molecular functional groups. The adiabatic flame temperatures were calculated according to the method presented by Turns [162].

These results appear to suggest that factors other than adiabatic flame temperatures might control the level of NO_x emissions. This matter will be discussed further in this paragraph. Figure 32c shows the correlations between NO_x normalized with ignition delay and the fraction of the molecular mass accounted by molecule-bound oxygen (See Figure 32d for the effect of molecular oxygen on ignition delay). It can be seen from Figure 32c that when the effect of ignition delay is excluded from the analysis in this way, the oxygen content of molecules has a clear and strong negative correlation with the NO_x. The decrease in NO_x due to higher oxygen content in the fuel molecules within the functional groups could be attributed to the decrease in adiabatic flame temperature with decreasing carbon chain length. This highlights the significance of adiabatic flame temperature in NO_x formation. Similar correlations between the oxygen content of fuel and adiabatic flame temperature with NOx emission were seen in the theoretical investigations of Nabi [181].

The effect of fuel molecular structure on NOx emissions was investigated in more detail in Figure 33. It should be noted, that the scale of Figure 33 is fine and that the trends discussed are very tentative in view of the standard error of mean (5.76 ppm) in the NOx measurements being of similar order as the changes in NOx shown in Figure 33. Figure 33a shows that oxygen bonded to the carbon chain of a molecule as an ether linkage has a positive correlation with NO_x emission. This is the opposite effect of that observed for other oxygen bearing molecules from Figure 32c. It is possible that this increase in NO_x for ethers was partly due to the slightly higher maximum in-cylinder temperatures (Figure 33b), resulting from the higher peak

HRR shown in Figure 34a, and somewhat higher adiabatic flame temperatures (Figure 33c) with increasing number of oxygen in the molecule as an ether linkage. Although ether linkages decrease the change in enthalpy during combustion, the fuel-bound oxygen also decreases the amount of N_2 produced in combustion reactions and therefore may result in the slightly higher adiabatic flame temperatures of ethers compared to the corresponding alkanes (calculation method presented in [162]). Many other experimental studies have, similarly, observed an increase in NO_x with increasing oxygen content of the fuel, e.g. [205].

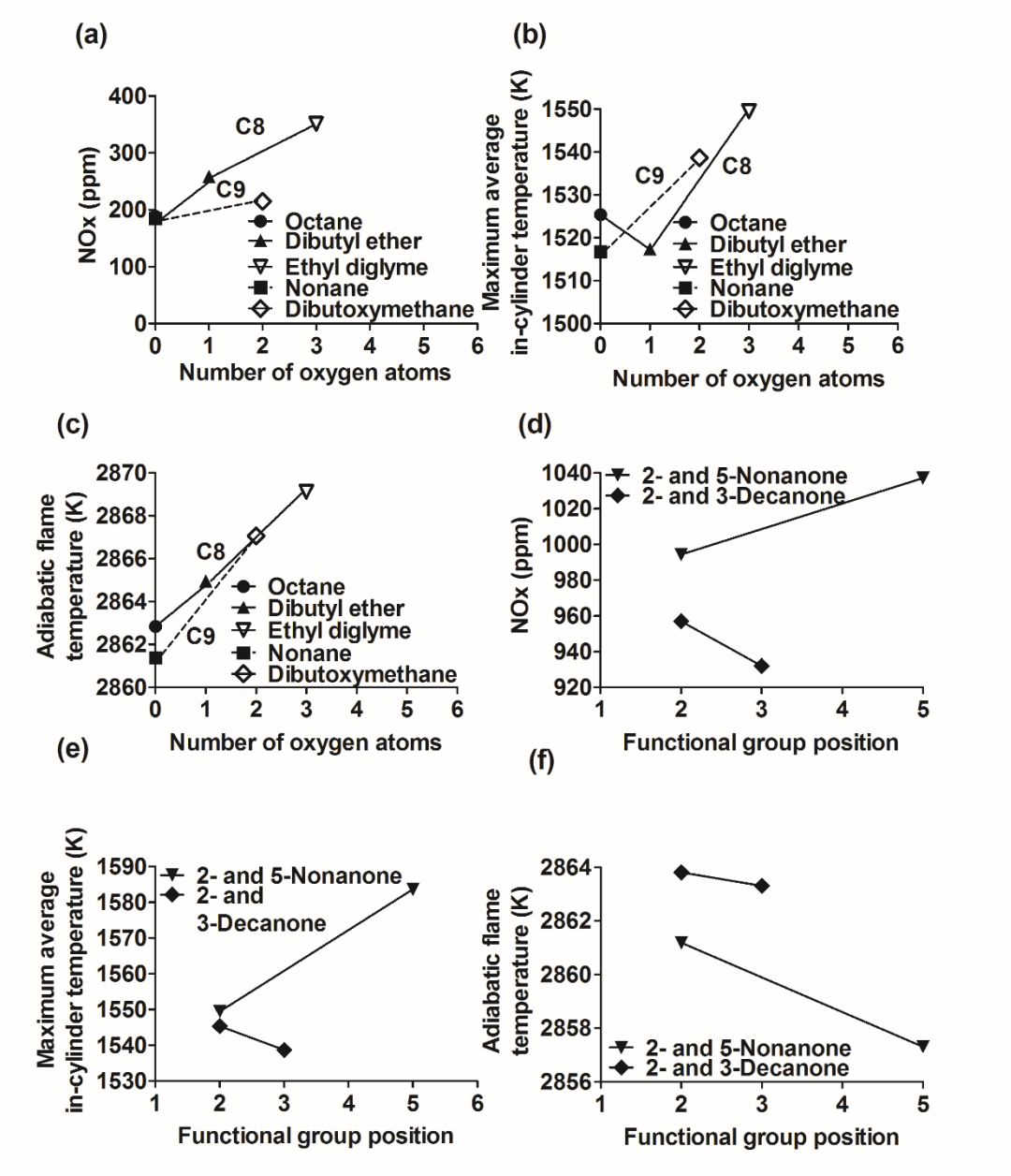

Figure 33. Changes in (a) NOx emissions, (b) maximum average in-cylinder temperature and (c) adiabatic flame temperature caused by adding of ether linkages to alkane structure, and the corresponding changes caused by moving a carbonyl along the carbon chain of a fuel molecule: (d), (e) and (f), respectively.

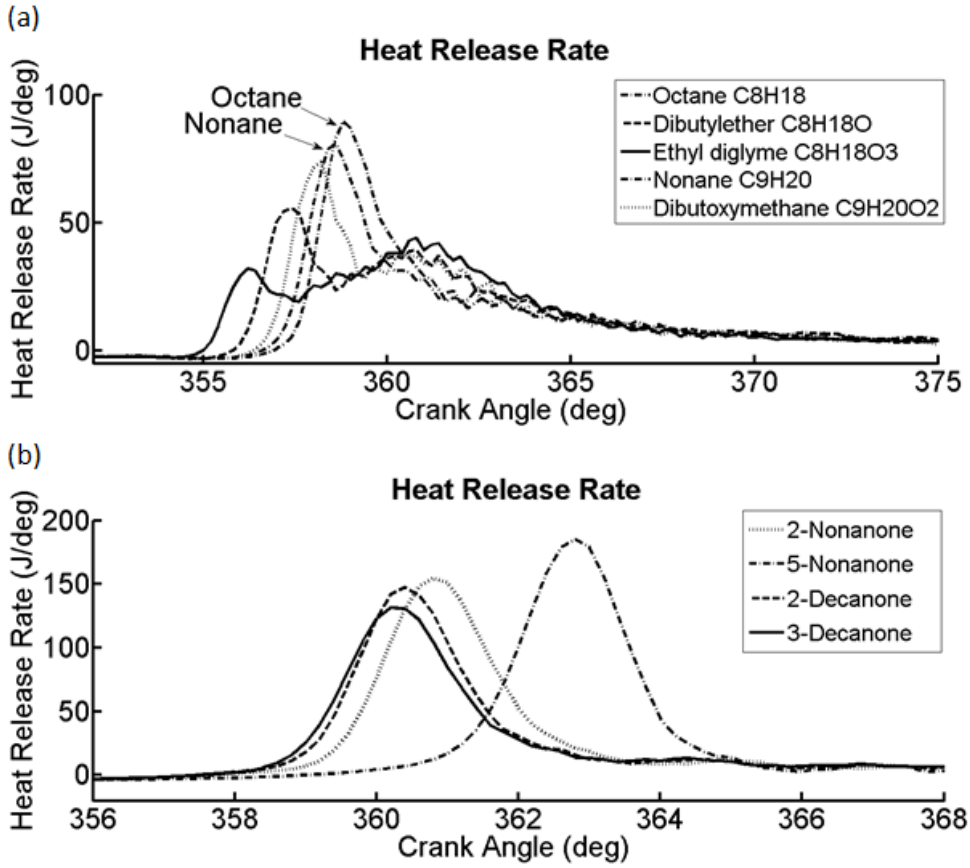

Figure 34. Effect of (a) the number of ether groups and (b) the location of a carbonyl group on heat release rate profile.

The location of a carbonyl group in a fuel molecule was observed to affect somewhat NO_x emission. Figure 33d shows that NO_x emissions were reduced by a small amount when moving a carbonyl group along the carbon chain towards the centre of the molecule in the case of decanone. It would appear that this small reduction in NO_x was due to the decreasing maximum in-cylinder temperature (Figure 33e) and decreasing adiabatic flame temperature (Figure 33f). In the case of nonanone, 5-nonanone had a later start of combustion and a larger premixed phase compared to 2-nonanone, as can be seen from Figure 34 b. This is believed to be the reason for the increase in the maximum in-cylinder temperature which, in turn, resulted in a 5% increase in NO_x emissions.

When comparing the NO_x levels of undecanoic acid to those of 10-undecenoic acid, adding a double bond to a carboxylic acid was observed to increase NO_x emissions significantly. This 50% rise in NO_x emissions is believed to be due to higher values

of both maximum in-cylinder temperature (29K increase) and adiabatic flame temperature (33K increase). In turn, the higher maximum in-cylinder temperature was the result of longer ignition delay and higher fraction of premixed-burned fuel.

5.3.10 Effect of fuel molecular structure on particulate matter

Particulate matter emissions usually originate from fuel-rich areas of the combustion chamber, where soot precursors and small particles combine together instead of being oxidized. PM consists of small primary nucleation particles (diameter 0-50 nm), which combine together to form accumulation particles (diameter 50-1000 nm), which subsequently can agglomerate further into even larger structures. The formation of particulates is influenced strongly by the extent of the premixed combustion phase, the in-cylinder temperature and oxygen availability. [248] With higher premixed phase, overly rich fuel regions are reduced, leading to formation of a smaller mass of particulates, although a large number of small nucleation particles are often recorded, as shown in Figure 35a (excluding the unexpectedly high number of nucleation particles for undecanoic acid). The rapid, high temperature combustion which is characteristic of the premixed phase, combined with good oxygen availability, curtail the relatively time-consuming reactions required for formation of large particulates. The consequence is that the number of large particulates is reduced as the maximum average temperature increases (Figure 35b), while the number of fine particles increases (Figure 35a). Longer ignition delays generally lead to larger premixed phases and higher in-cylinder temperatures and therefore they tend to decrease the mass of particle matter emissions. However, a decrease in the mass of particle matter emissions was observed from Figure 35c to generally result in the formation of a higher number of the smaller particles that are can be dangerous to human health than the larger particulates.

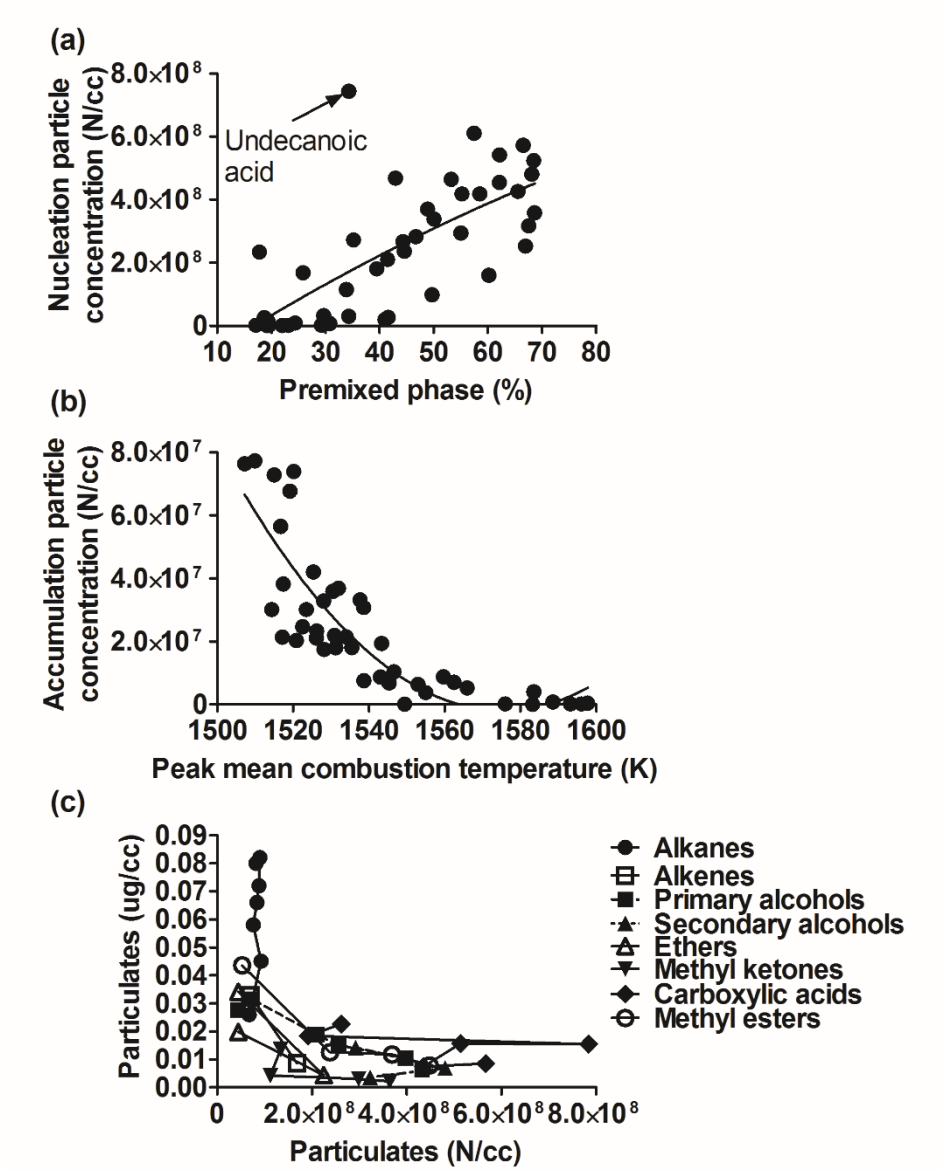

Figure 35. (a) Effect of premixed phase on nucleation particle concentration, (b) the effect of maximum average in-cylinder temperature on accumulation particle concentration and (c) the correlation between the number and mass of particulate emissions (excluding 1-octen-3-ol, 3,7-dimethyl-3-octanol and ethyl diglyme).

Figure 36 shows a tendency for the total particle mass to increase and the number of particles to decrease as the number of carbon atoms in a molecule increases. This is believed to be most likely as the result of the reduction in ignition delays with increasing number of carbon atoms (Figure 29a). As discussed above, shorter ignition delays result in smaller number of particles but greater particulate mass (see Figure 35). Figure 36c attempts to highlight the effect of molecule-bound oxygen on particulate mass emissions. In Figure 36c, the particulate mass emissions are normalized by dividing the mass the number of carbon atoms in the molecule multiplied by ignition delay; both these factors are known to affect the formation of particulate emissions. Figure 36c shows clearly that the molecule bound oxygen has a strong influence on reducing particulate emissions.

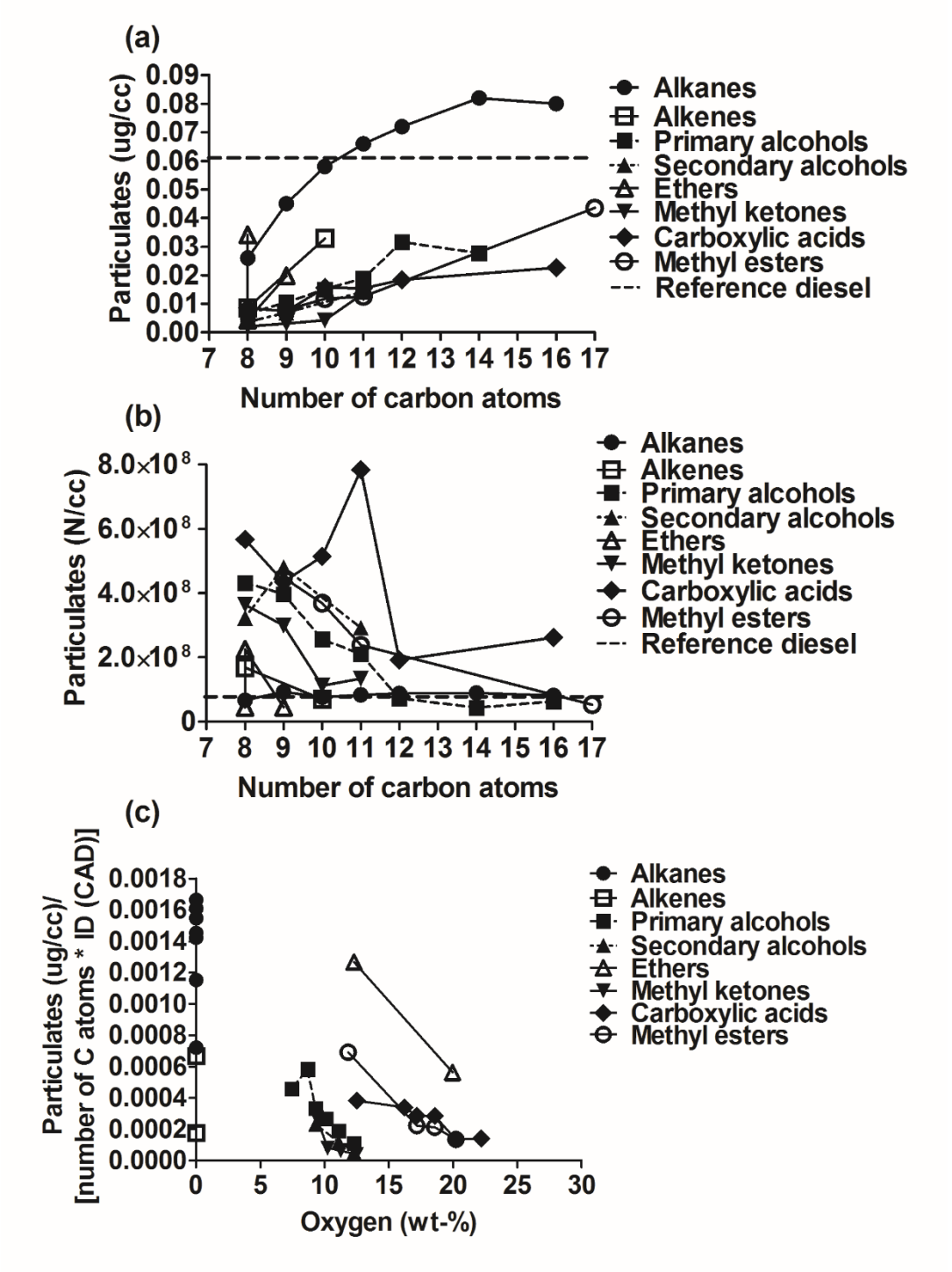

Figure 36. Effect of carbon chain length on number (a) and mass (b) of particulates in the 5-1000 nm size range emitted in the engine exhaust: (c) Effect of oxygen wt-% in the molecule on the formation of particulate mass normalized by the number of carbon atoms in the molecule multiplied by ignition delay.

The effect on PM emissions of adding oxygen to the carbon chain of a molecule as ether linkages was investigated for several molecules having the same number of carbon atoms, by comparing in Figure 37: octane to dibutyl ether and ethyl diglyme; and nonane to dibutoxymethane. Considering the two last compounds first, Figure 37a shows that the addition of two ether oxygen linkages to the non-oxygenated nonane results in an overall decrease in particulate number (both small nucleus particles and larger particulates). Considering the third C8 molecule, ethyl diglyme, it can be seen from Figure 37a that the particulate emission was greater than for the other C8 and C9 molecules. The reason for this observation is most likely to be a combination of chemical and physical properties of this compound. Firstly, the ignition delay for ethyl diglyme is the shortest at 2.4 CAD compared with the range of 3.25-4.5 CAD for the other four compounds. This could be expected to have increased slightly the amount of soot burned in the higher-soot-producing diffusion combustion phase. Furthermore the viscosity, boiling point and density for ethyl diglyme were the highest of these five molecules tested (Appendix II). Therefore, it is expected that the spray atomisation and spray impingement for ethyl diglyme would have been significantly worse, resulting in considerably higher soot formation rate, as observed in Figure 37a. These results are in agreement with several previous studies, which have reported a decrease in particulate emissions for several different ethers compared to diesel fuel [216,261,262].

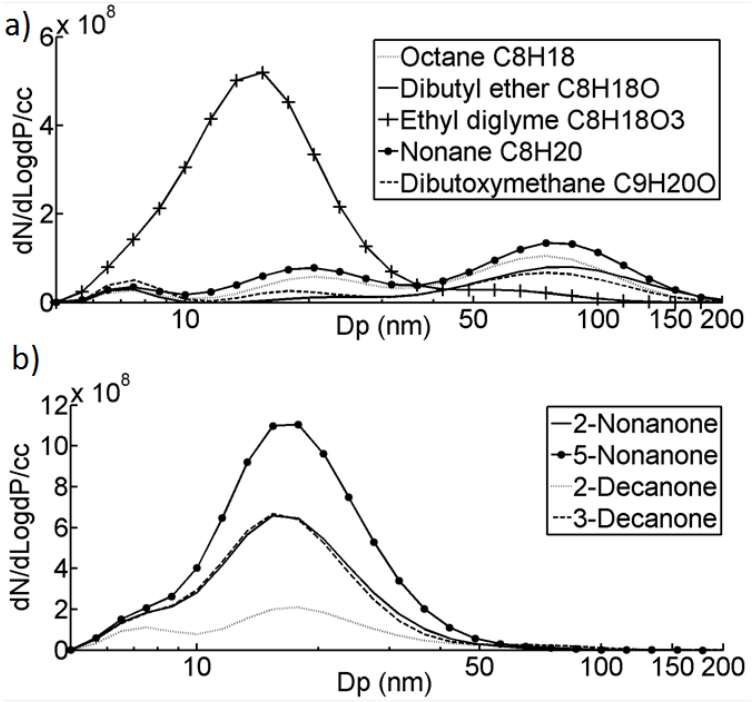

Figure 37. Effect on the size distribution of particulates 0-150 nm of (a) adding oxygen atoms in alkane structure as ether linkages; (b) moving the carbonyl group along the carbon chain of a molecule.

Figure 37b suggests that moving a carbonyl group towards the centre of the molecule increased the number of nucleation particles formed, both in the case of C9 and C10 molecules. Considering 2- and 3-decanone first, Figure 29b shows significant change in ignition delay; furthermore, the physical properties density, boiling point and viscosity are close in value for the two compounds. It is therefore quite possible, that the rise in nucleation particle number observed in Figure 37b is caused by the movement of the carbonyl group from the second to the third carbon atom for these C9 molecules. In contrast, in the case of 2- and 5-nonanone, the ignition delay is seen in Figure 29b to increase approximately 1.3 CAD, although the physical properties are no significantly different for these two compounds. As discussed previously, an increase in ignition delay leads to an increase in the number of nucleation particles and, for this reason, it is not possible to say whether the rise in nucleation particles seen in Figure 37a was due to the movement of the carbonyl group or due to the change in ignition delay.

When considering the effect of unsaturation on particulate emissions, adding a double bond to undecanoic acid to form 10-undecenoic acid was observed to decrease both the mass and the number of particulates. It is believed that this decrease in the number of particulates occurred as a result of the longer ignition delay and, thereby, larger premixed phase and higher in-cylinder temperature of 10-undecenoic acid compared to undecanoic acid.

5.4 Conclusions

Results have been presented on the effects of a large number of oxygenated functional groups on the auto ignition behaviour and exhaust gas emissions of a diesel research engine. The molecules considered included alkanes, alkenes, alcohols, ketones, carboxylic acids, methyl esters and ethers. The main molecular features affecting ignition delay appear to be the higher electronegativity of a fuel-bound oxygen atom compared to a fuel carbon atom, the way an oxygen atom is bonded to the carbon chain of the molecule, and the location of the oxygenated functional group in the molecule. These three features affect the ignition delay mainly through the changes in hydrogen abstraction and isomerisation. In general, fuel molecules with oxygenated functional groups had higher ignition delays than alkanes of the same carbon atom chain length. This may appear to be paradoxical in view of many observations in the literature that oxygenated biodiesel has shorter ignition delay than conventional fossil diesel fuel. However, the results presented here suggested that the lower ignition delay of commercial biofuels compared to diesel fuel, often observed by researchers, is mainly due to the longer hydrocarbon chains of the oxygenated biofuel molecules compared to the chain length of the hydrocarbon molecules in diesel fuel and the absence of cyclic compounds in biodiesel.

Both the engine in-cylinder temperature and the fuel adiabatic flame temperature were observed to influence exhaust levels of NO_x. Additionally, it was found that oxygen in the fuel molecular structure affected NO_x formation through several other factors, than merely though the ignition delay, such as the oxygen content. Generally, the particulate number in the exhaust gas was observed to increase with increasing size of the premixed phase, and the mass of particulates to decrease with increasing in-cylinder temperature. Furthermore, a small trade-off was observed between the

NO_x emissions and the mass of PM emissions with oxygen addition into the fuel molecule.

Turning now to the specific conclusions, these can be listed as follows:

5. Compared to alkanes, fuel molecules with an oxygenated functional group bonded to a carbon chain as a branch had higher ignition delays, higher NO_x emissions and lower particulate emissions.
6. Oxygen bonded to the fuel molecule as an ether linkage decreased the ignition delay, increased NOx levels and reduced PM emissions compared to alkanes.
7. Compared to carbonyl groups, alcohols had higher ignition delays, lower NO_x levels (excluding carboxylic acids), and slightly higher particulate emissions.
8. Carboxylic acids had similar ignition delays, lower NO_x levels and slightly lower particulate emissions than alcohols.
9. Methyl esters and methyl ketones had similar ignition delays, which were the lowest of the oxygenated fuel molecules, excluding ethers.
10. Methyl ketone combustion led to the formation of the highest NO_x levels, and the lowest particulate emissions of the oxygenated fuel molecules, excluding ethers.
11. Moving a hydroxyl group or carbonyl group closer to the centre of the carbon chain increased ignition delays, reduced NOx levels and increased particulate emissions.
12. Higher level of unsaturation led to higher ignition delays, higher NOx levels and lower particulate emissions.

In general, changing the molecular structure of the fuel can be used to alter the combustion profile and the exhaust gas emissions of a fuel.

Chapter 6

The effect of fuel molecular structure on the thermal engine efficiency of alcohols, carbonyl compounds and ethers

6.0 Introduction

The lower heating values of oxygenated fuels, compared to that for fossil diesel fuel, result in less work output being produced for each engine cycle from a fixed mass of fuel injected into the combustion chamber. This has been demonstrated in experiments with palm and canola oil methyl esters by Ozsezen et al. [263]. In order to achieve a given work output with biofuels, a higher volumetric injection rate is sometimes used (compared to that for fossil fuels), and this has been observed to lead to higher brake specific fuel consumption for biofuels [263–265]. However, the effect on engine efficiency of oxygen in the molecular structure of a fuel is not yet fully understood and is, therefore, explored further in this chapter.

Different experimental conditions and a wide variety of engines have been used in engine efficiency studies published in the literature and this variety makes comparisons between engine efficiency studies difficult. For example, a review article written by Azjargal [265] found that biodiesel addition to fossil diesel fuel in general reduces the engine efficiency, compared to that of fossil diesel fuel alone. However, several studies [263,264,266] have shown biodiesel to have similar engine efficiency to that of fossil diesel fuel, while some studies [267–270] have reported an increase in break thermal efficiency on order of around 0.5-5% percentage points with 20% biodiesel in biodiesel/diesel blends. In the case of alcohols, Kumar et al. [271] stated in a review article that alcohols, when added to fossil diesel fuel, can increase the engine efficiency due to the rapid combustion of alcohols. Imtenan et al. [99] showed that replacing 5% and 10% of jatropha biodiesel in B20 biodiesel/diesel blend with butanol increased the break thermal efficiency by 2.8 and 5.3 percentage points, respectively.

This chapter considers the effect of chemical and physical properties of a wide range of fuels on the thermal efficiency of a single cylinder diesel research engine. The impact on engine efficiency was considered using 43 mostly oxygen-bearing fuel

molecules, which could potentially in future be obtained from renewable sources. The 43 single-molecule fuels investigated included the molecules whose ignition and emissions have been investigated in chapters 4 and 5. In order to assist the interpretation of the results, a theoretical investigation is also presented, which examined the effect on efficiency of the injection timing and the rate of fuel energy release (heat release rate). For this theoretical investigation a zero-dimensional, non-adiabatic thermodynamic model was used which accounted explicitly for energy dissipation due to heat transfer and rejection of energy in the engine exhaust.

6.1.Experimental methods

6.1.1. Experimental conditions

The tests were conducted at the following engine running conditions: constant injection timing of 7.5 CAD before top dead centre (BTDC), 1200 rpm engine speed, 600 bar injection pressure, and 4 bar indicated mean effective pressure (IMEP). To detect any day-to-day drifts in the equipment and the instrumentation, reference diesel was repeatedly tested every day, as the first and last experiment of each day. In this way, a data set was created of 26 repeat tests with reference diesel. A statistical analysis of this set of 26 repeat tests allowed the mean value, standard deviation and the standard error of the mean value to be calculated for the measured indicated thermal efficiency as follows: the mean value of the 26 measurements of thermal efficiency was 38.09%, the standard deviation was 0.43 percentage points and the standard error of the mean value was 0.108 percentage points. Due to their high viscosity, some of the tested molecules were heated to 343 K, before injection into the combustion chamber. The molecules with elevated injection temperatures were alkanes and alcohols with carbon chain lengths longer than C11; also heated were 3,7-dimethyl-1-octano, 3,7-dimethyl-3-octanol, carboxylic acids with carbon chain length longer than C10, and methyl hexadecanoate. In order to reduce systematic errors arising from equipment drift or gradual changes of environmental conditions during each test period, the 43 fuels were tested in random sequence, so that fuels with similar structures, on homologous molecular series, were not tested consecutively on the same day or in the same test session.

6.1.2. Fuel molecules tested

The physical properties of the tested fuel molecules can be found in Appendix II. In total, 43 molecules of different molecular structures were tested, many of which included one or more oxygen atoms in their structure in a variety of sub-molecular functional group configurations. It should be noted, as mentioned previously, that due to the high viscosity of long chain molecules, fuel molecules larger than C11 were heated to 343 ±3K before injection in the engine combustion chamber.

6.2.Results and discussion

6.2.1. Effect of energy release rate on thermal engine efficiency

Figure 38a shows that the proportion of fuel burned in the premixed combustion phase was controlled strongly by the ignition delay period. Long delay periods of up to 8 CAD allowed more time for evaporation and mixing of the fuel with air and resulted in up to almost 60% of the injected fuel being burned in the premixed mode. On the other hand, short ignition delay periods of around 3.5 CAD curtailed the evaporation and mixing processes, resulting in some cases in only about 20% of the injected fuel burning in the premixed combustion mode and the other 80% in the diffusion-controlled mode. It should be noted, that while the period of ignition delay was largely controlled by the low temperature reaction kinetics of individual molecules, the amount of fuel premixed during this delay period was largely controlled by the compressed in-cylinder gas conditions (temperature and pressure) and the physical properties of the fuel (density, surface tension, boiling point and viscosity). The influences of physical fuel properties were exercised through the effect of those properties on spray formation (spray beak-up, penetration and droplet size distribution) and the rate at which the fuel spray vaporized and mixed with the surrounding highly turbulent and high-temperature air.

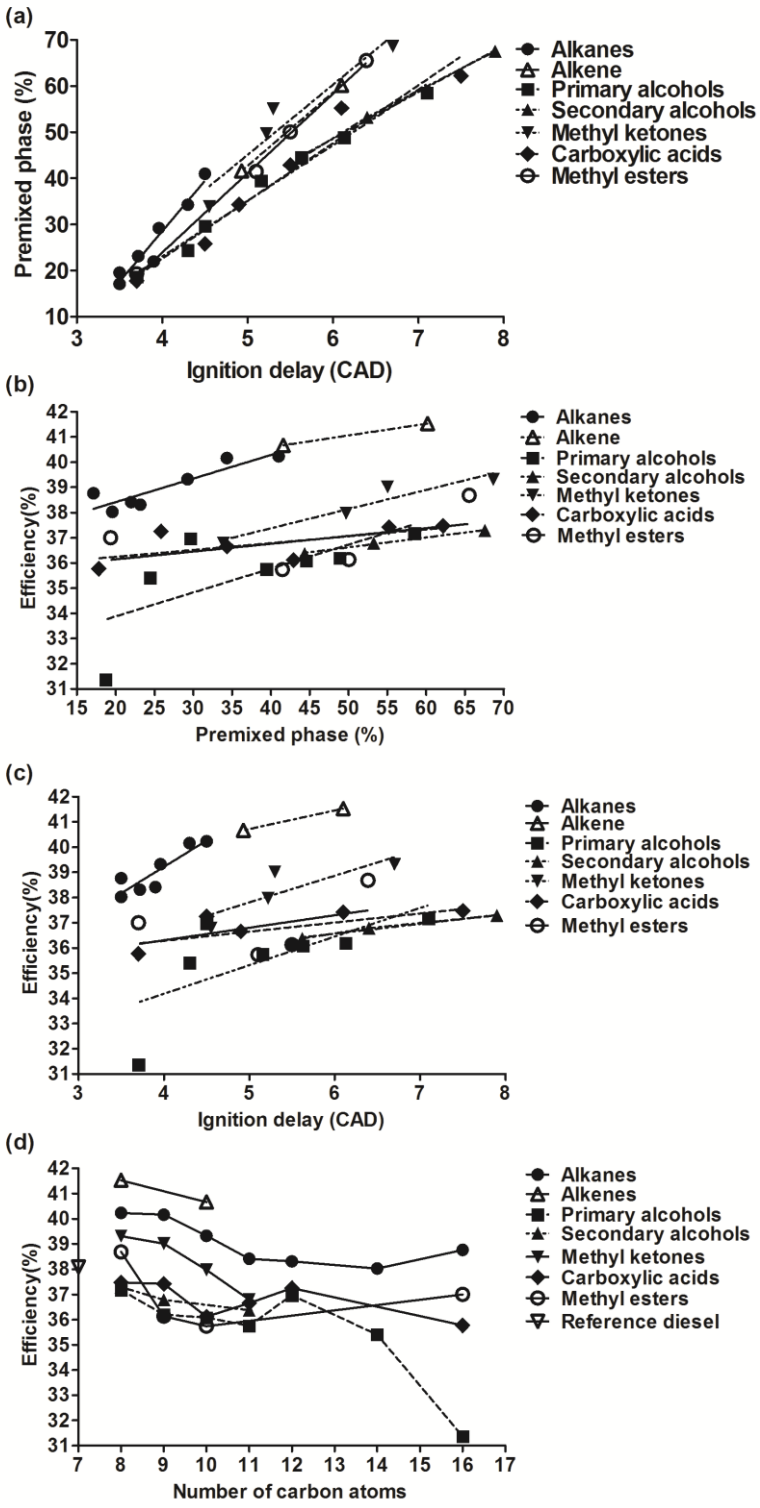

Figure 38. (a) Effect of ignition delay on the size of the premised combustion phase: effect of (a) magnitude of premixed combustion phase and (b) ignition delay on indicated engine thermal efficiency: (d) engine thermal efficiency of fuel molecules from different molecular groups.

Figure 38b shows that the engine indicated thermal efficiency was enhanced by more of the injected fuel being burned in the premixed mode. However, an increase in the premixed fuel percentage from 20% to 60% appeared to increase the engine efficiency by only about 2 or at most 3 percentage points (%-units). It is interesting, but not surprising, to see from Figure 38c that ignition delay has an influence on engine efficiency, through the control that the delay period has on the amount of fuel burned in the premixed mode (see Figure 38a). Figure 38c shows that an increase in ignition delay from 3.5 CAD to 7 CAD tends to raise the engine efficiency by about 2, or at most by 3, %-units. Figure 38b and Figure 38c show considerable scatter in the correlations for efficiency, for individual fuel groupings. Some of this scatter could be expected to be due to random experimental error in measuring the engine efficiency; with the standard error increasing the efficiency being at least ±0.43%-units (see section 1.3). It should also be noted, that when CA50 points in CAD were plotted against engine efficiency (not shown here), no correlation was observed when all of the molecules were considered together. When considering the fuel groupings alkanes had a good negative correlation: engine efficiency decreased when CA50 point occurred later in the engine cycle, as was expected because the shape of the HRR curves were similar for all of the alkanes with the peak heat release rate increasing with later ignition. However, no good correlations were observed for the oxygenated fuel groups. This suggests that both the timing and the shape of HRR have an effect on the engine efficiency.

6.2.2. Effect of chemical fuel properties on engine thermal efficiency

The tested molecules were grouped according to functional groups (alkanes, alkenes, alcohols, esters, etc.) in their molecular structure (see Appendix II). Figure 38d shows engine efficiency to decrease somewhat with increasing carbon chain length for all the functional groups. This decrease in efficiency with increasing carbon chain length is believed be the result of decreasing ignition delay when carbon chain is increased. In general, longer carbon chain molecules have shorter ignition delays which result in smaller premixed phases and thus in lower engine efficiency (see also Figure 38a

and Figure 38b). There is some support for this statement in the literature, for example Campos-Fernández et al. [193] observed that addition of 20%, 25% and 30% of butanol (C4) into fossil diesel fuel increased brake thermal efficiency slightly more than the corresponding additions of pentanol (C5); Balamurugan and Nalini [188] observed that the addition of 4% butanol into fossil diesel fuel increased the brake thermal efficiency by about 7.34 %-units more than the increase caused by the addition of 4% pentanol. Closer observation of Figure 38d suggests that the effect on efficiency beyond chain length of C11 is very small, save for the case of the very viscous primary alcohol hexadecanol (C16). Molecules with carbon chain length longer than C11 were heated prior to being injected into the combustion chamber and this may have had an effect of reducing the sensitivity of the efficiency to carbon chain length.

Figure 38d also suggests that alkanes and alkenes achieve higher engine thermal efficiency than oxygenated fuel molecules with the same carbon chain length. This suggestion is supported by the results of several other studies which have shown that, for example, methyl esters [186,272,273] and fatty acids [274,275] had lower engine efficiency than diesel fuel. The observed difference between the engine efficiency of alkanes and oxygenated fuel molecules was explored further in Figure 39a, which shows the energy release rates of several C9 molecules, one each of an alkane, methyl ketone, methyl ester, acid, and alcohol. Figure 39a shows distinctly different patterns of energy release between the alkane molecule (nonane) and the four oxygenated molecules, with nonane having shorter ignition delay, a smaller premixed combustion phase and a long diffusion controlled phase. The fact that nonane has higher efficiency than the oxygenated molecule (see Figure 38d) is, therefore, surprising. In principle, one might expect the oxygenated fuel molecules to have a higher engine efficiency than the alkane molecule (nonane), because the oxygenated molecules have the majority of their energy released rapidly and close to TDC, which is closer to the theoretical air-standard Otto-cycle which has the highest thermal engine efficiency amongst the internal combustion engine-related air-standard cycles with same compression ratio [1]. The effect of molecular oxygen on thermal efficiency is explored further in Figure 39b.

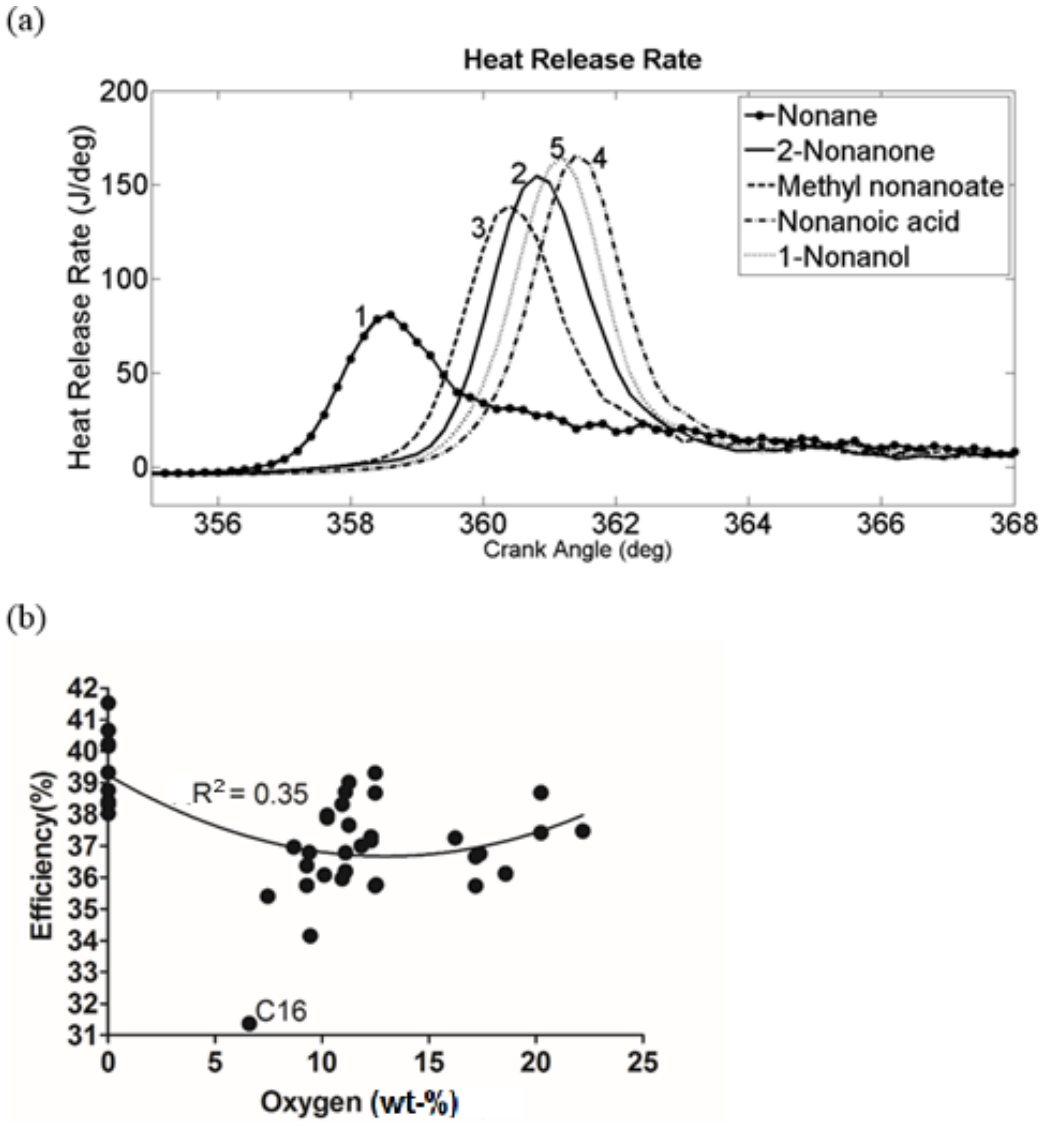

Figure 39. (a) Heat release rate of C9 molecules from five different functional groups (numbers indicate the general engine efficiency of the functional groups with 1 being the highest and 5 the lowest) and (b) the effect of fuel-bound oxygen on engine efficiency.

Figure 39b shows the thermal engine efficiency plotted against the percentage of oxygen (wt-%) in the various fuel molecules tested. Before discussing Figure 39b, it should be noted that hexadecanol, labelled C16 in Figure 39b, can be seen to have a very low efficiency of ~31% and further investigation of the energy release rate showed that hexadecanol combusted only partially and this is likely to have been due to its high viscosity (Appendix II) and likely poor combustible mixture preparation.

Figure 39b shows quite a poor correlation ($R^2 = 0.35$) between efficiency and wt-% of oxygen in the fuel molecule. Despite the poor correlation of Figure 39b, it is possible to see that the non-oxygenated molecules (plotted on the y-axis at zero wt-%) are clustered around an average efficiency of ~39.5% while the oxygen-bearing molecules are clustered around an average efficiency of ~38%. This is only a tentative observation, as the experimental error in measuring the thermal efficiency was estimated at ±0.43 %-units, which tend to swamp any effect that increasing molecular oxygen might have on efficiency. Reports in the literature on the likely effect of molecular oxygen on efficiency are not unequivocal [181,183,184,276], probably because any effect is likely to be small and not readily measured. According to Nabi [181], the fuel oxygen content has no effect on engine efficiency below 30 wt-% oxygen and has a negative correlation with efficiency with oxygen over 30 wt-%. Labeckas and Slavinskas [183] found that efficiency started to decline rapidly beyond 10 wt-% of rapeseed methyl ester added to fossil diesel fuel.

Figure 40 explores potential changes in engine efficiency caused by the following changes in the fuel molecular structure: Figure 40a, molecular branching; Figure 40b, moving either a hydroxyl or a carbonyl group along the carbon chain of a molecule; Figure 40c, the level of unsaturation (reduction in hydrogen/carbon ratio). Taken together, the data in Figure 40 does not indicate clear influences of these molecular features on engine thermal efficiency. Any influence of molecular branching (Figure 40a) appears to be small, no greater than ±0.5%-units and not significantly greater than the experimental error in the measurement of the engine thermal efficiency. Similarly, trends in engine efficiency versus the functional group position (Figure 40b) are not clear, with the ±0.75 %-units change in efficiency for individual molecular groups not being significantly greater than the experimental error in the measurement of the thermal engine efficiency (±0.43%). In Figure 40b, some of the homologous series (e.g. 1-, 2-, and 3-octanol; 1-, 2-, 3-nonanol; 1- and 2-undecanol) show the efficiency rising with transition of the hydroxyl group (OH) away from the primary position; this transition caused lengthening of the ignition delay period and is therefore consistent with Figure 38b and Figure 38c, which shows efficiency increasing with longer ignition delay, but this can only be considered as a tentative observation. Lastly, Figure 40c suggests that the degree of unsaturation is associated

with lower thermal efficiency which is inconsistent with the fact that greater level of unsaturation caused longer ignition delays.

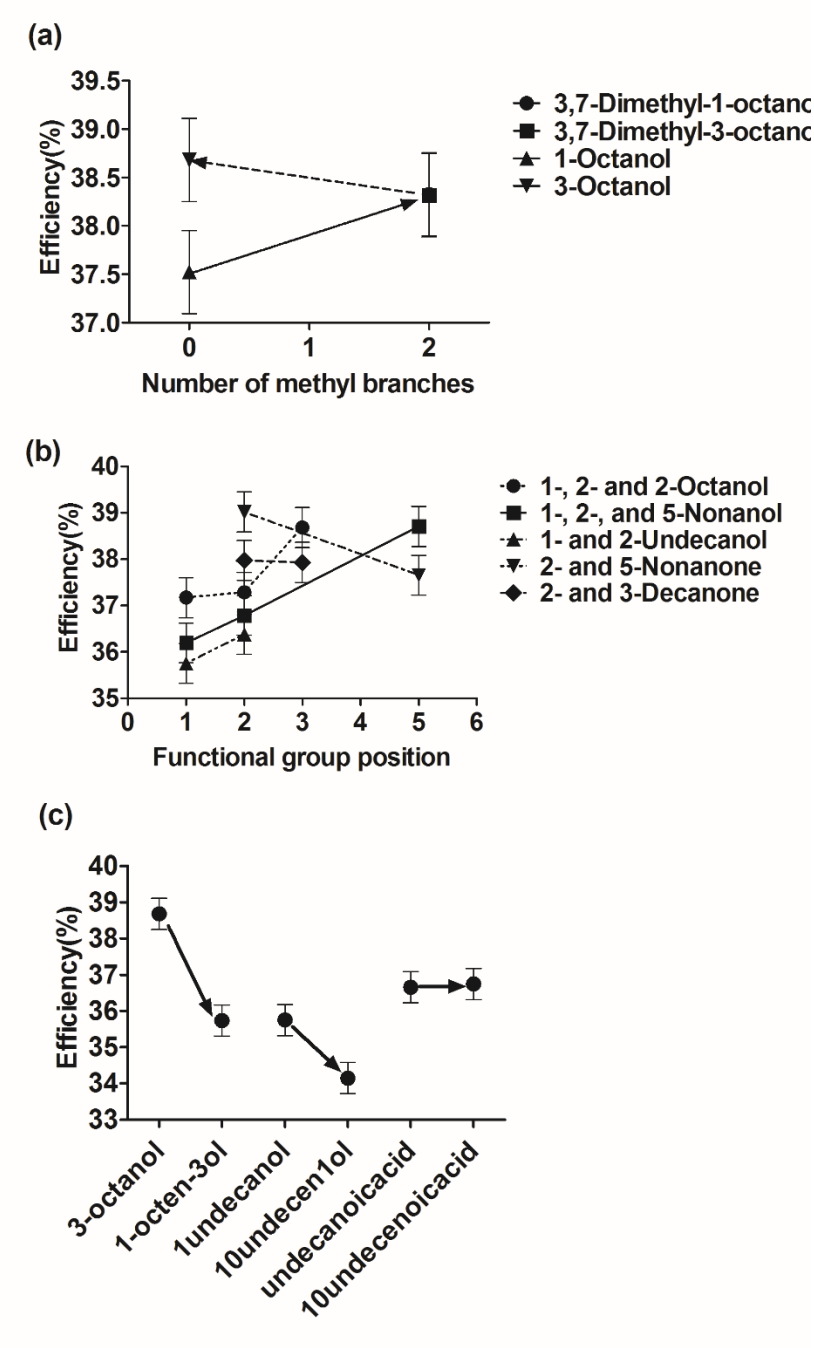

Figure 40. Effect on engine efficiency of (a) branching (arrows indicate the direction of adding two methyl branches to an alcohol), (b) moving a hydroxyl group or a carbonyl group along the carbon chain length of a fuel molecule and (c) level of unsaturation.

6.2.3. Effect of physical fuel properties on thermal engine efficiency

So far, the results presented appear to indicate that the only significant influence on thermal engine efficiency is that of ignition delay, with this influence likely to be exercised through changes in the shape of energy release rate (represented by the amount of premixed combustion). This section explores potential associations between fuel physical properties and thermal efficiency. Figure 41 shows the relation between efficiency and three major physical fuel properties. Starting with Figure 41a, considering all the data in Figure 41a together, it appears that there is a negative correlation between efficiency and fuel density, with molecules having low density showing higher efficiency and molecules with high density showing lower efficiency. However, closer examination of the individual molecular groups in Figure 41a indicates that not all the molecular groups show a negative correlation between efficiency and density. For example, the carboxylic acids and the esters show virtually no correlation between efficiency and density. Similarly, the primary and secondary alcohols also appear to show no clear correlation. This leaves the alkanes with a clear indication of a negative correlation between efficiency and density, although even the variation in density within the alkane group is small (about ±3.5% of the mean density value). It is therefore suggested that there is no clear evidence of a correlation between thermal engine efficiency and fuel density for the molecules shown in Figure 41a, save possibly in the case of alkane molecules, where a ±3.5% change in density appears to be associated negatively with a ±1% change in thermal efficiency.

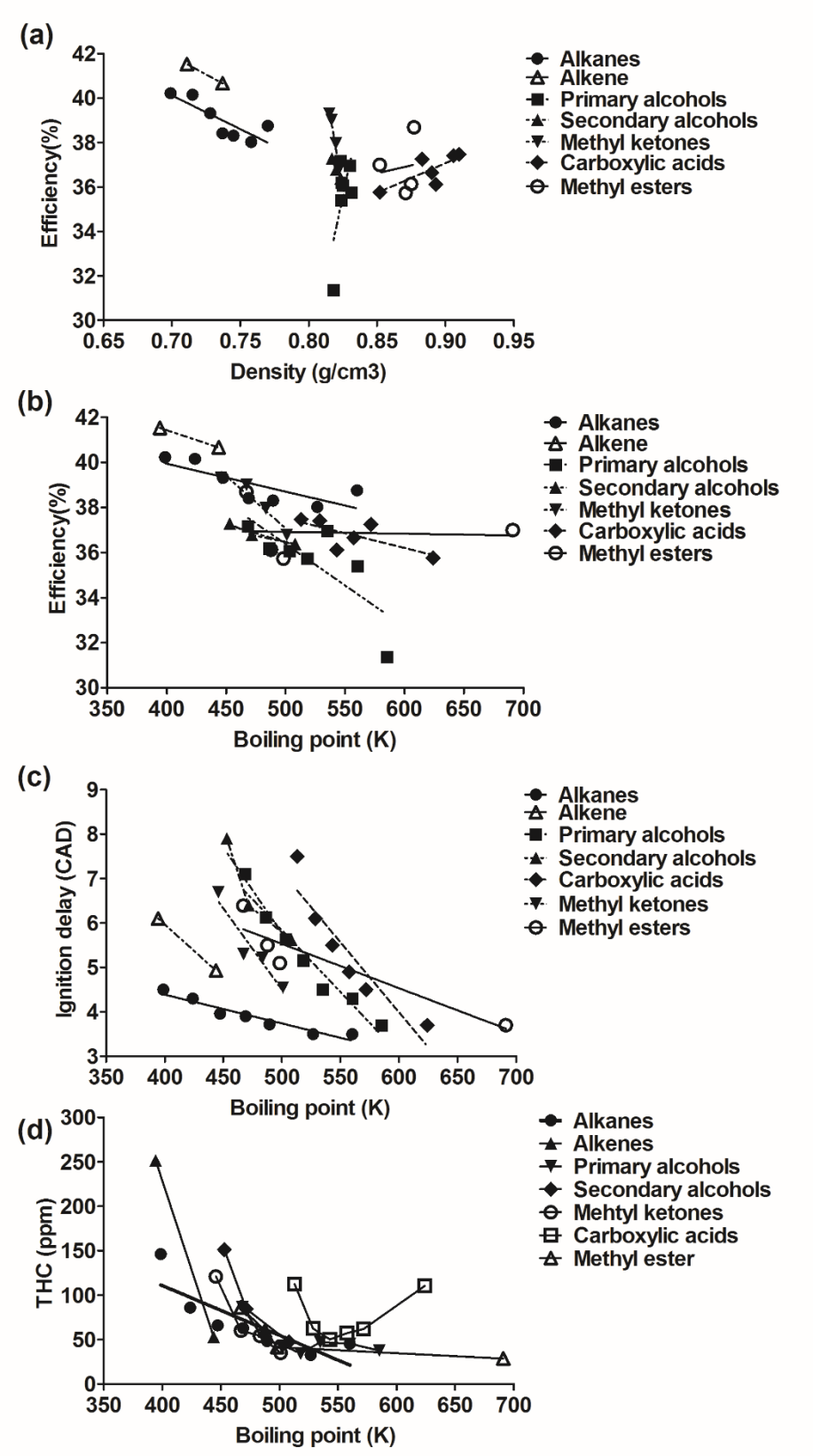

Figure 41. (a) The effect of density on engine efficiency; The effect of boiling point on (b) engine efficiency and (c) ignition delay; (d) The effect of boiling point on total unburned hydrocarbon emissions in the exhaust gas.

Moving onto the influence of fuel boiling point on thermal engine efficiency, Figure 41b suggests that there is a negative correlation between efficiency and boiling point, with higher boiling points leading to lower efficiency. This negative correlation between efficiency and boiling point can be seen in Figure 41b to hold, both, when all the fuel molecules are considered together, as well as when each individual molecular group is considered. However, the negative correlations are subject to considerable amount of scatter and, thereby, considerable uncertainty. Thus it is useful to consider, briefly, why molecules with high boiling points (less volatile) tend to result in lower efficiency. Potentially, any influence of the boiling point on efficiency may be because of its association with the ignition delay (Figure 41c): longer chain molecules, compared to shorter chain ones, tend to have higher boiling points but also shorter ignition delays as a result of their longer chains; in turn, the shorter ignition delays have been shown earlier in the study to be associated with lower engine efficiency (see Figure 39b and also Figure 38d). Additionally, molecules with high boiling points (i.e. less volatile) could have poorer mixing and poorer combustion. However, this potential effect on efficiency can be discounted here, because Figure 41d shows molecules with high boiling points (less volatile) to have relatively low levels of the unburned hydrocarbons in the exhaust gas. It is therefore possible to reach a conclusion that higher boiling point (less volatile) fuels tend to have shorter ignition delays and this could potentially lead to somewhat lower thermal efficiency.

Two other physical properties were explored in Figure 42 (viscosity and surface tension). Both these physical properties appear to have negative correlations with engine efficiency. One obvious explanation would be that higher viscosity and higher surface tension lead to poorer spray formation and air fuel mixing, resulting in lower combustion efficiency (less fuel being burned) This potential explanation and some additional ones will be discussed further below, using a cluster analysis of two distinctly different sets of molecules, alkanes and carboxylic acids.

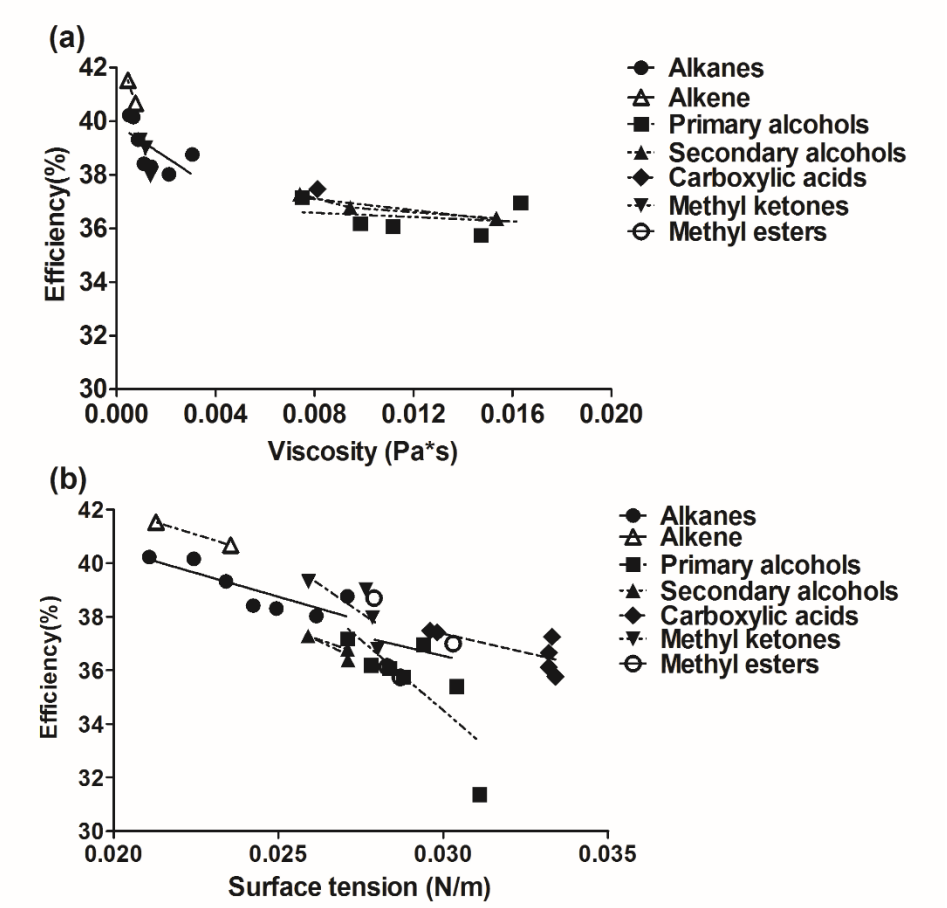

Figure 42. Effect of (a) viscosity and (b) surface tension on engine efficiency (data not available for all of the tested molecules, see Appendix II).

A closer observation of data clusters in Figure 41 and Figure 42 shows that the alkane set of molecules has, on average, higher engine efficiency (~39.5%) than carboxylic acids (~37.5%); alkanes also can be seen from these two figures to have substantially different physical fuel properties to those of the acids. The alkanes have lower density (mean 0.74 g/cm^3 compared with 0.89 g/cm^3 for the acids) lower boiling points (mean 474K compared to 556 K), lower viscosity (mean 0.0015 Pas compared to 0.008 Pas), lower surface tension (mean 0.024 Nm compared to 0.032 Nm), while the thermal engine efficiency for the alkanes is higher with mean value of 39.5% compared to 37.5% for the carboxylic acids. Plots of efficiency against THC and CO (not shown here) for these two sets of molecules showed, clearly, that unburned fuel and intermediate combustion products was not the reason for the lower efficiency of the acids compared to the alkane set of fuels, as both sets of fuels emitted approximately

similar levels of THC (alkanes mean 70 ppm; carboxylic acids mean 76 ppm) and CO (alkanes mean 237 ppm; carboxylic acids mean 267 ppm). In terms of particulate mass emissions, the alkanes in fact emitted somewhat higher particulate emissions in the exhaust (mean 0.06 μg/cm^3 compared to 0.015 μg/cm^3 for the acids) despite the higher engine efficiency of alkanes. Another potential explanation considered was that the energy rejected in the hot exhaust gases for the acids might have been greater than that for the alkanes, however his explanation was discounted as both sets of molecules had similar mean values of exhaust gas temperature (517K for alkanes and 513K for carboxylic acids). The final explanation considered for the higher average efficiency of alkanes compared to that of carboxylic acids related to the prolonged injection period for the acids (electronic pulse duration 684 μs) compared to that of the alkanes (pulse duration 578 μs), due to the lower calorific values of the acids (mean 33.8 kJ/kg compared to 44.5 kJ/kg for alkanes). Bearing in mind that a minimum electronic pulse duration of ~280 μs is required to cause fuel flow out of the injector, the net injection duration for the acids was ~36% greater than that for the alkanes. Therefore, the substantially longer injection period of the acids may be associated with their lower thermal efficiency compared to the thermal efficiency of the alkanes. The following paragraph will consider reasons why prolonged injection period for the acids may have led to their lower thermal engine efficiency.

Figure 43a compares the energy release rate of hexadecanoic acid with the release rates of three alkanes which were selected because they had nearly the same ignition delays and exhaust gas temperatures as those for the hexadecanoic acid (ignition delay 3.7 CAD, exhaust gas temperature 517 K). The three alkanes were: hexadecane (3.5 CAD, 520 K), tetradecane (3.5 CAD, 520 K) and dodecane (3.7 CAD, 519 K). Figure 43a shows that the early energy release rate for the acid was considerably lower, but during the diffusion controlled phase it was higher at a sustained level. In contrast, the early energy release rate for the alkanes was higher and close to TDC (premixed combustion mode); while the rate of diffusion controlled burning was lower than that of the acid. It is, therefore, likely that the higher and sustainable energy release rate in the expansion stroke for the acid resulted in higher energy loss by means of heat transfer to the increasing surface areas of the combustion chamber walls, and this may account for the lower efficiency of the acids compared to that for the alkanes. Figure 43b shows a similar comparison of heat release rates for another

acid, dodecanoic acid (ignition delay 4.5 CAD, exhaust gas temperature 516 K) and the release rate for two alkanes with similar values of ignition delay and exhaust gas temperature as those for the acid. The alkanes were: octane (4.5 CAD, 516 K) and nonane (4.3 CAD, 510 K). Figure 43b shows, as discussed above, that the acid had a higher and more sustained energy release rate during the expansion stroke which could potentially have led to higher energy dissipation through heat transfer and, thereby, to lower engine efficiency.

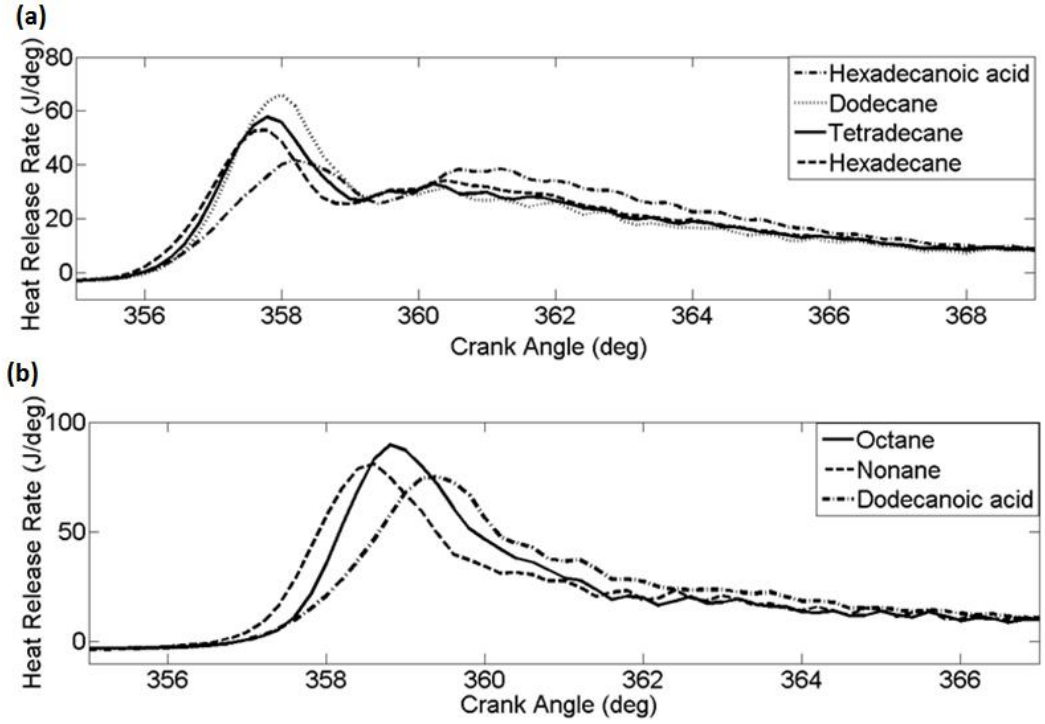

Figure 43. The heat release rates of alkanes and carboxylic acids with ignition delay around (a) 3.5 CAD (hexadecanoic acid, dodecane, tetradecane and hexadecane) and (b) 4.5 CAD (octane, nonane and dodecanoic acid).

6.2.4. Improvements in thermal engine efficiency that can be expected from modifying the energy release rate profile

The preceding sections of this chapter considered the effects of major fuel molecular features on thermal engine efficiency. The results have shown that molecular structural features appear to have a fairly small influence on thermal engine efficiency, of around ±1.5 %-units. Therefore, the experimental error in measuring

thermal engine efficiency (±0.43 %-units), and the added complexity of several physical fuel properties being highly correlated among themselves, introduce substantial challenges in investigating the effects of fuel properties on efficiency. That is, it is often difficult to disentangle which fuel properties have significant influence on engine thermal efficiency and through what mechanism these influences are being exercised. This section presents a simplified theoretical analysis which aims to assist in interpreting further the experimental results presented in the previous sections of this chapter. In particular, the following analysis aims to provide an answer to the question of how large a change in thermal efficiency could be expected when fuel properties are altered.

With very nearly 100% of the fuel supplied to the engine being combusted completely and converted to energy release, ultimately, the chemical and physical fuel properties can only influence thermal engine efficiency by modifying the timing and the rate at which energy is released from the fuel. In turn, the timing and profile of the rate at which energy is being released determines how much of the fuel energy is converted to useful mechanical work and how much of the fuel energy is dissipated unproductively through heat transfer and through rejection in the engine exhaust system. The influence of these factors on efficiency was examined with a zero-dimensional thermodynamic model, described in Stone [168]. The model was primarily used to examine how the energy release rate and the timing of energy release influence thermal efficiency. The model also provided information of whether low efficiency was caused by excessive energy dissipation in the exhaust and through heat transfer. The model therefore accounted explicitly for energy dissipation to the walls of the engine combustion chamber through heat transfer. The zero-dimensional model represented the naturally aspirated single cylinder engine used for the experiments presented earlier in this chapter. The contents of the engine cylinder were considered to be spatially uniform in terms of species, pressure, and temperature. The approach adopted was to use this model to simulate the effects on engine thermal efficiency of altering (a) the timing of energy release from the fuel, relative to the engine piston position, and (b) the profile of the energy release rate. The model and its numerical solution are explained in more detail in Appendix III.

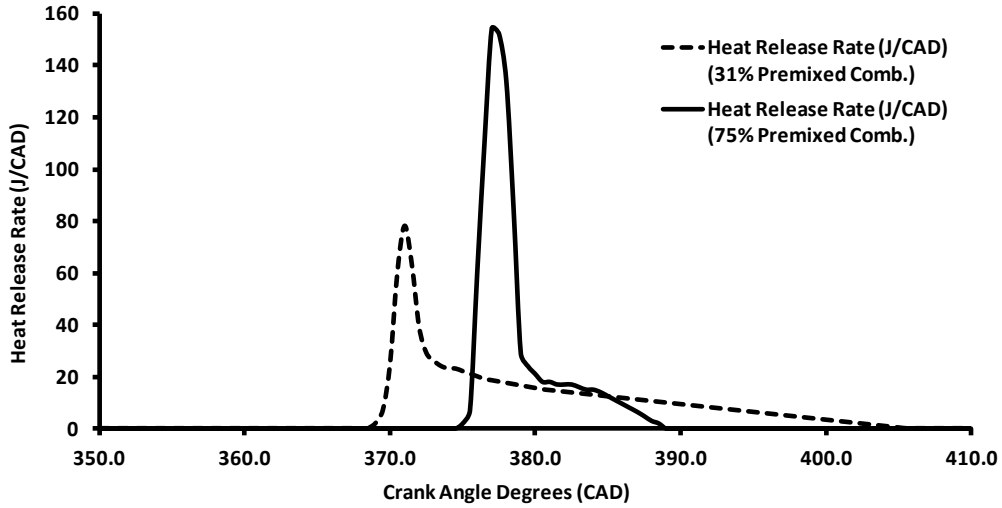

Figure 44. Arbitrarily defined heat release rates: Case 1 with low premixed and high diffusion-controlled energy release rate; and Case 2 with high premixed and low diffusion-controlled energy release rate.

The model was applied to two very different defined energy release patterns corresponding to Case 1 and Case 2 studied, as shown in Figure 44. While both energy release rates, when integrated, are equal to a total energy input from the fuel of 491 J, the energy released during the premixed controlled combustion phase in Case 1 is 31% and in Case 2 it is 75% of the total cycle energy of 491 J. In order to simulate optimised injection timing of a real engine, the Case 1 and Case 2 energy release rate patterns were kept constant in terms of their profile, but their timing in CAD was gradually varied so that the whole constant pattern of energy release rate sown in Figure 44 was advanced or retarded, relative to the engine TDC, by 0.5CAD at a time. That is, although the energy release was shifted in time (CAD), the pattern of energy release rate shown in Figure 44 was kept constant. For each 0.5 CAD shift in timing, the engine thermal efficiency was calculated as explained in Appendix III and the results plotted in Figure 45.

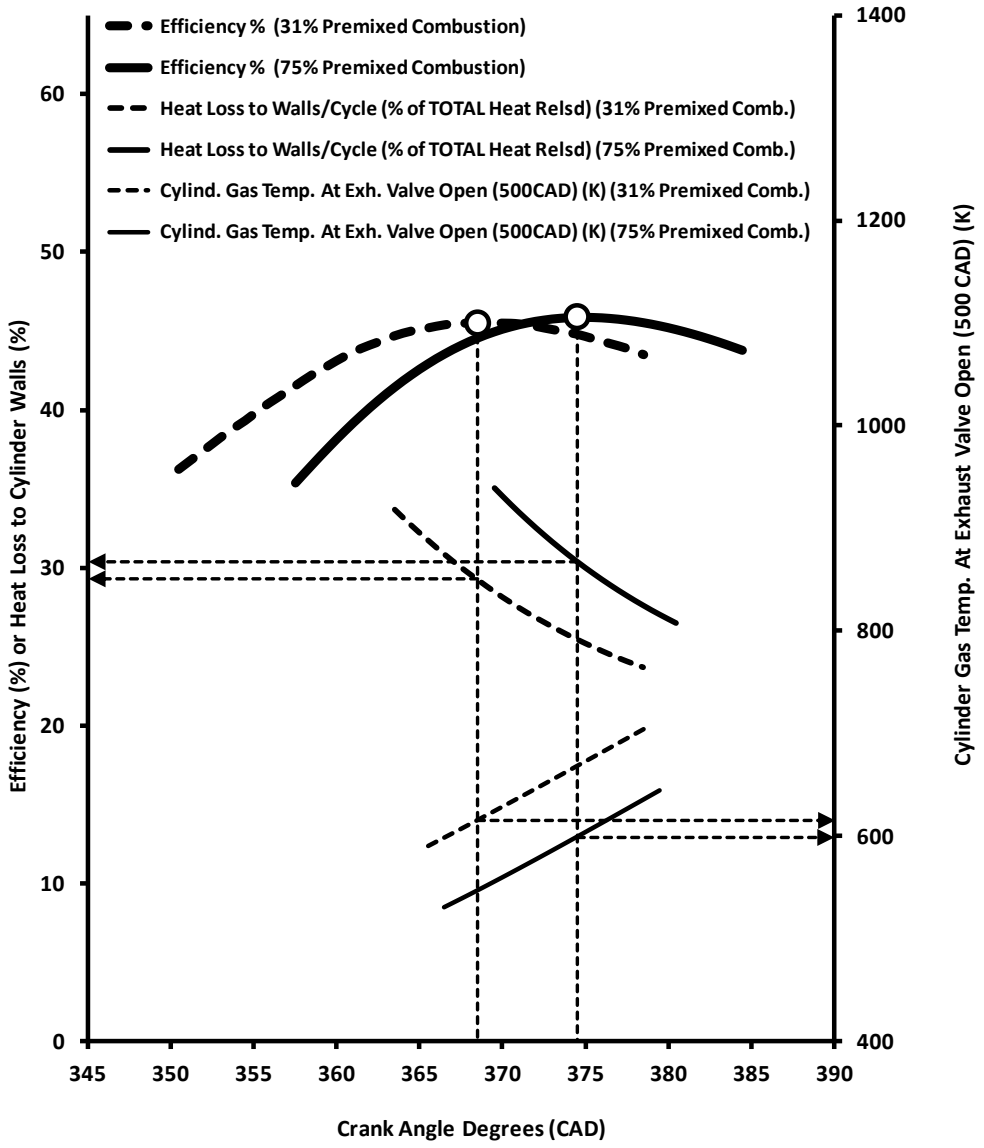

Figure 45. Simulated results for the effect on engine thermal efficiency of varying the start of energy release and altering the rates of energy release. Case 1 (broken curves) corresponds to 31% energy release in premixed combustion and Case 2 (solid curves) corresponds to 75% energy release in premixed combustion.

Figure 45 shows that for both Cases 1 and 2 of energy release rate profiles, the timing of energy release causes a significant variation in the thermal engine efficiency. However, the maximum (i.e. optimised) values of the engine thermal efficiency for Cases 1 and 2 are very similar at 44.0% and 44.8%, respectively. Therefore, according to this simulation, provided that the energy release timing is optimised (in

the case of a real engine that would be achieved through the injection timing) the two patterns of the energy release have only a small influence on the optimized value of engine thermal efficiency. Figure 45 gives a clear explanation why the timing-optimised efficiencies are almost the same for the two distinctly different energy release patterns of Case 1 and Case 2. The explanation is that the two different patterns of Case 1 and Case 2 caused trade-offs between energy losses by heat transfer and energy losses rejected in the exhaust gas. While the high (75%) premixed-controlled energy release rate of Case 2 raises the in-cylinder temperature, and hence the energy losses to the combustion chamber surfaces, the loss of energy in the exhaust is reduced when the exhaust valves open. Conversely, the low (31%) premixing controlled energy release rate of Case 1, with its short energy release period, results in somewhat higher energy loss in the exhaust gas but lower energy loss through heat transfer. The outcome, after optimization of the timing of energy release, is that the maximum efficiency for both patterns if roughly similar, with a difference in efficiency of only ~0.4 %-units.

The modelling results are useful in providing some assurance for the experimental results presented earlier in this chapter. Figure 38b and Figure 38c had shown that, over a wide range of fuel properties, the variation in experimentally measured thermal engine efficiency is fairly small at around ±1.5 to 2 %-units. Furthermore, when considering individual molecular groups, the variation in measured efficiency, with premixed phase ranging from 20% to 65%, is only about ±0.5 %-units, which is of similar magnitude to the results obtained from the theoretical model. It should be noted that the experimental results were conducted with fixed injection timing, while the modelling results (Figure 45) were obtained with optimised timing of energy release, which reduced further the effect of energy release profile on thermal efficiency. Therefore, it is reasonable to conclude that part of the scatter in the experimental results shown in Figure 38b and Figure 38c is likely to be a caused by the variations in the combustion timing for the different fuels. Finally, it is reasonable to conclude that there is significant evidence that wide variations in fuel properties exercise only a small influence on engine thermal efficiency.

6.3.Conclusions

The effects of chemical and physical fuel properties of 43 single component fuels on the thermal engine efficiency of a compression ignition engine were investigated experimentally. The combustion of several alkanes, alkenes and oxygenated molecules, namely alcohols, methyl ketones, methyl esters and carboxylic acids were investigated. The thermal efficiency of the diesel engine used appeared to be affected mostly by the rate and timing of energy release rate. Ignition delay, in particular, appears to have an influence on engine thermal efficiency, because it controls the amount of fuel burned during the premixed phase, which in turn defines the pattern and to some extent the timing of energy release. In turn, the ignition delay is controlled by the chemical and physical fuel properties. The specific results of this study on the influence of fuel properties on thermal efficiency (at fixed injection timing) are as follows:

1) Molecules with longer carbon chain length had lower thermal engine efficiency than shorter chain molecules. This can be explained by shorter ignition delay for longer molecules and, thereby, smaller premixed combustion phases.
2) Non-oxygen bearing hydrocarbons appear to have somewhat higher engine thermal efficiency than oxygenated molecules.
3) Fuel density did not appear to have a clear effect on thermal engine efficiency
4) Fuels with higher boiling points were observed to have lower engine thermal efficiency. It is suggested that this was due to association between fuel boiling point and ignition delay: molecules with higher boiling points generally had shorter ignition delays and their shorter ignition delays lead to lower thermal efficiency.

In addition to the experimental investigations, the influence of the timing and rate of energy release on engine thermal efficiency was examined with a zero dimensional thermodynamic model. The model showed that the timing of energy release rate was more important than the shape of the energy release rate. The model also affirmed that significant improvements in engine thermal efficiency require reductions in the

dissipation of energy from the engine cylinder contents to the surfaces of the combustion chamber and into the exhaust.

It can be concluded that fuel properties appear to have only a moderate influence on thermal efficiency of the diesel engine used for this study, and their influence on efficiency may be limited to 1 or 2 %-units when engine injection timing has been optimised. While the practical implications of this conclusion are that the fuel properties may not offer major opportunities for efficiency improvements, at the same time this allows the fuel developers to focus on optimising fuel properties for lower exhaust pollutant emissions without substantial detrimental trade-offs with thermal efficiency.

Chapter 7

The compression ignition and exhaust gas emissions of fuel molecules which can be produced from lignocellulosic biomass: levulinates, valeric esters and ketones

7.1 Introduction

This chapter deals with the combustion and emission characteristics of several fuel molecules which could be produced from lignocellulosic materials. Because of the future importance of such fuel molecules, the chapter begins with a brief review of published work on such fuels. This review is then followed by the presentation of a study, conducted by the author, which assesses the combustion and emission characteristics of several molecules which could be produced from lignocellulosic materials.

Fuels made from lignocellulosic biomass are potential second-generation biofuels. Lignocellulose includes the most abundant polymers on Earth and it is not likely to be a human food source [277]. Lignocellulosic biomass includes agricultural and forestry residues, herbaceous energy crops and it can be found in municipal solid waste. However, breaking the strong structure of lignocellulose and converting it to biofuel molecules involves rather complicated processes. The relative difficulty in developing commercially feasible technologies to do this is the main reason why lignocellulosic biofuels are not currently widely produced, until recently [278]. For example, the world's first wood-based renewable commercial fuel production started commercial operation in UPM Lappeenranta Biorefinery in Finland in January 2015 [279]. Lignocellulosic biomass can be converted into biofuels through thermal, biological and catalytic routes. The catalytic approach can be used to produce furfurals from lignocellulose through acid hydrolysis. The furfurals can, in turn, be converted into several chemicals, polymers, bioalcohols (e.g. ethanol), gasoline octane busters (e.g. 2-methylfuran and dimethylfuran) and levulinic acid. Levulinic acid is a versatile intermediate chemical, which can be processed further to produce biofuel molecules. The research for economically viable ways to produce levulinic acid from lignocellulose in large scale is ongoing: several possible pathways were described in the review articles by Rackemann and Doherty [280] and Deng et al.

[281]. Biofuel molecules such as 2-methylfuran, γ-Valerolactone, valeric esters and levulinates can be produced from levulinic acid [277]. A general chemical route to produce these biofuel molecules from lignocellulosic material is shown in Figure 46 [282]. Because esters are known to be viable biofuels for diesel engines [23,25,283], this study focused on the combustion of levulinates as well as valeric esters.

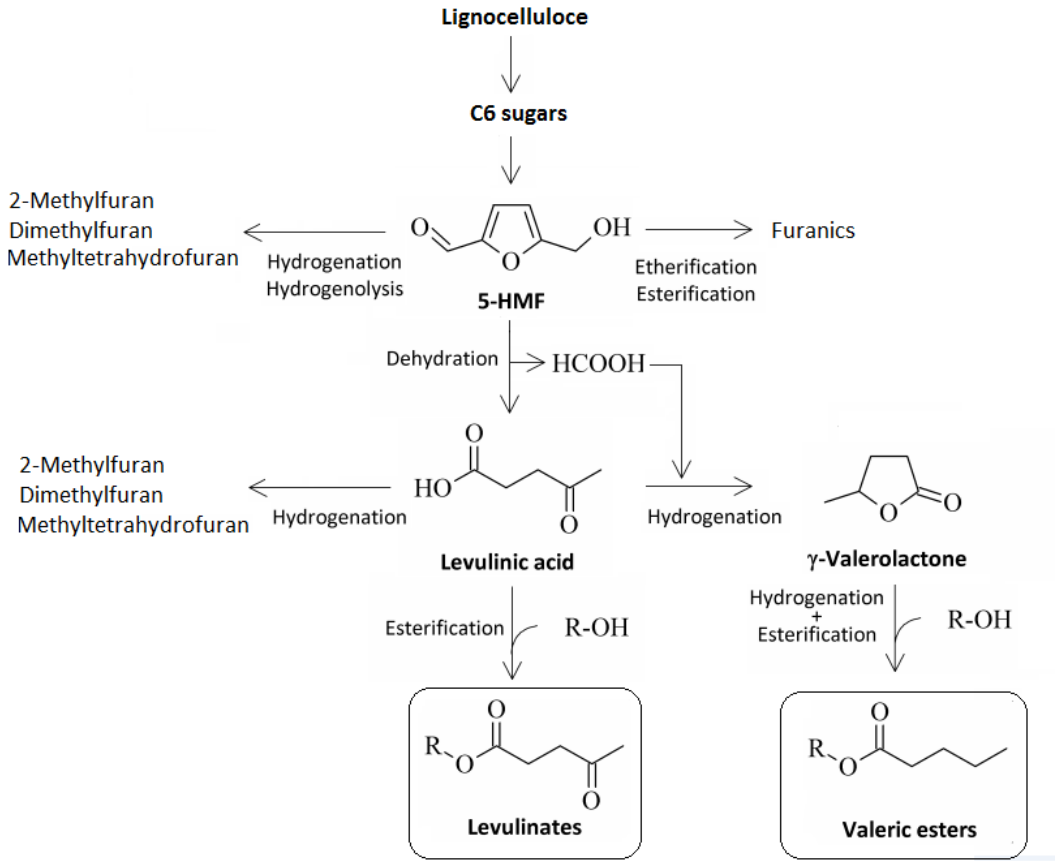

Figure 46. Production of levulinates and valeric esters from C6 sugars of lignocellulosic materials (adapted from [6]).

The levulinates are produced through esterification of levulinic acid and they have been proposed as fossil gasoline and diesel fuel extenders. When considering the physical properties of levulinates, methyl levulinates are potential gasoline additives, whereas ethyl and higher levulinates can potentially be used as diesel blend components. The boiling points of ethyl and higher levulinates are similar to those of the heavy gasoline compounds (over 475K) and correspond to the middle of the

diesel fuel boiling range. [284] The low cetane numbers of levulinates limit their blend proportion in diesel blends [6]. According to Joshi et al. [285], diesel blends with ethyl levulinate up to 15 v-% satisfy the ASTM D6751 and have improved cloud point, pour point and cold filter plugging point compared to diesel fuel. However, Chuck and Donnelly [286] concluded that butyl levulinate is a poor alternative for aviation kerosene because it is not miscible at low temperatures. Although several ways to produce alkyl levulinates have been developed, for example as described in a review article by Demolis et al. [287], only a small number of kinetic studies and engine studies are available on the oxidation of alkyl levulinates. Christensen et al. [284] tested ethyl levulinate and butyl levulinate as diesel blends in a 2008 model year Cummins ISB engine. With 10 v-% ethyl levulinate and 20 v-% butyl levulinate blends they observed no change in total hydrocarbon, CO, or PM exhaust gas emissions. The engine-out smoke number was reduced by 41.3% and 55%, respective of the two blends, while NO_x emissions were observed to increase by 0% and 4.6%, respectively. Janssen et al. [288] conducted experiments of 60, 70 and 80 v-% butyl levulinate/tetradecane blends in a single cylinder research engine. They observed that a reduction up to 95% (depending on the load) in particulate emissions could be achieved with butyl levulinate addition to tetradecane, compared to fossil diesel fuel. However, an increase was observed in hydrocarbon, CO and noise emissions for butyl levulinate/tetradecane blends compared to fossil diesel fuel. Nevertheless, Christensen et al. [284] concluded that commercial applications of levulinates would be challenging due to their poor solubility in diesel fuel at low temperatures and their low cetane number.

An alternative to esterification of the levulinic acid and use of the esters in diesel fuel blends is the hydrogenation of levulinic acid into valeric acid, which can then be esterified to produce valeric esters [286–289]. Compared to levulinates, valeric esters are less polar and have lower boiling points (Appendix II) and are therefore more appropriate to act as biofuels in blends with gasoline and diesel fuels [289]. According to Lange et al. [289], 20 v-% of ethyl valerate in gasoline meets the research and motor octane numbers of European gasoline specification (EN 228), whereas butyl valerates and higher valeric esters could be suitable for diesel blends. Lange et al. [289] reported that blends of pentyl valerate and diesel have higher volatility, compared to fatty acid methyl esters (FAME), and that blending pentyl

valerate with diesel improved cold flow properties more than blends of FAME, although FAME also has a lower cetane number. Very few studies have investigated the combustion kinetics and engine combustion of valerates and levulinates, and in the case of valerates such studies are particularity scarce. Research on the oxidation of ethyl or higher esters is generally scarce, mainly because methyl esters are the dominant compounds of current biodiesel fuels and, therefore, currently a main research focus. Combustion kinetic schemes for ethyl valerate and butyl valerate have been proposed by Dayma et al. [290], while Contino et al. [291] investigated the combustion of butyl and pentyl valerates in a single cylinder PSA DW10 engine. Contino et al. [291] concluded that, compared to diesel fuel, neither 20 v-% of butyl valerate or 20 v-% pentyl valerate added to diesel fuel resulted in significant changes in exhaust gas emissions or engine performance, despite an increase in ignition delay.

In the study reported here two levulinates, three valeric esters, two ketones, an ether and three alkanes were tested in a single cylinder diesel research engine with the aim of improving the understanding of their combustion characteristics, especially the ignition delay, and exhaust gas emissions of these potential lignocellulose-driven fuel molecules. Ketones, namely 3-heptanone and 5-nonanone, were tested because valeric acid, which can be esterified to produce valeric esters, can also be ketonized to form 5-nonanone and the 5-nonanone can subsequently be upgraded into several different hydrocarbons (such as straight chain alkanes and their isomers) using an acid catalyst [277]. These hydrocarbons include straight chain alkanes (e.g. nonane), and for this reason three such alkanes were tested in this study. Finally, an ether was included in the set of fuels tested so as to provide a different way of interpretation of oxygen in the molecular fuel structure than that in ketones and esters. It should be noted that in order to ensure reliable compression ignition of all the tested molecules, some of which have low cetane numbers, all the tests were conducted with 30 wt-% heptane added to each of the molecules investigated. The results of this study can be used to aid in selecting what stage lignocellulose should be chemically modified so as to produce a viable biofuel molecule with optimal combustion characteristics and exhaust gas emissions.

7.2 Experimental methods

7.2.1 Experimental conditions

The experiments were conducted at an engine speed of 1200 rpm, an engine load of 4 bar IMEP, injection pressure of 600 bars and intake air heated to 393K. Injection timing was kept fixed at 7.5 crank angle degrees before TDC. A reference diesel fuel test was conducted at the above test conditions at the beginning and at the end of each test day to create a long-term facility log. The data from these tests allowed the detection of any changes or day-to-day drifts in the equipment or the instrumentation. Based on this log with reference diesel fuel, the long term mean value of the NO_x emission was 807.24 ppm, the standard deviation of the mean NO_x was 44.7 ppm and standard error of the mean 5.53 ppm. The corresponding values for the mass of PM in the engine exhaust gas were 0.0081 µg/cc, 0.0013 µg/cc and 0.00066 µg/cc; and for the numbers of particulates in the engine exhaust gas they were $8.85*10^7$ N/cc, $3.90*10^7$ N/cc and $1.95*10^7$ N/cc, respectively.

7.2.2 Fuel molecules investigated

A number of fuel molecules, potentially obtainable from lignocellulosic biomass, were investigated; these molecules where two levulinates, three alkanes, three valeric esters, two ketones and an ether. Molecular structures of these molecules are shown in Figure 47 and their physical properties are listed in Appendix II [234,235,237,292,293]. Figure 47 shows the molecules grouped in the following manner, so as to allow easier comparison of the results of these molecules: molecules on each column have the same carbon chain length (C7, C9 or C10); molecules on each row are from the same structural group.

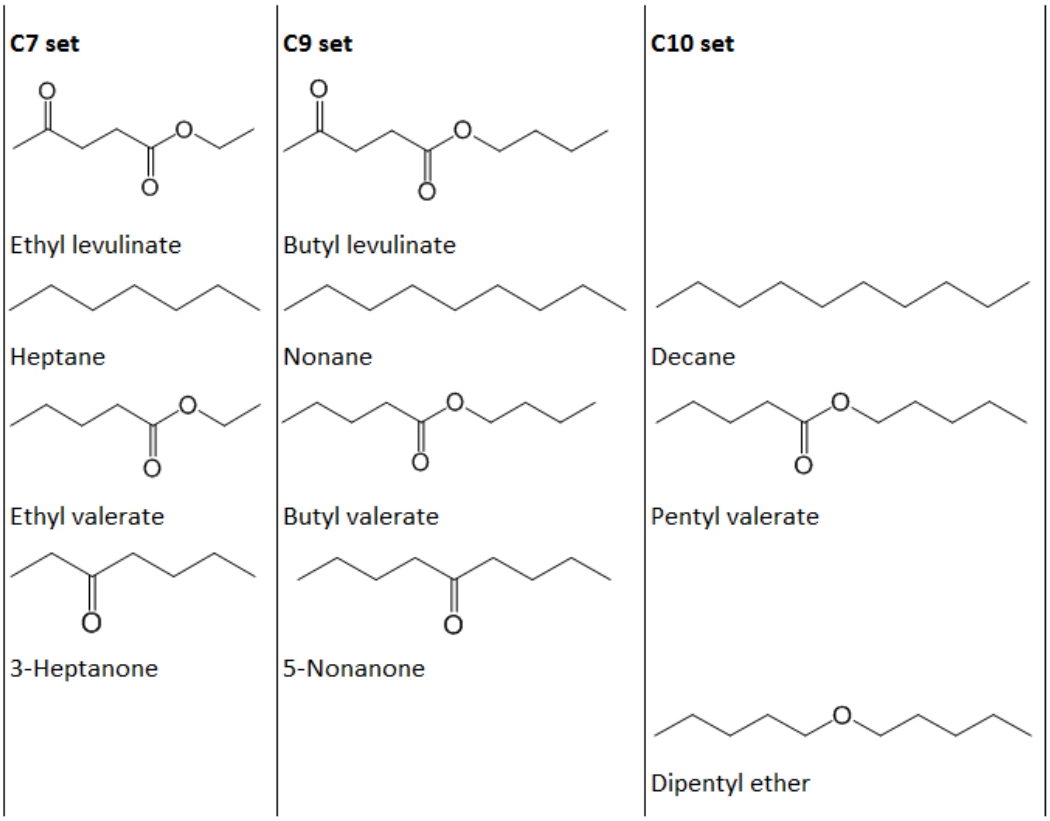

Figure 47. Tested molecule sets.

Initially, ethyl levulinate, butyl levulinate, ethyl valerate and butyl valerate were tested each one on its own, as pure compounds, and none of these fuel molecules were observed to ignite in the diesel engine. Therefore, in order to enable reliable ignition, heptane was added to all the tested molecules. Heptane was selected as the ignition improver due to its similar combustion qualities compared to fossil diesel fuel. The amount of heptane added was the same (wt-%) for all molecules to allow comparison between the combustion chemistries of the molecules. The quantity of heptane in the blends was decided after further tests were conducted with ethyl levulinate, because it had the shortest carbon chain length and the highest oxygen content of the tested molecules; therefore, it was the most difficult molecule to ignite. Mixtures with 20, 30 and 40 wt-% added heptane by mass were tried. It was found that 30 wt-% of heptane was the smallest amount of heptane that could be added to ethyl levulinate for reliable ignition, without a pronounced two-stage ignition. To allow the results from all the fuel molecules tested to be readily compared, 30 wt-% of heptane was added to all of the investigated molecules. The effect of heptane on

the combustion chemistry of the fuel mixtures is assumed to be similar in each test for the purposes of this study, because the same amount (wt-%) of heptane was added to each one of the molecules. Heptane interacts with the combustion of the molecules by donating radicals to the combustion mixture and, due to the same amount of heptane in the mixture, similar amounts of radicals from heptane may be expected to be available for each molecule at any given temperature.

The objectives of the experiments were to investigate the effects on ignition and pollutant emissions of the following structural changes in fuel molecules:

1. Adding a carbonyl group to an alkane to form a ketone.
2. Adding an ether linkage to an alkane to form an ether
3. Combining a carbonyl group and an ether linkage into an ester group to form a valeric ester
4. Adding a carbonyl group to the valeric ester to form a levulinate

7.3 Results and discussion

7.3.1 Effects of molecular structure on ignition delay

Longer ignition delays generally allow greater time for fuel to evaporate and mix with air, and therefore result in a greater portion of the injected fuel being burned rapidly close to TDC in premixed-combustion mode. Figure 48a shows, as expected, a positive correlation between the premixed phase quantity and ignition delay for alkanes and levulinates. Interestingly, ketones had a negative correlation and valeric esters no correlation between premixed phase and ignition delay when the premixed phase quantity was calculated as a percentage of energy injected, where the energy injected was defined as the chemical energy of the fuel injected during an engine cycle (Figure 48a). The data presented in Figure 48a is listed for each molecule in Appendix IV. It is suggested, that the unexpectedly small premixed phases of the ketone 3-heptanone and the ethyl valerate (Figure 48a) were caused by their lower percentages of total fuel combusted, compared to those of the other molecules in the same structural group. The lower combustion percentages resulted from the more difficult ignition of these molecules; for example, in the case of 3-heptanone only 61% of all the fuel energy was released during combustion, compared to the

corresponding value of 89% for 5-nonanone. In the case of ethyl valerate only 90% of all the injected fuel energy was released during combustion, compared to the 99% for both butyl and pentyl valerate. It should be noted, that although the correlation between the ignition delay and premixed percentage within the structural groups was not positive for all the compounds (as one would expect), Figure 48a shows that taken together, the data points for all compounds tested show a quite clear trend for the percentage of premixed combustion to increase when ignition delay becomes longer.

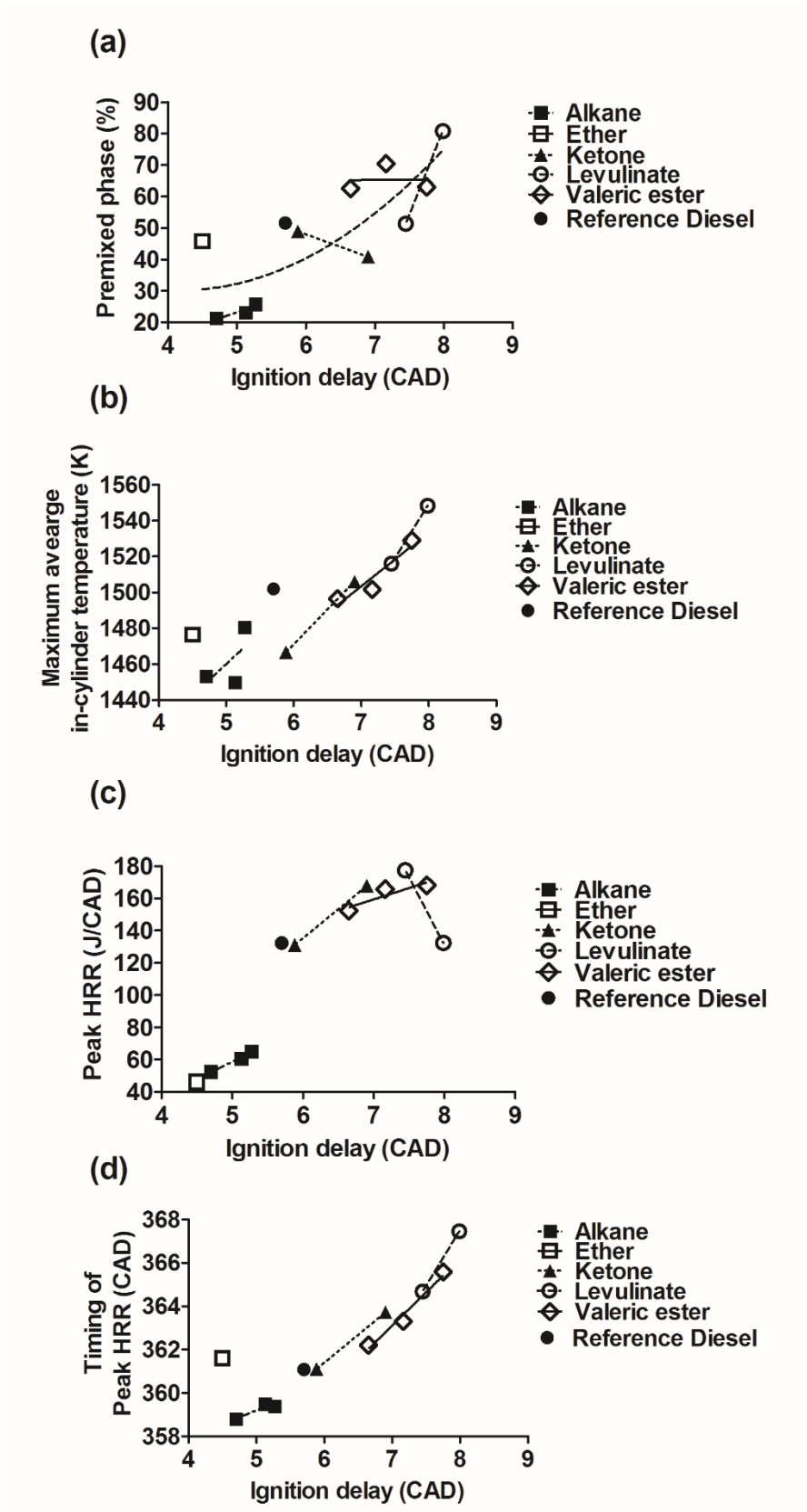

Figure 48. Effect of ignition delay on (a) premixed phase, b) in-cylinder temperature, (c) pHRR and (d) timing of pHRR.

Longer ignition delay was generally observed to result in higher in-cylinder temperature (Figure 48b), higher peak heat release rate (HRR) (Figure 48c) and later timing of the peak HRR (Figure 48d), as was expected. An exception to these trends was the levulinates, which did not show a rising peak HRR with increasing ignition delay (Figure 48c). The lower peak HRR of ethyl levulinate compared to that of butyl levulinate (Figure 48c) may be explained by the peak HRR occurring later in the expansion stroke for ethyl levulinate, as shown in Figure 49 (and Appendix IV), where the combustion volume is greater. Nevertheless, despite combustion in a larger volume, ethyl valerate can be seen from Fig. Figure 48b to reach a higher average combustion temperature. This can be explained by the substantially larger amount of premixed combustion of ethyl valerate (Figure 48a).

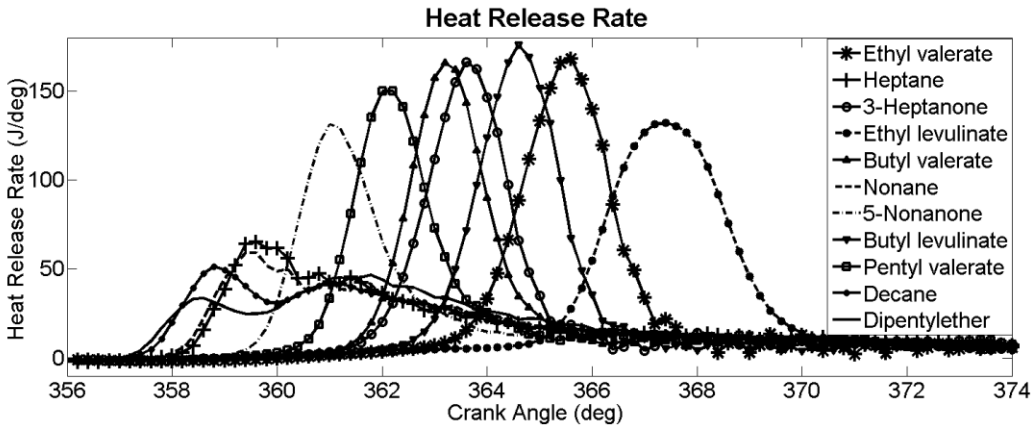

Figure 49. Heat release rates profiles of the tested molecules.

7.3.2 Ketones compared to alkanes

The effect of adding a carbonyl group to an alkane to form a ketone was investigated by comparing 3-heptanone to heptane and 5-nonanone to nonane Figure 50a shows that ketones had longer ignition delays compared to the corresponding alkanes. These results were supported by the findings of a previous study [294], in which six ketones were observed to have longer ignition delays than the corresponding alkanes. The later ignition of ketones, compared to alkanes, was suggested to be mainly caused by the oxygen atom in the carbonyl group of ketones. The carbonyl group is thought to

affect the ignition delay mainly through the changes in the two main steps of the chemical ignition mechanism: H-abstraction and isomerization. Several studies [3,251–253] have shown that the higher electronegativity of an oxygen atom, compared to that of carbon and hydrogen atoms, affects the strength of carbon-hydrogen bonds near the oxygen atom: the strength of the carbon-hydrogen bonds on the carbons next to the carbonyl group is weakened, but the strength of the carbon-hydrogen bonds on the next three carbon atoms of the chain are increased. Oxygen atom in the carbonyl group makes the overall H-abstraction from the oxygenated molecule more difficult than H-abstraction from the corresponding alkane molecules, thus increasing the ignition delay. In the case of isomerization, the rapid compression machine studies of Allen et al. [52] have showed that carbonyl group hinders the formation of a transition ring during isomerisation, compared to an alkane, and thus increases the ignition delay further. Furthermore, according to the low temperature oxidation experiments of Anderson and Hoare [252] and Hoare and Li [251], ketonyl peroxy radicals lead mainly to propagation reactions, instead of branching reactions through isomerization. This will contribute to the slower formation of a radical pool large enough to initiate and sustain ignition in the case of ketones compared to alkanes.

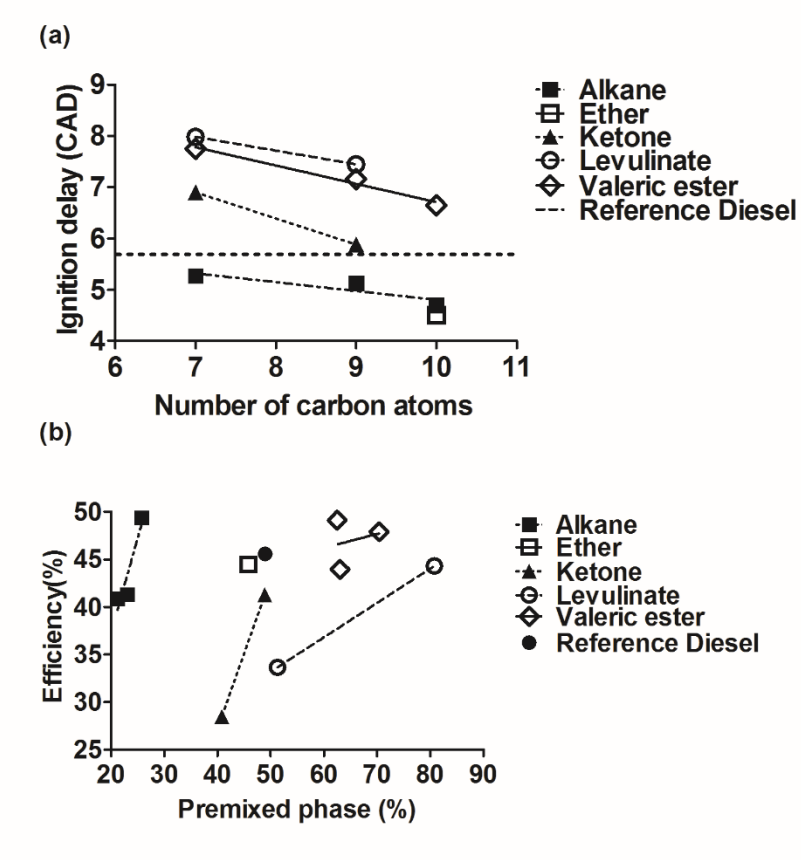

Figure 50. (a) Effect of the carbon chain length on ignition delay; (b) Effect of the magnitude of premixed phase on thermal engine efficiency.

7.3.3 Ethers compared to alkanes

Figure 50a shows that dipentyl ether (C10) had a 0.2 CAD shorter ignition delay than decane (C10). The shaft encoder resolution was 0.2 CAD and therefore this difference was deemed insignificant. It is interesting to note that dipentyl ether could perhaps be expected to have longer ignition delay than decane, based on the physical fuel properties of the two fuels: dipentyl ether has higher boiling point and surface tension values than decane (Appendix II) and could, therefore, be expected to have poorer spray atomisation and somewhat longer physical ignition delay. The fact that dipentyl ether and decane show similar values of ignition delay suggests that oxygen in the ether, which tends to shorten the ignition delay, offsets the opposing tendency of the physical properties. Considering first the chemistry of ether linkages, a laminar flow reactor study by Cai et al. [78], theoretical calculations of Ogura et al. [80] and shock tube experiments of Guan et al. [79] have shown that weakening in C-H bonds

caused by the oxygen atom in an ether linkage result in faster H-abstraction from an ether, compared to that for a corresponding alkane. When considering the isomerization reactions that follow, Cai et al. [78] observed that ethers can go through isomerization via hydrogen migration across the central oxygen atom. Additionally, the energy barrier of the peroxide decomposition, which will lead to further chain branching reactions, has been shown to be lower for ethers compared to the corresponding alkanes [78,80]. Hence, it is suggested that due to the faster H-abstraction and higher ability of the fuel peroxy radical to undergo isomerization, the ignition chemistry of ethers is faster than that of the corresponding alkanes, but that the higher values of some physical fuel properties of ethers hinder the ignition of ether compared to the ignition of alkanes. This suggestion was supported by a previous study [294], which showed that dibutyl ether (C8) had a significantly shorter ignition delay than octane (C8), despite the higher boiling point, higher surface tension and higher viscosity of dibutyl ether.

7.3.4 Valeric esters compared to ketones and ethers

Valeric esters have both a carbonyl group and an ether linkage in their structure as an ester group (Figure 47). Figure 50a shows that the ignition delays of valeric esters were higher than those of alkanes, ketones and the ether. Dayma et al. [290] showed, by both modelling and experimentally in a jet stirred reactor, that the higher ignition delays of valeric esters compared to the corresponding alkanes are caused mainly by the more difficult H-abstraction and the reduced ability of the fuel alkyl peroxy radicals to go through isomerization. The higher ignition delays of valeric esters compared to ketones or the ether are therefore partly explained by the differences in H-abstraction. As mentioned above, the H-abstraction from ethers is faster than from the corresponding alkanes but H-abstraction from ketones is slower than from the corresponding alkanes. When comparing the H-abstraction of ketones and esters, several studies have shown that the initial H-abstraction from a ketone occurs from the carbon atom next to the carbonyl group [3,251–253]; in the case of esters, H-abstraction is easiest from the carbon atom next to the ether oxygen [75,77,290]. The resulting ketone radical is more stable than the ester radical due to the presence of the ether oxygen in the ester group. Therefore, H-abstraction is easier

from a ketone compared to an ester [295]. This is suggested to have, partly, caused the shorter ignition delays of ketones compared to esters observed in Figure 50a.

When considering the isomerization of the fuel radical after H-abstraction, it was explained above that ethers may undergo isomerization more easily than the corresponding alkanes, but that the isomerization of molecules with a carbonyl group is more difficult than that of the corresponding alkanes. In the case of valeric esters, Dayma et al. [290] suggested that the fuel radicals of valeric esters react with oxygen to form peroxy compounds. Most of these peroxy compounds react further through isomerization, but they can also form ethyl pentanoates by HO_2 abstraction, hydrogen peroxides and oxygen through reaction with HO_2, or alkoxy compounds by combining with other peroxides. Additionally, several studies, e.g. Zhang and Boehman [92], have stated that the ester moiety imposes extra strain on the transition rings during isomerization, which may lower the rate of isomerization compared to the corresponding alkanes. It was suggested that the ester group may hinder the isomerisation more than a carbonyl group and that this would delay further the ignition of esters, compared to ketones and ethers.

7.3.5 Levulinates compared to valeric esters

Levulinates are 4-oxopentanoates with both a carbonyl group and an ester group, as shown in the molecular structures of ethyl levulinate and butyl levulinate in Figure 47. Compared to valeric esters, levulinates have one more carbonyl group in their structure. It was observed from Figure 50a that levulinates had the longest ignition delays of the tested molecules, slightly longer than the ignition delays of the corresponding valeric esters (longer by 0.23 CAD for C7 molecules and 0.28 CAD for C9 molecules). While the extra carbonyl group may contribute to the small increase in ignition delay over the delay for the esters, this small increase may also be explained, at least in part, by the higher boiling points and surface tension of levulinates (Appendix II) causing a potential deterioration in the injection fuel spray atomisation.

When considering the chemical fuel properties, it was suggested that the addition of a carbonyl group to valeric ester to form a levulinate hindered the ignition in a similar way to that of adding a carbonyl group to an alkane to form a ketone; that is, H-

abstraction becomes more difficult because the number of hydrogen atoms for H-abstraction is reduced by one and the C-H bonds close to the carbonyl group change, and the ability of a fuel peroxy radical to undergo isomerization is reduced. Interestingly, removing a carbonyl group from levulinate to form a valeric ester resulted in a significantly smaller decrease in ignition delay than when removing a carbonyl group from a ketone to form an alkane (Figure 50a). This could potentially be explained by greater decrease in the straight hydrocarbon chain length in the case of levulinates and valeric esters compared to the decrease for ketones and alkanes.

7.3.6 Effects of molecular structure on engine efficiency

Engine efficiency, which is defined as the conversion of fuel chemical energy to mechanical work, depends mainly on the air-fuel ratio and both the rate and timing of heat release from the fuel injected into the combustion chamber [1]. The maximum engine efficiency is, in general, achieved with an Otto-cycle-like combustion, where most of the fuel burns rapidly in the premixed combustion mode at TDC. Too early combustion will decrease engine efficiency because high in-cylinder pressures are reached during the compression stroke. Similarly, too late combustion will reduce engine efficiency because part of the energy released will be rejected with the engine exhaust gases. Figure 50b shows, as expected, positive correlations between engine efficiency and the quantity of fuel energy released during the premixed phase for all structural groups. Engine efficiency values of the molecules are presented in Appendix IV. In the case of valeric esters, the unexpectedly high engine efficiency of pentyl valerate (49.1%) could be explained by the timing of the pHRR: pHRR was reached closer to TDC in pentyl valerate combustion (362.2 CAD), compared to the combustions of ethyl valerate (350.8 CAD) and butyl valerate (363.3 CAD) (Figure 49). When all the data points are considered, however, there is no clear indication that a greater amount of premixed combustion has any considerable positive or negative influence on thermal engine efficiency. It should be noted, that valeric esters and the ether had higher, and ketones and levulinates lower, engine efficiency than the reference diesel (45.64%). When comparing the engine efficiencies of different molecular groups, however, it should be noted that the difference between several molecules were of the similar magnitude than the standard deviation of the mean efficiency of the reference diesel tests: 5-nonanone (41.3%) and nonane (41.4%);

ethyl valerate (44%), ethyl levulinate (44.3%); ethyl levulinate (44.3%) and dipentyl ether (44.5%); pentyl valerate (49.1%) and heptane (49.4%). It should be said that the above observations are only tentative ones, because the values for efficiency shown in Figure 50b are, on the whole, subject to considerable uncertainty, arising from the measurement of the fuel flow rate supplied to the engine combustion chamber. This involved measuring, (a) the flow rate supplied to the injector indirectly, from the movement of the enclosed UFVS piston, and (b) the fuel leakage rate from the injector; both there flow rates are very small and, individually, subject to considerable uncertainties; the net fuel flow rate to the combustion chamber, being the difference of these two small flow rates, is therefore subject to considerable error, which is expected to be reflected in the efficiency values shown in Figure 50b.

7.3.7 Effects of molecular structure on nitrogen oxides

NO_x emission formation in a compression ignition engine is affected by the fuel-bound oxygen, the global combustion temperature and availability of both oxygen and nitrogen from the air. It has been well established that the formation of NO_x emissions is mainly temperature controlled [1,205,245] and therefore significantly affected by the in-cylinder temperature. The combustion in-cylinder temperature, in turn, depends on the ignition delay, which affects the magnitude of the premixed combustion phase; in general, a longer ignition delay leads to a larger premixed phase releasing energy rapidly close to TDC, resulting in higher in-cylinder temperatures and greater formation of NO_x.

Following on from this discussion in the previous paragraph, Figure 51a and Figure 51b show the expected positive correlations between NO_x emission and both ignition delay and in-cylinder temperature for all molecular groups, excluding levulinates. The two levulinates show an opposing trend, which is suggested to occur due to the following reasons. Figure 49 shows ethyl levulinate to stand out in having a prolonged cool combustion with very little energy released, followed by a late large premixed combustion phase. The prolonged period prior to energy release for the ethyl levulinate results in the heat release occurring later in the engine expansion stroke when cylinder volume has increased, compared to the other compounds, which

causes a reduction in the overall premixed combustion temperature and thus also in NO_x formation.

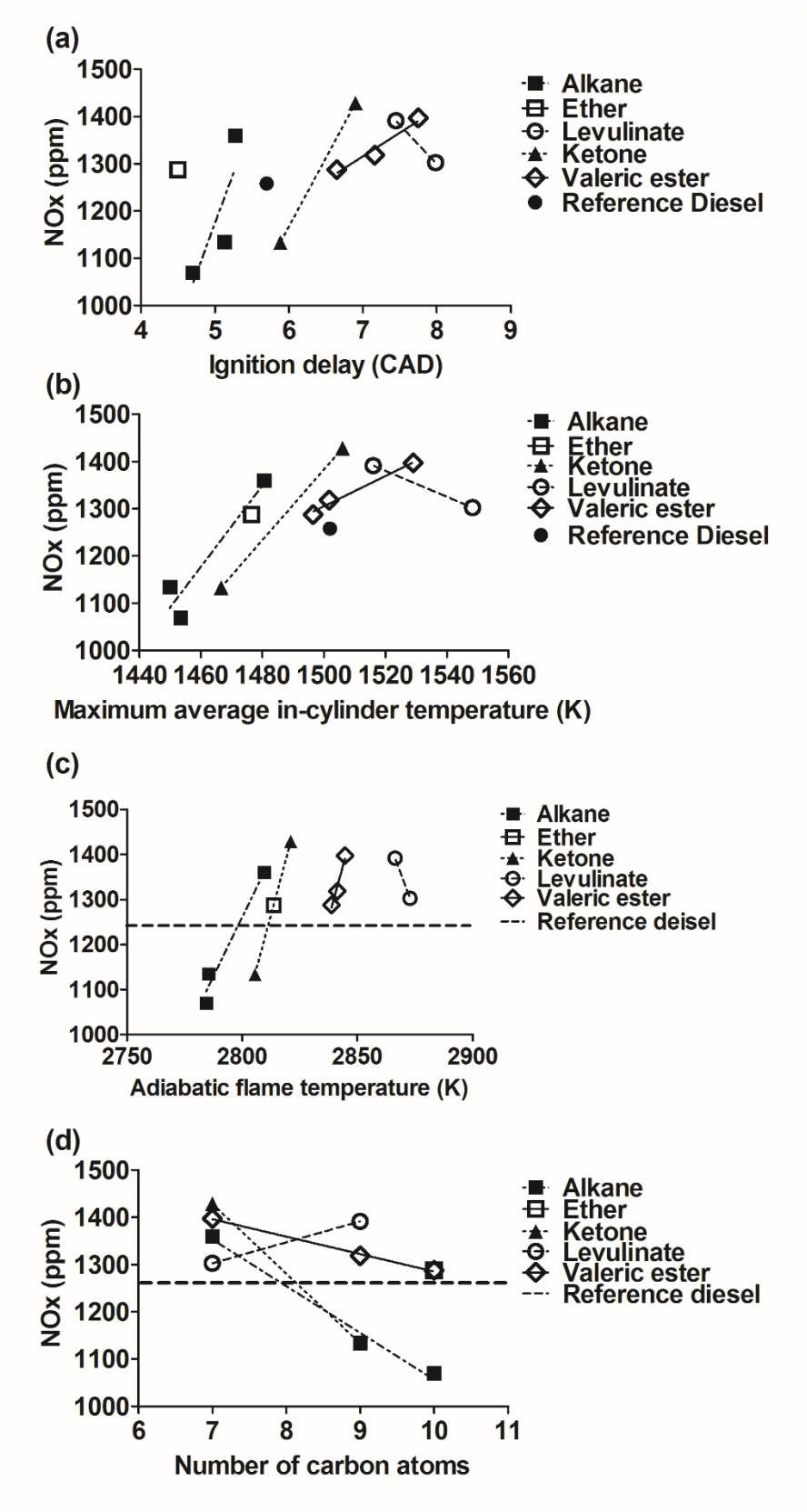

Figure 51. Changes in NO_x emissions caused by (a) ignition delay, (b) in-cylinder temperature, (c) adiabatic flame temperature and (d) carbon chain length.

Figure 51c shows NO_x plotted against the adiabatic flame temperature, which was calculated according to the method presented by Turns [162]. Figure 51c indicates a strong influence of adiabatic flame temperature on NO_x emission, save for the case of the two levulinates, where the opposing trend may have been caused by the reasons discussed above in relation to Figure 51a and Figure 51b.

Figure 51d shows the effect of the number of carbon atoms in the various fuel molecules on NO_x emission. The results in this figure reflect to a significant extent the effect of ignition delay on NO_x (Figure 51a). Molecules with a greater number of carbon atoms tend to have shorter ignition delays, and hence lower NO_x emission, than molecules with a lower number of carbon atoms for the reasons discussed previously in this chapter. It can also be observed from Figure 51d that the valeric esters have somewhat higher NOx emissions than the corresponding alkanes with the same number of carbon atoms. This appears to be related to the longer ignition delays of valeric esters compared to the alkanes, as can be seen in Figure 51a. As a closing comment on Figure 51, the number of data points for each molecular group is small (e.g. only two data points for ketones and levulinates) NO_x trends discussed are, to a considerable extent, tentative ones.

7.3.8 Effects of molecular structure on particulate matter

Figure 52 shows the results for particulate emissions. The trends in Figure 52a for individual compounds are not conclusive: the particulate mass of alkanes and ketones reduced slowly with the increasing in-cylinder temperature, as expected; however, the individual trends for the valeric esters and levulinates are not as expected (although the trend of levulinates might have been affected by the very late ignition of ethyl levulinate, shown in Figure 49). When all the data points in Figure 52a are taken together, there is a rather strong indication that higher in-cylinder temperature reduces the mass of particulates, as one would expect. Figure 52b shows that no clear correlation between the mass of particulates and the number of carbon atoms in the various fuel molecules tested was observed. Likewise, Figure 52c also suggests that there was no clear influence on the number of particulates of the number of carbon atoms in the molecules of the various tested compounds.

As in the case of the NO_x trends discussed above, the trends for particulates are, to a considerable extent, tentative ones due to the small number of data for individual molecular groups.

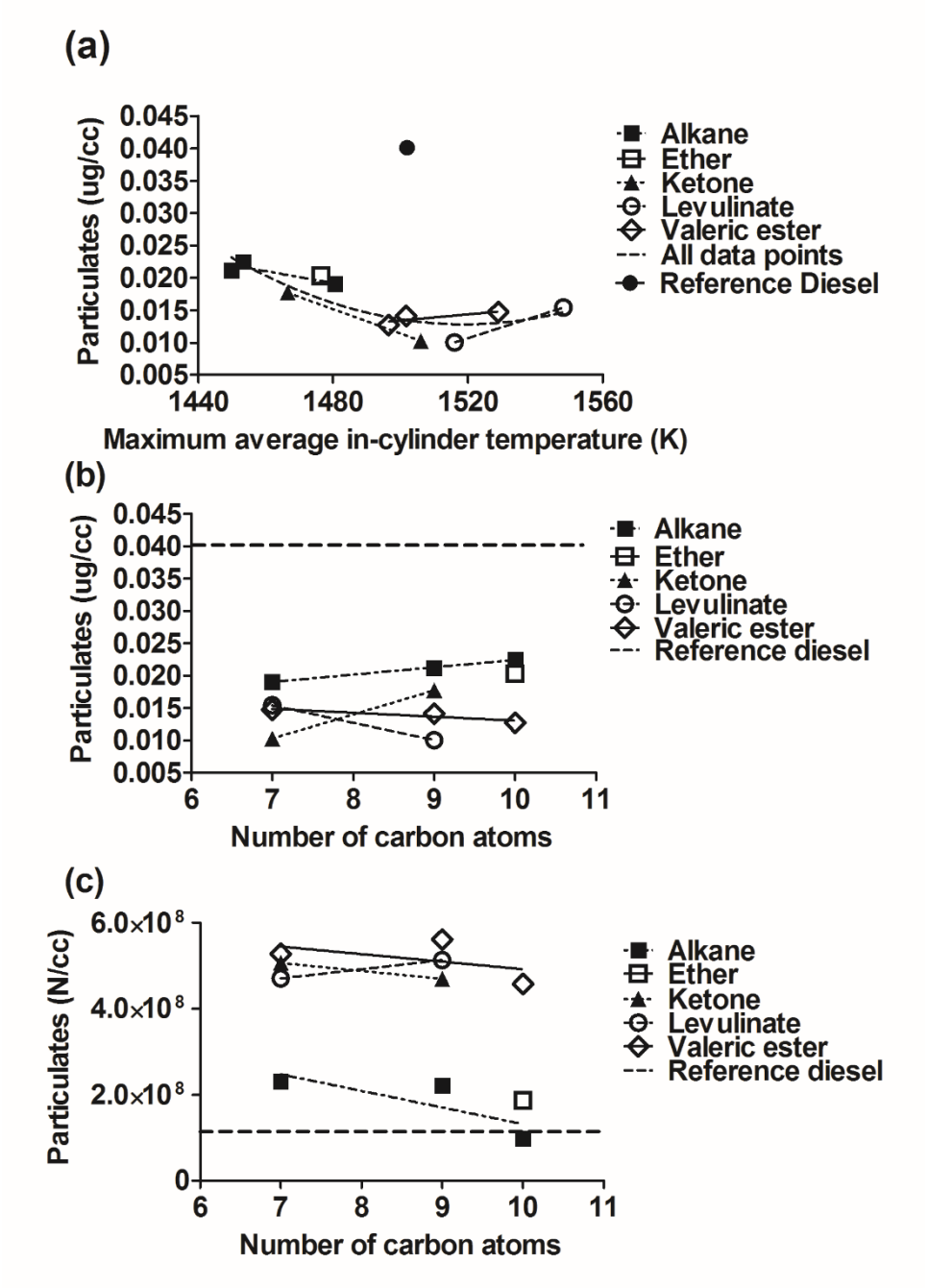

Figure 52. Effect of (a) in-cylinder temperature and (b) carbon chain length on the mass of particulates; (c) the effect of carbon chain length on the number of particulates in exhaust gas.

7.4 Conclusions

The compression ignition delays and exhaust gas emissions of several molecules, which, potentially, could be produced from lignocellulosic biomass were investigated. The tested molecules were levulinates, valeric esters, ketones, an ether and several alkanes. Ignition was ensured by testing each individual molecule with 30 wt-% heptane. The key results were as follows:

1. Ketones had longer ignition delays than alkanes because the carbonyl group makes H-abstraction more difficult from ketones, compared to alkanes, and also reduces the ability of the fuel peroxy radicals to undergo isomerization.
2. Dipentyl ether had a similar ignition delay to that of decane, despite the ether having an oxygen atom in its molecule embedded as an ether linkage. It is believed that the comparable delays occur because, in the case of the ester, physical properties (higher boiling point and higher surface tension) tend to increase the ignition delay while a chemical property (ether linkage) tends to reduce the ignition delay, with a result that both compounds end up with comparable ignition delay periods
3. Valeric esters ignited later than ketones, ethers and alkanes. This was suggested to occur because the ester group results in more difficult H-abstraction and isomerization for valeric esters compares to ketones, ethers and alkanes.
4. Levulinates had slightly longer ignition delays compared to the corresponding valeric esters, most likely due to the additional carbonyl group in the structure of levulinates.
5. Valeric esters and the ether had similar engine efficiency than the reference diesel fuel.
6. Ketones and levulinates had slightly lower thermal engine efficiency than the reference diesel fuel.
7. NO_x emissions appeared to be affected by both the in-cylinder temperatures and the adiabatic flame temperatures of the tested molecules.

8. NO_x emissions of the oxygenated molecules were higher compared to those of alkanes, but no consistent difference was observed between the NO_x emissions of the oxygenated molecule groups.
9. The oxygenated molecules produced less of the heavy particulates but more of the light, smaller particulates compared to both alkanes and reference diesel fuel.
10. No real difference in the mass or the number of particulate emissions was observed between the structural groups tested.

As to be expected, the oxygen bearing molecules show a clear reduction in particulate mass, when compared with the non-oxygen bearing molecules and the fossil diesel fuel used as the reference test fuel. There is however, in the case of the oxygen bearing molecules a penalty in terms of an increase in the number of particulates (compared to reference diesel fuel and non-oxygenated molecules) which is particularly relevant due to recently introduced legislation to additional control the number of emitted particles for vehicle engines. The customary penalty of oxygen bearing molecules in terms of some increase in NO_x can also be seen in the results presented in this paper. In terms of engine thermal efficiency, some of the oxygen bearing molecules, especially the levulinates, have shown efficiency levels similar to those of the non-oxygen bearing molecules. It should be noted, however, that some of the trends discussed in the paper are, to a considerable extent, only tentative and more data are necessary before firm conclusions could be drawn. Nevertheless, there is considerable evidence from the results that the oxygen bearing compounds tested, which could potentially be obtained from lignocellulosic materials, can potentially be used as diesel fuel extenders and would warrant further detailed investigations, including tests in diesel-engine vehicles.

Chapter 8

Compression ignition and pollutant emissions of large alkylbenzenes

8.1 Introduction

Diesel fuels, gasoline fuels, and aviation jet fuels are complex mixtures of several hundred chemical compounds. Alkyl aromatics represent a significant fraction of all of these fuels and have thus been used as fuel surrogates in combustion experiments. Diesel fuels in general consist of approximately 30% paraffins, 25% alkyl-cyclohexanes, 20% polycyclic naphthenoaromatic compounds, 15% alkyldecalines and 10% alkylbenzenes with the carbon chain length ranging from 10 to 22 [296]. In order to develop new efficient and environmentally friendly engine fuels the combustion characteristics of the various compounds in the fuel have to be understood in detail. The combustion of paraffins has been widely researched, but the combustion chemistry of alkyl aromatics has been researched less and is not as well understood.

Aromatic compounds, in general, consist of an aromatic ring and one or several alkyl chains bonded to the ring. This study focuses on the combustion characteristics, especially ignition delay and exhaust gas emissions, of alkylbenzenes having one aromatic ring and one straight alkyl chain. The combustion mechanism of the simplest alkylbenzene, that is toluene, has been widely researched e.g. in rapid compression machines and in shock tubes and is relatively well understood [296–300]. However, only a few studies have been conducted on the low temperature ignition chemistry of alkylbenzenes having longer alkyl chains than toluene. Furthermore, engine studies of alkylbenzenes are even scarcer, with only a few engine studies of toluene combustion being available [301–303].

Studies of combustion mechanisms suggest that alkylbenzenes with longer alkyl chains may combust through similar mechanisms to those of toluene, except for the low-temperature reactions, when H-abstractions occurs from the alkyl chain. Recently, reaction mechanisms have been suggested for various alkylbenzenes. These include: ethylbenzene, as a result of theoretical calculations by Altarawneh et

al. [304] and jet-stirred reactor experiments conducted by Husson et al. [305]; propylbenzene through shock tube experiments conducted by Gudiyella and Brezinsky [306], flame studies by Wang et al. [307] and calculations by Altarawneh and Dlugogorski [308]; butybenzene through experiments with a rapid compression machine conducted by Roubaud et al. [309], and combined rapid compression machine experiments and modelling by Ribaucour et al. [310] and Husson et al. [311,312], and experiments conducted in a shock tube and a rapid compression machine by Nakamura [312]; and alkylbenzenes ranging from propylbenzene up to decylbenzene, through modelling based on experiments conducted on a jet-stirred reactor by Battin-Leclerc et al. [313]. Based on these studies, the general combustion mechanism of alkylbenzenes, having long alkyl chains, was found to start with the consumption of the alkyl chain, due to the stability of the benzene ring. The importance of H-abstractions from the alkyl carbons increases with increasing alkyl chain length. As combustion progresses, the relatively stable benzyl radicals react mainly in termination reactions and thus increase the ignition delay of alkylbenzenes compared to that of alkanes.

This study investigates the combustion characteristics and exhaust gas emissions of three alkylbenzenes, namely heptylbenzene, octylbenzene and dodecylbenzene, in a single cylinder direct injection research engine. Additionally, the effect of using a corresponding alkane/toluene mixture as fuel, instead of an alkylbenzene, was investigated, for comparison. Furthermore, the effect of the phenyl group in the alkylbenzenes was compared to the effect of the hydroxyl group in alcohols. The hydroxyl group was used for comparison with the phenyl group because the hydroxyl group is one of the most common functional groups in the currently commercially available biofuels, and its combustion characteristics are therefore rather well understood.

8.2 Experimental methods

8.2.1 Experimental conditions

The combustion experiments were conducted with injection timing of 7.5 CAD before TDC, 600 bar injection pressure, 1200 rpm engine speed and 4 bar IMEP. An

experiment with reference diesel fuel was carried out at the beginning and at the end of each test day, always at the same engine operating conditions, to allow the detection of any day-to-day drifts in the instrumentation or the equipment. Based on the eight reference diesel tests conducted during this test programme, the mean value of NO_x emissions was 790 ppm, standard deviation of the mean was 16.83 ppm and standard error of the mean 6.87 ppm. The corresponding values for the number of particulates in the engine exhaust gas were mean $1.15*10^8$ N/cc, standard deviation $3.12*10^7$ N/cc and standard error $1.27*10^7$ N/cc; for the mass of PM and standard error 0.0013 µg/cc.

8.2.2 Fuel molecules investigated

In order to investigate combustion of alkylbenzenes with one straight alkyl chain, three alkylbenzenes, three alcohols and seven alkanes were tested. Additionally, four alkane/toluene mixtures were tested. The tested molecules and mixtures were divided into three sets shown in Figure 53 based on the alkyl chain length of the alkylbenzene. Each of the three sets included: an alkylbenzene, with alkyl chain length of C7, C8 and C12, respectively for the sets 1, 2 and 3; primary alcohol with C7,C8 and C12 carbon chain length, respectively, for the sets 1, 2 and 3; an alkane with one carbon atom longer chain length than the alkyl chain of the alkylbenzene, that is C8, C9 and C13 chain length, respectively, for the sets 1, 2 and 3; and an alkane with the same alkyl chain length, that is C7, C8 and C12, respectively, for the sets 1, 2 and 3. Additionally, each set had an alkane/toluene mixture in which the toluene was mixed with C6, C7 and C11 alkanes, respectively, for the sets 1, 2 and 3, so that the total number of non-aromatic carbon atoms in the alkane/toluene mixtures were the same as that for the alkylbenzene (i.e. C8, C9 and C13) in the same set. The physical properties of the tested molecules are listed in Appendix II [234].

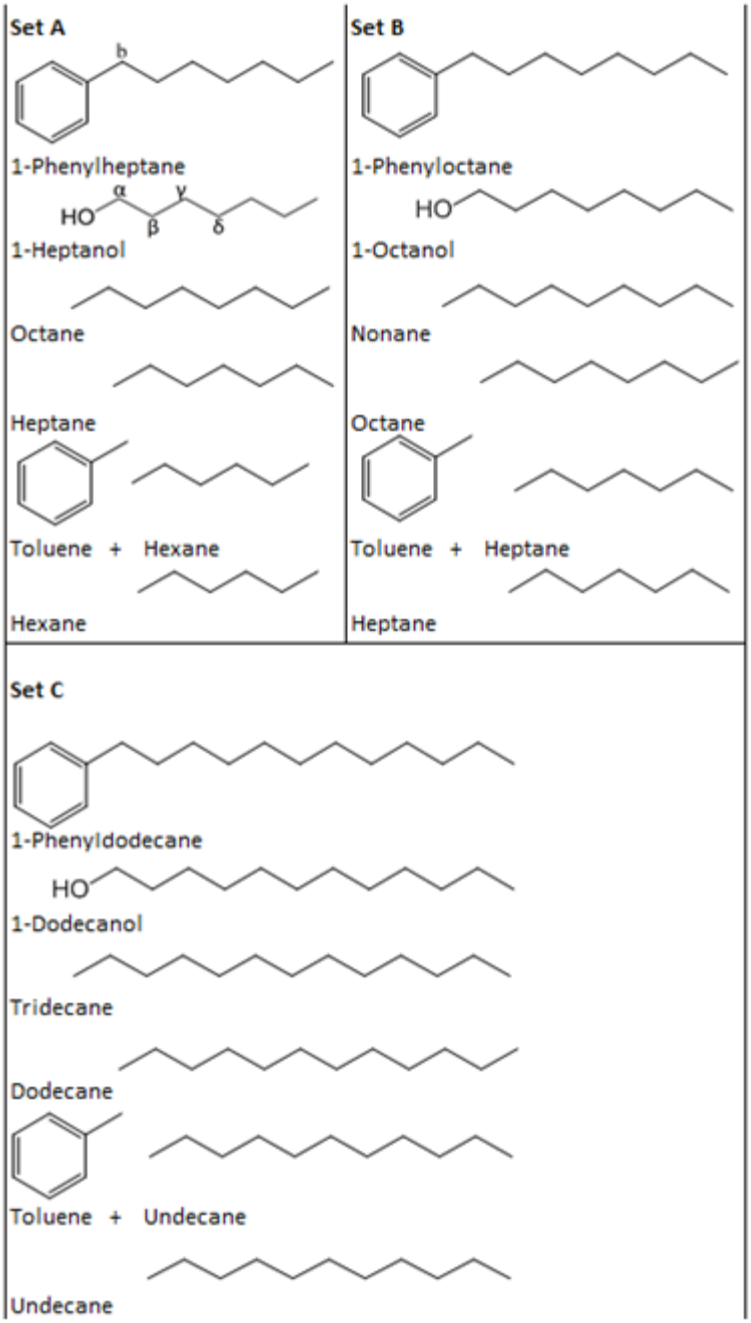

Figure 53. Tested molecules which were divided into three sets based on the alkyl chain length of the alkyl benzenes, with molecules on each row having similar molecular structures.

The percentage of toluene in the alkane/toluene mixtures was kept as small as possible to prevent the slow toluene combustion from dominating the alkane/toluene combustion of the mixtures so as to allow comparisons between the different mixtures. Therefore, the toluene percentage of the three alkane/toluene mixtures was decided based on the combustion of hexane/toluene mixture, because it was the most

difficult of the toluene mixtures to ignite in the diesel engine due to the short carbon chain length of hexane. The volumetric concentration (v- %) of hexane in the mixture was decided through a brief investigation in which the toluene/hexane mixtures of 0, 10, 20 and 30 v-% of toluene in hexane were tested. The mixture with highest v-% of toluene in hexane not exhibiting a two-stage-like ignition was observed to be the 20 v-% mixture. On-stage combustion was desirable for all of the tested fuel molecules, because comparison between one-stage and two-stage combustion would not have allowed comparisons between the value and timing of the pHRR or the combustion phasing. Hence, 20 v-% of toluene was used for all three alkane/toluene mixtures.

The three sets of molecules allowed the effect on both ignition characteristics and engine emissions to be investigated, when the following structural changes were made to the fuel:

1. Adding a phenyl group to an alkane
2. A comparison of adding an alkane to a hydroxyl group instead of a phenyl group
3. Having an alkyl chain bonded to the phenyl group compared to a "separate alkyl" chain of the toluene in toluene/alkane mixtures

It should be mentioned that instead of the toluene molecule a more logical choice of phenyl group molecule would have been benzene due to its lack of a methyl group bonded to the aromatic ring. However toluene was used instead of benzene due to safety considerations relating to the toxicity of benzene.

8.3 Results and discussion

The following sections of this chapter focus on a detailed analysis of molecular structure of the tested compounds on ignition delay and engine exhaust gas emissions.

8.3.1 Adding a phenyl group to an alkane

The effect of adding a phenyl group to an alkane was investigated by comparing the alkylbenzenes to alkanes having the same carbon chain length as the alkyl chain of the alkylbenzene. Figure 54a shows the effect on ignition delay of adding a phenyl group to an alkane. It is interesting to note in Figure 54a that the addition of the phenyl group to an alkane hardly has a significant effect on ignition delay. In the case of heptylbenzene (C7) and octylbenzene (C8), the ignition delays are almost identical to those of heptane and octane. However, in the case of dodecylbenzene (C12), the ignition delay is higher than that of dodecane by 0.8 CAD. It is suggested that this difference in ignition delay between dodecylbenzene and dodecane is caused by early ignition, when the ignition resistance of the phenyl group had a more significant effect. That is, when the C12 alkyl benzene and alkane ignited 2 to 3 CAD before TDC, in the somewhat lower temperatures of the compressed air in the engine cylinder, compared to the later ignition of the corresponding C7 and C8 molecules. Figure 54b shows that, as was expected, the percentage of fuel burned in the premixing controlled combustion phase is similar for the alkylbenzenes and the corresponding alkanes, due to the similar values of their ignition delays (Figure 54a). The values of ignition delays and peak heat release rates (pHRR) of the tested molecules are listed in Appendix V.

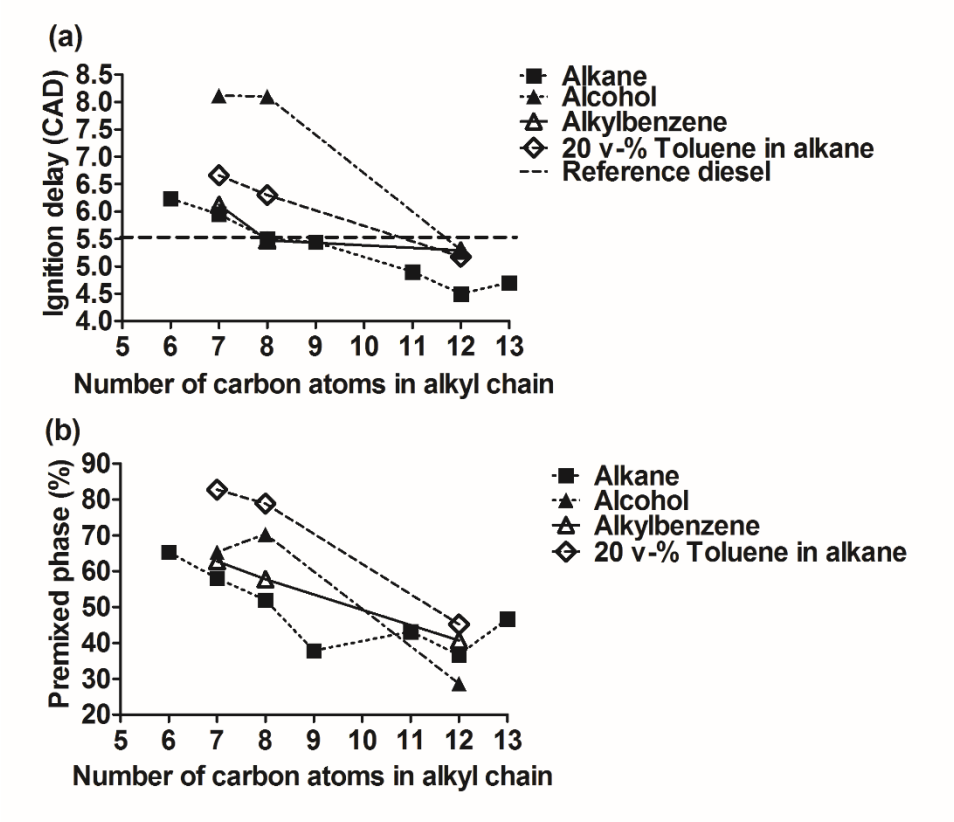

Figure 54. Effect of the alkyl chain length on ignition delay, where the alkyl chain in toluene/alkane mixtures is considered as a sum of the one carbon atom in the methyl group of toluene and the number of carbon atoms in the alkane.

Interestingly, Figure 55 shows that the alkylbenzenes had a substantially different pattern of heat release rate than the corresponding alkanes, despite the similarities between the ignition delays and premixed phases of these two groups (Figure 54). The alkylbenzenes can be observed from Figure 55 to ignite at similar timing as the alkanes, but the initial rate of heat release of the alkylbenzenes was much slower, thereby shifting the bulk of the premixed combustion of alkylbenzenes to later crank angle timings than the timings of alkanes. A possible explanation for these observations is as follows.

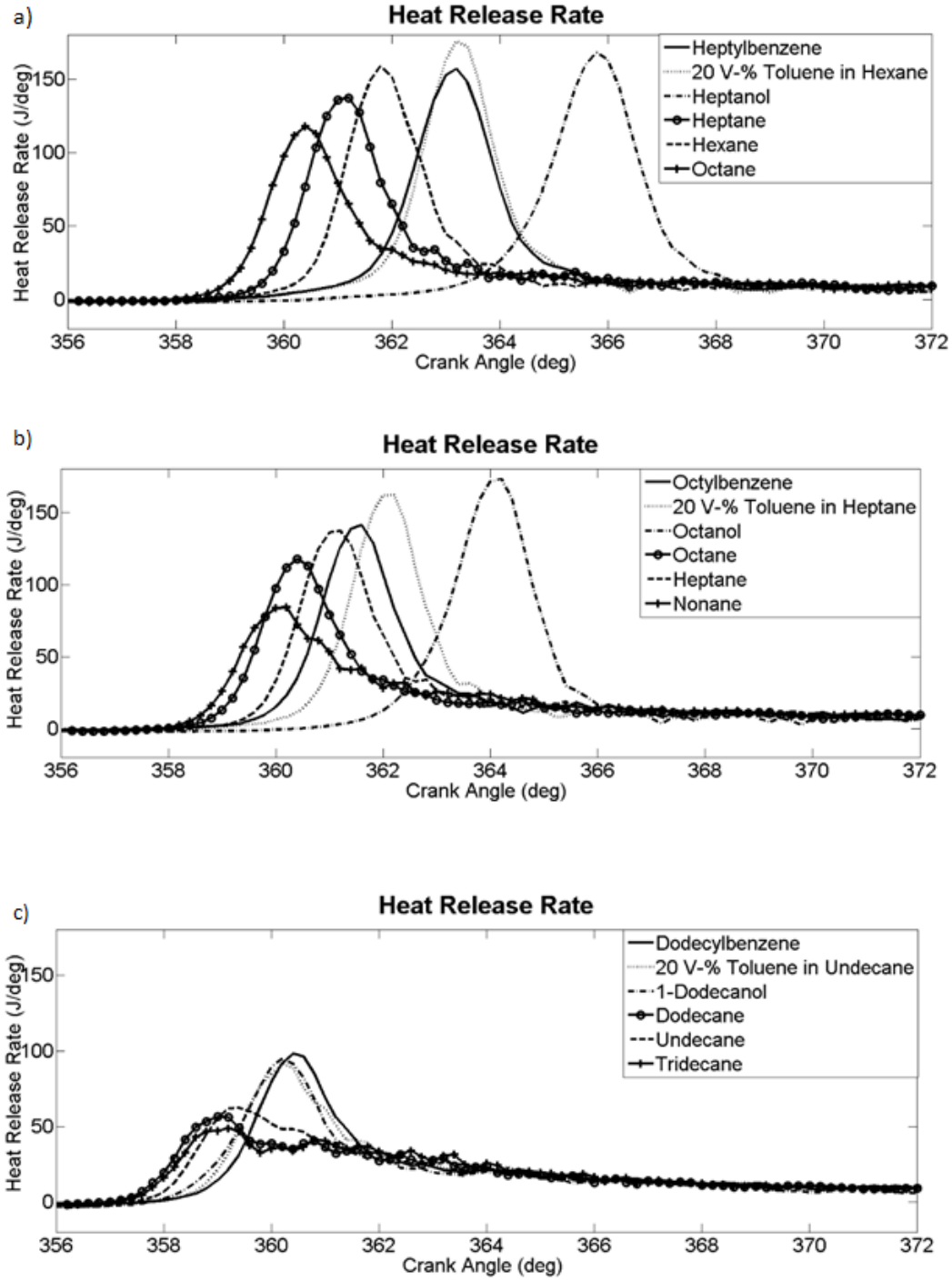

Figure 55. Heat release rates of the three tested molecule sets: (a) See A; (b) Set B; (c) Set C

First, consider the H-abstraction from the fuel molecule. Because the aromatic ring is rather stable, the ignition delay of alkyl benzenes is largely determined by their alkyl chains. The main difference between an alkane and an alkylbenzene is the

benzylic carbon of alkylbenzenes (labelled, for example, *b* in heptylbenzene, Figure 53). Published studies conducted on ignition and oxidation of alkylbenzenes with long alkyl chains state that these molecules are mainly consumed by H-abstraction from the alkyl chain and by cleavage of the benzylic C-C bond [304–313]. Since the alkyl chain of the alkylbenzenes had the same chain length as that of the alkanes (e.g. octylbenzene and octane, Figure 53 Set B), the ignition delays of the three alkylbenzenes have approximately similar values as the ignition delays of the three corresponding alkanes (Figure 54).

Secondly, consider the further reactions following H-abstraction from the fuel molecule. Figure 55 indicates that once ignition has occurred, the alkanes proceed straight away to rapid combustion of the already premixed fuel, while in the case of alkylbenzenes, combustion following ignition proceeds initially at a significantly slower rate until sometime later when the premixed fuel is finally rapidly consumed. These contrasting behaviours can be explained by the alkyl radicals (which are formed though H-abstraction from an alkyl chain) reacting more readily with oxygen to give branching agents through isomerization compared to the more stable benzylic radicals (which are formed through the abstraction of H atom from the benzylic carbon, labelled *b* in Figure 53). Benzyl radicals are resonance stabilized and therefore mainly react in termination reactions of the combustion chain reaction mechanism [296]. This tendency of benzyl radicals to act as a radical sink during combustion has been shown experimentally by several studies in the case of toluene [301,303,314]. The formation of the benzylic radicals is therefore suggested to be the main reason for the slower initial combustion of alkylbenzenes compared to alkanes (Figure 55). Additionally, the aromatic ring of alkylbenzenes is assumed to hinder the formation of transition rings during isomerization of fuel peroxy radicals, compared to alkanes, thus hindering the initial build-up of heat release rate further [309,310,313].

8.3.2 Phenyl group compared to a hydroxyl group

When comparing alkylbenzenes to alcohols, both having the same alkyl chain length, the hydroxyl group was observed from Figure 54a to result in longer ignition delays than the phenyl group of the C7 (heptylbenzene and 1-heptanol) and C8

(octylbenzene and 1-Octanol) molecules. Alkylbenzenes have higher boiling points, density and surface tension compared to the alcohols (Appendix II), so one would expect the spray quality, evaporation and air-fuel mixing of alkylbenzenes to be poorer than that of alcohols: yet the alkyl benzenes showed shorter ignition delays than alcohols. Therefore, the differences in ignition delays between alkylbenzenes and alcohols could be assumed to be mainly due to the combustion chemistry.

Several studies [71,239] have shown that the higher electronegativity of the oxygen atom, compared to that of carbon and hydrogen atoms, in the hydroxyl group makes the H-abstraction from alcohols more difficult than from alkanes of the same carbon chain length. Therefore, the longer ignition delays of alcohols compared to alkylbenzenes are suggested to occur partly due to the more difficult H-abstraction from alcohols caused by the higher electronegativity of the hydroxyl group compared to that of the phenyl group [315,316]: H- abstraction from alpha carbon of an alcohol (labelled α, for example, in 1-heptanol, Figure 53) becomes easier than from the allylic-like benzyl carbon, but the abstraction of the beta, gamma and delta hydrogens (labelled β,γ and δ ,for example, in 1-heptanol, Figure 53) becomes more difficult than abstraction of the corresponding hydrogens of a alkylbenzene.

It should be noted, that no real difference in ignition delays was observed from Figure 54a for the C12 molecules (dodecylbenzene and dodecanol). This suggests that the effect of the functional group on ignition delay decreases with increasing carbon chain length and that when the alkyl chain increases from C7 and C8 to C12, the alkyl chain largely dominates ignition chemistry with the hydroxyl and phenyl groups having virtually insignificant influences on the ignition delay.

8.3.3 Breaking up an alkylbenzene into an alkane and toluene

In order to investigate the effect of breaking an alkylbenzene (e.g. heptylbenzene) into an alkane (e.g. hexane) and toluene, the single molecule alkylbenzenes were compared to bimolecular alkane/toluene mixtures, where the alkane was one carbon atom shorter than the alkyl chain of the alkylbenzene, so that the total number of carbon atoms (that were not within a cyclic structure) of an alkane/toluene mixture was the same as that of the corresponding alkylbenzene; for example, toluene (C7)

in hexane (C6) mixture was compared with heptylbenzene. Figure 54a shows that the toluene/alkane mixtures increased the ignition delay compared to the corresponding alkylbenzenes in the case of C7 (hexane/toluene mixture and heptylbenzene) and C8 (heptane/hexane mixture and octylbenzene) molecules. Interestingly, in the case of the C 12 molecules (undecane/toluene mixture and dodecylbenzene), no difference in the ignition delay was observed from Figure 54a. These results suggest that the effect on ignition delay of breaking the alkylbenzene into an alkane and toluene decreases with increasing alkyl chain length.

In the case of alkane/toluene mixtures, Klotz et al. [317] suggested that a butane/toluene blend can be modelled by using the model predictions of the individual molecules, and that the interactions between toluene and alkane molecules during combustion is limited to sharing the radical pool. Therefore, the ignition delays of alkylbenzenes compared to those of alkane/toluene mixtures (Figure 54a) were thought to be shorter mainly because of the one carbon atom longer alkyl chains of alkylbenzenes. Compared to the results discussed above, which showed alkanes to result in earlier ignition and faster initial HRR compared to the alkylbenzenes with the same alkyl chain length (Figure 54a), this result highlights the significance of the effect of carbon chain length on ignition delay

8.3.4 Effect of phenyl group on nitrogen oxides

Nitrogen oxides (NO_x) form in diesel engines mainly through a thermal mechanism driven by the oxidation of nitrogen in air; also, to lesser extent, by the conversion of fuel bound nitrogen, and through reactions between the hydrocarbon fuel and nitrogen in air. Due to the dominance of the thermal mechanism, most of the NO_x emissions are produced at high in-cylinder temperatures [245]. The engine in-cylinder gas temperature is highly dependent on the timing and magnitude of the premixed combustion phase. In turn, the magnitude and the timing of the premixed phase are greatly influenced by how long the ignition delay is. This point is illustrated in Figure 56, which shows strong correlations between the ignition delay and premixed phase, ignition delay and pHRR, as well as ignition delay and timing of pHRR.

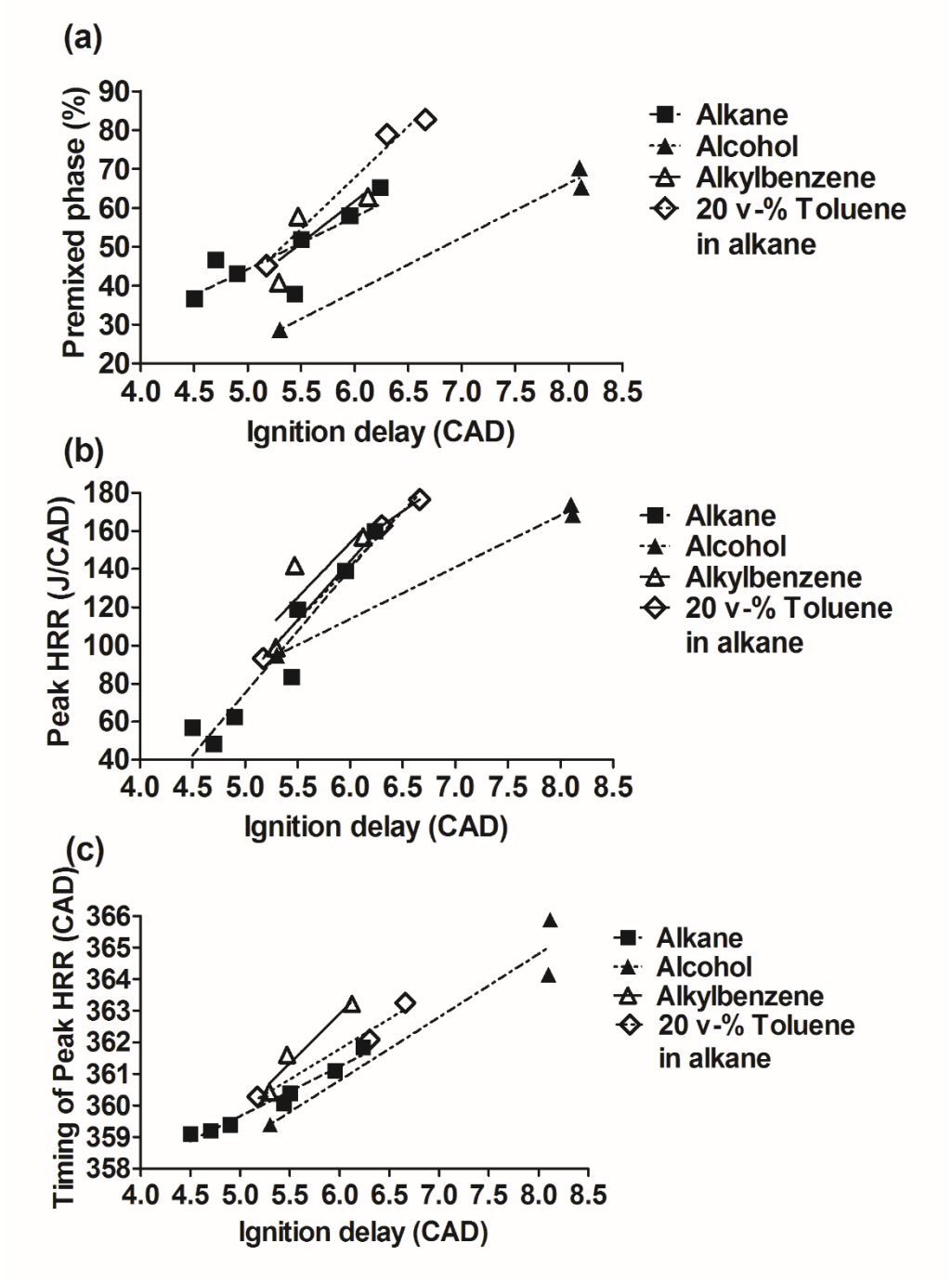

Figure 56. Correlations of ignition delay with (a) premixed phase, (b) pHRR and (c) timing of pHRR.

Figure 57a and Figure 57b show a general trend of increasing NO_x emission with increasing ignition delay and increasing premixed phase. Interestingly, alkylbenzenes seem to have the best correlation between the NO_x emission and ignition delay in Figure 57b. Two fuels appear to depart from this trend, namely heptanol (ignition delay 8.1 CAD) and toluene/hexane mixture (ignition delay 6.7 CAD). The reasons for the low NOx emissions for these two fuel molecules are not apparent: heptanol, for example, combusted at relatively high in-cylinder temperatures (1576K in Figure 57c) due to the high percentage of premixed combustion, despite late combustion (Figure 55); similarly, the toluene/hexane mixture combusted at high in-cylinder temperatures of 1548K. One possible explanation for the low NOx emissions of heptanol and toluene/hexane mixture, despite their relatively high in-cylinder temperatures, is that the premixed phases for these two fuels occurred just as the piston had started the expansion stroke and it is possible that localised flame cooling might have occurred by the intense local turbulence generated by gasses moving out of the piston bowl into the piston pumping clearance volume.

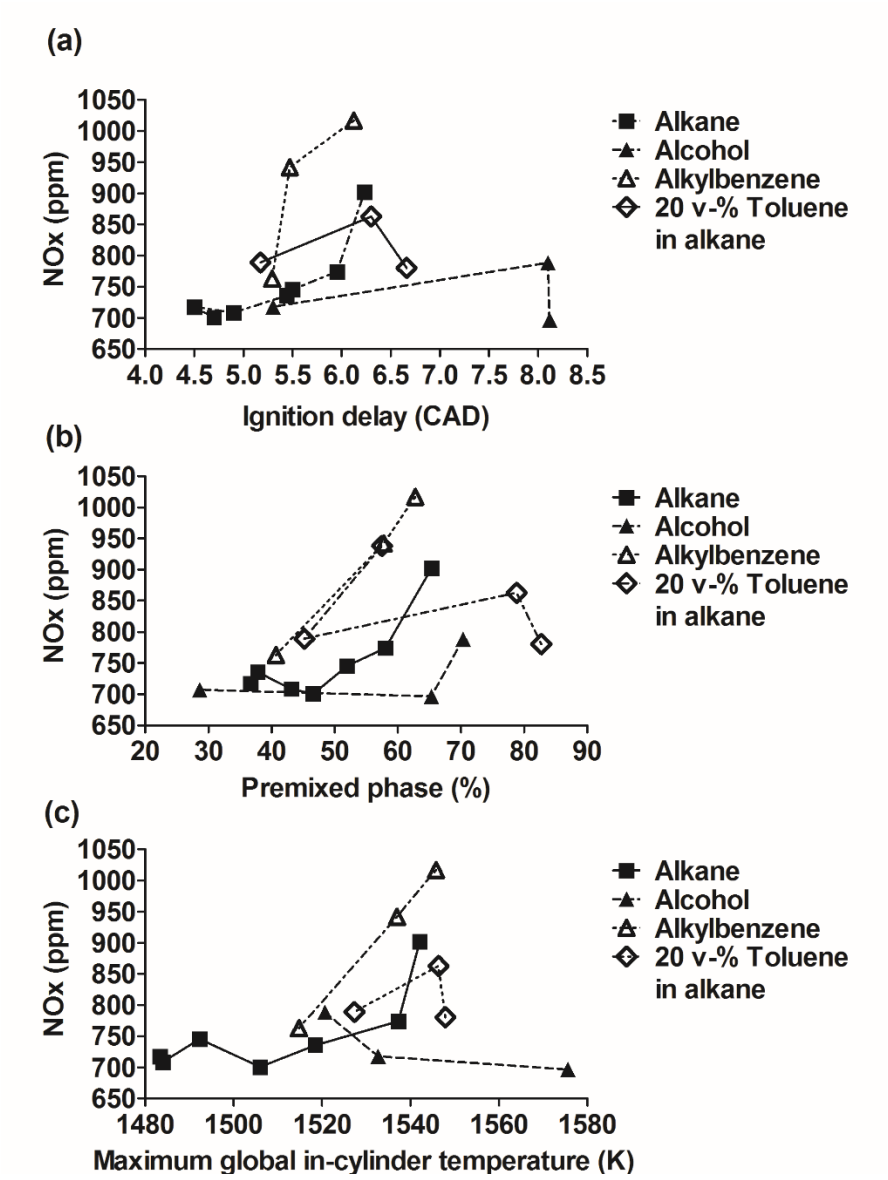

Figure 57. NO_x emissions as function of (a) ignition delay, (b) percentage of fuel burned during premixed phase and (c) in-cylinder temperature.

Close observation of Figure 57 indicates a tendency for the cyclic structures (alkylbenzenes and alkane/toluene mixtures) to produced higher levels of NO_x emissions compared to alkanes and alcohols. In the case of alkylbenzenes, Figure 57c shows that they had high in-cylinder temperatures despite the short ignition delays (Figure 57a), possibly reflecting their high adiabatic flame temperatures (the adiabatic flame temperatures were calculated for a stoichiometric mixture at constant pressure assuming no dissociation [162]). In the case of alkane/toluene mixtures, the high NO_x emissions were caused by the high in-cylinder temperatures (Figure 57c).

8.3.5 Effect of phenyl group on particulate matter

Particulate matter is formed when small particles combine together to form bigger agglomerates, usually in the fuel-rich areas of the combustion chamber. The particulates can be divided in to two categories based on their size: small primary nucleation particles (diameter 0-50 nm) and larger accumulation particles (diameter 50-1000 nm). The small particles can penetrate human respiratory defences more easily than the large particles. [248] The formation of particulates is mainly effected by fuel structure, equivalence ratio, as well as in-cylinder temperature and oxygen availability during the oxidation process.

The mass of particulates was observed from Figure 58a not to change significantly for carbon chain lengths below C8 but to increase for chain lengths above C8 with the increasing chain length. Figure 58b shows that molecules with longer carbon chain lengths generally had a smaller particulate number count. It is suggested that these changes in the mass and number of particulates with increasing carbon chain length are partly due to the decrease in both the proportion of fuel burned during the premixed phase and the in-cylinder temperature. Poorer mixing indicated by the smaller premixed phase results in easier formation of the heavier accumulation particles.

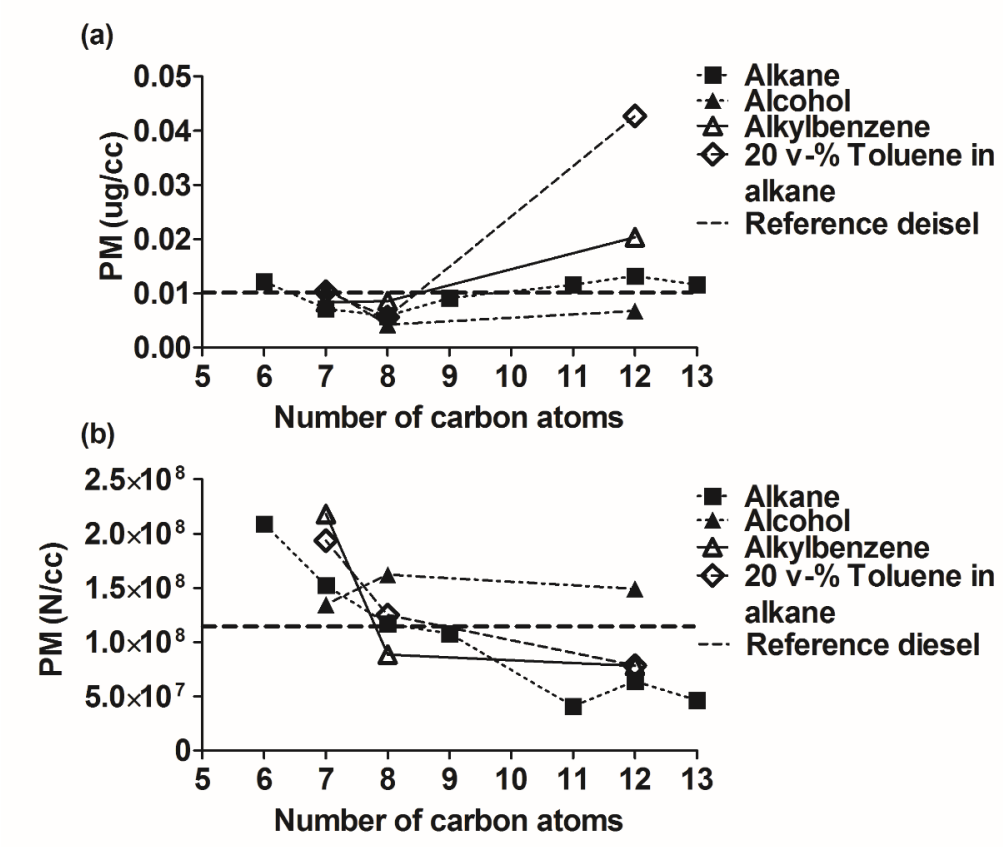

Figure 58. The (a) mass and (b) number of particulate emissions of each structural group.

Alcohols can be seen from Figure 58a to have the lowest particulate mass, compared to the tested hydrocarbon molecules, and from Figure 58b to have the highest number of small particulates. This is consistent with a previous study [294] which showed that increasing oxygen content in the fuel molecule tends to decrease the particulate emissions in the exhaust. It should also be noted, that the cyclic compounds (alkylbenzenes and alkane/toluene mixtures) produced heavier particulates than alkanes or alcohols. This result is supported e.g. by Xiao et al. [301], who recorder an increase in smoke when toluene was added to heptane.

8.4 Conclusions

The phenyl group was observed to have a significant effect on ignition delay and exhaust gas emissions of compression ignition combustion when compared to the corresponding alkanes and alcohols. It was suggested, based on the diesel engine experiments, that the ignition delays of the three tested alkylbenzenes with long alkyl chains can be explained by the general combustion mechanism suggested by previous studies for alkylbenzenes with short alkyl chains.

The more detailed key results were as follows:

1. Adding a phenyl group to an alkane by replacing a primary hydrogen atom with a phenyl group to form an alkylbenzene had no significant effect on ignition delay for the C7 and C8 molecules. This highlights the significance of the alkyl chain length on ignition delay.
2. The initial heat release rate of alkylbenzenes was slower than that of alkanes. This was suggested to occur due to both the more difficult H-abstraction and the lower ability of fuel radicals to undergo isomerization for alkyl benzenes, compared to alkanes, caused by the phenyl group.
3. Adding a hydroxyl group to an alkane, instead of a phenyl group, increased the ignition delay more significantly than the addition of a phenyl group for C7 and C8 molecules, although no change was observed in the case of C12 molecules. It was suggested that the hydroxyl group had a more significant increasing effect on ignition delay than the phenyl group due to the slightly high electronegativity of an oxygen atom in the hydroxyl group compared to that of the phenyl group.
4. Breaking an alkylbenzene into two constituent parts of an alkane and toluene increased the ignition delay. This increase in ignition delay was suggested to occur because of the longer alkyl chains of alkyl benzenes compared to the alkane/toluene mixtures.
5. Aromatic compounds (alkylbenzenes and alkane/toluene mixtures) were observed to produce higher levels of NO_x emissions compared to alkanes and the alcohols. This was attributed to the higher in-cylinder temperatures of the cyclic compounds compared to those of alkanes and alcohols.

6. Cyclic compounds produced heavier (larger) particulates in the exhaust gas than alkanes or alcohols.

It was concluded that the changes in combustion characteristics and engine emissions when comparing alkylbenzenes to alkanes and alcohols are mainly affected by the length of the alkyl chain and the number of the rather stable benzyl radicals formed. Further experiments are required in order to understand the degree to which the alkyl chain compensates the decrease in alkylbenzene reactivity caused by the relatively stable benzyl radicals.

Chapter 9

Combustion characteristics and engine exhaust gas emissions of several diesel refinery streams

9.1 Introduction

Petroleum diesel fuel is produced from crude oil by fractional distillation, which results in a mixture of molecules with carbon chain lengths of mainly 8-21 carbon atoms [296]. This mixture often undergoes several refining processes before commercial petroleum diesel is produced. For example, the aromatic compounds of the mixture are hydrogenated to open the aromatic rings, thus producing cycloparaffins and straight chain molecules; hydrotreatment opens the cyclic structures further and can saturate unsaturated molecules. [318–320] Therefore, understanding the combustion of both individual molecules and mixtures of molecules is highly desirable when developing efficient and environmentally friendly fuels. In order to gain further understanding of the combustion characteristics of molecule mixtures, seven petroleum diesel refinery streams, provided by British Petroleum, and blends of these streams were investigated. The refinery streams included three paraffin ones, a non-dearomatized hydrotreated stream, a dearomatized hydrotreated stream, RME and SME.

9.2 Experimental methods

9.2.1 Experimental conditions

The experiments were conducted at an engine speed of 1200 rpm, 600 bar injection pressure, 4 bar IMEP; and with a fixed injection timing of 7.5 CAD before top dead centre. A 7-hole Delphi diesel injector EJDR00504Z was used to inject the fuel to the combustion chamber. Tests with reference diesel fuel were conducted at the beginning and at the end of each test day in order to detect any day-to-day changes in the instrumentation or the experimental equipment. This generated six sets of repeated tests with reference diesel fuel, which allowed assessment of the repeatability of various combustion and exhaust emission measurements. Considering the repeatability of emission measurements, the mean value for NOx

was 733 ppm for the six reference diesel tests, the standard deviation of the mean was 16.9 ppm and the standard error of the mean was 7.6 ppm. The corresponding values for PM mass were: 0.0049 µg/cc, 0.00131 µg/cc and 0.000653 µg/cc; for the number of particulates the corresponding data was: 92.7 $*10^6$ N/cc, 22.0$*10^6$ N/cc and 1.10$*10^6$ N/cc.

9.2.2 Data analysis

In this experiment series, the premixed combustion phase was calculated as the ratio of energy released between SOC and the maximum of second derivative of heat release rate profile to the amount of energy released between SOC and EOC.

9.2.3 Fuel samples investigated

Seven diesel refinery streams, which included two biodiesels, were investigated experimentally. These seven streams and their physical properties are presented in Appendix VI. To allow better analysis of the combustion characteristics of the streams, each one was qualitatively analysed by the author using a gas chromatography-mass spectrometer (GC-MS). The main six compounds detected in each stream, as well as in the reference diesel, and the abbreviations used for the streams are presented in Table 7.

Table 7. The six main compounds in each of stream based on GC-MS analysis.

Stream	Compound
C10 - C14 Paraffins (ShortParaffins)	Decane Tridecane Undecane Dodecane
C14 - C17 Paraffins (Paraffins)	Tridecane Dodecane Tetradecane Pentadecane Hexadecane Undecane
Heavy paraffins (HP)	Tridecane Dodecane Hexadecane, 2,6,10-trimethyl- Eicosane, 2-methyl- Nonadecane, 3-methyl- Eicosane, 2-methyl-
Dearomatised Hydrotreated (DH)	Decane Undecane Dodecane, 4-cyclohexyl- Cyclohexane, 1-methyl-3-propyl- 9-Eicosene, (E)- 1-Octadecyne Sulfurous acid, 2-ethylhexyl heptadecyl ester
Non-Dearomatised Hydrotreated (NonDH)	Tetradecane Tridecane Dodecane Undecane Tetradecane 1-Decanol, 2-hexyl-
FAME (SME)	9-Octadecenoic acid, methyl ester, (E)- Decane Hexadecanoic acid, methyl ester Methyl stearate Methyl 9-eicosenoate Eicosanoic acid, methyl ester
FAME (RME)	9,12-Octadecadienoic acid (Z,Z)-, methyl ester Hexadecanoic acid, methyl ester Decane Methyl stearate Eicosanoic acid, methyl ester Methyl 9-eicosenoate
Reference diesel fuel	Decane Undecane Dodecane

	Tridecane Tetradecane Pentadecane

In addition to the seven individual refinery streams listed above, some of the streams were blended together so as to generate six further streams. Therefore, in total, 17 fuels (7 streams, 6 blends and reference diesel fuel) were available for combustion tests, including the reference diesel. The GC-MS analysis showed that the composition of the HP refinery stream had strong similarities to the reference diesel fuel (~60% similar compounds; a more detailed list of the main compounds in these two samples can be found in Appendix VII). Therefore the HP stream was considered to be the base one for all the six blends. In this way, all the blends were prepared with 50 v-% of HP, with the balance of 50% of the blend made from other streams, so as to form blends similar to the reference diesel fuel.

Table 8 presents the composition of each of the six blends. Both DH and NonDH streams were added to HP stream, so as to make a blend, which allowed investigation of the effect of aromatic and cyclic molecules on combustion. Next, some of NonDH in NonDH/HP blend was replaced with either Paraffin or ShortParaffins in order to observe the significance of straight chain alkanes in a diesel fuel-like mixture. Additionally, a biodiesel/diesel blends was simulated by replacing part of both NonDH and ShortParaffins in the HP/NonDH/ShortParaffins blend with RME. Lastly, so as to investigate the effect of aromatic and cyclic compounds on combustion further, the NonDH in the HP/NonDH/ShortParaffins/RME blend was replaced with DH.

Table 8. Tested stream blends

Blend number	Blend	HP (v-%)	NonDh (v-%)	Dh (v-%)	Paraffin (v-%)	Short Paraffin (v-%)	RME (v-%)
1	HP / DH	50	50	0	0	0	0
2	HP / NonDH	50	0	50	0	0	0
3	HP / NonDH / Paraffins	50	25	0	25	0	0
4	HP / NonDH / ShortParaffins	50	25	0	0	25	0
5	HP / NonDH / ShortParaffins / RME	50	10	0	0	20	20
6	HP / DH / ShortParaffins / RME	50	0	10	0	20	20

9.3 Results and discussion

9.3.1 Effect of fuel composition on the heat release rate

Figure 59a shows that the CN values of the individual streams (see Appendix VI for CN of streams) correlated well with the observed ignition delay times, as was expected. Additionally, Figure 59a shows that in the case of blends, their ignition delays correspond closely to their CN, when the CN of the blends was calculated based on the CN of the individual streams and their v-% in the blends. Figure 59b, Figure 59c and Figure 59d show the expected positive correlations between the ignition delay and the premixed combustion phase, peak HRR and timing of peak HRR, respectively.

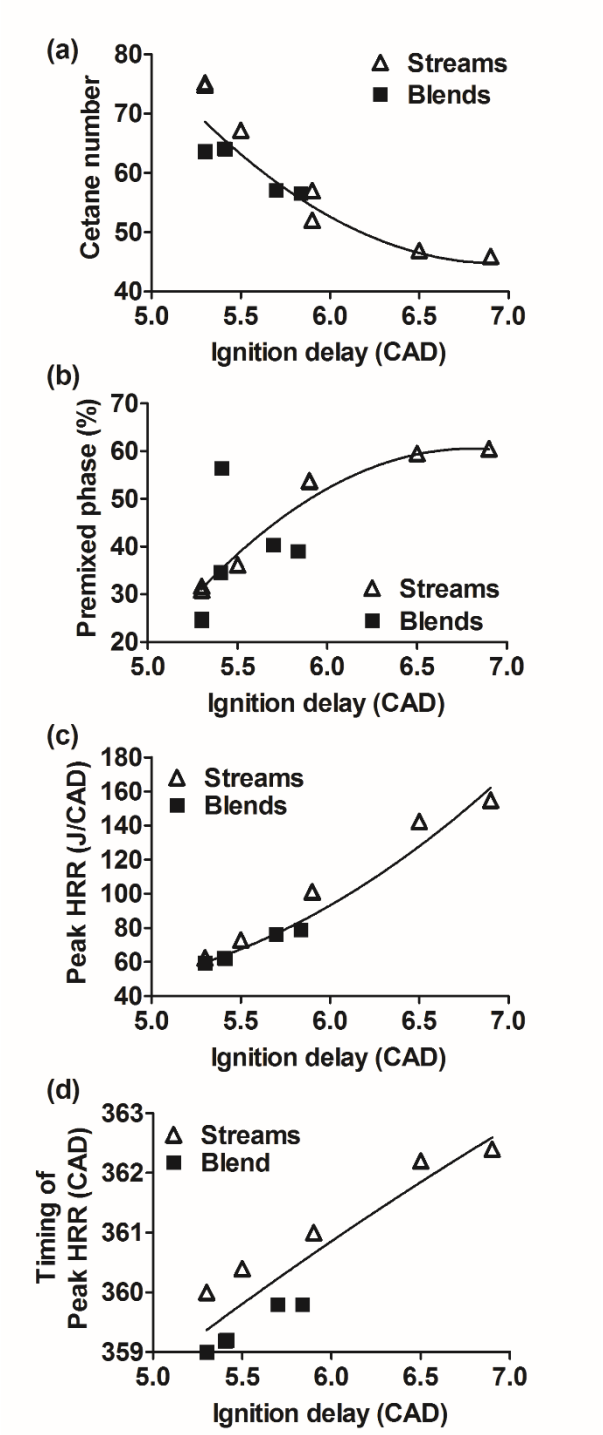

Figure 59. Correlations between ignition delay and (a) cetane number, (b) premixed phase; (c) peak HRR; (d) timing of the peak HRR.

When considering the ignition delays of streams, Figure 60 shows that the three paraffin streams ignited almost simultaneously around 357.8 CAD, and before any of the other fuel samples, as was expected due to their high cetane numbers, arising due to the high content of alkanes with long, straight carbon chains. It should be noted that Heavy Paraffins stream had a slightly slower initial HRR and reached the peak HRR 0.4 CAD after the two other paraffin streams. It is suggested that, in addition to mainly long chain alkanes, the Heavy Paraffins stream might also have included some branched alkanes, which would have slowed the initial HRR. The two biodiesels, SME and RME, ignited at 358.2 CAD, slightly later than the Paraffin streams and before the Hydrotreated streams. This order of ignition was explained by the molecular structure of the streams as follows: methyl ethers of the biodiesel streams had longer ignition delays, compared to the alkanes of the Paraffin streams, due to the presence of oxygen in the ester group and, consequently, the higher electronegativity of the oxygen atom in the ester group, compared to the electronegativity of a carbon atom or a hydrogen atom; the Hydrotreated streams ignited after both alkanes and methyl esters due to the higher content of cyclic and aromatic structures in these streams. These results were in agreement with the conclusions of Chapter 4 and Chapter 5 of this thesis. Figure 60 also shows that the reference diesel fuel ignited between the two biodiesels and the two hydrotreated streams, as was expected, due to the mixture of paraffins, cyclic and aromatic structures in the reference diesel fuel.

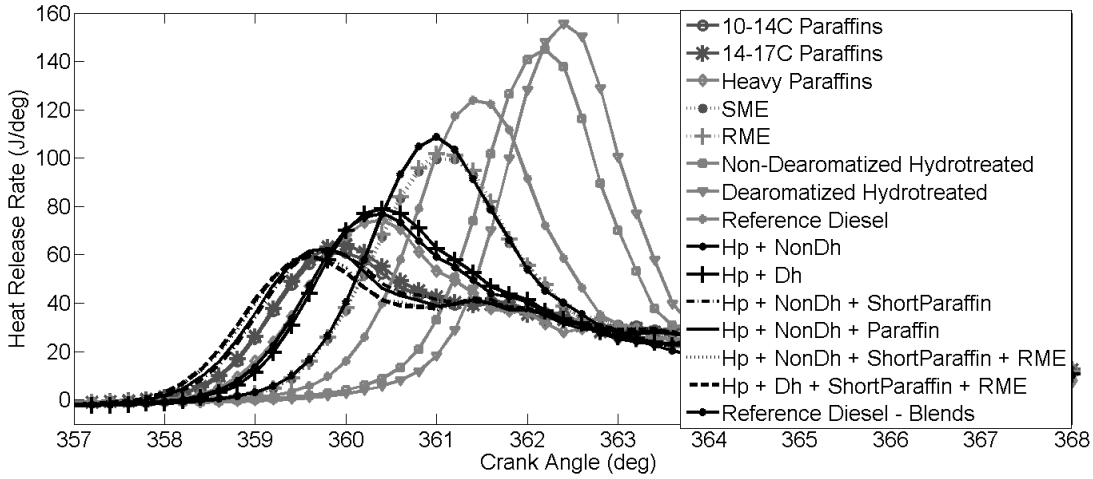

Figure 60. Heat release rate profiles of the tested blends (the grey lines present the HRR of streams and the black lines the HRR of blends).

In the case of stream blends, Figure 60 shows that adding 50 v-% of either the NonDH stream or the DH stream to the HP stream (i.e. blends 1 and 2 in Table 8) slightly increased the ignition delay, and as a result caused increase in the premixed phase and in the value of the peak HRR, compared to the corresponding results for the HP stream alone (Table 9). Interestingly, the timing of peak HRR of 360.4 CAD was retarded by 0.6 CAD. It is suggested, tentatively, that this retardation occurred due to the higher amount of energy released from the aromatic and cyclic structures of the blends 1 and 2, compared to the energy released from the alkanes of the HP stream: although the aromatic and cyclic structures required more energy to be broken down compared to alkanes, and thus increased the ignition delay, once the combustion of the easily ignitable alkanes in the blends 1 and 2 had released enough energy for the aromatic and cyclic structures to break, they resulted in a faster increase in the HRR compared to the alkanes of the HP stream.

Table 9. Main results of the combustion experiments conducted with diesel fuel refinery streams and their blends.

Fuel sample	Ignition delay (CAD)	Premixed phase (%)	Peak HRR (J)	Timing of peak HRR (CAD)
10-14C Paraffins	5.3	30.9	62.5	360.0
14-17C Paraffins	5.3	31.7	62.4	360.0
Heavy Paraffins	5.5	36.2	73.0	360.4
RME	5.9	53.7	101.3	361.0
SME	5.9	53.8	101.1	361.0
Dearomatized Hydrotreated	6.9	60.5	155.0	362.4
Non-Dearomatized Hydrotreated	6.5	59.5	142.5	362.2
Blend 1	5.8	39.0	79.0	359.8
Blend 2	5.7	40.3	76.3	359.8
Blend 3	5.4	34.6	62.2	359.2
Blend 4	5.4	56.4	62.1	359.2
Blend 5	5.3	24.5	59.3	359.0
Blend 6	5.3	24.9	59.5	359.0

Considering now blends 3 and 4 in Table 8 replacing 25 v-% of the NonDH steam in the HP/NonDH blend (blend 2 in Table 8) with either Paraffin to form blend 3 or ShortParaffins to form blend 4, reduced the ignition delay, the premixed phase and the peak HRR, as well as retarded the timing of peak HRR, as was expected. The HRR profile of these two blends was similar to that of the ShortParaffins and Paraffins streams (Figure 60). This result highlights the significance of the effect of the fast-igniting alkanes on compression ignition combustion.

Considering now blend 5, replacing some of both NonDH and ShortParaffins of the HP/NonDH/ShortParaffins blend (blend 4) with RME to form the HP/NonDH/ShortParaffins/RME blend (blend 5 in Table 8) had no significant effect on either the ignition delay or the timing of peak HRR. However, the premixed phase was reduced significantly. It is suggested that the diffusion combustion phase became larger partly because 5 v-% of ShortParaffins was replaced with RME, which was more difficult to ignite than ShortParaffins. However, on the other hand, the replacement of 15 v-% of the NonDH stream with RME would have been expected to increase the premixed phase. Considering, finally, blend 6, this was prepared by replacing the NonDH stream with DH stream in the HP/NonDH/ShortParaffins/RME

blend (blend 5) to form a HP/DH/ShortParaffins/RME blend (blend 6 in Table 8) Figure 60 shows that this had no significant effect on the HRR, with both blends 5 and 6 having similar HRR patterns. These results again highlight the effect of the fast igniting alkanes on combustion, and also suggest that interaction between molecules in fuel mixtures has a significant effect on combustion characteristics.

9.3.2 Effect of fuel composition on NOx emissions

NO_x emissions are formed mainly through the Fennimore mechanism in compression ignition engines and the chemistry is formulated by the extended Zeldovich system of reactions. Therefore, higher combustion temperatures tend to lead to higher formation rates and higher NOx levels in the engine exhaust gas. Figure 61 shows that, as expected, NO_x emissions increased with increasing: ignition delay (Figure 61 a), premixed phase amount (Figure 61 b), peak HRR (Figure 61 c), and in-cylinder temperature (Figure 61 d). The lack of a good positive correlation in Figure 61d between NO_x concentration and mean gas temperature suggests that other factors, than the average in-cylinder temperature, have an effect on the level of NO_x exhaust emission. One such factor might be the oxygen content of fuel. It should be noted, however, that the two biodiesels with oxygen content do not have NOx levels which are part of the trend shown in Figure 61d (see also Table 10). Another factor that may lead to poor correlation in Figure 61d might be that the average in-cylinder temperature may not be a good representation of the local flame temperature which is, after all, responsible for the production of NO_x. Small differences in local temperature could be very important for NO_x formation rate (due to the exponential relation between this rate and temperature) but do not alter the average in-cylinder temperature significantly.

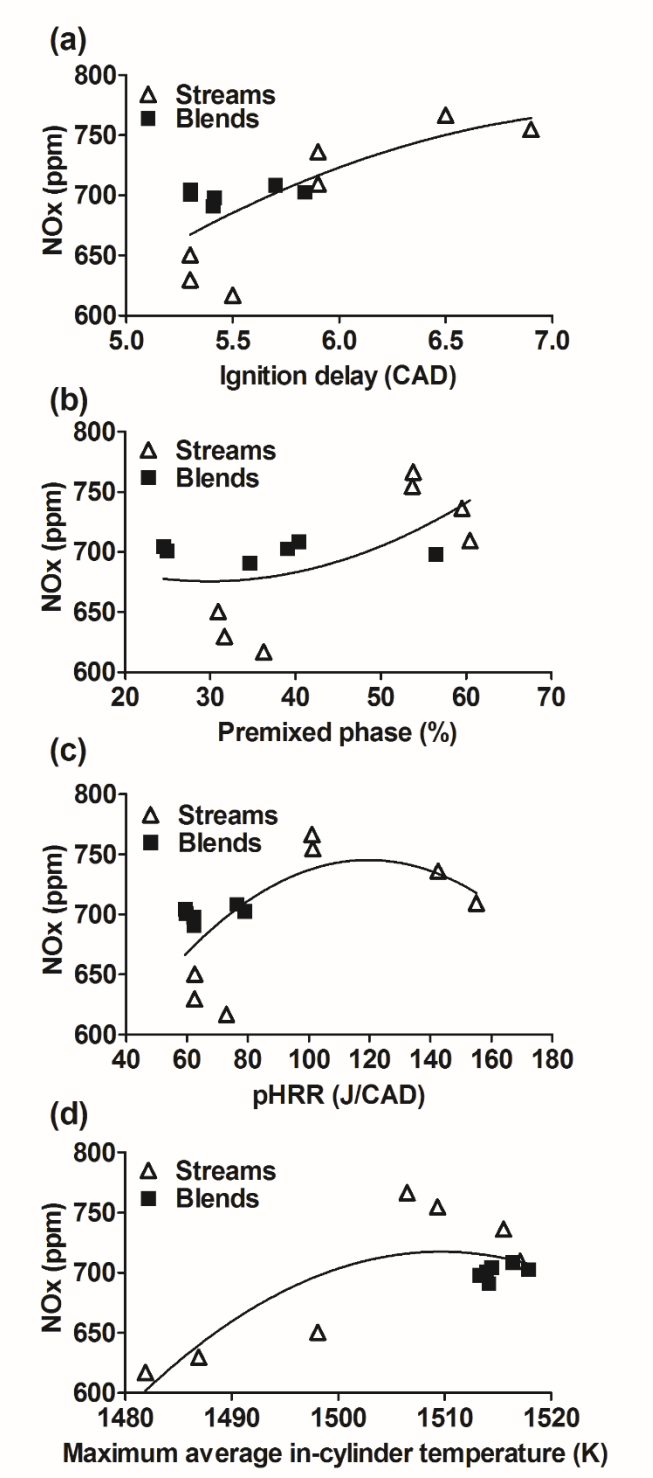

Figure 61. Effect on NOx of (a) ignition delay, (b) premixed phase, (c) peak HRR and (d) in-cylinder temperature.

Table 10. Main exhaust gas emissions of the combustion experiments conducted with diesel fuel refinery streams and their blends.

Fuel sample	NOx (ppm)	THC (ppm)	Particulates N (n/cc)	Particulates m (yg/cc)
10-14C Paraffins	650.5	135.8	5.2E+07	0.0140
14-17C Paraffins	629.7	121.3	5.2E+07	0.0200
Heavy Paraffins	616.9	114.8	5.6E+07	0.0200
RME	709.5	126.5	1.3E+08	0.0060
SME	736.3	133.0	1.3E+08	0.0070
Dearomatized Hydrotreated	754.8	191.2	1.2E+08	0.0020
Non-Dearomatized Hydrotreated	766.5	179.0	6.9E+07	0.0200
Blend 1	702.8	168.7	2.8E+08	0.0230
Blend 2	708.6	153.8	2.2E+08	0.0160
Blend 3	691.2	134.7	4.9E+07	0.0130
Blend 4	698.1	141.9	5E+07	0.0120
Blend 5	704.5	222.5	1.1E+08	0.0120
Blend 6	701.0	150.4	1.1E+08	0.0090

9.3.3 Effect of fuel composition on THC emissions

Incomplete combustion of fuel results in formation of unburned hydrocarbons. Generally, better mixing of air and fuel reduces the concentration of THC in the engine exhaust gas due to more complete combustion. Figure 62a shows a good negative correlation between the concentration of total hydrocarbons in the engine exhaust and the premixed combustion, excluding the two data points for the two hydrotreated streams. The high levels of THC for the two hydrotreated streams (NonDh 179.0 ppm; Dh 191.2 ppm) can be explained by the higher content of cyclic and aromatic structures, compared to the other streams. These structures are more difficult to break down, requiring longer sustained period of high temperature for complete oxidation. Returning to Figure 62b, considering the effect of fuel physical properties on THC emissions, higher fuel density was observed to increase THC

emissions (Figure 62b). One blend, that is the HP/NonDH/ShortParaffins/RME blend (blend 5) had particularly high level of THC emissions (222.5ppm), which may be attributable to particularly poor mixing of air and fuel (see also Figure 62a, showing a very low premixed proportion of ~25% for this blend). Turning now to Figure 62c, a positive but rather poor correlation can be observed between THC emissions and fuel kinematic viscosity, if the HP stream (7.5 cSt and 114.8 ppm) is excluded. Both the positive correlations between THC emissions and fuel density and viscosity are suggested to occur because fuels with higher density and high viscosity can generally lead to poorer mixing of fuel and air.

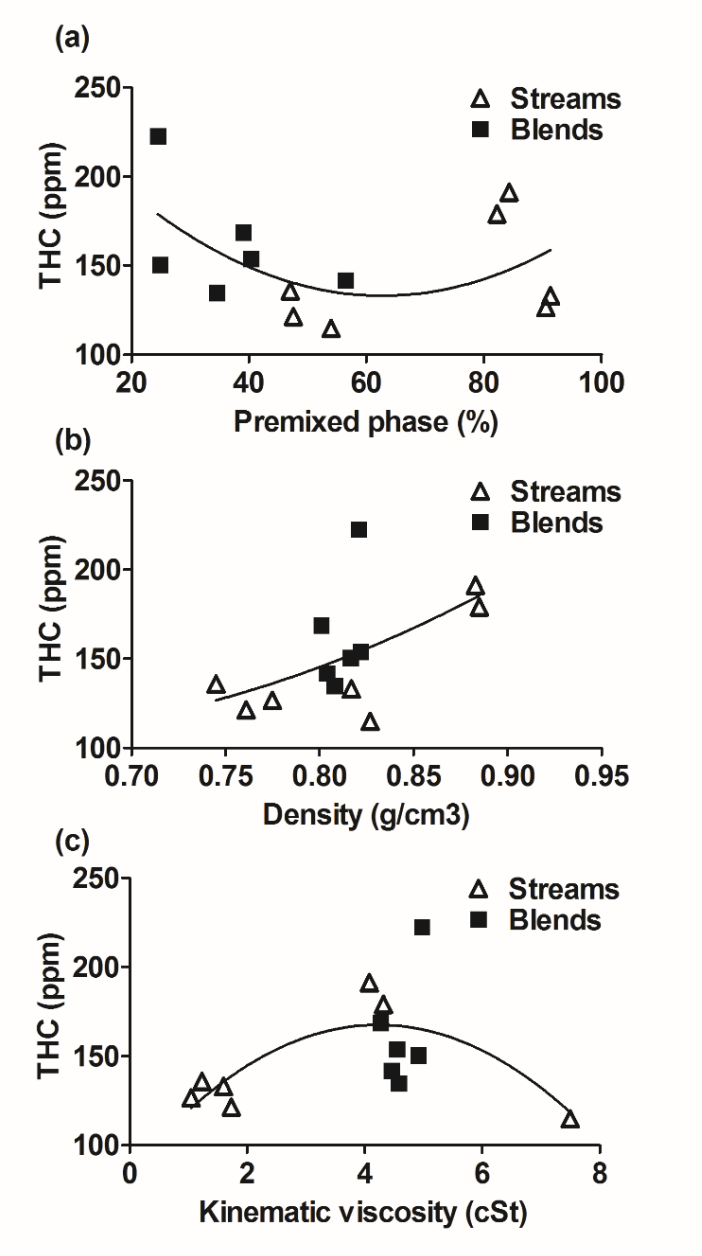

Figure 62. The effect on total hydrocarbon emissions in engine exhaust gas of (a) premixed combustion phase, (b) fuel density and (c) fuel kinematic viscosity (Viscosity and density of the blends was calculated based on the corresponding values of the streams and their v-% in the blend).

9.3.4 Effect of fuel composition on particulate emissions

Figure 63 shows the results for particulate emissions and, as observed in previous chapters of this thesis, trends of particulates are generally poorer and the results are less straightforward to interpret compared to the NO_x emissions. Considering first the number of particulates, Figure 63a shows that the number of particulates in the exhaust gas did no correlate with the premixed combustion phase, whereas the results suggest a positive correlation between the number of particulates and the in-cylinder temperature (Figure 63b). Considering now the mass of particulates, there did not seem to be any correlation between mass and premixed combustion phase (Figure 63c). On the other hand, the results in Figure 63d suggest that increasing in-cylinder temperature for the streams, excluding the NonDH stream (1516 K; 0.20 μg/cc), was associated with the lower number of particulates. The high mass of particulates for the NonDH stream , observed in Figure 63c, was probably due to the higher content of cyclic and aromatic structures, which have difficult ignition, compared to the other streams, and which require higher temperatures and longer periods at high temperatures before they can oxidise fully. To observe a trade-off in Figure 63b and Figure 63d between mass and size of particulates with respect to in-cylinder temperature is likely to be because at high temperatures the rate of formation of more ultrafine particles increases in fuel rich areas off the spray, while at the same time particulate oxidation accelerates in the leaner regions of the combustion chamber. Therefore, in principle, it is possible to produce many very small and almost massless particles (i.e. increase the number of particles), by means of oxidation.

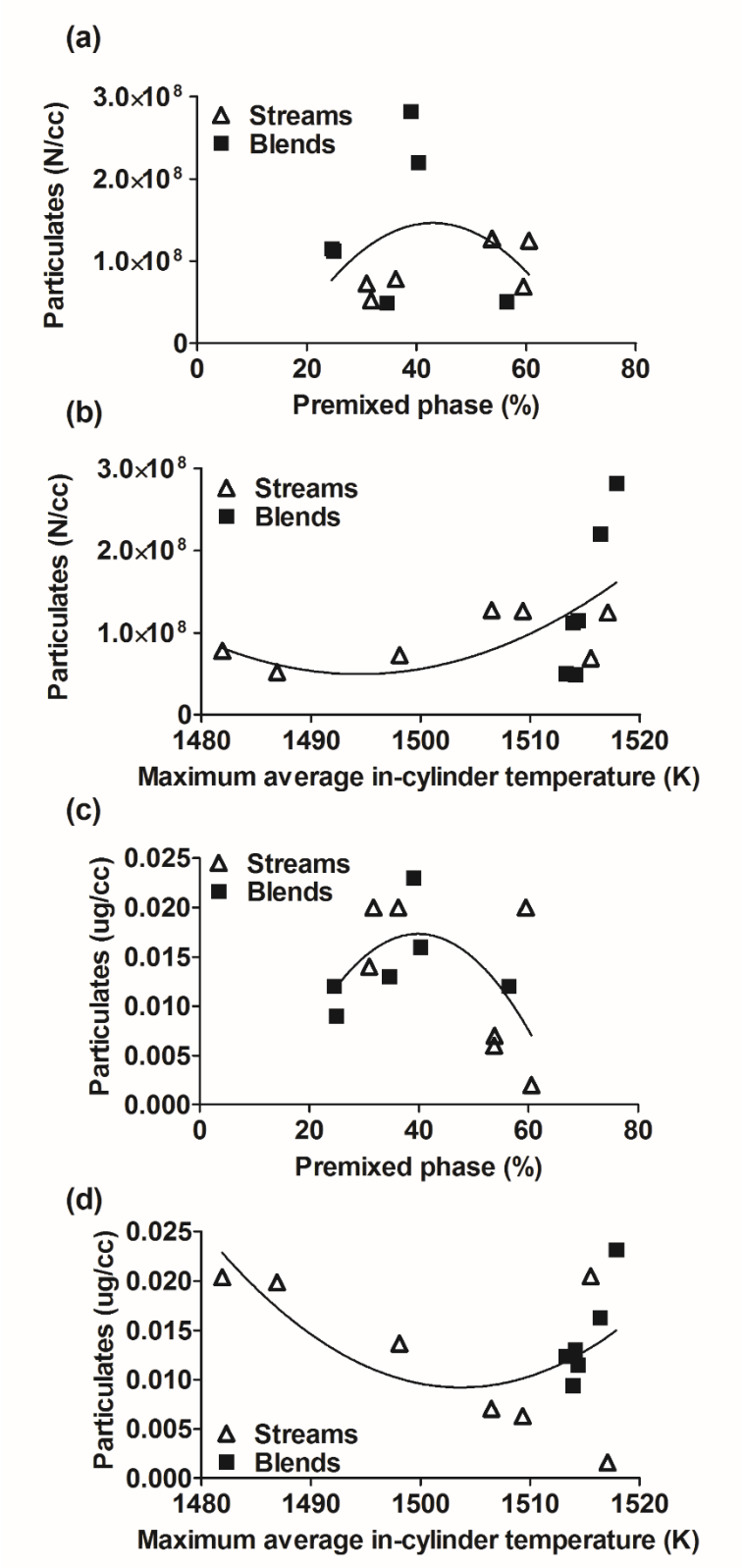

Figure 63. The effect on number of particulates of (a) premixed phase and (b) in-cylinder temperature: The effect on mass of particulates of (c) premixed phase and (d) in-cylinder temperature.

Figure 64 demonstrates clearly this trade-off between number and mass of particulates, but only in the case of the streams. In contrast, in the case of blends, there appears to be a poor positive correlation, rather than a trade-off, between particulate number and mass. One possible explanation is that the dominance of the HP stream (50 v-% in all blends) dominates the chemical and physical properties of the blends and leaves less scope for trends to develop. In contrast the streams have widely different chemical and physical properties.

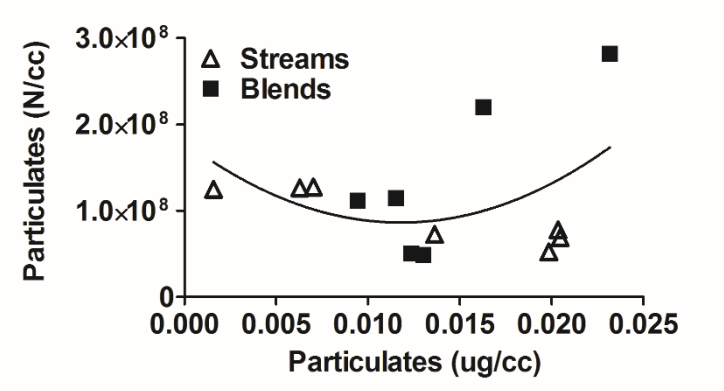

Figure 64. Correlation between the number and mass of particulates in engine exhaust gas.

9.4 Conclusions

It can be concluded, that blending a variety of molecules to form a fuel can alter significantly the compression ignition and the formation of exhaust gas emissions from a diesel engine, depending on the composition of the fuel. The specific conclusions for this chapter on refinery streams and fluid blends are as follows:

1. The tested fuel samples can be listed as follows according to the increasing ignition delay: Paraffin streams (alkanes), RME and SME (methyl esters), reference diesel fuel, Hydrotreated streams (high content of cyclic and aromatic structures). This order was explained by the molecular composition of the streams and these results were in agreement with the other experimental

studies conducted for this thesis and presented in chapters Chapter 4 and Chapter 5.

2. Alkanes had a significant effect on compression ignition combustion, with 20 v-% or more paraffins seeming to dominate the combustion characteristics of a stream blend.
3. NO_x emissions were observed to be controlled mainly by the combustion temperature, corresponding to the different molecular compositions of the streams.
4. THC emissions were reduced with better fuel-air mixing, excluding the hydrotreated streams. It was suggested that the poor combustion of the aromatic and cyclic compounds in the hydrotreated streams resulted in high THC emissions, despite their large premixed combustion phases.
5. High fuel density and high fuel kinematic viscosity were associated with high THC emissions.
6. A shift from a smaller number of heavy particulates to a larger number of light particulates was observed with increasing in-cylinder temperature. This was suggested to occur due to simultaneous acceleration with temperature of the formation of new nanoparticles in the fuel rich areas and greater oxidation of formed particles in leaner areas of the combustion chamber.
7. The mass of particulates decreased with more efficient mixing of fuel and air due to survival of fewer precursors and particulates from oxidation.
8. The non-aromatised hydrotreated stream produced more particulates, compared to the other streams, and this was associated with the high content of aromatic and cyclic compounds, despite a large premixed combustion phase.

It can be summarised, that although the molecules in the diesel refinery streams interact during combustion in terms of their kinetic mechanisms, the combustion characteristics of these streams and their blends can be mainly explained by the same principles as the combustion experiments of the individual compounds discussed in Chapter 4, Chapter 5 and Chapter 8.

Chapter 10

Conclusions and recommendations for future work

10.1 Conclusions

The aim of this PhD project was to systematically investigate the effect of chemical and physical fuel properties of several potential alternative fuels on combustion characteristics, exhaust gas emissions and thermal efficiency of a diesel engine, so as to aid in the development of energy efficient and environmentally friendly future fuels. It was concluded based on the literature review that the differences between fossil diesel fuel combustion and the combustion of potential alternative biofuels are mainly caused by the higher oxygen content, and the lower content of cyclic and aromatic structures of alternative fuels compared to fossil diesel fuel. However, experimental studies comparing the combustion of different alternative fuels in a diesel engine are scarce in the published literature. Therefore, several systematic experimental studies investigating the effect of fuel molecular structure on compression ignition, formation of pollutant exhaust gas emissions and engine thermal efficiency were conducted in a single cylinder direct injection diesel engine during this PhD project. The experiments were done with fixed injection timing, 4 bar IMEP, 1200 rpm engine speed and 600 bar injection pressure.

First, the compression ignition and exhaust gas emissions of long chain alcohols were investigated because ethanol-diesel blends are currently commercially available and the longer chain alcohols with better ignition qualities have been proposed as alternative diesel engine fuels. The main conclusions of this study were as follows:

1) Alcohol molecules with chain lengths from C8 to C16 were observed to have longer ignition delays compared to the corresponding alkanes. The delayed ignition of alcohols compared to the ignition of alkanes was suggested to occur mainly due to the higher electronegativity of the oxygen atom present in alcohols, compared to that of carbon and hydrogen atoms in hydrocarbon molecules: the high electronegativity of oxygen atoms makes the overall hydrogen abstraction from alcohols more difficult, compared to alkanes, and decreases the ability of fuel molecules to initiate further branching reactions through isomerization

2) Due to the long ignition delays, alcohol combustion developed higher in-cylinder temperatures, compared to alkanes, which tended to increase the NOx emissions. Additionally, the larger premixed phases of alcohols, compared to alkanes, resulted in lower mass of particulate emissions and higher number of particulates in the exhaust gas.
3) Moving the hydroxyl group towards the centre of the alcohol carbon chain increased the ignition delay. This increase in ignition delay was suggested to be caused mainly by the increasing amount of chemical bonds within the alcohol being affected by the high electronegativity of the oxygen atom when the hydroxyl group was moved towards the centre of the molecule. Interestingly, NOx emissions decreased with increasing ignition delay, despite the increasing in-cylinder temperature. This reduction in NOx emissions was suggested to be caused by both the decrease in adiabatic flame temperatures and the later combustion: the later combustion was assumed to result in a shorter overall time during which the in-cylinder temperature remained high, partly due to possible flame quenching and lower NOx formation rate. As was expected, due to the larger premixed phases, the longer ignition delays resulted in the formation of greater number of small nucleation particulates.
4) Higher degree of unsaturation in both alkanes and alcohols resulted in longer ignition delays, increased NOx emissions (due to an increase in both the maximum average in-cylinder temperature and the adiabatic flame temperature), as well as in an increase in the number of particulates and a reduction in the mass of particulates, as was expected from the literature review.
5) Higher degree of branching in alcohols increased the ignition delay and the number of PM particles, similarly to the higher degree of unsaturation, as was expected from the literature review. Interestingly, NOx emissions decreased slightly with increasing degree of branching, despite the increase in both premixed phase and the maximum average in-cylinder temperature, perhaps partly due to a decrease in the adiabatic flame temperature.

The effects of a carbonyl group and an ether group within the fuel molecule on compression ignition and exhaust gas emissions were also investigated. Ethers and

ketones were included in the study because they have been suggested as potential diesel engine fuels; esters were included in the study because they are the main component of bio-diesel; and carboxylic acids were also included so as to confirm theories regarding ignition chemistry. Additionally, the combustion of these carbonyl and ether molecules were compared to the combustion of the alcohols discussed above. The main conclusions of this study were as follows:

6) Compared to the corresponding alkanes, fuel molecules with a carbonyl, ester or carboxylic group in their structure had longer ignition delays. It was suggested that the later ignition of the oxygenated fuel molecules in question, compared to alkanes, were caused by the high electronegativity of the oxygen atom(/s), as was the case when comparing the ignition delays of alcohols and alkanes in the previous study. The longer ignition delays of carbonyl compounds, compared to alkanes, resulted in higher NO_x emissions and lower particulate emissions.
7) Moving a carbonyl group closer to the centre of the carbon chain increased ignition delay and reduced NOx emission, similarly to when a hydroxyl group was moved towards the centre of a molecule. Unlike moving the hydroxyl group, however, the moving of a carbonyl group increased the number of nucleation particulates.
8) Ether group was observed to decrease the ignition delay compared to the corresponding alkanes, unlike the carbonyl compounds. The faster ignition of ethers, compared to the corresponding alkanes, was attributed to the ether linkage because based on the literature review the ether linkages enhances the H-abstraction from fuel molecules and does not to hinder the isomerization of fuel peroxy radicals. However, compared to alkanes, ethers produced higher NOx levels due to an increase in both the in-cylinder temperature and the adiabatic flame temperature. Ethers resulted in lower PM emissions compared to alkanes, as was expected based on the literature.
9) Compared to the carbonyl molecules, perhaps excluding carboxylic acids, alcohols had longer ignition delays. This was suggested to be mainly caused by the higher electronegativity and higher polarity of the hydroxyl group compared to the carbonyl group. The shorter ignition delays of carbonyl

molecules, compared to alcohols, lead to higher NO_x levels (excluding carboxylic acids) and slightly lower particulate emissions.

10) Methyl esters and methyl ketones had similar ignition delays, which were the lowest of the tested oxygenated fuel molecules, excluding ethers. Methyl ketone combustion led to the formation of the highest NO_x levels, and the lowest particulate emissions of the tested oxygenated fuel molecules, excluding ethers.

Thirdly, the effect of fuel molecular structure on engine thermal efficiency was investigated both experimentally by considering the combustion efficiency of the molecules tested in the two previous studies, and with a zero dimensional thermodynamic model. The main conclusions of this study were as follows:

11) Molecules with longer carbon chain length had lower thermal engine efficiency than shorter chain molecules. This was explained by a decrease in ignition delay, and therefore in premixed phase, with increasing carbon chain length of a fuel molecule.
12) Hydrocarbons had higher thermal engine efficiency than oxygenated molecules. Additionally, no obvious correlation between engine efficiency and the amount of oxygen atoms in the fuel molecule was observed. It was therefore concluded that further analysis was required on the effect of heat release rate shape on thermal engine efficiency – especially considering that the experiments were conducted with a fixed injection timing.
13) Fuel density did not have a clear effect on thermal engine efficiency. However, the boiling point of fuel had a negative correlation with the engine efficiency, perhaps due to the association between fuel boiling point and ignition delay: molecules with higher boiling points generally had shorter ignition delays than molecules with lower boiling points. Additionally, high fuel density and high fuel surface tension were both observed to reduce a small amount (1 or 2 percentage points) engine thermal efficiency. This reduction in efficiency was suggested to be caused by the reduced spray area and lower rate of air-fuel mixing with increased values of these two physical fuel properties.
14) The zero dimensional thermodynamic model showed that the timing of heat release rate is more important than the shape of the heat release rate itself, i.e.

the amount of fuel burned during the premixing controlled combustion phase was less important than the timing of the heat release.

15) It was concluded, that besides their effect on ignition delay, fuel properties do not have a substantial effect on the engine thermal efficiency. While the practical implications of this conclusion are that the fuel properties may not offer substantial opportunities for efficiency improvements, at the same time the fuel developers may be free to optimize the fuel structure for lower exhaust pollutant emissions with minimum negative influence on thermal engine efficiency.

Next, the knowledge achieved from the above three studies was applied to explain the compression ignition and exhaust gas emissions of ketones, an ether, valeric esters and levulinates, which could be produced from lignocellulosic biomass. Ignition was ensured by testing each individual molecule when mixed with 30 wt-% heptane. The main conclusions of this study were as follows:

16) Ketones had longer ignition delays than alkanes, as was expected from reports of previous studies in the literature.
17) Dipentyl ether ($C_{10}H_{22}O$) had a similar ignition delay to that of decane ($C_{10}H_{22}$). It was suggested that the similar delay values occurred because, in the case of the ester, physical properties (higher boiling point and higher surface tension) tend to increase the ignition delay while a chemical property (ether linkage) tends to reduce the ignition delay, with a result that both compounds with the same carbon chain length end up with comparable ignition delay periods
18) Valeric esters had longer ignition delays than the ether and alkanes, as was expected based on the previous published studies. Valeric esters also ignited later than the corresponding ketones. This later ignition was attributed partly to the harder H-abstraction from valeric esters compared to ketones, caused by the less stable nature of an ester radial formed after the H-abstraction, compared to a ketone radical.
19) Levulinates had slightly longer ignition delays compared to the corresponding valeric esters due to the additional carbonyl group in the structure of levulinates.

20) Oxygenated molecules produced higher NO_x emissions compared to alkanes, as was expected based on both the literature and the previous studies reported in this thesis. However, no consistent difference was observed between the NO_x emissions, or the particulate emissions, of the oxygenated molecule groups.

The next major study investigated the compression ignition and exhaust gas emissions of alkyl benzenes. Alkyl benzenes were considered as examples of cyclic molecules, the concentration of which tends to be significantly higher in fossil diesel fuel compared to that in alternative fuels. The main conclusions of this study were as follows:

21) Adding a phenyl group to C7 and C8 alkanes to form alkylbenzenes had no significant effect on ignition delay. Nonetheless, the initial heat release rate of the two alkylbenzenes was slower than that of the corresponding alkanes. This was suggested to occur due to both the more difficult H-abstraction from alkylbenzenes, compared to alkanes, and their lower ability to undergo isomerization.
22) Hydroxyl group addition to C7 and C8 alkanes was observed to increase the ignition delay more than the addition of a phenyl group. This interesting result was suggested to occur mainly due to the high electronegativity of the hydroxyl group compared to that for the phenyl group.
23) Breaking an alkylbenzene into two constituent parts of an alkane and toluene increased the ignition delay. This was explained by the longer alkyl chains of the alkylbenzenes compared to those for the alkane/toluene mixtures.
24) As was expected, based on the literature review, cyclic compounds (alkylbenzenes and alkane/toluene mixtures) were observed to produce higher levels of NO_x emissions compared to the corresponding alkanes and alcohols, perhaps because of the higher in-cylinder temperatures. Additionally, cyclic compounds produced heavier (larger) particulates in the exhaust gas than alkanes or alcohols, as was expected from the literature review.

In the next major study, the compression ignition and exhaust gas emissions of seven fossil crude refinery streams were investigated. The streams were supplied by BP and

they were obtained from the fossil crude oil refining process. Additionally, blends of these refinery streams were also investigated. The main conclusions of this study were as follows:

25) Although the streams were complicated mixtures of several compounds, it was possible to predict their ignition delays compared to each other based on the ten most common compounds of each stream and the information gained in the previous studies presented in this thesis.
26) 20 v-% or more of paraffins in fuel dominated the combustion characteristics.
27) Increasing the content of aromatic and cyclic compounds in the fuel increased the concentration of THC in the exhaust gas, despite the increased premixed phase. Additionally, high fuel kinematic viscosity and high density were associated with high THC emissions.
28) Increasing the content of aromatic and cyclic compounds in the fuel also resulted in production of more particulate emissions, despite the increase in premixed phase.

In general, the experimental studies showed that oxygenated fuel molecules resulted in longer ignition delays compared to alkanes of the same carbon chain length. These longer ignition delays of oxygenated fuels compared to those of alkanes may appear to be paradoxical in view of many observations in the literature, according to which oxygenated FAME biofuels, especially biodiesel, have shorter ignition delays than conventional fossil diesel fuel. However, the results presented here suggest that the lower ignition delay of commercial biodiesels, compared to diesel fuel, is mainly due to the longer hydrocarbon alkyl chains of the oxygenated biodiesel molecules, compared to the chain lengths of the hydrocarbon molecules in diesel fuel. Additionally, the absence or lower amount of cyclic and aromatic compounds in biodiesels, compared to fossil diesel fuel, decreases the ignition delay of biodiesel fuels further. When considering the exhaust gas emissions, it is especially interesting, that although oxygen in the molecular fuel structure decreased the particulate emissions, at the same time it increased the number of small particulates. Arguably, the smaller particulates are more dangerous to human health than the larger particulates, because they can penetrate deeper into the human respiratory system.

It can be summarized, based on this work, that the oxygen content in alternative fuels has a significant effect on the combustion characteristics, formation of pollutant exhaust gas emissions and engine thermal efficiency. This indicates that modifying the molecular structure of the fuel can be used to achieve an environmentally friendly fuel, consistent with high engine efficiency. It can also be tentatively suggested that the development of new structures of alternative fuels can have as a primary focus reducing the pollutant exhaust gas emissions (especially by addressing the trade-off between NOx and particulate emissions), because the thermal engine efficiency of a diesel engine is not substantially altered by changes in fuel molecular structure. The experimental work conducted shows that several oxygenated fuel molecules, namely alcohols, ketones, esters, carboxylic acids and ethers, could be used as B100 alternative fuels in diesel engines based on their ignition characteristics. Additionally, several oxygenated molecules, which could be obtained from lignocellulose, could be potentially used as diesel fuel extenders. The results of this study can be used to aid the selection and development of alternative fuels with environmentally friendly combustion and emission characteristics and high thermal efficiency.

10.2 Claims of originality

It is believed that IFFMS, the system developed for measuring the fuel sample flow to the injector of the compression ignition engine, is novel. The main advantage of this system was that combined with a precision mass balance, which measured the injector spill flow rate, the injection rate into the combustion chamber could be measured and recorded continuously during an engine test run. This allowed accurate calculations of engine thermal efficiency and of the amount of fuel that was burned during the premixing controlled combustion phase.

Several of the molecules investigated in this work, such as ketones, valeric esters and levulinates, had not previously been tested in a diesel engine and/or not compared to the other tested molecules. Additionally, the experimental setup allowed testing small amounts of the carboxylic acids which could not be tested in conventional diesel engines due to their corrosive nature and relatively high cost.

To this date, this PhD project has resulted in the publication of three journal papers with two other submitted papers awaiting publication. A list of these papers is presented in the introduction section of this dissertation.

10.3 Recommendations for future work

Based on the work presented in this thesis, it is possible to make several recommendations for future work. When considering the effect of changes in the fuel molecular structure on compression ignition combustion, ketones were concluded to be a promising potential fuel additive for diesel engines based on their ignition characteristics. However, the engine research on ketone combustion is still relatively scarce and the effect of a carbonyl group and the location of this group were only briefly studied during this work. Therefore, a systematic fundamental study could be conducted to investigate the effect on combustion of a carbonyl group in comparison to a double bond; a carbon branch; an ether group; a hydroxyl group; or another carbonyl group. Additionally, the studies could focus on e.g. how the high NOx levels of ketones could be reduced, perhaps by adding another compound to the fuel. Furthermore, the combustion of levulinates and valeric esters with long carbon chains could be investigated, as well as the combustion of other molecules with potential to be formed from lignocellulosic biomass.

Besides the chemical kinetics of ignition, the effect of physical fuel properties on combustion characteristics could also be investigated further. Especially studies with optical engines on the effect of physical fuel properties on heat release rate would provide valuable information for the selection of alternative fuels.

In the case of engine thermal efficiency, further studies are required to understand the effect of the shape of heat release rate on engine efficiency. Therefore, systematic studies where the ignition timing or the CA50 would be held constant but the shape of heat release rate would be varied should be conducted.

When considering engine exhaust gas emissions, further work could be conducted on the effect of oxygen in the fuel molecular structure on particulate emissions. It is known, based on this and previous work, that the NOx formation depends on the in-cylinder temperature, timing of heat release rate and adiabatic flame temperature.

However, the mechanisms through which these three main factors affect NOx formation are not yet fully understood.

Appendix I

Properties of the reference diesel fuel.

CORYTON advanced fuels

Certificate of Analysis

Fuel Blend No:	CAF-G11/407	**Contact:**	Jeanette Angerstein
Fuel Type:	BP EN590 B0	**Order No:**	P000027145
Customer:	BP	**Date:**	08/05/2012

Test	Method	Unit	Limit		Result
			Min	Max	
Cetane Number	ASTM D613		52.0	54.0	53.2
Cetane Index	EN ISO 4264		Report		51.5
Density @ 15°C	EN ISO 3675	kg/L	0.833	0.837	0.8319
Flash Point	EN ISO 2719	°C	55	-	61.0
Polycyclic Aromatics	EN 12916	% m/m	3	6	2.9
Total Aromatics	EN 12916	% m/m	Report		29.3
Sulfur	EN ISO 2846	mg/kg	-	10.0	6.2
Carbon Residue (on 10% DR)	EN ISO 10370	% m/m	-	0.20	0.02
Ash	EN ISO 6245	% m/m	-	0.01	<0.001
Water Content	IP 439	mg/kg	-	200	76.0
Total Contamination	EN ISO 12662	mg/kg	Report		4.1
Copper Corrosion	EN ISO 2160	Rating	Report		1a
FAME	EN 14078	% v/v	Report		<0.2
Oxidation Stability	EN ISO 12205	g/m^3	-	25	2
Strong Acid Number	ASTM D974	mgKOH/g	-	0.02	0
Lubricity Correct WSD	EN ISO 12156-1	micron	-	400	390
Viscosity @ 40°C	ASTM D445	mm^2/s	2.30	3.30	2.463
Cloud Point	EN ISO 23015	°C	Report		-9
CFPP	EN 116	°C	Report	-5	-21
Distillation					
E250	EN ISO 3405	% v/v	Report		42.6
E350	EN ISO 3405	% v/v	Report		95.8
IBP	EN ISO 3405	°C	Report		160.7
10% Volume Evaporated	EN ISO 3405	°C	Report		197.9
20% Volume Evaporated	EN ISO 3405	°C	Report		216.7
30% Volume Evaporated	EN ISO 3405	°C	Report		230.9
40% Volume Evaporated	EN ISO 3405	°C	Report		246.2
50% Volume Evaporated	EN ISO 3405	°C	245	-	260.7
60% Volume Evaporated	EN ISO 3405	°C	Report		275.3
70% Volume Evaporated	EN ISO 3405	°C	Report		289.9
80% Volume Evaporated	EN ISO 3405	°C	Report		307.3
90% Volume Evaporated	EN ISO 3405	°C	Report		328.9
95% Volume Evaporated	EN ISO 3405	°C	345	350	345.8
FBP	EN ISO 3405	°C	-	370	356.5
Residue	EN ISO 3405	% v/v	Report		1.4

Date:	08/05/2012
Signed:	

Coryton Advanced Fuels Ltd
The Manorway
Stanford-le-Hope
Essex SS17 9LN, UK

Tel: +44 (0)1375 665707
Fax: + 44 (0)1375 678904
Email: admin@corytonfuels.co.uk
Website: www.corytonfuels.co.uk

Appendix II

Properties of the molecules used in the experimental studies discussed in chapters 4-8 [234].

Fuel molecule	Test temperature (K)	Boiling point (K)	Density at 25°C (g/ml)	Surface tension at 25°C (N/m)	Dynamic Viscosity at 25°C (Pa*s)
Chapters 4, 5 and 6					
Alkane					
Octane	305	398.83	0.699	0.0211	0.00051
Nonane	305	423.97	0.715	0.0224	0.00067
Decane	305	447.3	0.728	0.0234	0.00086
Undecane	305 and 343	469.08	0.737	0.0242	0.00110
Dodecane	343	489.47	0.745	0.0249	0.00139
Tetradecane	343	526.73	0.758	0.0262	0.00211
Hexadecane	343	560.01	0.77	0.0271	0.00306
Alkene					
1-octene	305	394.44	0.711	0.0213	0.00045
1-decene	305	443.75	0.737	0.0236	0.00076
Alcohol					
1-octanol	305 and 343	468	0.823	0.0271	0.00749
2-octanol	305	453	0.817	0.0259	0.00741
3-octanol	305 and 343	448	0.818	0.0263	0.00690
1-octen-3-ol	305	448 [235]	0.830 [292]	0.0281 [237]	-
1-nonanol	305	486	0.824	0.0278	0.00985
2-nonanol	305	472	0.82	0.0271	0.00944
5-nonanol	305	468	0.818	0.0273	0.00903
1-decanol	305 and 343	503	0.825	0.0284	0.01117
1-decen-3-ol	305	489 [292]	0.837 [292]	0.0290 [237]	-
1-undecanol	305 and 343	518	0.831	0.0288	0.01473
2-undecanol	305	508	0.823	0.0271	0.01536
10-undecen-1-ol	305 and 343	523 [292]	0.850 [292]	0.0303 [237]	-

3,7-dimethyl-1-octanol	343	485	0.832 [292]	0.028	0.01366
3,7-dimethyl-3-octanol	343	469	0.826	0.0268	0.01106
1-dodecanol	343	535	0.83	0.0294	0.01634
1-tetradecanol	343	560	0.824	0.0304 [237]	-
1-hexadecanol	343	585	0.818 [292]	0.0311 [237]	-
Ketone					
2-octanone	305	446	0.815	0.0259	0.00096
2-nonanone	305	467	0.817	0.0277	0.00117
5-nonanone	305	463 [235]	0.826 [292]	0.0265 [237]	-
2-decanone	305	483	0.82	0.0279	0.00136
3-decanone	305	477 [235]	0.825 [292]	0.0271 [237]	-
2-undecanone	305	501	0.822	0.028	-
Carboxylic acid					
Octanoic acid	305	513	0.910 [292]	0.0296	-
Nonanoic acid	305 and 343	529	0.902 [292]	0.0298	0.00812
Decanoic acid	343	543	0.893 [292]	0.0332 [237]	-
Undecanoic acid	343	557.35	0.89	0.0332 [237]	-
10-undecenoic acid	343	549	0.912 [292]	0.0335 [237]	-
Dodecanoic acid	343	571.85	0.883 [292]	0.0333 [237]	-
Hexadecanoic acid	343	624.15	0.852 [292]	0.0334 [237]	-
Ester					
Methyl octanoate	305 and 343	467 [235]	0.877 [292]	0.0279 [237]	-
Methyl nonanoate	305 and 343	488	0.875 [292]	0.0283 [237]	-
Methyl decanoate	305	498 [235]	0.871 [292]	0.0287 [237]	-
Methyl hexadecanoate	343	691 [235]	0.852 [292]	0.0303 [237]	-
Ether					
Ethyl diglyme	305	462.15	0.904	0.0268	0.00124
Dibutyl ether	305	413.44	0.764	0.0224	0.00062

Dibutoxymethane	305	454 [237]	0.834 [238]	0.0262 [237]	0.000964 [250]

Chapter 7

Fuel molecule	Boiling point (K)	Density at 25°C [292] (g/ml)	Surface tension at 25°C (N/m)	Dynamic Viscosity at 25°C (Pa*s)
Alkane				
Heptane	372	0.682	0.0000	0.00039
Nonane	424	0.715	0.0224	0.00067
Decane	447	0.730	0.0000	0.00086
Ketone				
3-Heptanone	421	0.818	0.0000	0.00075
5-Nonanone	462.6 [292]	0.826 [235]	0.0000	-
Ether				
Dipentyl ether	460	0.785	0.0000	0.00161
Valerate				
Ethyl valerate	274	0.875	0.0000	0.00847 [237]
Butyl valerate	274	0.868	0.0000	-
Pentyl valerate	274	0.865	0.0000	-
Levulinate				
Ethyl levulinate	274	1.016	0.0000	-
Butyl levulinate	274	0.974	0.0000	-

Chapter 8

Fuel molecule	Boiling point (K)	Density at 25°C (g/ml)	Surface tension at 25°C (N/m)	Dynamic Viscosity at 25°C (Pa*s)
Alkane				
Hexane	342	0.656	0.0000	0.00030
Heptane	372	0.682	0.0000	0.00039
Octane	399	0.699	0.0211	0.00051
Nonane	424	0.715	0.0224	0.00067
Undecane	469	0.737	0.0242	0.00110
Dodecane	489	0.745	0.0249	0.00139
Tridecane	509	0.754		0.00172
Alcohol				
1-Methanol	338	0.787	0.0000	0.00054
1-Heptanol	449	0.82	0.0000	0.00578
1-Octanol	468	0.823	0.0271	0.00749
1-Dodecanol	535	0.83	0.0294	0.01634

Phenyl alkane				
1-Phenylheptane	519	0.853	0.0000	0.00192
1-Phenyloctane	538	0.853	0.0000	0.00237
1-Phenyldodecane	601	0.849	0.0000	0.00495

Appendix III

A zero-dimensional thermodynamic model (Section 6.2.4).

A zero-dimensional model of the engine cylinder contents is considered, with the contents being spatially uniform in terms of species, pressure, and temperature. The instantaneous net energy input to the engine cylinder contents is given by equation (E 11) below [168]:

$$\frac{dQ_{hr}}{d\theta} - \frac{dQ_{ht}}{d\theta} = \frac{\gamma}{\gamma-1} p \frac{dV}{d\theta} + \frac{1}{\gamma-1} V \frac{dp}{d\theta} \qquad \text{(E 11)}$$

Where $\frac{\mathrm{dQ_{hr}}}{\mathrm{d\theta}}$ is the instantaneous energy release from the combustion of the fuel, $\frac{\mathrm{dQ_{ht}}}{\mathrm{d\theta}}$ is the instantaneous energy transfer (heat transfer) to/from the walls of the engine combustion chamber, and p and V are the instantaneous pressure and volume of the engine cylinder contents and $\frac{\mathrm{dp}}{\mathrm{d\theta}}$ and $\frac{\mathrm{dV}}{\mathrm{d\theta}}$ are their derivatives with respect to crank angle. Rearranging equation (E 11) leads to equation (E 12).

$$\frac{dp}{d\theta} = \left[\frac{\frac{dQ_{hr}}{d\theta} - \frac{dQ_{ht}}{d\theta} - \frac{\gamma}{\gamma-1} p \frac{dV}{d\theta}}{\frac{1}{\gamma-1} V} \right] \qquad \text{(E 12)}$$

The above equation (E 12) was discretised and integrated numerically with respect to crank angle to yield the instantaneous cylinder gas pressure. The instantaneous discretised value of $\frac{\Delta Q_{hr}}{\Delta \theta}$, required in the discretised form of equation (E 12), is defined arbitrarily in Figure 44 and it corresponds to two case studies of special interest: one with a low percentage of premixed combustion; and, the other with a high percentage of this parameter. And the instantaneous discretised value of $\frac{\mathrm{dQ_{ht}}}{\mathrm{d\theta}}$, required in equation

(E 12), was evaluated using the Woschni heat transfer model for diesel engines[168]. The calculation of the instantaneous pressure, based on equation (E 12) above, allows the evaluation of indicated engine work over an engine cycle, as well as the energy rejected in the engine exhaust; the Woschni model allows the calculation of energy dissipated over the cycle by means of heat transfer; and the integration of the two energy release rate profiles in Figure 44 allows the calculation of the energy input from the fuel to the engine cycle, for each profile; finally, the ratio of cycle indicated work and cycle energy input from the fuel allows the calculation of the engine thermal efficiency for the two energy release rate profiles of Figure 44. Table 11 lists the parameters required for calculations of $\frac{dp}{d\theta}$ from equation

(E 12) above. The Table 11 also includes the parameters needed for the Woschni heat transfer model [168].

Table 11. The values of various variables used in the theoretical modelling of energy release

ENGINE GEOMETRIC PARAMETERS	
Compression Ratio	18.2
Connecting Rod Length (m)	0.16
Stroke (m)	0.086
Bore(m)	0.086
Displacement Volume (l)	0.5
THERMODYNAMIC MODEL PARAMETERS	
BDT at start of compression stroke (CAD)	180
TDC at end of compression stroke (CAD)	360
BDC at end of expansion stroke (CAD)	540
Ratio of specific heat capacities (compression process)	1.4
Ratio of specific heat capacities (expansion process)	1.33
Compression Stroke Starting Pressure at BDC (bar)	1.013
Compression Stroke Starting Temperature at BDC (K)	300
Trapped Mass (g)	0.59
Engine Speed (rpm)	1200

Engine Cylinder Wall Temperature (K)	373
Piston Crown Wall Temperature (K)	473
Timing of Exhaust Valve Opening (CAD)	500
Cylinder Press After Exhaust Valve Open (bar)	1.013
Total heat release/cycle (both 31% and 75% pre-mix) fixed (J)	491
Indicated mean effective pressure engine at start of combustion timing for maximum efficiency (bar)	4.5
ENGINE HEAT TRANSFER MODEL	
Woschni C1 Constant (Gas Exchange)	6.18
Woschni C1 Constant (Compression)	2.28
Woschni C1 Constant (Combustion and Expansion)	2.28
Woschni C2 Constant (Gas Exchange)	0
Woschni C2 Constant (Compression)	0
Woschni C2 Constant (Combustion and Expansion)	0.00324
Adjusted value of Constant of Proportionality in Woschni Equation	68

The model simulation commences at BDC, at the start of compression stroke (i.e. at 180 CAD) and at each successive 0.5 CAD increment the value of $\frac{dp}{d\theta}$ is calculated from equation (E 12) which, in turn, allows the evaluation of the instantaneous pressure for the engine cylinder contents. At each crank angle increment the approximate value of $\frac{\Delta Q_{ht}}{\Delta\theta}$ is read from Figure 44 (depending on Case 1 or Case 2 heat profile). Also at each crank angle increment the appropriate value of $\frac{\Delta Q_{ht}}{\Delta\theta}$ is calculated from the Woschni model using the parameters listed in Table 11. The simulation continues until the crank angle at which the exhaust valves open (i.e. 500 CAD), when the pressure of the cylinder contents is set equal to the atmospheric pressure so as to represent the exhaust blow-down and energy dissipation in the in the real engine. The simulation then continues beyond 500 CAD, with the cylinder contents pressure fixed at the atmospheric value, until 540 CAD (i.e. BDC) is reached, when the simulation ends. Therefore, the simulation covers one complete engine power revolution of 360 CAD and ignores the induction and exhaust strokes which in a real engine would add another 360 CAD to make up a four

stroke cycle. Once the simulation has ended the thermal efficiency is calculated from the following equation (E 13):

$$\eta = \frac{\sum_{\theta=180}^{\theta=540}(p*\frac{dV}{d\theta})}{\sum_{\theta=180}^{\theta=540}\frac{dQ_{hr}}{d\theta}} = \frac{\text{indicated work done}}{\text{net energy input from fuel}} \quad \text{(E 13)}$$

The numerator in equation (E 13) represents the integral of indicated (cylinder gas) work and denominator the integral (total) of energy released from the fuel.

Appendix IV

Results of the combustion tests (Chapter 7).

Fuel molecule	Ignition delay	Premixed phase	Maximum average in-cylinder temperature	Peak HRR	Timing of Peak HRR	Engine efficiency
	(CAD)	(%)	(K)	(J/CAD)	(CAD)	(%)
Alkane						
Heptane	5.3	25.7	1481	65.0	359.4	49.4
Nonane	5.1	23.0	1450	60.5	359.5	41.4
Decane	4.7	21.2	1453	52.4	358.8	40.9
Ether						
Dipentyl ether	4.5	45.8	1476	46.0	361.6	44.5
Ketone						
3-Heptanone	6.9	40.8	1506	167.6	363.7	28.5
5-Nonanone	5.9	48.9	1467	131.0	361.1	41.3
Levulinate						
Ethyl levulinate	8.0	80.8	1548	132.4	367.5	44.3
Butyl levulinate	7.4	51.3	1516	177.4	364.7	33.7
Valerate						
Ethyl valerate	7.8	63.0	1529	168.0	365.6	44.0
Butyl valerate	7.2	70.4	1502	165.6	363.3	47.9
Pentyl valerate	6.6	62.5	1496	152.2	362.2	49.1

Appendix V

Ignition delay and pHRR of the tested molecule sets (Chapter 8).

	Set A		Set B		Set C	
Molecular group	ID	pHRR	ID	pHRR	ID	pHRR
Alkylbenzene (CX)	6.1	156.9	5.5	141.8	5.3	98.9
Alcohol	8.1	168.4	8.1	173.8	5.3	94.7
Alkane long (CX+1)	5.5	118.8	5.4	83.5	4.7	48.6
Alkane (CX)	6.0	139.2	5.5	118.8	4.5	57.0
20 v-% Toluene in Alkane	6.7	176.4	6.3	162.6	5.2	93.1
Alkane short (CX-1)	6.2	159.9	6.0	139.2	4.9	62.4

Appendix VI

Physical properties of the diesel refinery streams (Chapter 9).

Stream	CN	Kinematic viscosity (cST)	Density(g/ml)
10-14C Paraffins	74.8	1.23	0.745
14-17C Paraffins	75.2	1.73	0.761
Heavy Paraffins	67.2	7.5	0.827
RME	52	4.08	0.883
SME	57	4.32	0.885
Dearomatized Hydrotreated	45.9	1.05	0.775
Non-Dearomatized Hydrotreated	46.9	1.6	0.817

Appendix VII

Main compounds in the reference diesel fuel and the Heavy Paraffins stream obtained with GC-MS (Chapter 9)

Reference diesel fuel		Heavy paraffins
(5.beta.)Pregnane-3,20.beta.-diol, 14.alpha.,18.alpha.-[4-methyl-3-oxo-(1-oxa-4-azabutane-1,4-diyl)]-, diacetate	Decane, 2-cyclohexyl-	1-Decanol, 2-hexyl-
1,5:2,4-Dimethanopentalene-3,6-diol, octahydro-	Disulfide, di-tert-dodecyl	2-methylhexacosane
1,5:2,4-Dimethanopentalene-3,6-diol, octahydro-	Disulfide, di-tert-dodecyl	3-Ethyl-3-methylheptadecane
11,14-Eicosadienoic acid, methyl ester	Dodecane	4-Dehydroxy-N-(4,5-methylenedioxy-2-nitrobenzylidene)tyramine
1-Decanol, 2-hexyl-	Dodecane, 1-fluoro-	Disulfide, di-tert-dodecyl
1-Dodecanol, 2-methyl-, (S)-	Eicosane	Dodecane
1-Ethyl-4-methylcyclohexane	Falcarinol	Eicosane, 2-methyl-
1-Heptanol, 2,4-diethyl-	Heptacosane	Heptacosane
1-Heptatriacotanol	Hydrocinnamic acid, o-[(1,2,3,4-tetrahydro-2-naphthyl)methyl]-	Nonadecane, 3-methyl-
1-Nonylcycloheptane	Malonic acid, heptadecyl 4-methylpent-2-yl ester	Nonane, 4,5-dimethyl-
1-Octanol, 2-butyl-	Malonic acid, isobutyl tetradecyl ester	Octadecanoic acid, 2-oxo-, methyl ester
1-Phenyl-1-butene	Naphthalene, 1,2,3,4-tetrahydro-5-methyl-	Sulfurous acid, butyl tetradecyl ester
2(1H)-Isoquinolinecarboximidamide, 3,4-dihydro-	Nonadecane	Tetradecane
2,5-Octadecadiynoic acid, methyl ester	Octadecane, 1-chloro-	Tetradecane, 2,6,10-trimethyl-

2-Propen-1-ol, 3-(2,6,6-trimethyl-1-cyclohexen-1-yl)-	Oleyl alcohol, trifluoroacetate	Tetradecane, 3-methyl-
3-Hexene, 3-ethyl-2,5-dimethyl-	tert-Hexadecanethiol	Tridecane
9-Eicosyne	Tetradecane	Hexadecane, 2,6,10-trimethyl-
Benzene, 1,2,3-trimethyl-	Tetradecane, 1-chloro-	
Benzene, 1-ethyl-2-methyl-	Tetradecane, 2,6,10-trimethyl-	
Benzene, 1-ethyl-4-methyl-	Tetrapentacontane, 1,54-dibromo-	
Benzene, propyl-	trans-Decalin, 2-methyl-	
Bicyclo[3.1.1]heptan-3-ol, 6,6-dimethyl-2-methylene-, [1S-(1.alpha.,3.alpha.,5.alpha.)]-	trans-p-mentha-1(7),8-dien-2-ol	
Carbonic acid, heptadecyl propyl ester	Tridecane	
cis-1-Chloro-9-octadecene	Undecane	
cis-p-mentha-1(7),8-dien-2-ol	Undecane, 2-cyclohexyl-	
Cyclodecane, methyl-	Oxirane, tetradecyl-	
Cyclohexanecarboxylic acid, 3-phenylpropyl ester	p-Cymene	
Cyclohexanol, 5-methyl-2-(1-methylethyl)-, (1.alpha.,2.alpha.,5.alpha.)-	Sulfurous acid, 2-ethylhexyl octadecyl ester	
Cyclopropane, 1-(2-methylbutyl)-1-(1-methylpropyl)-	tert-Hexadecanethiol	
Decane		

References

[1] Heywood JB. Internal combustion engine fundamentals. McGraw-Hill Inc.; 1988.

[2] Fiorese G, Catenacci M, Verdolini E, Bosetti V. Advanced biofuels: Future perspectives from an expert elicitation survey. Energy Policy 2013;56:293–311. doi:10.1016/j.enpol.2012.12.061.

[3] Badra J, Elwardany AE, Khaled F, Vasu SS, Farooq A. A shock tube and laser absorption study of ignition delay times and OH reaction rates of ketones: 2-Butanone and 3-buten-2-one. Combust Flame 2014;161:725–34. doi:10.1016/j.combustflame.2013.10.001.

[4] Martínez I. Termodinámica básica y aplicada. Dossat; 1992.

[5] Bawse MA, Reve SD, Saraf MR. Carbon Number Distribution by Gas Chromatography for Identification of Outlying Diesel Sample. . AdMet 2012 2012;Paper No. .

[6] Yanowitz J, Ratcliff MA, McCormick RL, Taylor JD, Murphy MJ. Compendium of Experimental Cetane Numbers. 2014.

[7] Stone R. Introduction to Internal Combustion Engines. 3rd ed. Society of Automotive Engineers; 1999.

[8] Lee SY, Kim HM, Cheon S. Metabolic engineering for the production of hydrocarbon fuels. Curr Opin Biotechnol 2014;33C:15–22. doi:10.1016/j.copbio.2014.09.008.

[9] Steen EJ, Kang Y, Bokinsky G, Hu Z, Schimrer A, McClure A, et al. Microbial production of fatty-acid-derived fuels and chemicals from plant biomass. Nature 2010;463:559–62. doi:10.1038/nature08721.

[10] Schirmer A, Rude MA, Li X, Popova E, del Cardayre SB. Microbial Biosynthesis of Alkanes. Science (80-) 2010;329:559–62. doi:10.1126/science.1187936.

[11] Huber GW, Iborra S, Corma A. Synthesis of Transportation Fuels from Biomass: Chemistry, Catalysts, and Engineering. Chem Rev 2006;106:4047. doi:10.1021/cr068360d.

[12] Hoekman SK, Broch A, Robbins C, Ceniceros E, Natarajan M. Review of biodiesel composition, properties, and specifications. Renew Sustain Energy Rev 2012;16:143–69. doi:10.1016/j.rser.2011.07.143.

[13] Ejim CE, Fleck BA, Amirfazli A. Analytical study for atomization of biodiesels and their blends in a typical injector: Surface tension and viscosity effects. Fuel 2007;86:1534–44.

[14] Knothe G. A comprehensive evaluation of the cetane numbers of fatty acid methyl esters. Fuel 2014;119:6–13. doi:10.1016/j.fuel.2013.11.020.

[15] Yuan W, Hansen A, Zhang Q. Vapor pressure and normal boiling point predictions for pure methyl esters and biodiesel fuels. Fuel 2005;84:943–50. doi:10.1016/j.fuel.2005.01.007.

[16] Atabani AE, Silitonga AS, Ong HC, Mahlia TMI, Masjuki HH, Badruddin IA, et al. Non-edible vegetable oils: A critical evaluation of oil extraction, fatty

acid compositions, biodiesel production, characteristics, engine performance and emissions production. Renew Sustain Energy Rev 2013;18:211–45. doi:10.1016/j.rser.2012.10.013.

[17] Abbaszaadeh A, Ghobadian B, Omidkhah MR, Najafi G. Current biodiesel production technologies: A comparative review. Energy Convers Manag 2012;63:138–48. doi:10.1016/j.enconman.2012.02.027.

[18] Borugadda VB, Goud V V. Biodiesel production from renewable feedstocks: Status and opportunities. Renew Sustain Energy Rev 2012;16:4763–84. doi:10.1016/j.rser.2012.04.010.

[19] Aransiola EF, Ojumu TV, Oyekola OO, Madzimbamuto TF, Ikhu-Omoregbe DIO. A review of current technology for biodiesel production: State of the art. Biomass and Bioenergy 2014;61:276–97. doi:10.1016/j.biombioe.2013.11.014.

[20] Adewale P, Dumont M-J, Ngadi M. Recent trends of biodiesel production from animal fat wastes and associated production techniques. Renew Sustain Energy Rev 2015;45:574–88. doi:10.1016/j.rser.2015.02.039.

[21] Bharathiraja B, Chakravarthy M, Kumar RR, Yuvaraj D, Jayamuthunagai J, Kumar RP, et al. Biodiesel production using chemical and biological methods – A review of process, catalyst, acyl acceptor, source and process variables. Renew Sustain Energy Rev 2014;38:368–82. doi:10.1016/j.rser.2014.05.084.

[22] Daud NM, Sheikh Abdullah SR, Abu Hasan H, Yaakob Z. Production of biodiesel and its wastewater treatment technologies: A review. Process Saf Environ Prot 2014;94:487–508. doi:10.1016/j.psep.2014.10.009.

[23] Ashraful AM, Masjuki HH, Kalam MA, Rizwanul Fattah IM, Imtenan S, Shahir SA, et al. Production and comparison of fuel properties, engine performance, and emission characteristics of biodiesel from various non-edible vegetable oils: A review. Energy Convers Manag 2014;80:202–28. doi:10.1016/j.enconman.2014.01.037.

[24] Silitonga AS, Masjuki HH, Mahlia TMI, Ong HC, Chong WT, Boosroh MH. Overview properties of biodiesel diesel blends from edible and non-edible feedstock. Renew Sustain Energy Rev 2013;22:346–60. doi:10.1016/j.rser.2013.01.055.

[25] Kumar N, Varun, Chauhan SR. Performance and emission characteristics of biodiesel from different origins: A review. Renew Sustain Energy Rev 2013;21:633–58.

[26] Takase M, Zhao T, Zhang M, Chen Y, Liu H, Yang L, et al. An expatiate review of neem, jatropha, rubber and karanja as multipurpose non-edible biodiesel resources and comparison of their fuel, engine and emission properties. Renew Sustain Energy Rev 2015;43:495–520. doi:10.1016/j.rser.2014.11.049.

[27] Sarathy SM, Oßwald P, Hansen N, Kohse-Höinghaus K. Alcohol combustion chemistry. Prog Energy Combust Sci 2014;44:40–102. doi:10.1016/j.pecs.2014.04.003.

[28] Baeyens J, Kang Q, Appels L, Dewil R, Lv Y, Tan T. Challenges and opportunities in improving the production of bio-ethanol. Prog Energy Combust Sci 2015;47:60–88. doi:10.1016/j.pecs.2014.10.003.

[29] Vohra M, Manwar J, Manmode R, Padgilwar S, Patil S. Bioethanol production: Feedstock and current technologies. J Environ Chem Eng 2014;2:573–84. doi:10.1016/j.jece.2013.10.013.

[30] Haghighi Mood S, Hossein Golfeshan A, Tabatabaei M, Salehi Jouzani G, Najafi GH, Gholami M, et al. Lignocellulosic biomass to bioethanol, a comprehensive review with a focus on pretreatment. Renew Sustain Energy Rev 2013;27:77–93. doi:10.1016/j.rser.2013.06.033.

[31] Kang Q, Apples L, Tna T, Dewil R. Bioethanol from Lignocellulosic Biomass: Current Findings Determine Research Priorities. Sci World J 2014;2014:13. doi:10.1155/2014/298153.

[32] Cann AF, Liao JC. Pentanol isomer synthesis in engineered microorganisms. Appl Microbiol Biotechnol 2010;85:893–9.

[33] Jin C, Yao M, Liu H, Lee CF, Ji J. Progress in the production and application of n-butanol as a biofuel. Renew Sustain Energy Rev 2011;15:4080–106. doi:10.1016/j.rser.2011.06.001.

[34] Morone A, Pandey RA. Lignocellulosic biobutanol production: Gridlocks and potential remedies. Renew Sustain Energy Rev 2014;37:21–35. doi:10.1016/j.rser.2014.05.009.

[35] Saini M, Hong Chen M, Chiang C-J, Chao Y-P. Potential production platform of n-butanol in Escherichia coli. Metab Eng 2015;27:76–82. doi:10.1016/j.ymben.2014.11.001.

[36] Zhang F, Rodriguez S, Keasling JD. Metabolic engineering of microbial pathways for advanced biofuels production. Curr Opin Biotechnol 2011;22:775–83. doi:10.1016/j.copbio.2011.04.024.

[37] Nozzi NE, Desai SH, Case AE, Atsumi S. Metabolic engineering for higher alcohol production. Metab Eng 2014;25:174–82. doi:10.1016/j.ymben.2014.07.007.

[38] Singh V, Mani I, Chaudhary DK, Dhar PK. Metabolic Engineering of Biosynthetic Pathway for Production of Renewable Biofuels. Appl Biochem Biotechnol 2014;172:1158–71. doi:10.1007/s12010-013-0606-3.

[39] Zhang K, Sawaya MR, Eisenberg DS, Liao JC. Expanding metabolism for biosynthesis of nonnatural alcohols. Proc Natl Acad Sci United States Am PNAS, Proc Natl Acad Sci 2008;105:20653–8. doi:10.1073/pnas.0807157106.

[40] Youngquist JT, Schumacher MH, Rose JP, Raines TC, Politz MC, Copeland MF, et al. Production of medium chain length fatty alcohols from glucose in Escherichia coli. Metab Eng 2013;20:177–86. doi:10.1016/j.ymben.2013.10.006.

[41] Arcoumanis C, Bae C, Crookes R, Kinoshita E. The potential of di-methyl ether (DME) as an alternative fuel for compression-ignition engines: A review. Fuel 2008;87:1014–30. doi:10.1016/j.fuel.2007.06.007.

[42] Sezer İ. Thermodynamic, performance and emission investigation of a diesel engine running on dimethyl ether and diethyl ether. Int J Therm Sci 2011;50:1594–603. doi:10.1016/j.ijthermalsci.2011.03.021.

[43] Azizi Z, Rezaeimanesh M, Tohidian T, Rahimpour MR. Dimethyl ether: A

review of technologies and production challenges. Chem Eng Process Process Intensif 2014;82:150–72. doi:10.1016/j.cep.2014.06.007.

[44] Sorenson SC. Dimethyl Ether in Diesel Engines: Progress and Perspectives. J Eng Gas Turbines Power 2000;123:652–8. doi:10.1115/1.1370373.

[45] Rakopoulos DC, Rakopoulos CD, Giakoumis EG, Dimaratos AM. Characteristics of performance and emissions in high-speed direct injection diesel engine fueled with diethyl ether/diesel fuel blends. Energy 2012;43:214–24.

[46] Melin K, Hurme M. Evaluation of lignocellulosic biomass upgrading routes to fuels and chemicals. Celluloce Chem Technol 2010;44:117–37. doi:05769787.

[47] Li T, Suzuki M, Ogawa H. Effects of ethyl tert-butyl ether addition to diesel fuel on characteristics of combustion and exhaust emissions of diesel engines. Fuel 2009;88:2017–24. doi:10.1016/j.fuel.2009.02.041.

[48] Weberdemenezes E, Dasilve R, Cataluna R, Ortega R. Effect of ethers and ether/ethanol additives on the physicochemical properties of diesel fuel and on engine tests. Fuel 2006;85:815–22. doi:10.1016/j.fuel.2005.08.027.

[49] Goh E-B, Baidoo EEK, Burd H, Lee TS, Keasling JD, Beller HR. Substantial improvements in methyl ketone production in E. coli and insights on the pathway from in vitro studies. Metab Eng 2014;26C:67–76. doi:10.1016/j.ymben.2014.09.003.

[50] Goh EB, Baidoo EEK, Keasling JD, Beller HR. Engineering of Bacterial Methyl Ketone Synthesis for Biofuels. Appl Env Microbiol 2012;78:70–80. doi:PMCID: PMC3255637 En.

[51] Anbarasan P, Baer ZC, Sreekumar S, Gross E, Binder JB, Blanch HW, et al. Integration of chemical catalysis with extractive fermentation to produce fuels. Nature 2012;491:235–9. doi:10.1038/nature11594.

[52] Allen JW, Scheer AM, Gao CW, Merchant SS, Vasu SS, Welz O, et al. A coordinated investigation of the combustion chemistry of diisopropyl ketone, a prototype for biofuels produced by endophytic fungi. Combust Flame 2014;161:711–24. doi:10.1016/j.combustflame.2013.10.019.

[53] Faravelli T, Gaffuri P, Ranzi E, Griffiths JF. Detailed thermokinetic modelling of alkane autoignition as a tool for the optimization of performance of internal combustion engines. Fuel 1998;77:147–55.

[54] Semenov NN. Some problems in Chemical Kinetics and Reactivity. Pergamon Press; 1959. doi:10.1016/B978-0-08-009197-6.50002-3.

[55] Warnatz J, Maas U, Dibble RW. Combustion: Physical and Chemical Fundamentals, Modeling and Simulation, Experiments, Pollutant Formation. Springer Science & Business Media,; 2006.

[56] Franz G, Sheldon RA. Oxidation. Ullmann's Encycl. Ind. Chem., Wiley-VCH Verlag GmbH & Co. KGaA; 2000.

[57] Westbrook CK. Research Progress and Future Directions at the Interface Between Next Generation Biofuels and Advanced Engines 2009.

[58] Glassman I, Yetter RA. Combustion. vol. 4. Elsevier Inc.; 2008.

[59] Saxena P, Peters N, Williams FA. An analytical approximation for high-temperature autoignition times of higher alkanes. Combust Flame 2007;149:79–90.

[60] Brezinsky K, Litzinger TA, Glassman I. The high temperature oxidation of the methyl side chain of toluene. Int J Chem Kinet 1984;16:1053–74.

[61] Griffths JF, Barnard J. Flame and combustion. SpringerChapman & Hall; 1995.

[62] Kemnitz CR, Mackey JL, Loewen MJ, Hargrove JL, Lewis JL, Hawkins WE, et al. Origin of Stability in Branched Alkanes. Chem A Eur J 2010;16:6942–9.

[63] Ji C, Sarathy S, Veloo PS, Westbrook CK, Egolfopoulos FN. Effects of fuel branching on the propagation of octane isomers flames. Combust Flame n.d.;159:1426–36.

[64] Liu N, Sarathy S, Westbrook CK, Egolfopoulos FN. Ignition of non-premixed counterflow flames of octane and decane isomers. Proc Combust Inst 2013;34:903–10.

[65] Westbrook CK, Pitz WJ, Sarathy SM, Mehl M. Detailed chemical kinetic modeling of the effects of CC double bonds on the ignition of biodiesel fuels. Proc Combust Inst 2013;34:3049–56. doi:10.1016/j.proci.2012.05.025.

[66] Sun H, Law CK. Kinetics of Hydrogen Abstraction Reactions of Butene Isomers by OH Radical. J Phys Chem A n.d.;114:12088–98.

[67] Mehl M, Vanhove G, Pitz WJ, Ranzi E. Oxidation and combustion of the n-hexene isomers: A wide range kinetic modeling study. Combust Flame 2008;155:756–72. doi:10.1016/j.combustflame.2008.07.004.

[68] Minetti R, Roubaud A, Therssen A, Ribaucour M, Sochet LR. The chemistry of pre-ignition of n-pentane and 1-pentene. Combust Flame n.d.;118:213–20.

[69] Frédérique Battin-Leclerc, Anne Rodriguez, Benoit Husson, Olivier Herbinet, Pierre-Alexandre Glaude, Zhandong Wang, Zhanjun Cheng and FQ, Battin-Leclerc F, Rodriguez A, Husson B, Herbinet O, Glaude PA, et al. Products from the Oxidation of Linear Isomers of Hexene. J Phys Chem 2014;118:673–83.

[70] Prabhu SK, Bhat RK, Miller DL, Cernansky NP. 1-Pentene oxidation and its interaction with nitric oxide in the low and negative temperature coefficient regions. Combust Flame 31996;104:377–90.

[71] Heufer KA, Bugler J, Curran HJ. A comparison of longer alkane and alcohol ignition including new experimental results for n-pentanol and n-hexanol. Proc Combust Inst 2013;34:511–8.

[72] Black G, Curran HJ, Pichon S, Simmie JM, Zhukov V. Bio-butanol: Combustion properties and detailed chemical kinetic model. Combust Flame n.d.;157:363–73.

[73] Weber BW, Kumar K, Zhang Y, Sung C-J. Autoignition of n-butanol at elevated pressure and low-to-intermediate temperature. Combust Flame 2011;158:809–19. doi:10.1016/j.combustflame.2011.02.005.

[74] Mani Sarathy S, Park S, Weber BW, Wang W, Veloo PS, Davis AC, et al. A comprehensive experimental and modeling study of iso-pentanol combustion.

Combust Flame 2013;160:2712–28. doi:10.1016/j.combustflame.2013.06.022.

[75] Wang Q-D, Wang X-J, Liu Z-W, Kang G-J. Theoretical and kinetic study of the hydrogen atom abstraction reactions of ethyl esters with hydrogen radicals. Chem Phys Lett 2014;616-617:109–14. doi:10.1016/j.cplett.2014.10.032.

[76] Lin KC, Lai JYW, Violi A. The role of the methyl ester moiety in biodiesel combustion: A kinetic modeling comparison of methyl butanoate and n-butane. Fuel 2012;92:16–26. doi:10.1016/j.fuel.2011.05.014.

[77] Osmont A, Catoire L, Gökalp I, Swihart MT. Thermochemistry of C−C and C−H Bond Breaking in Fatty Acid Methyl Esters. Energy & Fuels 2007;21:2027–32.

[78] Cai L, Sudholt A, Lee DJ, Egolfopoulos FN, Pitsch H, Westbrook CK, et al. Chemical kinetic study of a novel lignocellulosic biofuel: Di-n-butyl ether oxidation in a laminar flow reactor and flames. Combust Flame 2014;161:798–809. doi:10.1016/j.combustflame.2013.10.003.

[79] Guan L, Tang C, Yang K, Mo J, Huang Z. Experimental and Kinetic Study on Ignition Delay Times of Di-n-butyl Ether at High Temperatures. Energy Fuels 2014;28:5489–96. doi:10.1021/ef500873e.

[80] Ogura T, Miyoshia A, Koshi M. Rate coefficients of H-atom abstraction from ethers and isomerization of alkoxyalkylperoxy radicals. Phys Chem Chem Phys 2007;9:5133–42. doi:10.1039/B706388A.

[81] Al Rashidi MJ, Davis AC, Sarathy SM. Kinetics of the high-temperature combustion reactions of dibutylether using composite computational methods. Proc Combust Inst 2015;35:385–92. doi:10.1016/j.proci.2014.05.109.

[82] Puhan S, Saravanan N, Nagarajan G, Vedaraman N. Effect of biodiesel unsaturated fatty acid on combustion characteristics of a DI compression ignition engine. Biomass and Bioenergy 2010;34:1079–88. doi:10.1016/j.biombioe.2010.02.017.

[83] Lapuerta M, Armas O, Rodríguez-Fernández J. Effect of the Degree of Unsaturation of Biodiesel Fuels on NOx and Particulate Emissions. SAE Int J Fuels Lubr 2009;1:1150–8. doi:10.4271/2008-01-1676.

[84] Benjumea P, Agudelo J., Agudelo AF. Effect of the Degree of Unsaturation of Biodiesel Fuels on Engine Performance, Combustion Characteristics, and Emissions. Energy Fuels 2011;25:, 77–85 : doi:10.1021/ef101096x.

[85] Wang W, Gowadagiri S, Oehlschlaeger MA. Comparative Study of the Autoignition of Methyl Decenoates, Unsaturated Biodiesel Fuel Surrogates. Energy Fuesl 2013;27:5527–32. doi:10.1021/ef4012593.

[86] Yilmaz N, Vigil FM, Benalil K, Davis SM, Calva A. Effect of biodiesel–butanol fuel blends on emissions and performance characteristics of a diesel engine. Fuel 2014;135:46–50. doi:10.1016/j.fuel.2014.06.022.

[87] Merola SS, Tornatore C, Iannuzzi SE, Marchitto L, Valentino G. Combustion process investigation in a high speed diesel engine fuelled with n-butanol diesel blend by conventional methods and optical diagnostics. Renew Energy 2014;64:225–37. doi:10.1016/j.renene.2013.11.017.

[88] Wei L, Cheung CS, Huang Z. Effect of n-pentanol addition on the combustion,

performance and emission characteristics of a direct-injection diesel engine. Energy 2014;70:172–80. doi:10.1016/j.energy.2014.03.106.

[89] Campos-Fernandez J, Arnal JM, Gomez J, Lacalle N, Dorado MP. Performance tests of a diesel engine fueled with pentanol/diesel fuel blends. Fuel 2013;107:866–72. doi:10.1016/j.fuel.2013.01.066.

[90] da Silva G. Oxidation of Carboxylic Acids Regenerates Hydroxyl Radicals in the Unpolluted and Nighttime Troposphere. J Phys Chem 2010;114:6861–9.

[91] Tran LS, Sirjean B, Glaude PA, Fournet R, Battin-Leclerc F. Progress in detailed kinetic modeling of the combustion of oxygenated components of biofuels. Energy 2012;43:4–18.

[92] Zhang Y, Boehman AL. Experimental study of the autoignition of C8H16O2 ethyl and methyl esters in a motored engine. Combust Flame 2010;157:546–55. doi:10.1016/j.combustflame.2009.09.003.

[93] Buyukkaya E. Effects of biodiesel on a DI diesel engine performance, emission and combustion characteristics. Fuel 2010;89:3099–105. doi:10.1016/j.fuel.2010.05.034.

[94] Sahoo PK, Das LM. Combustion analysis of Jatropha, Karanja and Polanga based biodiesel as fuel in a diesel engine. Fuel 2009;88:994–9. doi:10.1016/j.fuel.2008.11.012.

[95] Özener O, Yüksek L, Ergenç AT, Özkan M. Effects of soybean biodiesel on a DI diesel engine performance, emission and combustion characteristics. Fuel 2014;115:875–83. doi:10.1016/j.fuel.2012.10.081.

[96] Sakthivel G, Nagarajan G, Ilangkumaran M, Gaikwad AB. Comparative analysis of performance, emission and combustion parameters of diesel engine fuelled with ethyl ester of fish oil and its diesel blends. Fuel 2014;132:116–24. doi:10.1016/j.fuel.2014.04.059.

[97] Awad S, Loubar K, Tazerout M. Experimental investigation on the combustion, performance and pollutant emissions of biodiesel from animal fat residues on a direct injection diesel engine. Energy 2014;69:826–36. doi:10.1016/j.energy.2014.03.078.

[98] Park SH, Lee CS. Applicability of dimethyl ether (DME) in a compression ignition engine as an alternative fuel. Energy Convers Manag 2014;86:848–63. doi:10.1016/j.enconman.2014.06.051.

[99] Imtenan S, Masjuki HH, Varman M, Rizwanul Fattah IM, Sajjad H, Arbab MI. Effect of n-butanol and diethyl ether as oxygenated additives on combustion–emission-performance characteristics of a multiple cylinder diesel engine fuelled with diesel–jatropha biodiesel blend. Energy Convers Manag 2015;94:84–94. doi:10.1016/j.enconman.2015.01.047.

[100] Sivalakshmi S, Balusamy T. Effect of biodiesel and its blends with diethyl ether on the combustion, performance and emissions from a diesel engine. Fuel 2013;106:106–10. doi:10.1016/j.fuel.2012.12.033.

[101] Paul A, Bose PK, Panua R, Debroy D. Study of performance and emission characteristics of a single cylinder CI engine using diethyl ether and ethanol blends. J Energy Inst 2015;88:1–10. doi:10.1016/j.joei.2014.07.001.

[102] Qi DH, Chen H, Geng LM, Bian YZ. Effect of diethyl ether and ethanol

additives on the combustion and emission characteristics of biodiesel-diesel blended fuel engine. Renew Energy 2011;36:1252–8. doi:10.1016/j.renene.2010.09.021.

[103] Kajitani S, Usisaki H, Clasen E, Campbell S, Al. E. MTBE for Improved Diesel Combustion and Emissions? SAE Tech Pap 1994;941688. doi:10.4271/941688.

[104] Mehl M, Pitz WJ, Westbrook CK, Yasunaga K, Conroy C, Curran HJ. Autoignition behavior of unsaturated hydrocarbons in the low and high temperature regions. Proc Combust Inst 2011;33:201–8.

[105] Kuo KK-Y. Principles of combustion. John Wiley & Sons, Inc.; 2005.

[106] Ali MA, Violi A. Reaction Pathways for the Thermal Decomposition of Methyl Butanoate. J Org Chem 2013;78:5898–908. doi:10.1021/jo400569d.

[107] Westbrook CK. Chemical kinetics of hydrocarbon ignition in practical combustion systems. Proc Combust Inst 2000;28:1563–77.

[108] Nandi MK, Jacobs DC, Liotta FJ, Kesling Jr HS. The preformance of peroxide-based cetane improvement additive in different diesel fuels. SAE 1994.

[109] Mardani A, Tabejamaat S. Effect of hydrogen on hydrogenGÇômethane turbulent non-premixed flame under MILD condition. Hyceltec 2009 Conf 2010;35:11324–31.

[110] Wang F, Mi J, Li P, Zheng C. Diffusion flame of a CH4/H2 jet in hot low-oxygen coflow. Int J Hydrogen Energy 2011;36:9267–77.

[111] Christodoulou F, Megaritis A. Experimental investigation of the effects of separate hydrogen and nitrogen addition on the emissions and combustion of a diesel engine. Int J Hydrogen Energy 2013;38:10126–40.

[112] Bose PK, Maji D. An experimental investigation on engine performance and emissions of a single cylinder diesel engine using hydrogen as inducted fuel and diesel as injected fuel with exhaust gas recirculation. 2nd Int Work Hydrog 2nd Int Work Hydrog 2009;34:4847–54.

[113] Gomes Antunes JM, Mikalsen R, Roskilly AP. An experimental study of a direct injection compression ignition hydrogen engine. Int J Hydrogen Energy 2009;34:6516–22.

[114] Gupta HN. Fundamentals Of Internal Combustion Engines. Prentice-Hall Of India Pvt. Limited; 2006.

[115] Desantes JM, Payri R, Garcia A, Manin J. Experimental Study of Biodiesel Blends Effects on Diesel Injection Processes. Energy & Fuels 2009;23:3227–35.

[116] Dernotte J, Hespel C, Foucher F, Houillie S, Mounaim-Rousselle C. Influence of physical fuel properties on the injection rate in a Diesel injector. Fuel 2012;96:153–60.

[117] Pandey RK, Rehman A, Sarviya RM. Impact of alternative fuel properties on fuel spray behavior and atomization. Renew Sustain Energy Rev 2012;16:1762–78. doi:10.1016/j.rser.2011.11.010.

[118] Lee CS, Park SW, Kwon S Il. An Experimental Study on the Atomization and

Combustion Characteristics of Biodiesel-Blended Fuels. Energy & Fuels 2005;19:2201–8.

[119] Gao J, Deng J, Li C, Dang F, Liao Z, Wu Z, et al. Experimental study of the spray characteristics of biodiesel based on inedible oil. Biotechnol Adv 2009;27:616–24.

[120] Mohan B, Yang W, Yu W. Effect of internal nozzle flow and thermo-physical properties on spray characteristics of methyl esters. Appl Energy 2014;129:123–34. doi:10.1016/j.apenergy.2014.04.109.

[121] No S-Y. How Vegetable Oils and Its Derivatives Affect Spray Characteristics in CI Engines- A Review. At Sprays 2011;21:87–105. doi:10.1615/AtomizSpr.v21.i1.60.

[122] Lahane S, Subramanian KA. Effect of different percentages of biodiesel–diesel blends on injection, spray, combustion, performance, and emission characteristics of a diesel engine. Fuel 2015;139:537–45. doi:10.1016/j.fuel.2014.09.036.

[123] Mohan B, Yang W, Tay KL, Yu W. Experimental study of spray characteristics of biodiesel derived from waste cooking oil. Energy Convers Manag 2014;88:622–32. doi:10.1016/j.enconman.2014.09.013.

[124] Erazo JA, Parthasarathy R, Gollahalli S. Atomization and combustion of canola methyl ester biofuel spray. Fuel 2010;89:3735–41. doi:10.1016/j.fuel.2010.07.022.

[125] Agarwal AK, Dhar A, Gupta JG, Kim W Il, Choi K, Lee CS, et al. Effect of fuel injection pressure and injection timing of Karanja biodiesel blends on fuel spray, engine performance, emissions and combustion characteristics. Energy Convers Manag 2015;91:302–14. doi:10.1016/j.enconman.2014.12.004.

[126] Galle J, Defruyt S, Van de Maele C, Rodriguez RP, Denon Q, Verliefde A, et al. Experimental investigation concerning the influence of fuel type and properties on the injection and atomization of liquid biofuels in an optical combustion chamber. Biomass and Bioenergy 2013;57:215–28. doi:10.1016/j.biombioe.2013.07.004.

[127] Park SH, Cha J, Kim HJ, Lee CS. Effect of early injection strategy on spray atomization and emission reduction characteristics in bioethanol blended diesel fueled engine. Energy 2012;39:375–87.

[128] Park SH, Suh HK, Lee CS. Nozzle flow and atomization characteristics of ethanol blended biodiesel fuel. Renew Energy 2010;35:144–50. doi:10.1016/j.renene.2009.06.012.

[129] Suh HK, Lee CS. Experimental and analytical study on the spray characteristics of dimethyl ether (DME) and diesel fuels within a common-rail injection system in a diesel engine. Fuel 2008;87:925–32.

[130] Kim W Il, Lee K, Lee CS. Spray and atomization characteristics of isobutene blended DME fuels. J Nat Gas Sci Eng 2015;22:98–106. doi:10.1016/j.jngse.2014.11.015.

[131] Guan L, Tang C, Yang K, Mo J, Huang Z. Effect of di-n-butyl ether blending with soybean-biodiesel on spray and atomization characteristics in a common-rail fuel injection system. Fuel 2015;140:116–25.

doi:10.1016/j.fuel.2014.09.104.

[132] Quoc HX, Brun M. Study on Atomization and Fuel Droplet Size Distribution in Direct Injection Diesel Spray. SAE Tech Pap Ser 1994.

[133] Wang X, Huang Z, Kuti OA, Zhang W, Nishida K. Experimental and analytical study on biodiesel and diesel spray characteristics under ultra-high injection pressure. Int J Heat Fluid Flow 2010;31:659–66.

[134] Mancaruso E, Sequino L, Vaglieco BM. First and second generation biodiesels spray characterization in a diesel engine. Fuel 2011;90:2870–83. doi:10.1016/j.fuel.2011.04.028.

[135] Wu Z, Zhu Z, Huang Z. An experimental study on the spray structure of oxygenated fuel using laser-based visualization and particle image velocimetry. Fuel 2006;85:1458–64.

[136] Bang SH, Lee CS. Fuel injection characteristics and spray behavior of DME blended with methyl ester derived from soybean oil. Fuel 2010;89:797–800. doi:10.1016/j.fuel.2009.10.009.

[137] Sagna K, Almeida AD. A study of droplet evaporation. Am J Mod Phys 2013;2:71–6.

[138] Law CK. Recent advances in droplet vaporization and combustion. Prog Energy Combust Sci 1982;8:171–201.

[139] Godsave GAE. Studies of the combustion of drops in a fuel spray: The burning of single drops of fuel. Fourth Symp Combust 1953:818–30.

[140] Spalding DB. Combustion of fuel particles. Fuel 1951;30.

[141] Hsiao GC, Meng H, Yang V. Pressure-coupled vaporization response of n-pentane fuel droplet at subcritical and supercritical conditions. Proc Combust Inst 2011;33:1997–2003.

[142] Sazhin SS, Abdelghaffar WA, Sazhina EM, Heikal MR. Models for droplet transient heating: Effects on droplet evaporation, ignition, and break-up. Int J Therm Sci 2005;44:610–22.

[143] Faeth GM. Current status of droplet and liquid combustion. Prog Energy Combust Sci 1977;3:191–224.

[144] Liu L, Bi Q cheng, Liu W min, Qi F cheng, Bi X gang. Experimental and Theoretical Investigation on Rapid Evaporation of Ethanol Droplets and Kerosene Droplets During Depressurization. Microgravity Sci Technol 2011;23:89–97.

[145] Nakaya S, Fujishima K, Tsue M, Kono M, Segawa D. Effects of droplet diameter on instantaneous burning rate of isolated fuel droplets in argon-rich or carbon dioxide-rich ambiences under microgravity. Proc Combust Inst 2013;34:1601–8. doi:10.1016/j.proci.2012.05.086.

[146] Siebers D. Liquid-Phase Fuel Penetration in Diesel Sprays. Int Congr Expo 1998.

[147] Chiang CH. Axisymmetric calculations of three-droplet interactions. At Sprays 1993;3:91–107. doi:10.1615/AtomizSpr.v3.i1.50.

[148] Sahu S, Hardalupas Y, Taylor AMKA. Simultaneous droplet and vapour-phase measurements in an evaporative spray by combined ILIDS and PLIF

techniques. Exp Fluids 2014;1673. doi:10.1007/s00348-014-1673-0.

[149] Xue J. Combustion characteristics, engine performances and emissions of waste edible oil biodiesel in diesel engine. Renew Sustain Energy Rev 2013;23:350–65. doi:10.1016/j.rser.2013.02.039.

[150] Daho T, Vaitilingom G, Sanogo O, Ouiminga SK, Segda BG, Valette J, et al. Study of droplet vaporization of various vegetable oils and blends of domestic fuel oil-cottonseed oil under different ambient temperature conditions. Int Conf Lignocellul Ethanol 2012;46:653–63.

[151] Al Qubeissi M, Sazhin SS, Crua C, Turner J, Heikal MR. Modelling of biodiesel fuel droplet heating and evaporation: Effects of fuel composition. Fuel 2015. doi:10.1016/j.fuel.2015.03.051.

[152] Sazhin SS, Al Qubeissi M, Kolodnytska R, Elwardany AE, Nasiri R, Heikal MR. Modelling of biodiesel fuel droplet heating and evaporation. Fuel 2014;115:559–72. doi:10.1016/j.fuel.2013.07.031.

[153] Birouk M, Toth SL. Vaporization and Combustion of a Soybean Biodiesel Droplet in Turbulent Environment at Elevated Ambient Pressure. Combust Sci Technol 2015;187:937–52. doi:10.1080/00102202.2014.991867.

[154] Park SH, Kim HJ, Lee CS. Macroscopic spray characteristics and breakup performance of dimethyl ether (DME) fuel at high fuel temperatures and ambient conditions. Fuel 2010;89:3001–11.

[155] Han S, Kim J, Bae C. Effect of air–fuel mixing quality on characteristics of conventional and low temperature diesel combustion. Appl Energy 2014;119:454–66. doi:10.1016/j.apenergy.2013.12.045.

[156] Gao Y, Chow WK. A brief review on combustion modelling. Int J Archit Sci 2005;6:38–69.

[157] Arregle J, Lopez JJ, Garcia JM, Fenollosa C, Garcia A. Development of a zero-dimensional Diesel combustion model. Part 1: Analysis of the quasi-steady diffusion combustion phase. Appl Therm Eng 2003;23:1301–17.

[158] Yamane K, Ueta A, Shimamoto Y. Influence of Physical and Chemical Properties of Biodiesel Fuel on Injection, Combustion and Exhaust Emission Characteristics in a DI-CI Engine. Fifth Int Symp Diagnostics Model Combust Intern Combust Engines 2001.

[159] Gokalp I, Chauveau C, Simon O, Chesneau X. Mass transfer from liquid fuel droplets in turbulent flow. Combust Flame 1992;89:286–98.

[160] Birouk M, Fabbro SC. Droplet evaporation in a turbulent atmosphere at elevated pressure – Experimental data. Proc Combust Inst 2012.

[161] Birouk M, Gökalp I. Current status of droplet evaporation in turbulent flows. Prog Energy Combust Sci 2006;32:408–23.

[162] Turns S. An Introduction to Combustion: Concepts and Applications. McGraw-Hill Science; 2011.

[163] Maqua C, Castanet G, Grisch F, Lemoine F, Kristyadi T, Sazhin SS. Monodisperse droplet heating and evaporation: Experimental study and modelling. Int J Heat Mass Transf 2008;51:3932–45.

[164] Kemenov KA, Pope SB. Molecular diffusion effects in LES of a piloted

methane–air flame. Combust Flame 2011;158:240–54.

[165] Mardani A, Tabejamaat S, Ghamari M. Numerical study of influence of molecular diffusion in the Mild combustion regime. Combust Theory Model 2010;14:747–74.

[166] Kelly-Zion PL, Pursell CJ, Booth RS, VanTilburg AN. Evaporation rates of pure hydrocarbon liquids under the influences of natural convection and diffusion. Int J Heat Mass Transf 2009;52:3305–13.

[167] Poling BP, Prausnitz JM, O'Connel JP. The Properties of Gases and Liquids. McGraw-Hill Professional; 2000.

[168] Stone R. Introduction to Internal Combustion Engines. 4th ed. Palgrave Macmillan; 2012.

[169] Hoskin DH, Edwards CF, Siebers DL. Ingition Delay Performance Versus Composition of Model Fuels. SAE Tech Pap Ser 1992.

[170] Lyn WT. Study of burning rate and nature of combustion in diesel engines. Symp Combust 1963;9:1069–82.

[171] Sornek RJ, Dobashi R, Hirano T. Effect of turbulence on vaporization, mixing, and combustion of liquid-fuel sprays. Combust Flame 2000;120:479–91.

[172] Tompkins BT, Song H, Bittle JA, Jacobs TJ. Efficiency considerations for the use of blended biofuel in diesel engines. Appl Energy 2012;98:209–18.

[173] Kasiraman G, Nagalingam B, Balakrishnan M. Performance, emission and combustion improvements in a direct injection diesel engine using cashew nut shell oil as fuel with camphor oil blending. Energy 2012;47:116–24.

[174] Demirbas A. Calculation of higher heating values of biomass fuels. Fuel 1997;76:431–4.

[175] Friedl A, Padouvas E, Rotter H, Varmuza K. Prediction of heating values of biomass fuel from elemental composition. Pap Present 9th Int Conf Chemom Anal Chem Pap Present 9th Int Conf Chemom Anal Chem 2005;544:191–8.

[176] Fassinou WF. Higher heating value (HHV) of vegetable oils, fats and biodiesels evaluation based on their pure fatty acids' HHV. Energy 2012;45:798–805.

[177] Mehta PS, Anand K. Estimation of a Lower Heating Value of Vegetable Oil and Biodiesel Fuel. Energy & Fuels 2009;23:3893–8.

[178] Sadrameli SM, Seames W, Mann M. Prediction of higher heating values for saturated fatty acids from their physical properties. Fuel 2008;87:1776–80.

[179] Demirbas A. Prediction of Higher Heating Values for Biodiesels from Their Physical Properties. Energy Sources, Part A Recover Util Environ Eff 2009;31:633–8.

[180] Demirbas A. Relationships derived from physical properties of vegetable oil and biodiesel fuels. Fuel 2008;87:1743–8.

[181] Nabi M. Theoretical investigation of engine thermal efficiency, adiabatic flame temperature, NOx emission and combustion-related parameters for different oxygenated fuels. Appl Therm Eng 2010;30:839–44.

[182] Arbab MI, Masjuki HH, Varman M, Kalam MA, Imtenan S, Sajjad H. Fuel properties, engine performance and emission characteristic of common

biodiesels as a renewable and sustainable source of fuel. Renew Sustain Energy Rev 2013;22:133–47.

[183] Labeckas G, Slavinskas S. The effect of rapeseed oil methyl ester on direct injection Diesel engine performance and exhaust emissions. Energy Convers Manag 2006;47:1954–67. doi:10.1016/j.enconman.2005.09.003.

[184] Agarwal AK, Das LM. Biodiesel Development and Characterization for Use as a Fuel in Compression Ignition Engines. J Eng Gas Turbines Power 2000;123:440–7.

[185] Vallinayagam R, Vedharaj S, Yang WM, Lee PS, Chua KJE, Chou SK. Combustion performance and emission characteristics study of pine oil in a diesel engine. Energy 2013;57:344–51.

[186] Chauhan BS, Kumar N, Cho HM. A study on the performance and emission of a diesel engine fueled with Jatropha biodiesel oil and its blends. Energy 2012;37:616–22. doi:10.1016/j.energy.2011.10.043.

[187] Can Ö. Combustion characteristics, performance and exhaust emissions of a diesel engine fueled with a waste cooking oil biodiesel mixture. Energy Convers Manag 2014;87:676–86. doi:10.1016/j.enconman.2014.07.066.

[188] Balamurugan T, Nalini R. Experimental investigation on performance, combustion and emission characteristics of four stroke diesel engine using diesel blended with alcohol as fuel. Energy 2014;78:356–63. doi:10.1016/j.energy.2014.10.020.

[189] Zhang Q, Yao M, Zheng Z, Liu H, Xu J. Experimental study of n-butanol addition on performance and emissions with diesel low temperature combustion. Energy 2012;47:515–21. doi:10.1016/j.energy.2012.09.020.

[190] Şahin Z, Aksu ON. Experimental investigation of the effects of using low ratio n-butanol/diesel fuel blends on engine performance and exhaust emissions in a turbocharged DI diesel engine. Renew Energy 2015;77:279–90. doi:10.1016/j.renene.2014.11.093.

[191] Zheng Z, Li C, Liu H, Zhang Y, Zhong X, Yao M. Experimental study on diesel conventional and low temperature combustion by fueling four isomers of butanol. Fuel 2015;141:109–19. doi:10.1016/j.fuel.2014.10.053.

[192] Karabektas M, Hosoz M. Performance and emission characteristics of a diesel engine using isobutanol–diesel fuel blends. Renew Energy 2009;34:1554–9. doi:10.1016/j.renene.2008.11.003.

[193] Campos-Fernandez J, Arnal JM, Gomez J, Dorado MP. A comparison of performance of higher alcohols/diesel fuel blends in a diesel engine. Appl Energy 2012;95:267–75.

[194] Li L, Wang J, Wang Z, Liu H. Combustion and emissions of compression ignition in a direct injection diesel engine fueled with pentanol. Energy 2015;80:575–81. doi:10.1016/j.energy.2014.12.013.

[195] Kannan TK, Marappan R. Study of performance and emission characteristics of a diesel engine using thevetia peruviana biodiesel with diethyl ether blends. Eur J Sci Res 2010;43:563–70. doi:1450216X.

[196] Rakopoulos DC, Rakopoulos CD, Giakoumis EG, Papagiannakis RG, Kyritsis DC. Influence of properties of various common bio-fuels on the combustion

and emission characteristics of high-speed DI (direct injection) diesel engine: Vegetable oil, bio-diesel, ethanol, n-butanol, diethyl ether. Energy 2014;73:354–66. doi:10.1016/j.energy.2014.06.032.

[197] Sakhrieh A, Abu-Nada E, Al-Hinti I, Al-Ghandoor A, Akash B. Computational thermodynamic analysis of compression ignition engine. Int Commun Heat Mass Transf 2010;37:299–303.

[198] EU directive 2007/46/EC of 5 September 2007 establishing a framework for the approval of motor vehicles and their trailers, and of systems, components and separate technical units intended for such vehicles [2007] OJ 263/1 n.d. http://ec.europa.eu/enterprise/sectors/automotive/documents/directives/directive-2007-46-ec_en.htm (accessed April 24, 2015).

[199] Pulkrabek WW. Engineering fundamentals of the internal combustion engine. vol. 2. Pearson Prentice Hall; 2004.

[200] United States Enviromental Protection Agency n.d. http://www.epa.gov/ (accessed April 25, 2015).

[201] Shahir VK, Jawahar CP, Suresh PR. Comparative study of diesel and biodiesel on CI engine with emphasis to emissions—A review. Renew Sustain Energy Rev 2015;45:686–97. doi:10.1016/j.rser.2015.02.042.

[202] Westbrook CK. Biofuels Combustion. Annu Rev Phys Chem 2013;64:201–19. doi:10.1146/annurev-physchem-040412-110009.

[203] Ban-Weiss GA, Chen JY, Buchholz BA, Dibble RW. A numerical investigation into the anomalous slight NOx increase when burning biodiesel; A new (old) theory. Biofuels Transp 2007;88:659–67.

[204] Hoekman SK, Robbins C. Review of the effects of biodiesel on NOx emissions. Fuel Process Technol 2012;96:237–49. doi:10.1016/j.fuproc.2011.12.036.

[205] Palash SM, Kalam MA, Masjuki HH, Masum BM, Rizwanul Fattah IM, Mofijur M. Impacts of biodiesel combustion on NOx emissions and their reduction approaches. Renew Sustain Energy Rev 2013;23:473–90. doi:10.1016/j.rser.2013.03.003.

[206] Lapuerta M, Octavio A, Rodriguez-Fernandez J, Armas O, Rodriguez-Fernandez J. Effect of biodiesel fuels on diesel engine emissions. Prog Energy Combust Sci 2008;34:198–223.

[207] Serrano L, Lopes M, Pires N, Ribeiro I, Cascão P, Tarelho L, et al. Evaluation on effects of using low biodiesel blends in a EURO 5 passenger vehicle equipped with a common-rail diesel engine. Appl Energy 2015;146:230–8. doi:10.1016/j.apenergy.2015.01.063.

[208] Peirce DM, Alozie NSI, Hatherill DW, Ganippa LC. Premixed Burn Fraction: Its Relation to the Variation in NOx Emissions between Petro- and Biodiesel. Energy Fuels 2017;27:3838–52. doi:10.1021/ef4006719.

[209] Giakoumis EG, Rakopoulos CD, Dimaratos AM, Rakopoulos DC. Exhaust emissions with ethanol or n-butanol diesel fuel blends during transient operation: A review. Renew Sustain Energy Rev 2013;17:170–90. doi:10.1016/j.rser.2012.09.017.

[210] Labeckas G, Slavinskas S, Mažeika M. The effect of ethanol–diesel–biodiesel

blends on combustion, performance and emissions of a direct injection diesel engine. Energy Convers Manag 2014;79:698–720. doi:10.1016/j.enconman.2013.12.064.

[211] Guarieiro LLN, Guerreiro ET de A, Amparo KK dos S, Manera VB, Regis ACD, Santos AG, et al. Assessment of the use of oxygenated fuels on emissions and performance of a diesel engine. Microchem J 2014;117:94–9. doi:10.1016/j.microc.2014.06.004.

[212] Rakopoulos DC, Rakopoulos CD, Giakoumis EG, Dimaratos AM, Kyritsis DC. Effects of butanol–diesel fuel blends on the performance and emissions of a high-speed DI diesel engine. Energy Convers Manag 2010;51:1989–97. doi:10.1016/j.enconman.2010.02.032.

[213] Chen Z, Liu J, Han Z, Du B, Liu Y, Lee C. Study on performance and emissions of a passenger-car diesel engine fueled with butanol–diesel blends. Energy 2013;55:638–46. doi:10.1016/j.energy.2013.03.054.

[214] Zhu Y, Chen Z, Liu J. Emission, efficiency, and influence in a diesel n-butanol dual-injection engine. Energy Convers Manag 2014;87:385–91. doi:10.1016/j.enconman.2014.07.028.

[215] Chen Z, Wu Z, Liu J, Lee C. Combustion and emissions characteristics of high n-butanol/diesel ratio blend in a heavy-duty diesel engine and EGR impact. Energy Convers Manag 2014;78:787–95. doi:10.1016/j.enconman.2013.11.037.

[216] Thomas G, Feng B, Veeraragavan A, Cleary MJ, Drinnan N. Emissions from DME combustion in diesel engines and their implications on meeting future emission norms: A review. Fuel Process Technol 2014;119:286–304. doi:10.1016/j.fuproc.2013.10.018.

[217] Cinar C, Can Ö, Sahin F, Yucesu HS. Effects of premixed diethyl ether (DEE) on combustion and exhaust emissions in a HCCI-DI diesel engine. Appl Therm Eng 2010;30:360–5. doi:10.1016/j.applthermaleng.2009.09.016.

[218] Sharma YC, Singh B, Upadhyay SN. Advancements in development and characterization of biodiesel: A review. Fuel 2008;87:2355–73. doi:10.1016/j.fuel.2008.01.014.

[219] Tree DR, Svensson KI. Soot processes in compression ignition engines. Prog Energy Combust Sci 2007;33:272–309. doi:10.1016/j.pecs.2006.03.002.

[220] Bergthorson JM, Thomson MJ. A review of the combustion and emissions properties of advanced transportation biofuels and their impact on existing and future engines. Renew Sustain Energy Rev 2015;42:1393–417. doi:10.1016/j.rser.2014.10.034.

[221] Zhang Z-H, Balasubramanian R. Influence of butanol–diesel blends on particulate emissions of a non-road diesel engine. Fuel 2014;118:130–6. doi:10.1016/j.fuel.2013.10.059.

[222] Yoon SH, Cha JP, Lee CS. An investigation of the effects of spray angle and injection strategy on dimethyl ether (DME) combustion and exhaust emission characteristics in a common-rail diesel engine. Fuel Process Technol 2010;91:1364–72. doi:10.1016/j.fuproc.2010.04.017.

[223] Shakya BM, Harold MP, Balakotaiah V. Modeling and analysis of dual-layer

NOx storage and reduction and selective catalytic reduction monolithic catalyst. Chem Eng J 2014;237:109–22.

[224] Schönborn A. Influence of the molecular structure of biofuels on combustion in a compression ignition engine. 2009.

[225] Hellier PR. The Molecular Structure of Future Fuels. University College London, 2013.

[226] Instruments H. MEXA 9100HEGR instructions manual. 1984.

[227] Cambustion. DMS500 Particulate Spectrometer User Manual 2003.

[228] Poiling B, Prausnitz J, O'Connel J. The Properties of Gases and Liquids. 5th ed. McGraw-Hill Professional; 5 edition; 200AD.

[229] Welz, Oliver. Judit Zádor, John D. Savee, Leonid Sheps, David L. Osborn and CAT. Low-Temperature Combustion Chemistry of n-Butanol: Principal Oxidation Pathways of Hydroxybutyl Radicals. J Phys Chem 2013;117:11983–2001.

[230] Tang C, Wei L, Man X, Zhang J, Huang Z, Law CK. High temperature ignition delay times of C5 primary alcohols. Combust Flame 2013;160:520–9.

[231] Zhu Y, Davidson DF, Hanson RK. 1-Butanol ignition delay times at low temperatures: An application of the constrained-reaction-volume strategy. Combust Flame 2014;161:634–43. doi:10.1016/j.combustflame.2013.06.028.

[232] Bayraktar H. An experimental study on the performance parameters of an experimental CI engine fueled with diesel–methanol–dodecanol blends. Fuel 2008;87:158–64. doi:10.1016/j.fuel.2007.04.021.

[233] Ramírez AI, Aggarwal SK, Som S, Rutter TP, Longman DE. Effects of blending a heavy alcohol (C20H40O with diesel in a heavy-duty compression-ignition engine. Fuel 2014;136:89–102. doi:10.1016/j.fuel.2014.06.039.

[234] Yaws CL. Yaws' Handbook of Thermodynamic and Physical Properties of Chemical Compounds. 2003.

[235] Lide D. CRC Handbook of Chemistry and Physics, 85th Edition. 85th ed. CRC Press; 2004.

[236] Sigma-Aldrich 2015. http://www.sigmaaldrich.com/united-kingdom.html (accessed January 3, 2015).

[237] ChemSpider| Search and share chemistry. http://www.chemspider.com/ (accessed January 16, 2015).

[238] Lambiotte&Cie 1999. http://www.lambiotte.com/Butylal-product_view.htm?id=61 (accessed January 16, 2015).

[239] Yeung C, Thomson MJ. Experimental and kinetic modeling study of 1-hexanol combustion in an opposed-flow diffusion flame. Proc Combust Inst 2013;34:795–802.

[240] Sarathy SM, Vranckx S, Yasunaga K, Mehl M, Oßwald P, Metcalfe WK, et al. A comprehensive chemical kinetic combustion model for the four butanol isomers. Combust Flame 2012;159:2028–55.

[241] Cai J, Yuan W, Ye L, Cheng Z, Wang Y, Zhang L, et al. Experimental and kinetic modeling study of 2-butanol pyrolysis and combustion. Combust Flame 2013;160:1939–57. doi:10.1016/j.combustflame.2013.04.010.

[242] Vanhove G, Ribaucour M, Minetti R. On the influence of the position of the double bond on the low-temperature chemistry of hexenes. Proc Combust Inst 2005;30:1065–72. doi:10.1016/j.proci.2004.08.042.

[243] Silke EJ, Curran HJ, Simmie JM. The influence of fuel structure on combustion as demonstrated by the isomers of heptane: a rapid compression machine study. Proc Combust Inst 2005;30:2639–47. doi:10.1016/j.proci.2004.08.180.

[244] Ribaucour M, Minetti R, Sochet LR, Curran HJ, Pitz WJ, Westbrook CK. Ignition of isomers of pentane: An experimental and kinetic modeling study. Proc Combust Inst 2000;28:1671–8. doi:10.1016/S0082-0784(00)80566-4.

[245] Saravanan S, Nagarajan G, Anand S, Sampath S. Correlation for thermal NOx formation in compression ignition (CI) engine fuelled with diesel and biodiesel. Energy 2012;42:401–10. doi:10.1016/j.energy.2012.03.028.

[246] Fang Q, Fang J, Zhuang J, Huang Z. Effects of ethanol–diesel–biodiesel blends on combustion and emissions in premixed low temperature combustion. Appl Therm Eng 2013;54:541–8. doi:10.1016/j.applthermaleng.2013.01.042.

[247] Rakopoulos DC, Rakopoulos CD, Papagiannakis RG, Kyritsis DC. Combustion heat release analysis of ethanol or n-butanol diesel fuel blends in heavy-duty DI diesel engine. Fuel 2011;90:1855–67. doi:10.1016/j.fuel.2010.12.003.

[248] Kittelson DB. Engines and nanoparticles. J Aerosol Sci 1998;29:575–88. doi:10.1016/S0021-8502(97)10037-4.

[249] Xue J, Grift TE, Hansen AC. Effect of biodiesel on engine performances and emissions. Renew Sustain Energy Rev 2011;15:1098–116. doi:10.1016/j.rser.2010.11.016.

[250] Palczewska-Tulinska M, Szafranski A. Selected Physiochemisal Properties of Dibutoxymethane. J Chem Eng Data 2000;45:988–90. doi:10.1021/je/0000701.

[251] Hoare DE, Li T-M. The combustion of simple ketones I— Mechanism at “low” temperatures. Combust Flame 1968;12:136–44. doi:10.1016/0010-2180(68)90089-8.

[252] Anderson D, Hoare DE. The combustion of methyl isopropyl ketone and methyl t-butyl ketone. Combust Flame 1969;13:511–20. doi:10.1016/0010-2180(69)90091-1.

[253] Zhou C-W, Simmiea JM, Currana HJ. Ab initio and kinetic study of the reaction of ketones with ȮH for T = 500–2000 K. Part I: hydrogen-abstraction from H3CC(O)CH3–x(CH3)x, x = 0 - 2. Phys Chem Chem Phys 2011;13:11175–92. doi:10.1039/C0CP02754E.

[254] Peralta-Yahya P, Zhang F, del Cardayre SB, Keasling JD. Microbial engineering for the production of advanced biofuels. Nature 2012;488:320–8. doi:10.1038/nature11478.

[255] Fisher EM, Pitz WJ, Curran HJ, Westbrook CK. Detailed chemical kinetic mechanisms for combustion of oxygenated fuels. Proc Combust Inst 2000;28:1579–86. doi:10.1016/S0082-0784(00)80555-X.

[256] Koivisto E, Ladommatos N, Gold M. Systematic study of the effect of the hydroxyl functional group in alcohol molecules on compression ignition and exhaust gas emissions. Fuel 2015;153:650–63. doi:10.1016/j.fuel.2015.03.042.

[257] Mayo DW, Miller FA, Hannah RW. Course Notes on the Interpretation of Infrared and Raman Spectra. John Wiley & Sons; 2004.

[258] Anslyn E, Dougherty D. Modern Physical Organic Chemistry. University Science Books; 2006.

[259] Carey F, Sundberg R. Advanced Organic Chemistry: Part A: Structure and Mechanisms. Springer Science & Business Media,; 2007.

[260] Okuyama T, Maskill H. Organic Chemistry: A Mechanistic Approach. Oxford University Press; 2013.

[261] Górski K, Sen AK, Lotko W, Swat M. Effects of ethyl-tert-butyl ether (ETBE) addition on the physicochemical properties of diesel oil and particulate matter and smoke emissions from diesel engines. Fuel 2013;103:1138–43. doi:10.1016/j.fuel.2012.09.004.

[262] Beatrice C, Di Blasio G, Guido C, Cannilla C, Bonura G, Frusteri F. Mixture of glycerol ethers as diesel bio-derivable oxy-fuel: Impact on combustion and emissions of an automotive engine combustion system. Appl Energy 2014;132:236–47. doi:10.1016/j.apenergy.2014.07.006.

[263] Ozsezen AN, Canakci M, Turkcan A, Sayin C. Performance and combustion characteristics of a DI diesel engine fueled with waste palm oil and canola oil methyl esters. Fuel 2009;88:629–36. doi:10.1016/j.fuel.2008.09.023.

[264] Monyem A, Gerpen HV. The effect of biodiesel oxidation on engine performance and emissions. Biomass and Bioenergy 2001;20:317–25.

[265] Azjargal J. The comparison of combustion characteristics and performances of diesel engine fueled with biodiesel and diesel blends. Strateg. Technol. (IFOST), 2014 9th Int. Forum, Cox's Bazar: IEEE; 2014, p. 313–7. doi:10.1109/IFOST.2014.6991129.

[266] Tsolakis A, Megaritis A, Wyszynski M, Theinnoi K. Engine performance and emissions of a diesel engine operating on diesel-RME (rapeseed methyl ester) blends with EGR (exhaust gas recirculation). Energy 2007;32:2072–80. doi:10.1016/j.energy.2007.05.016.

[267] Gogoi TK, Baruah DC. A cycle simulation model for predicting the performance of a diesel engine fuelled by diesel and biodiesel blends. Energy 2010;35:1317–23. doi:10.1016/j.energy.2009.11.014.

[268] Bueno AV, Velásquez JA, Milanez LF. Heat release and engine performance effects of soybean oil ethyl ester blending into diesel fuel. Energy 2011;36:3907–16. doi:10.1016/j.energy.2010.07.030.

[269] Raheman H, Phadatare AG. Diesel engine emissions and performance from blends of karanja methyl ester and diesel. Biomass and Bioenergy 2004;27:393–7. doi:10.1016/j.biombioe.2004.03.002.

[270] Lin Y-C, Lee W-J, Hou H-C. PAH emissions and energy efficiency of palm-biodiesel blends fueled on diesel generator. Atmos Environ 2006;40:3930–40. doi:10.1016/j.atmosenv.2006.02.026.

[271] Kumar S, Cho JH, Park J, Moon I. Advances in diesel-alcohol blends and their effects on the performance and emissions of diesel engines. Renew Sustain Energy Rev 2013;22:46–72.

[272] Aydin H, Bayindir H. Performance and emission analysis of cottonseed oil methyl ester in a diesel engine. Renew Energy 2010;35:588–92. doi:10.1016/j.renene.2009.08.009.

[273] Ndayishimiye P, Tazerout M. Use of palm oil-based biofuel in the internal combustion engines: Performance and emissions characteristics. Energy 2011;36:1790–6. doi:10.1016/j.energy.2010.12.046.

[274] Ramadhas AS, Jayaraj S, Muraleedharan C. Characterization and effect of using rubber seed oil as fuel in the compression ignition engines. Renew Energy 2005;30:795–803. doi:10.1016/j.renene.2004.07.002.

[275] Altın R, Çetinkaya S, Yücesu HS. The potential of using vegetable oil fuels as fuel for diesel engines. Energy Convers Manag 2001;42:529–38. doi:10.1016/S0196-8904(00)00080-7.

[276] An H, Yang WM, Li J, Zhou DZ. Modeling study of oxygenated fuels on diesel combustion: Effects of oxygen concentration, cetane number and C/H ratio. Energy Convers Manag 2015;90:261–71. doi:10.1016/j.enconman.2014.11.031.

[277] Centi G, Lanzafame P, Perathoner S. Analysis of the alternative routes in the catalytic transformation of lignocellulosic materials. Catal Today 2011;167:14–30. doi:10.1016/j.cattod.2010.10.099.

[278] Hayes DJM. Second-generation biofuels: why they are taking so long. Wiley Interdiscip Rev Energy Environ 2013;2:304–34. doi:10.1002/wene.59.

[279] Harrela P. UPM LAPPEENRANTA BIOREFINERY IS IN COMMERCIAL PRODUCTION. http://www.upm.com/EN/MEDIA/All-news/Pages/UPM-Lappeenranta-Biorefinery-is-in-commercial-production-001-Mon-12-Jan-2015-11-30.aspx (Accessed 2.3.2015) n.d. http://www.upm.com/EN/MEDIA/All-news/Pages/UPM-Lappeenranta-Biorefinery-is-in-commercial-production-001-Mon-12-Jan-2015-11-30.aspx (accessed March 2, 2015).

[280] Rackemann D, Doherty WO. The conversion of lignocellulosics to levulinic acid. Biofuels, Bioprod Biorefining 2011;5:198–214. doi:10.1002/bbb.267.

[281] Deng W, Zhang Q, Wang Y. Catalytic transformations of cellulose and its derived carbohydrates into 5-hydroxymethylfurfural, levulinic acid, and lactic acid. Sci China Chem 2015;58:29–46. doi:10.1007/s11426-014-5283-8.

[282] Serrano DP, Coronado JM, Melero JA. Conversion of cellulose and hemicellulose into platform molecules: Chemical routes. Final Biorefiney Conf. - EuroBioRef Present., Brussels: EuroBioRef; 2014, p. 41.

[283] Rajasekar E, Selvi S. Review of combustion characteristics of CI engines fueled with biodiesel. Renew Sustain Energy Rev 2014;35:390–9. doi:10.1016/j.rser.2014.04.006.

[284] Christensen E, Williams A, Paul S, Burton S, McCormick RL. Properties and Performance of Levulinate Esters as Diesel Blend Components. Energy Fuels 2011;25:5422–8. doi:10.1021/ef201229j.

[285] Joshi H, Moser BR, Toler J, Smith WF, Walker T. Ethyl levulinate: A potential bio-based diluent for biodiesel which improves cold flow properties. Biomass and Bioenergy 2011;35:3262–6. doi:10.1016/j.biombioe.2011.04.020.

[286] Chuck CJ, Donnelly J. The compatibility of potential bioderived fuels with Jet A-1 aviation kerosene. Appl Energy 2014;118:83–91. doi:10.1016/j.apenergy.2013.12.019.

[287] Démolis A, Essayem N, Rataboul F. Synthesis and Applications of Alkyl Levulinates. ACS Sustain Chem Eng 2014;2:1338–52. doi:10.1021/sc500082n.

[288] Janssen A, Pischinger S, Muether M. Potential of Cellulose-Derived Biofuels for Soot Free Diesel Combustion. SAE Int J Fuels Lubr 2010;3:70–84. doi:10.4271/2010-01-0335.

[289] Lange J-P, Price R, Ayoub PM, Louis J, Petrus L, Clarke L, et al. Valeric Biofuels: A Platform of Cellulosic Transportation Fuels. Angew Chemie Int Ed 2010;49:4479–83. doi:10.1002/anie.201000655.

[290] Dayma G, Halter F, Foucher F, Togbe C, Mounami-Rousselle C, Dagaut P, et al. Experimental and Detailed Kinetic Modeling Study of Ethyl Pentanoate (Ethyl Valerate) Oxidation in a Jet Stirred Reactor and Laminar Burning Velocities in a Spherical Combustion Chamber. Energy Fuels 2012;26:4735–48. doi:10.1021/ef300581q.

[291] Contino F, Dagaut P, Dayma G, Halter F, Foucher F, Mounaïm-rousselle C. Combustion and Emissions Characteristics of Valeric Biofuels in a Compression Ignition Engine. J Energy Eng 2013;140:1943–7897. doi:10.1061/(ASCE)EY.1943-7897.0000161.

[292] Sigma-Aldrich 2015. http://www.sigmaaldrich.com/united-kingdom.html (accessed January 16, 2015).

[293] Indraswati N, Mudjijati, Wicaksana F, Hindarso H. Density and Viscosity for a Binary Mixture of Ethyl Valerate andHexyl Acetate with 1-Pentanol and 1-Hexanol at 293.15 K, 303.15 K,and 313.15 K. J Chem Eng Data 2001;46:134–7. doi:10.1021/je0001431.

[294] Koivisto E, Ladommatos N, Gold M. The influence of various oxygenated functional groups in carbonyl and ether compounds on compression ignition and exhaust gas emissions. Submitt to Fuel 2015.

[295] Fersner A, Karty JM, Mo Y. Why Are Esters and Amides Weaker Carbon Acids than Ketones and Acid Fluorides? Contributions by Resonance and Inductive Effects. J Org Chem 2009;74:7245–53. doi:10.1021/jo901225t.

[296] Battin-Leclerc F. Detailed chemical kinetic models for the low-temperature combustion of hydrocarbons with application to gasoline and diesel fuel surrogates. Prog Energy Combust Sci 2008;34:440–98. doi:10.1016/j.pecs.2007.10.002.

[297] Tian Z, Pitz WJ, Fournet R, Glaude PA, Battin-Leclerc F. A detailed kinetic modeling study of toluene oxidation in a premixed laminar flame. Proc Combust Inst 2011;33:233–41. doi:10.1016/j.proci.2010.06.063.

[298] Zhang L, Cai J, Zhang T, Qi F. Kinetic modeling study of toluene pyrolysis at low pressure. Combust Flame 2010;157:1686–97.

doi:10.1016/j.combustflame.2010.04.002.

[299] Brezinsky K. The high-temperature oxidation of aromatic hydrocarbons. Prog Energy Combust Sci 1986;12:1–24. doi:10.1016/0360-1285(86)90011-0.

[300] Sakai Y, Miyoshi A, Koshi M, Pitz WJ. A kinetic modeling study on the oxidation of primary reference fuel-toluene mixtures including cross reactions between aromatics and aliphatics. Proc Combust Inst 2009;32 I:411–8. doi:10.1016/j.proci.2008.06.154.

[301] Xiao Z, Ladommatos N, Zhao H. The effect of aromatic hydrocarbons and oxygenates on diesel engine emissions. Proc Inst Mech Eng Part D J Automob Eng 2000;214:307–32. doi:10.1243/0954407001527448.

[302] Hellier P, Ladommatos N, Allan R, Rogerson J. Combustion and emissions characteristics of toluene/n-heptane and 1-octene/n-octane binary mixtures in a direct injection compression ignition engine. Combust Flame 2013;160:2141–58. doi:10.1016/j.combustflame.2013.04.016.

[303] Machrafi H, Cavadias S, Gilbert P. An experimental and numerical analysis of the HCCI auto-ignition process of primary reference fuels, toluene reference fuels and diesel fuel in an engine, varying the engine parameters. Fuel Process Technol 2008;89:1007–16. doi:10.1016/j.fuproc.2008.03.007.

[304] Altarawneh MK, Dlugogorski BZ, Kennedy EM, Mackie JC. Rate constants for reactions of ethylbenzene with hydroperoxyl radical. Combust Flame 2013;160:9–16. doi:10.1016/j.combustflame.2012.08.008.

[305] Husson B, Ferrari M, Herbinet O, Ahmed SS, Glaude P-A, Battin-Leclerc F. New experimental evidence and modeling study of the ethylbenzene oxidation. Proc Combust Inst 2013;34:325–33. doi:10.1016/j.proci.2012.06.002.

[306] Gudiyella S, Brezinsky K. High pressure study of n-propylbenzene oxidation. Combust Flame 2012;159:940–58. doi:10.1016/j.combustflame.2011.09.013.

[307] Wang Z, Li Y, Zhang F, Zhang L, Yuan W, Wang Y, et al. An experimental and kinetic modeling investigation on a rich premixed n-propylbenzene flame at low pressure. Proc Combust Inst 2013;34:1785–93. doi:10.1016/j.proci.2012.05.006.

[308] Altarawneh M, Dlugogorski BZ. Reactions of HO2 with n-propylbenzene and its phenylpropyl radicals. Combust Flame 2014. doi:10.1016/j.combustflame.2014.11.007.

[309] Roubaud A, Lemaire O, Minetti R, Sochet L. High pressure auto-ignition and oxidation mechanisms of o-xylene, o-ethyltoluene, and n-butylbenzene between 600 and 900 K. Combust Flame 2000;123:561–71. doi:10.1016/S0010-2180(00)00174-7.

[310] Ribaucour M, Roubaud A, Minetti R, Sochet LR. The low-temperature autoignition of alkylaromatics: Experimental study and modeling of the oxidation of n-butylbenzene. Proc Combust Inst 2000;28:1701–7. doi:10.1016/S0082-0784(00)80570-6.

[311] Husson B, Bounaceur R, Tanaka K, Ferrari M, Herbinet O, Glaude PA, et al. Experimental and modeling study of the oxidation of n-butylbenzene. Combust Flame 2012;159:1399–416.

doi:10.1016/j.combustflame.2011.12.006.

[312] Nakamura H, Darcy D, Mehl M, Tobin CJ, Metcalfe WK, Pitz WJ, et al. An experimental and modeling study of shock tube and rapid compression machine ignition of n-butylbenzene/air mixtures. Combust Flame 2014;161:49–64. doi:10.1016/j.combustflame.2013.08.002.

[313] Battin-Leclerc F, Warth V, Bounaceur R, Husson B, Herbinet O, Glaude P-A. The oxidation of large alkylbenzenes: An experimental and modeling study. Proc Combust Inst 2015;35:349–56. doi:10.1016/j.proci.2014.05.087.

[314] Darcy D, Nakamura H, Tobin CJ, Mehl M, Metcalfe WK, Pitz WJ, et al. An experimental and modeling study of surrogate mixtures of n-propyl- and n-butylbenzene in n-heptane to simulate n-decylbenzene ignition. Combust Flame 2014;161:1460–73. doi:10.1016/j.combustflame.2013.12.006.

[315] Huheey J. The Electronegativity of Groups. J Phys Chem 1965;69:3284–91. doi:10.1021/j100894a011.

[316] Huheey J. The Electronegativity of Multiply Bonded Groups. J Phys Chem 1966;70:2086–92. doi:10.1021/j100879a003.

[317] Klotz SD, Brezinsky K, Glassman I. Modeling the combustion of toluene-butane blends. Symp Combust 1998;27:337–44. doi:10.1016/S0082-0784(98)80421-9.

[318] Gary JH, Handwerk GE, Kaiser MJ. Petroleum Refining: Technology and Economics. 5th ed. CRC Press; 2007.

[319] Spleight JG, Ozum B. Petroleum Refining Processes. CRC Press; 2001.

[320] Fahim MA, Taher AA-S, Elkilani A. Fundamentals of Petroleum Refining. Elsevier; 2009.